SCIENCE CHINA
Earth Sciences

•RESEARCH PAPER•

March 2023 Vol.66 No.3: 594–608
https://doi.org/10.1007/s11430-021-1056-6

The development process of a temperate montane peatland and its controlling factors since the middle Holocene

Yanmin DONG[1,2], Hongkai LI[1,2*], Shengzhong WANG[1,2] & Hongshi HE[1,3]

[1] *Key Laboratory of Geographical Process and Ecological Security in Changbai Mountains, Ministry of Education, School of Geographical Sciences, Northeast Normal University, Changchun 130024, China;*
[2] *State Environmental Protection Key Laboratory of Wetland Ecology and Vegetation Restoration, Northeast Normal University, Changchun 130024, China;*
[3] *School of Natural Resources, University of Missouri, MO 65211, USA*

Received December 28, 2021; revised December 9, 2022; accepted December 29, 2022; published online February 23, 2023

Abstract Peatlands are some of the largest carbon reservoirs in terrestrial ecosystems and play a key role in the global carbon cycle. Understanding peatland development, carbon accumulation processes, and the peatland response to varying forcing factors over different temporal and spatial scales helps reveal the underlying processes and general patterns of these ecosystems. To assess the role of climate and local conditions in peatland development, the basal samples from 23 peat cores and three well dated long peat cores were used to explore peatland initiation, lateral expansion, and carbon accumulation rate in the Baijianghe peatland located in the Changbai Mountains, Northeast China. Our results reveal that the Baijianghe peatland was initiated from forest conditions at 7.9 cal. kyr BP and then expanded laterally by paludification. The rapid expansion between 5 and 4 cal. kyr BP likely resulted from high precipitation and gentle topography. The mean carbon accumulation rates of the three long peat cores were 36.3, 39.1 and 48.4 g C m^{-2} yr^{-1}, respectively, which are higher than rates from the northern peatlands. Both climate and local conditions have exerted an important influence on carbon accumulation rates in the Baijianghe peatland since the middle Holocene. The carbon accumulation patterns between 5 and 1.5 cal. kyr BP were probably linked to local conditions rather than climatic settings, including topography, hydrological conditions, and plant composition. The consistently decreasing carbon accumulation rate values at all locations within the BJH peatland over the last 1.5 cal. kyr BP suggests that climate is the primary control. This study highlights the varying primary controls on the process of peatland development and reveals the important role of local conditions in carbon accumulation.

Keywords Paludification, Peatland lateral expansion, Carbon accumulation rate, Northeast China, Middle Holocene

Citation: Dong Y, Li H, Wang S, He H. 2023. The development process of a temperate montane peatland and its controlling factors since the middle Holocene. Science China Earth Sciences, 66(3): 594–608, https://doi.org/10.1007/s11430-021-1056-6

1. Introduction

Although peatlands occupy a relatively small fraction of the terrestrial land surface (ca. 3%) (Frolking et al., 2011; Xu et al., 2018), they store 500±100 Pg of carbon, which represents approximately 30% of the present day global soil organic carbon pool (Yu, 2011; Yu et al., 2021). Since natural peatlands function as carbon dioxide (CO_2) reservoirs and are sources of atmospheric methane (CH_4), they play an important role in the global carbon cycle (Loisel et al., 2017). The response of the global peatland carbon cycle to future climate change remains uncertain (Ise et al., 2008; Dorrepaal et al., 2009; Frolking et al., 2011; Charman et al., 2015; Gallego-Sala et al., 2018; Loisel et al., 2021). Recent studies have suggested that increasing temperatures enhance net primary productivity (NPP), which could play a greater role

* Corresponding author (email: lihk431@nenu.edu.cn)

© Science China Press 2023

in the long-term accumulation of carbon compared to decomposition (Charman et al., 2013). However, the responses of different types of peatlands (such as bogs and fens) to climate change may be different (Yu, 2006; Loisel and Yu, 2013; Yu et al., 2014; Treat et al., 2016). For example, Yu (2006) found that the rate carbon accumulated in fens in continental western Canada exceeded that in bogs during the same period. Improving our understanding of peatland carbon dynamics and the controlling factors, therefore, will help to predict the fate of the peatland carbon pool within future climate contexts (Yu et al., 2014; Xing et al., 2015a; Loisel et al., 2017; Gallego-Sala et al., 2018).

Given the complexity of peatlands, various external factors that exhibit local- to continental-scale variability regulate their development (Charman, 2002; Yu et al., 2009; Ruppel et al., 2013; Charman et al., 2015). Climate is a dominant regulator of carbon accumulation in peatlands over larger and longer spatiotemporal scales (Yu et al., 2009; Jones and Yu, 2010; Gallego-Sala et al., 2018). Primary production and decay processes in peatlands are greatly affected by temperature and precipitation (Charman et al., 2015). Previous studies have suggested that the carbon accumulation rate (CAR) is greater under wetter and warmer conditions and lower under drier and colder conditions (Charman et al., 2013, 2015; Mathijssen et al., 2016; Panait et al., 2017). Furthermore, the capacity of a peatland to sequester carbon depends to a large degree on the composition of the dominant plant species; hence, changes in species composition will potentially have a considerable effect on carbon accumulation (van Bellen et al., 2011; Loisel and Yu, 2013; Lacourse and Davies, 2015, Mathijssen et al., 2016; Panait et al., 2017), which is not fully understood (Charman et al., 2015). Local conditions (such as topography and hydrology) could mediate the influence of climate on vegetation succession, subsequently affecting the CAR of peatland (van Bellen et al., 2011; Lacourse and Davies, 2015; Panait et al., 2017; Mathijssen et al., 2019). For example, van Bellen et al. (2011) found that CAR was highly variable among cores recovered from boreal Quebec, Canada, suggesting that local topography and/or hydrology may mediate the influence of climate on carbon accumulation. Loisel and Yu (2013) found that peat accumulation across Patagonia did not correlate with climatic parameters. They emphasized the local scale controls (such as vegetation succession and peatland self-regulation mechanisms) on peat accumulation. Hence, both climatic and local factors should be considered when evaluating carbon dynamics in peatlands.

To date, most studies dealing with the climate sensitivity of carbon accumulation have focused on northern peatlands (~45°N to 70°N in latitude) where ombrotrophic bogs are widespread (Loisel et al., 2017; Gallego-Sala et al., 2018), but few studies have investigated peatlands in mid-latitude regions where fens are widespread (Wang et al., 2014; Xing et al., 2015a). Northeast China (NE China) contains the largest area of peatland and represents 48% of the total wetland area in China (Niu et al., 2012; Xing et al., 2015a). However, little is known about the sensitivity of peatlands to past climate, carbon accumulation, and the forcing factors of CAR in NE China. Some investigations have focused on peatland initiation and carbon accumulation over regional scales (Zhao et al., 2014; Wang et al., 2014; Zhang et al., 2015; Xing et al., 2015a, 2015b), while control over local scales has not been fully addressed (Dong et al., 2021). The few long-term records of CAR obtained from the Changbai Mountains were restricted to the Hani (Cai et al., 2013), Baijianghe (Xia et al., 2019), and Jinchuan peatlands (Sun et al., 2019). Xia et al. (2019) found that the Baijianghe peatland had its highest CAR between 750 and 580 cal. yr BP under comparatively wet and probably warm conditions and low CAR under cold and dry climates during the Little Ice Age (LIA). However, the results are based on only one core and should be treated with caution. It would be meaningful, therefore, to study carbon accumulation patterns and various forcing factors over local scales using multiple cores to improve our understanding of the processes underpinning peatland carbon accumulation.

In this study, the Baijianghe (BJH) peatland, a montane peatland in the Changbai Mountains of NE China, was selected as the study site. Twenty-three basal peat ages were used to explore the peatland initiation and expansion processes that have occurred since the middle Holocene. The CAR values were calculated based on three well dated peat cores. The relationships between CAR and climate, plant composition, and topography are discussed in this study as they relate to the following objectives: (1) to identify the development of the BJH peatland over time, including when and how the peatland was initiated and how it laterally expanded, (2) to estimate the rate of long-term carbon accumulation in the BJH peatland, and (3) to understand how peatland development and carbon accumulation change under the influence of changing climate and local conditions.

2. Study site

The Baijianghe peatland (42°09′59″N, 126°44′10″E, 778 m a.s.l.) is located in the Changbai Mountains, Jilin Province, NE China (Figure 1a and 1b). The climate here is humid and temperate within the East Asia summer monsoon (EASM) climate zone (Wang and LinHo, 2002; Stebich et al., 2015). The mean annual temperature is 3.3°C, with a mean warmest month (July) temperature of 20.8°C and mean coldest month (January) temperature of −17.8°C. The mean annual precipitation is 773 mm, with the rainy season extending from May to September, which accounts for approximately 80% of the total annual rainfall (Figure 1c). The vegetation is

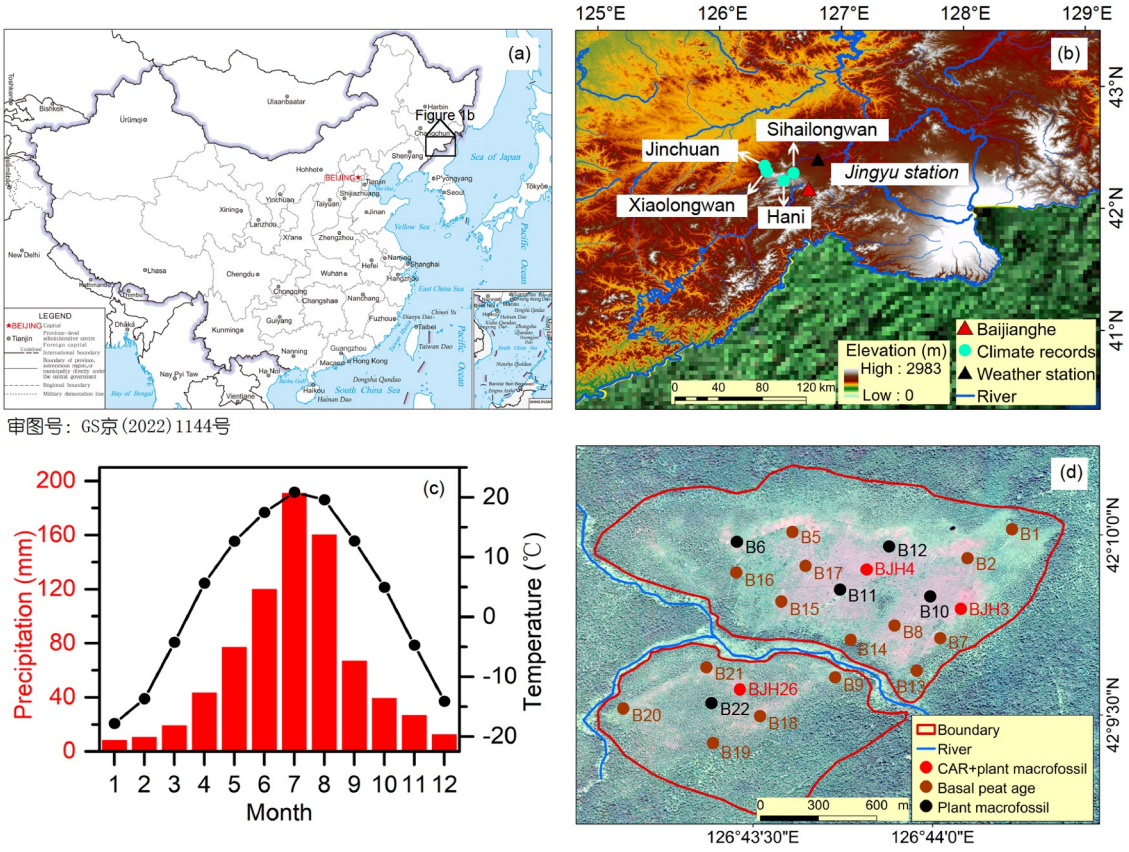

Figure 1 (a) Map showing the location of the Baijianghe (BJH) peatland. (b) The BJH peatland and nearby palaeoclimate records, including those from Jinchuan peatland (Zhang et al., 2019a), the Hani peatland (Hong et al., 2005), the Sihailongwan Maar lake (Stebich et al., 2015), and the Xiaolongwan Maar lake (Chu et al., 2014). (c) Precipitation and temperature patterns of the BJH peatland. The values shown are mean monthly temperature and precipitation records from the Jingyu station for the period between 1955 and 2015. (d) Sampling points in the BJH peatland are considered in this study.

dominated by temperate mixed conifer and broadleaf deciduous forest (Stebich et al., 2015). The BJH peatland is surrounded by a *Larix olgensis* forest with accompanying species, including *Betula platyphylla*, *Quercus mongolica*, *Tilia mandshurica*, *Abies nephrolepis*, *Picea jezoensis*, *Juglans mandshurica*, and *Acer mono*.

The total area of the BJH peatland is approximately 1.89 km^2 and is divided into two parts by the river flowing from west to east (Figure 1d). Rainfall and surface runoff from the surrounding mountains are the main sources of water supply for the peatland. The vegetation in the BJH peatland is highly heterogeneous: the northeast part is dominated by herbaceous plants such as *Carex* spp., *Menyanthes trifoliata*, *Iris setosa*, and *Equisetum hyemale*. Shrubs cover less than 20% of the area, and *Sphagnum* spp. is widely distributed across the site (Appendix Figure S1a, https://link.springer.com). In the northwest of the peatland, the shrub coverage is extremely high (>90%), and is largely dominated by *Potentilla fruticosa* with a small amount of *Betula ovalifolia* and *Ledum palustre* (Appendix Figure S1b). The peatland in the southern part is dominated by *Larix olgensis-Betula ovalifolia-Carex* spp.-*Sphagnum* spp. communities (Appendix Figure S1c).

3. Material and methods

3.1 Peat sampling

The peat depth was surveyed in detail using a manual peat corer at 93 points (Figure 2a). Three long peat cores (BJH3, BJH4, and BJH26, red dots in Figure 1d) were retrieved for plant macrofossil analysis and CAR calculation (Appendix Figure S2). The basal ages of these three long cores and another 20 cores (core locations depicted by the black and brown dots in Figure 1d) were used to explore the process of peatland initiation and lateral expansion. Since in most cores, the lithological characteristics of the bottom layers changed gradually from mineral deposits to peat (Appendix Figure S3), the lower-most sample in each core that had a total organic carbon (TOC) content of over 15% (Chai, 1990) was defined as the basal peat deposit. After recording the sedimentary features in the cores and photographing them (Appendix Figures S2–S3), all cores were segmented *in situ* at 1 cm intervals. The samples were then sealed in labelled bags for transport to the laboratory. The stratigraphic features and plant composition of the three long peat cores were described based on visual field inspection and plant macrofossil analysis.

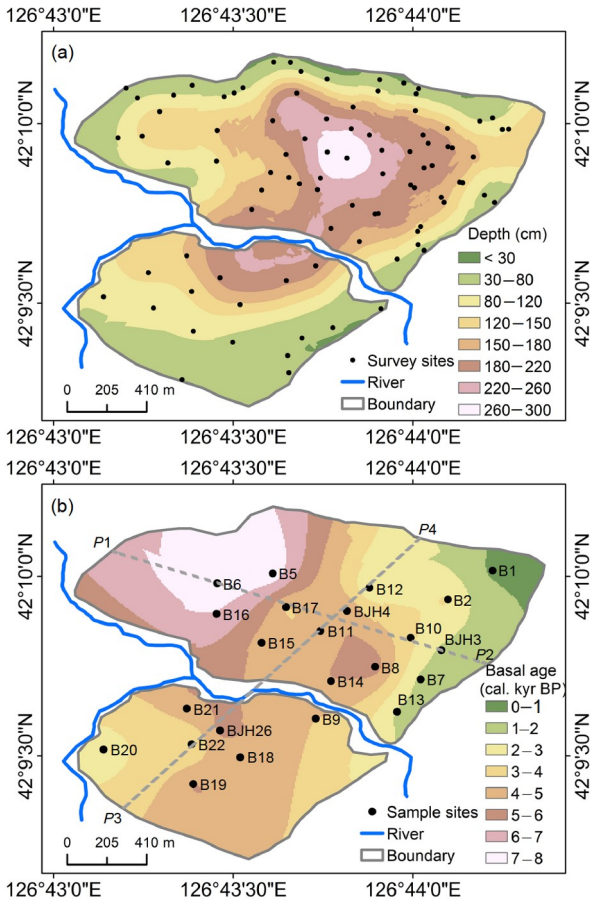

Figure 2 (a) Peat thickness distribution according to 93 surveyed sites and (b) pattern of peatland lateral expansion according to 23 basal ages from the BJH peatland. The grey dashed lines in (b), *P*1–*P*2, and *P*3–*P*4, refer to the section lines that are shown in Figure 6, extending from the northwest to the southeast and from the southwest to the northeast, respectively.

3.2 AMS^{14}C dating and age-depth model

Accelerator mass spectrometry ^{14}C (AMS ^{14}C) was used to date the peat samples. For the three long peat cores, the dating points were selected based on changes in colour, plant composition, and humification features of the peat (Table 1). *Sphagnum* spp., seeds, and above-ground portions of *Carex* spp. were selected as the dating materials. Bulk peat was also used for highly decomposed layers. All dated samples were treated using standard acid-alkali-acid treatments (Olsson, 1986) before they were prepared for synthesized graphite targets with a high vacuum system at Northeast Normal University. AMS ^{14}C measurements were conducted in the NTUAMS laboratory at Taiwan University.

Age-depth models for the three long peat cores were established using the Bacon program (Blaauw and Christen, 2011) with the rbacon package within the R statistical software (Blaauw et al., 2019; R Development Core Team, 2019). The ^{14}C ages of the basal peat samples were calibrated using the Oxcal 4.4 online calibration tool with the IntCal20 curve (Bronk, 2009; Reimer et al., 2020). All calibrated ^{14}C ages used in this study are expressed as calibrated millennium years before present (1 cal. kyr BP=1,000 cal. yr BP).

Based on 23 basal peat ages together with the peat depths of 93 survey points, the peat thickness distribution and pattern of peatland lateral expansion were plotted using the Kriging method in ArcMap 10.3 (Figure 2).

3.3 Dry bulk density, total organic carbon and carbon accumulation rate

Subsamples of undisturbed peat (2 cm^3) from each layer were taken to determine the dry bulk density (DBD) by the dry-weight method. After drying and pulverizing, TOC values were measured using an elemental analyser (EURO VECTOR EA3000). The CAR was calculated using the following formula (Tolonen and Turunen, 1996):

$$\mathrm{CAR} = c \times d \times r / 1000, \quad (1)$$

where c is the content of organic carbon (g C g^{-1} dry weight), d represents the dry bulk density (g cm^{-3}), and r is the rate of peat accumulation (mm yr^{-1}).

3.4 Plant macrofossil analysis

Plant macrofossils were analysed at 2 cm intervals for core BJH3, 3 cm intervals for cores BJH4 and BJH26, and at 1 cm intervals for cores B6, B10, B11, B12, and B22. The semi-quantitative method (Barber et al., 2003) was used for the macrofossil analyses. Fifteen views of each sample under the stereomicroscope (magnification: 10–40×) were first used to calculate the average proportions of five plant components: woody, herbaceous, *Sphagnum* spp., *Polytrichum* spp., and unidentified organic matter (UOM). For *Sphagnum* spp. component, the species or section level were further identified under a light microscope (magnification: 40–200×) and divided into *Sphagnum magellanicum*, *Sphagnum palustre*, *Sphagnum* sect. *Cuspidata*, *Sphagnum* sect. *Acutifolia*, and *Sphagnum* sect. *Subsecunda*. The relative abundance of each component or species was expressed as average volumetric percentages within the total sample.

4. Results

4.1 Basal ages and peatland lateral expansion

The thickness of the peat in the BJH peatland gradually increases from its edge to the centre, ranging from 30 to 300 cm, with an average of approximately 170 cm (Figure 2a). According to basal peat ages, peat formation was initiated at 7.9 cal. kyr BP in the northwest of the BJH peatland. Subsequent lateral expansion occurred from the northwest to the southeast before 4 cal. kyr BP and south-

Table 1 Radiocarbon dating (AMS ^{14}C) results for the three long peat cores (BJH3, BJH4, and BJH26) and the basal peat samples of the Baijianghe peatland

Core	Lab number	Sample ID	Depth (cm)	Material dated	^{14}C age±error (yr BP±yr)	Calibrated age (±2σ, cal. yr BP)	Mean calibrated age (cal. yr BP)
BJH3	NENUR10468	BJH3-1	31	*Sphagnum* spp.	226±58	128–232	180
	NENUR10620	BJH3-2	50	*Sphagnum* spp.	373±64	305–516	411
	NENUR10470	BJH3-3	74	*Carex* spp.	488±58	439–565	502
	NENUR10472	BJH3-4	112	Seed	1,028±60	790–1,061	926
	NENUR10473	BJH3-5	130	*Carex* spp.	1,191±59	961–1,191	1,076
	NENUR10474	BJH3-6	150	Seed	1,321±61	1,171–1,345	1,258
	NENUR10475	BJH3-7	171	Bulk peat	1,857±60	1,690–1,925	1,808
BJH4	NENUR10621	BJH4-1	5	Seed	Modern	−49–−43	−46
	NENUR10622	BJH4-2	14	*Sphagnum* spp.	369±63	304–513	409
	NENUR10457	BJH4-3	26	*Sphagnum* spp.	485±60	433–565	499
	NENUR10458	BJH4-4	50	*Carex* spp.	854±58	675–834	755
	NENUR10459	BJH4-5	66	*Carex* spp.	1,097±58	915–1,151	1,033
	NENUR10460	BJH4-6	90	*Carex* spp.	1,250±61	1,056–1,294	1,175
	NENUR10461	BJH4-7	126	*Sphagnum* spp.	1,710±61	1,510–1,731	1,621
	NENUR10462	BJH4-8	150	*Sphagnum* spp.	1,756±65	1,529–1,820	1,675
	NENUR10464	BJH4-9	200	*Sphagnum* spp.	1,886±64	1,695–1,945	1,820
	NENUR10465	BJH4-10	226	*Sphagnum* spp.	1,930±63	1,712–1,996	1,854
	NENUR10466	BJH4-11	266	Bulk peat	2,898±62	2,865–3,214	3,040
	NENUR10467	BJH4-12	300	Bulk peat	4,383±62	4,842–5,081	4,962
BJH26	NENUR10714	BJH26-1	30	*Sphagnum* spp.	419±68	312–543	428
	NENUR10715	BJH26-2	50	*Carex* spp.	1,207±71	971–1,279	1,125
	NENUR10716	BJH26-3	71	*Carex* spp.	1,731±89	1,411–1,823	1,617
	NENUR10717	BJH26-4	98	*Sphagnum* spp.	2,032±76	1,746–2,154	1,950
	NENUR10718	BJH26-5	130	*Carex* spp.	2,272±73	2,058–2,490	2,274
	NENUR10719	BJH26-6	149	Seed	2,562±82	2,366–2,784	2,575
	NENUR10720	BJH26-7	176	*Carex* spp.	3,607±73	3,701–4,095	3,898
	NENUR10721	BJH26-8	200	Bulk peat	4,576±72	5,037–5,472	5,255
Basal sample	NENUR10662	B1	48	Bulk peat	511±62	459–650	555
	NENUR10663	B2	216	Bulk peat	2,950±77	2,921–3,276	3,099
	NENUR10664	B5	200	*Carex* spp.	7,103±73	7,739–8,038	7,889
	NENUR10665	B6	155	Bulk peat	6,863±69	7,578–7,844	7,711
	NENUR10666	B7	128	Bulk peat	1,750±78	1,510–1,829	1,670
	NENUR10667	B8	220	Bulk peat	4,780±68	5,437–5,604	5,521
	NENUR10668	B9	200	Bulk peat	3,648±66	3,827–4,145	3,991
	NENUR10669	B10	200	*Carex* spp.	3,065±66	3,075–3,402	3,239
	NENUR10670	B11	248	*Carex* spp.	3,851±65	4,084–4,425	4,255
	NENUR10679	B12	230	Bulk peat	2,056±65	1,829–2,155	1,992
	NENUR10680	B13	99	Bulk peat	1,947±63	1,714–2,003	1,859
	NENUR10681	B14	236	*Carex* spp.	4,361±69	4,831–5,082	4,957
	NENUR10671	B15	150	Bulk peat	4,117±84	4,426–4,836	4,631
	NENUR10672	B16	100	Bulk peat	6,093±92	6,740–7,170	6,955
	NENUR10673	B17	150	Bulk peat	3,634±82	3,812–4,157	3,985
	NENUR10674	B18	148	Bulk peat	4,143±89	4,505–4,852	4,679
	NENUR10675	B19	100	*Carex* spp.	4,359±87	4,818–5,300	5,059
	NENUR10676	B20	84	Bulk peat	2,478±84	2,357–2,738	2,548
	NENUR10677	B21	150	Bulk peat	4,103±85	4,423–4,833	4,628
	NENUR10678	B22	116	*Carex* spp.	2,711±81	2,717–3,061	2,889

west to northeast after that (Figure 2b). The expansion rate was low between 7.9 and 5 cal. kyr BP. The peatland increased to 26% of its present area during this period, followed by a rapid lateral expansion between 5 and 4 cal. kyr BP with the area increasing to 60% of the present. Then, its expansion rate subsequently decreased constantly, and the area reached approximately 90% of its present coverage at 2 cal. kyr BP (Figure 2b).

4.2 Age-depth model

The age-depth model of cores BJH3, BJH4, and BJH26 revealed a development history of 1.7, 4.9, and 5 cal. kyr BP, respectively (Figure 3). However, all three long peat cores showed varying peat accumulation rates. The peat accumulation rate of core BJH26 ranged between 0.02 and 0.17 cm yr^{-1} with a mean of 0.05 cm yr^{-1}. Cores BJH3 and BJH4 showed a similar mean peat accumulation rate of 0.1 cm yr^{-1}, although the rates ranged between 0.05 and 0.2 cm yr^{-1} and 0.01 and 0.3 cm yr^{-1}, respectively. Core BJH3 had its lowest peat accumulation rate, 0.06 cm yr^{-1}, between 1.7 and 1.3 cal. kyr BP but a higher rate of 0.11 cm yr^{-1} since 1 cal. kyr BP. Core BJH4 had its lowest peat accumulation rate of 0.02 cm yr^{-1} during the period 4.9 to 3.1 cal. kyr BP, after which the highest peat accumulation rate of 0.22 cm yr^{-1} occurred between 2 and 1.5 cal. kyr BP. Core BJH26 also revealed that its lowest peat accumulation rate, 0.02 cm yr^{-1}, occurred during the period between 5 and 3.1 cal. kyr BP, which was followed by a relatively high rate of 0.05 cm yr^{-1} between 2.8 and 1.1 cal. kyr BP (Figure 4e).

4.3 Carbon accumulation rate

Cores BJH3 and BJH4 showed a range of DBD values from 0.02 to 0.56 g cm^{-3} and 0.03 to 0.44 g cm^{-3}, respectively, and the same mean of 0.13 g cm^{-3}. Core BJH26 had the highest mean DBD of 0.26 g cm^{-3} among the three examined cores, with values varying between 0.02 and 0.64 g cm^{-3} (Figure 4a). It is worth noting that the highest DBD values were from the early period of peat accumulation.

In terms of TOC, core BJH26 had the lowest mean value of 38%, though the TOC ranged from 23% to 48%. In cores BJH3 and BJH4, the TOC ranged from 26% to 53% with a mean of 40% and from 21% to 54% with a mean of 45%, respectively (Figure 4b).

The average CAR of the three long peat cores was highest in core BJH3, which had a mean of 48.4 g C m^{-2} yr^{-1} and a range of 10.9 to 90.1 g C m^{-2} yr^{-1}. Cores BJH26 and BJH4 showed relatively low CARs with mean values of 39.1 g C m^{-2} yr^{-1} and 36.3 g C m^{-2} yr^{-1} and ranges of 4.2 to 82.5 g C m^{-2} yr^{-1} and 10.7 to 189.3 g C m^{-2} yr^{-1}, respectively (Figure 4f). The CAR for core BJH3 peaked during the early period (1.7–1.5 cal. kyr BP) of peat accumulation, after which it declined gradually. The CAR in BJH4 was lower during the period 4.9 to 2 cal. kyr BP, followed by a sharp increase from 2 to 1 cal. kyr BP. The CAR at core BJH26 was steady between 5 and 3 cal. kyr BP, after which the CAR increased until 1 cal. kyr BP, with the lowest values occurring from 1 cal. kyr BP (Figure 4f).

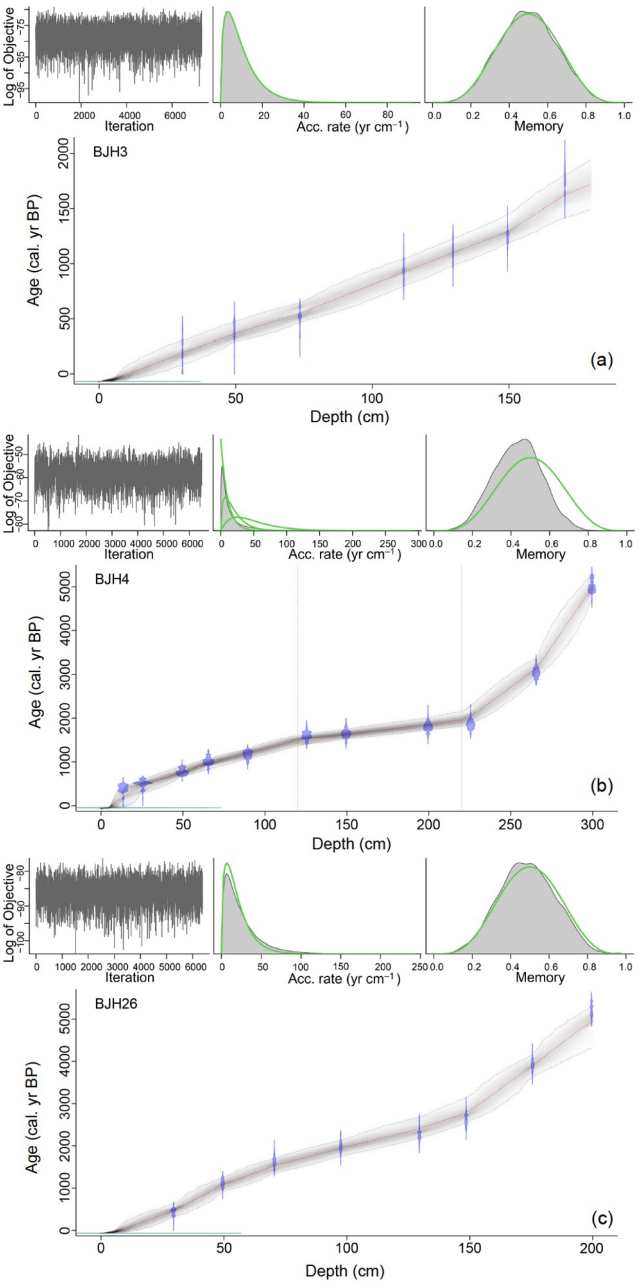

Figure 3 Age-depth models produced by Bacon within the R software package for cores (a) BJH3, (b) BJH4, and (c) BJH26. The blue line indicates the ^{14}C range and the red line is the weighted mean average. Grey shaded areas show the 95% confidence intervals of the estimated age, with darker greys indicating more likely ages.

4.4 Vegetation development

In general, the plant composition varied greatly along the

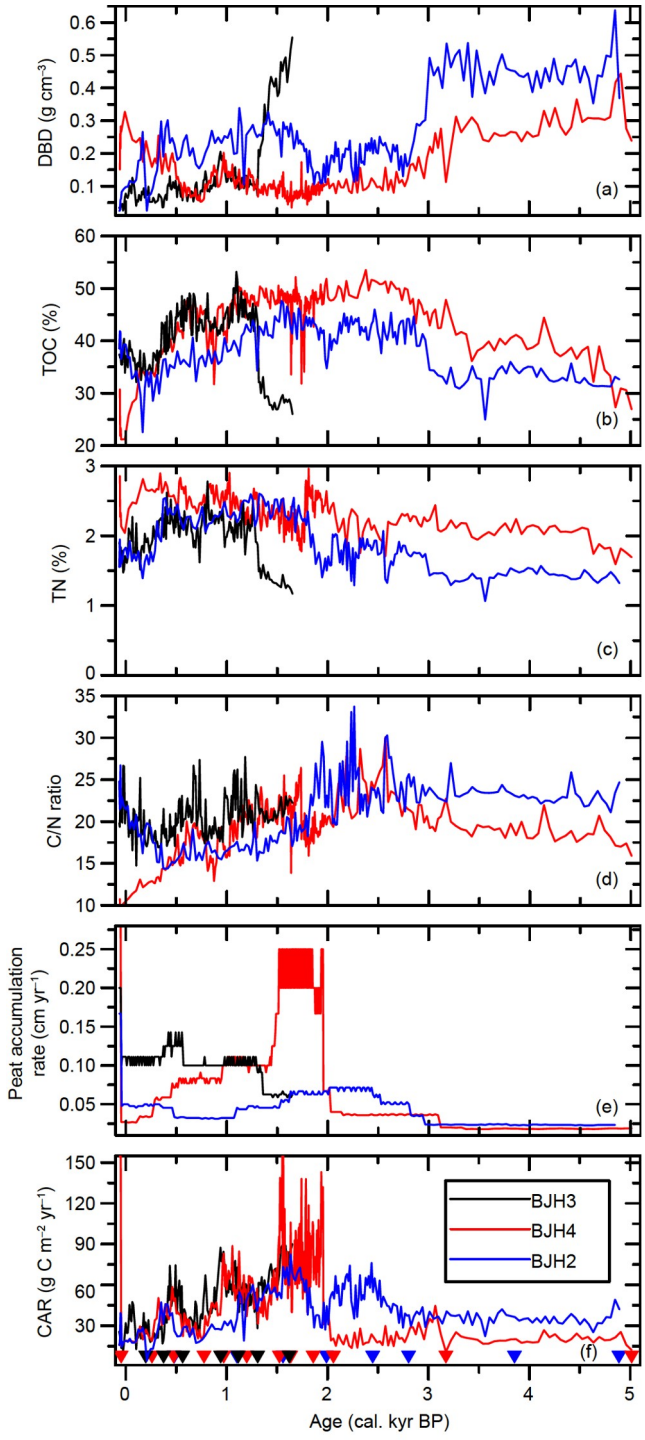

Figure 4 Peat characteristics of cores BJH3, BJH4, and BJH26. (a) Dry bulk density (DBD), (b) total organic carbon content (TOC), (c) total nitrogen (TN), (d) carbon/nitrogen ratio (C/N ratio), (e) peat accumulation rate, and (f) carbon accumulation rate (CAR). The black, red, and blue triangles indicate the AMS ^{14}C dating points of cores BJH3, BJH4 and BJH26, respectively.

three long peat cores (Figure 5, Appendix Figures S4–S6 and Appendix Table S1). Unidentified organic matter (UOM) dominated core BJH3 between 1.7 and 1.3 cal. kyr BP, after which the percentage of herbaceous material increased and dominated the core between 1.3 and 0.3 cal. kyr BP. *Sphagnum* spp. constituted the highest percentage of the remains within core BJH3 over the last 0.3 cal. kyr BP. Core BJH4 was dominated by UOM between 4.9 and 3.7 cal. kyr BP. Woody remains dominated the core between 3.7 and 2.1 cal. kyr BP with relatively high percentages. Between 2.1 and 1.4 cal. kyr BP, the core was dominated by *Sphagnum* spp. and after 1.4 cal. kyr BP, herbaceous material were dominant. Core BJH26 was dominated by UOM and woody remains between 5 and 2.9 cal. kyr BP, after which the percentage of *Sphagnum* spp. and *Polytrichum* spp. increased and dominated the core between 2.4 and 1.8 cal. kyr BP (Figure 5). This was followed by herbaceous material, which was dominant between 1.8 and 0.3 cal. kyr BP.

There were significant negative correlations between the woody content and CAR for cores BJH4 and BJH26 (r=−0.27, p<0.05 and r=−0.34, p<0.05, respectively). A similar but not significant relationship also occurred with core BJH3. There was a significant positive correlation between the *Sphagnum* spp. content and CAR in core BJH4 (r=0.46, p<0.01) (Appendix Table S2), and the highest CAR corresponded with the most abundant *Sphagnum* spp. remains during the period 2.1 to 1.4 cal. kyr BP (Figure 5c and 5d). However, core BJH3 shows a negative correlation between *Sphagnum* spp. content and CAR (r=−0.49, p<0.01) from 1.7 cal. kyr BP, but this negative correlation was not significant in core BJH26 (Figure 5e and 5f) (Appendix Table S2).

5. Discussion

5.1 Paludification or terrestrialization

Peatland generally develops in two different ways: terrestrialization, where a water body is filled with peat and sediments due to autogenic succession or decreasing water level, and paludification, where dryland is converted to peatland due to rising water levels (Chai, 1990; Rydin and Jeglum, 2013). The process of terrestrialization is characterized by systematically younger peat basal ages from the edge to the centre, and paludification is the opposite (Charman, 2002; Lacourse et al., 2019). In the BJH peatland, peat formation was initiated in the northwest of the peatland at 7.9 cal. kyr BP, rather than the most depressed part in the centre (Figure 2). The peat basal ages become younger gradually from the edge to the centre along the northwest–southeast direction between 7.9 and 4 cal. kyr BP. The distribution pattern of basal ages seems to imply that the BJH peatland experienced terrestrialization after initiation. However, field investigations, analysis of the plant composition of the collected bottom peat samples, and analyses of the geochemical properties show characteristics of paludifi-

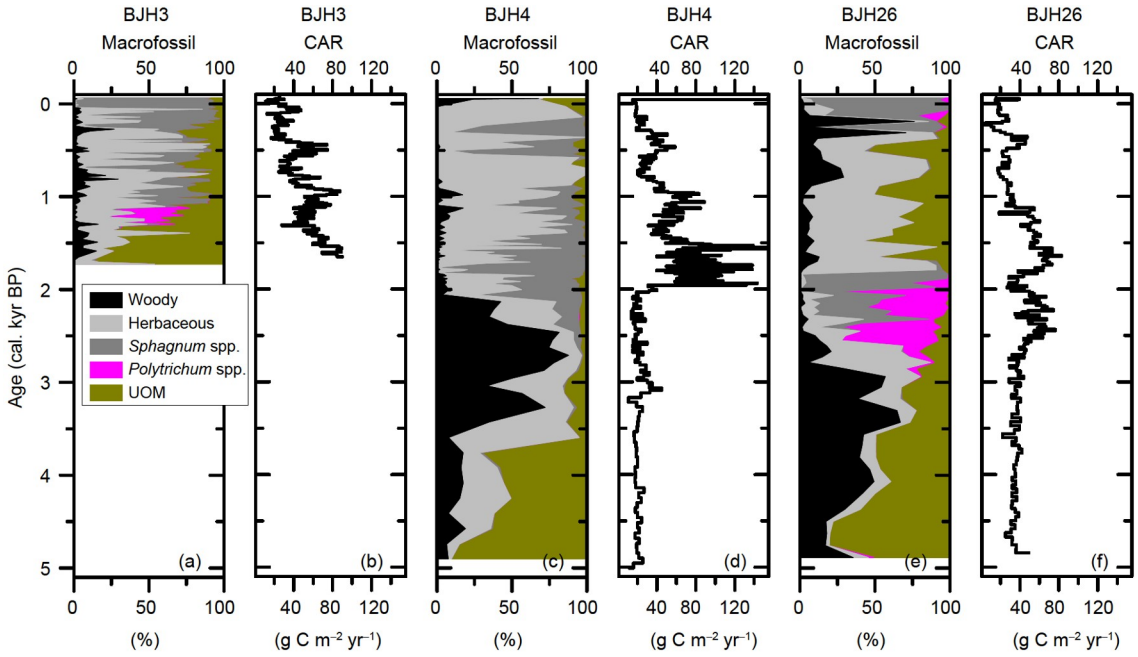

Figure 5 The relationship between plant composition and CAR of the three long peat cores from BJH3 ((a)–(b)), BJH4 ((c)–(d)), and BJH26 ((e)–(f)).

cation. First, woody remains occur at the bottom of peat cores based on visual field inspection and plant macrofossil analyses, which indicates terrestrial conditions, rather than a water body, were prevalent before peat initiation (Appendix Figures S2–S7). Second, the carbon/nitrogen (C/N) ratio is generally above 10 in the three long peat cores and bottom peat samples of each dated core, indicating nonaquatic conditions during peat initiation and expansion in the BJH peatland (Meyers, 1994) (Figure 4d and Appendix Figure S8). Third, palaeoclimate records from the same region showed that the climate was warm and wet between 7.9 and 4 cal. kyr BP (Chu et al., 2014; Stebich et al., 2015; Zheng et al., 2017; Zhang et al., 2020), which is not conducive for terrestrialization but benefits the process of paludification. The slope of the BJH peatland is quite gentle, and the low-lying topography at the centre of the basin may have been connected to the ancient river course (Figures 2a and 6), leading to the basin being less prone to being waterlogged over long periods. Therefore, we believe that the BJH peatland was initiated from forest conditions and then expanded laterally by paludification. The results also demonstrate that determining process of peatland development based only on the basal age distribution may be inadequate. The characteristics of peat deposition, plant composition, and climatic conditions should be fully considered.

5.2 Peatland lateral expansion and the connection to climate and topography

The lateral expansion of peatlands can be driven by autogenic succession, but the speed of the process can increase significantly due to favourable climate and topography. The higher water table induced by the climate and the relatively gentle slope would result in faster lateral expansion (Korhola, 1996; Ruppel et al., 2013). A strong correlation between hydroclimatic variability and peatland development has been reported in other peatland systems of the Changbai Mountains (Zhang et al., 2019a, 2019b). According to the climate record at Sihailongwan Maar Lake, which is 16 km away, there was increased precipitation around the Changbai Mountains between 7.9 and 5 cal. kyr BP (Stebich et al., 2015), but the rate of lateral expansion in the BJH peatland was low during that period (Figure 7a and 7c). This might be because the increased precipitation may have been offset by higher evaporation induced by the high summer insolation and regional temperatures (Figure 7g and 7h) (Laskar et al., 2004; Stebich et al., 2015). Consequently, the effective precipitation, and thus the water table in the BJH peatland, may have been not high enough to facilitate lateral expansion.

The highest rates of lateral expansion in the BJH peatland occurred between 5 and 4 cal. kyr BP, which correspond to the highest precipitation identified in the records for Sihailongwan Maar Lake (Stebich et al., 2015) (Figure 7a and 7c). A study of the Jinchuan peatland, approximately 20 km away, showed almost the same pattern in the timing of the initiation and lateral expansion, with the expansion rate peaking between 5 and 4 cal. kyr BP (Figure 7b) (Zhang et al., 2019a). Many climate records in NE China suggest consistently wetter conditions between 5 and 4 cal. kyr BP (Figure 7d–7f) (Hong et al., 2005; Chen et al., 2014; Chu et al., 2014). The summer insolation and temperature decreased

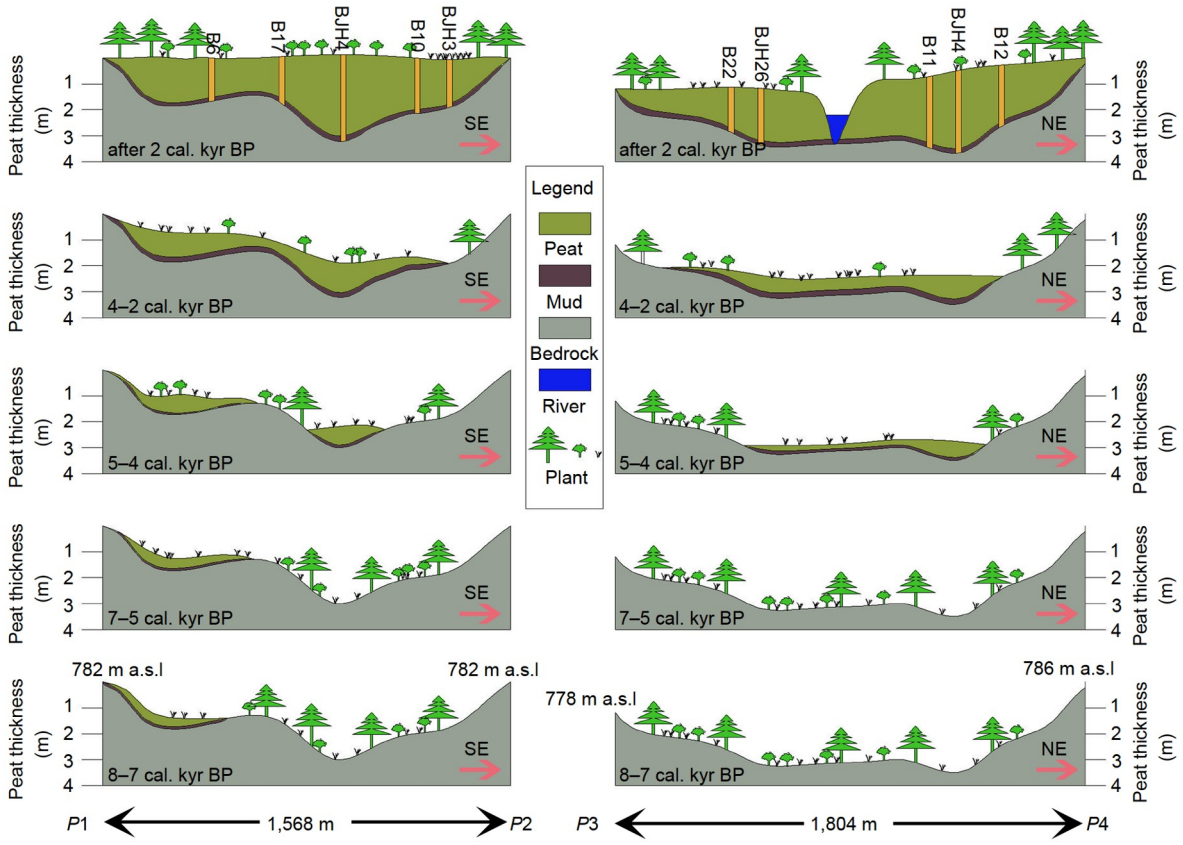

Figure 6 Schematic diagram of the inferred lateral expansion and vertical accumulation of the northwest-southeast (*P*1–*P*2 in Figure 2b) and southwest-northeast (*P*3–*P*4 in Figure 2b) sections crossing the BJH peatland. The inferences are based on the peat depth, basal age, plant composition and topographic map. Note that the time windows considered are uneven.

during this period (Laskar et al., 2004; Stebich et al., 2015), but they were still warmer than in the following 4 cal. kyr BP. The abundant precipitation and lower but still warm temperatures decreased the evaporation and raised the water table in the peatland, which promoted the lateral expansion of the peatland. The lateral expansion slowed down from 4 cal. kyr BP to the present in response to reduced precipitation (Stebich et al., 2015) (Figure 7). Although the decreased summer insolation and regional temperatures could reduce evaporation and result in a higher water table for the peatland, such an effect could be offset by decreasing regional precipitation.

In addition to climate forcing, local topography is another important factor that impacts peatland development (Mäkilä, 1997; Mäkilä and Moisanen, 2007; Loisel et al., 2013). In the BJH peatland, the highest lateral expansion rate was between 5 and 4 cal. kyr BP and mainly occurred in the relatively flat regions from the northeast to the southwest of the peatland, indicating that the flat topography was conducive to lateral expansion (Figures 2 and 6). The steep topography of the northern margin has restricted peatland enlargement in this area after peat initiation. This also limited the expansion and accumulation of peat between core B17 and BJH4 due to surface runoff (Figure 6). Furthermore, the direction of lateral expansion changed from the southwest to the northeast at approximately 4 cal. kyr BP, which was also due to the greater slope in the southwest direction than in the northeast direction (Figure 2).

5.3 CAR and its connection with climate and plant composition

Higher CAR values are expected under warmer and wetter conditions (Charman et al., 2013, 2015; Panait et al., 2017; Bunsen and Loisel, 2020). However, CARs were low in cores BJH4 and BJH26 under warm and wet climatic conditions between 4.9 and 2.1 cal. kyr BP and 5 to 2.9 cal. kyr BP, respectively (Figures 5 and 7) (Laskar et al., 2004; Dykoski et al., 2005; Stebich et al., 2015). Moreover, the highest CARs in cores BJH4 and BJH26 occurred between 2.1 and 1.4 cal. kyr BP and between 1.8 and 1.4 cal. kyr BP, respectively, corresponding to relatively cold and dry conditions. We supposed that the local conditions, such as topography, hydrology, plant composition, and initial conditions may have also played an important role during the process of carbon accumulation in the BJH

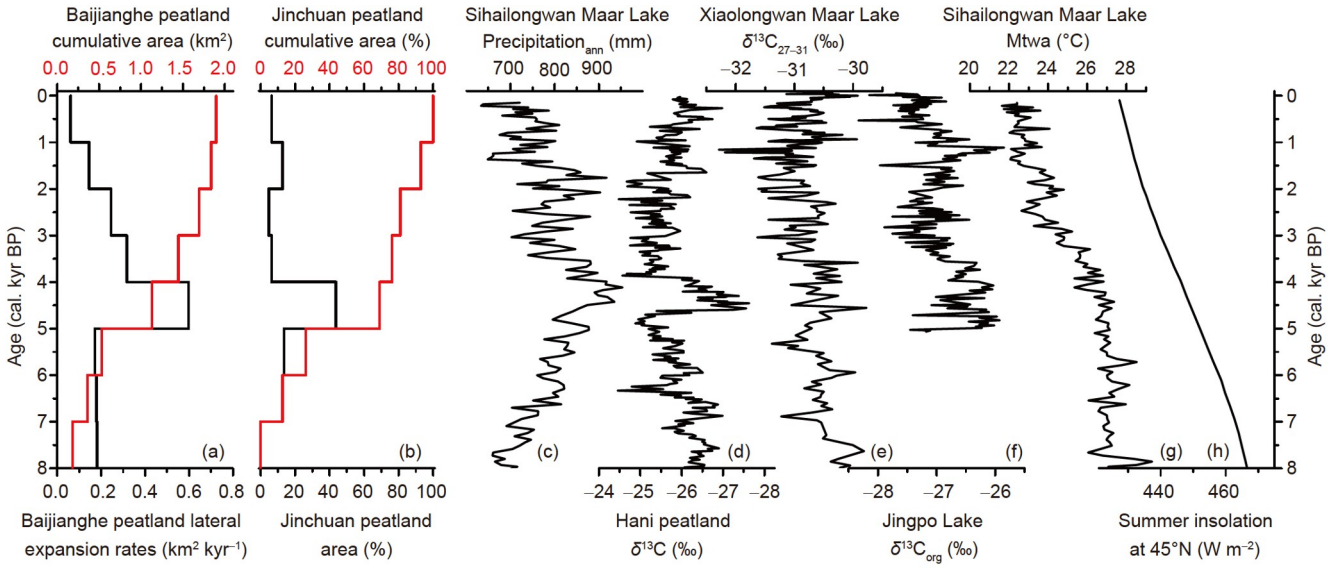

Figure 7 The history of peat lateral expansion in the BJH peatland from 8 cal. kyr BP to the present and its connection with other records. (a) The rates of peat lateral expansion (black solid line) and the accumulative areas (red solid line) in the BJH peatland. (b) The areas (black solid line) and the accumulated areas (red solid line) of peat establishment for the expansion episode at the Jinchuan peatland (Zhang et al., 2019a). (c) Reconstructed mean annual precipitation in Sihailongwan Maar Lake (Stebich et al., 2015). (d) Cellulose $\delta^{13}C$ record from the Hani peatland (Hong et al., 2005). (e) The $\delta^{13}C_{27-31}$ time series from Xiaolongwan Maar Lake (Chu et al., 2014). (f) The $\delta^{13}C_{org}$ record from Jingpo Lake (Chen et al., 2014). (g) The reconstructed mean temperature of the warmest month (July) for Sihailongwan Maar Lake (Stebich et al., 2015). (h) Summer solar insolation at 45°N (Laskar et al., 2004).

peatland.

It has been suggested that peat accumulation appears to have been greatly influenced by local environmental factors such as topography and hydrology, especially during the early-stage succession of peatland development (Holmquist and MacDonald, 2014; Charman et al., 2015). For the BJH peatland, the highest DBD and low TOC values in the early periods of cores BJH4 (4.9 to 2.1 cal. kyr BP) and BJH26 (5 to 2.9 cal. kyr BP) indicate that mineral matter represents a considerable proportion of the peat deposits and that the deposition conditions were unstable while the BJH peatland was undergoing the transition from forest to peatland. The species composition of the BJH peatland did not change significantly under the relatively wet and warm conditions that occurred between 5 and 3 cal. kyr BP (Laskar et al., 2004; Stebich et al., 2015). Woody remains persistently dominate in cores BJH4 and BJH26 during the early periods of peat accumulation, showing low peat accumulation rates and CAR values (Figure 5 and Appendix Table S3). Furthermore, the sedimentary compositions of cores BJH4 and BJH26 might have been influenced by water flow induced by low-lying topography and slope, which were unsuitable for the growth of plants and accumulation of peat (Figure 6). The composition of core BJH26 might even have been influenced by the flood pulse of the river (Figure 2a). Therefore, during the early developmental periods of the BJH peatland, the CAR was mainly affected by initial conditions, species composition, and topography.

In the middle periods of carbon accumulation shown in cores BJH4 (2.1 to 1.5 cal. kyr BP) and BJH26 (2.9 to 1.5 cal. kyr BP), the decreased DBD, increased TOC, and change in plant composition from woody to herbaceous/*Sphagnum* spp. suggest that peat deposition was stable and that the influence of the initial conditions had gradually disappeared. The precipitation and temperature decreased after 3 cal. kyr BP in the Changbai Mountains (Stebich et al., 2015), corresponding to the increased CAR and the altered plant composition in cores BJH4 and BJH26 (Figure 5), indicating that local hydrological conditions and plant composition might be the primary factors influencing CAR during these periods. However, another explanation might be that the lower temperatures restrained peat decomposition and promoted carbon accumulation (Ise et al., 2008; Dorrepaal et al., 2009). The C/N ratio of peat is often used as a proxy for decomposition degree, with lower ratios indicating higher states of peat decomposition (Kuhry and Vitt, 1996). However, the C/N ratio in core BJH4 did not obviously increase between 2.1 and 1.4 cal. kyr BP, and the highest CARs correspond to the decreasing C/N ratio in core BJH26 between 2 and 1.5 cal. kyr BP (Figure 4d). This meant that the effects of decomposition cannot account for the CAR changes during the middle periods of carbon accumulation in the BJH peatland.

It has also been suggested that *Sphagnum* spp. remains decompose slowly in acidic environments (Bragazza and Freeman, 2007), which contributes to the high CAR values in bogs (van Bellen et al., 2011; Panait et al., 2017). However, this is only the case for core BJH4 in our study. Core BJH4 was dominated by hygrophilous *Sphagnum* spp. (mainly *Sphagnum magellanicum* and *Sphagnum Cuspidata*) be-

tween 2.1 and 1.4 cal. kyr BP, indicating that the location of core BJH4 was probably a hollow or lawn and experienced relatively wet conditions during this period. For core BJH26, *Sphagnum* remains are associated with lower CAR values between 2.4 and 1.8 cal. kyr BP. The macrofossils in this interval were dominated by dry moss (*Sphagnum Acutifolia* and *Polytrichum* spp.), indicating that the core location might have once been a hummock with a drier habitat. The correlation between *Sphagnum* spp. and CAR varied among different peat cores due to the influence of microtopography and local hydrology. The CAR values might be higher in wetter locations, such as hollows or lawn and lower in dry locations, such as on hummocks, despite identical climate conditions.

The CAR values decreased over the last 1.5 cal. kyr BP across the BJH peatland despite different plant species identified at each sample site (Figure 8a–8b). This indicates that the influence of plant composition on the CAR during that time was limited, with climatic conditions, therefore, potentially being the primary factor affecting CAR. The simultaneous decreasing CAR over the last 1.5 cal. kyr BP, as shown from the analysis of each core collected from the BJH peatland, corresponds to decreasing summer insolation, seasonality, and regional temperatures across Northeast China (Figure 8c–8f) (Laskar et al., 2004; Chen et al., 2014; Stebich et al., 2015). Moreover, this period provides an opportunity to examine the sensitivity of carbon accumulation in the BJH peatland to climate events such as the Medieval Climate Anomaly (MCA) (1,150 to 800 cal. yr BP) and the LIA (400 to 50 cal. yr BP) (Mann et al., 2009). The CAR values were high during the MCA and low during the LIA (Figure 8). High summer insolation and temperatures during the MCA could extend the length of the growing season and increase the NPP (Nemani et al., 2003; Jones and Yu, 2010; Charman et al., 2015). Meanwhile, high temperatures would also increase the rate of peat decomposition through accelerated microbial activity (Ise et al., 2008; Dorrepaal et al., 2009). However, a database of peat profiles across the high northern latitudes suggests that the NPP variability has a greater role in determining long-term carbon accumulation than decomposition (Charman et al., 2013). This is supported by an analysis of carbon accumulation based on 54 peat cores from NE China, which suggests that the role of decomposition is less important than the effect of NPP in determining long-term carbon accumulation in NE China (Xing et al., 2015b). In addition, high precipitation during the MCA also increased carbon accumulation due to the stimulation of peat growth and the reduction in peat decomposition driven by high water content (Lupascu et al., 2014; Charman et al., 2015). Thus, climatic conditions, especially the interaction between temperature and precipitation, acted as the primary control on the CAR in the BJH peatland over the past 1.5 cal. kyr BP.

Overall, climate, local hydrological conditions, and plant composition have important influences on CAR in the BJH peatland, though the role of the primary factor varied between the different periods. During the early period of carbon accumulation in the peatland, the CAR was mainly affected by initial conditions, plant composition, and topography. In the middle period of carbon accumulation, hydrological conditions and associated plant composition had a greater influence on the CAR, with the CAR being higher in the wet hollows/lawns. During the last 1.5 cal. kyr BP, despite the differences in plant composition among the three locations, the CARs simultaneously decreased, which should be related to unfavourable climatic conditions, such as lower solar insolation and seasonality, lower regional temperature, and/or less precipitation.

5.4 High carbon accumulation rate in the BJH peatland

According to some studies, the long-term rate of carbon accumulation in the northern peatlands averaged between 18.6 and 23 g C m^{-2} yr^{-1} during the Holocene (Yu et al., 2009; Loisel et al., 2014). However, the mean carbon accumulation rates of the three long peat cores in the BJH peatland were 36.3, 39.1 and 48.4 g C m^{-2} yr^{-1}, respectively, higher than rates from the northern peatlands. This may have resulted from the following three reasons. First, the higher solar insolation in mid-latitude areas compared to the northern peatland areas might increase the photosynthetic rate of plants and the NPP (Gallego-Sala et al., 2018). Relatively high CARs values can also be observed in other peatlands in mid-latitude areas, such as the Hengduan Mountains region and the Zoige Plateau in China (34.9 and 33 g C m^{-2} yr^{-1}, respectively) (Liu et al., 2020; Wang et al., 2015), warm temperate peatlands in Pennsylvania (27.3 g C m^{-2} yr^{-1}) (Cai and Yu, 2011), and northeastern North America (28.5–45 g C m^{-2} yr^{-1}) (Charman et al., 2015). Second, the mean annual precipitation and temperatures of the BJH far exceed those of the northern peatlands (Yu et al., 2009). Warm conditions could provide a longer growing season, which plays an important role in producing higher long-term rates of carbon accumulation (Charman et al., 2013). Wet climatic conditions, and thus high water level conditions, could restrict decomposition and promote peat accumulation. Last, the CAR records from the BJH peatland are much shorter than those from the northern peatlands, which may have resulted in less decomposition and higher CAR values (Clymo, 1984).

The CAR in the BJH peatland was also higher than that in the Sanjiang Plain (13.3 g C m^{-2} yr^{-1}) in NE China during the Holocene (Wang et al., 2014). This may have resulted from the peatlands in the Changbai Mountains suffering from less flooding than the Sanjiang Plain, although they are both

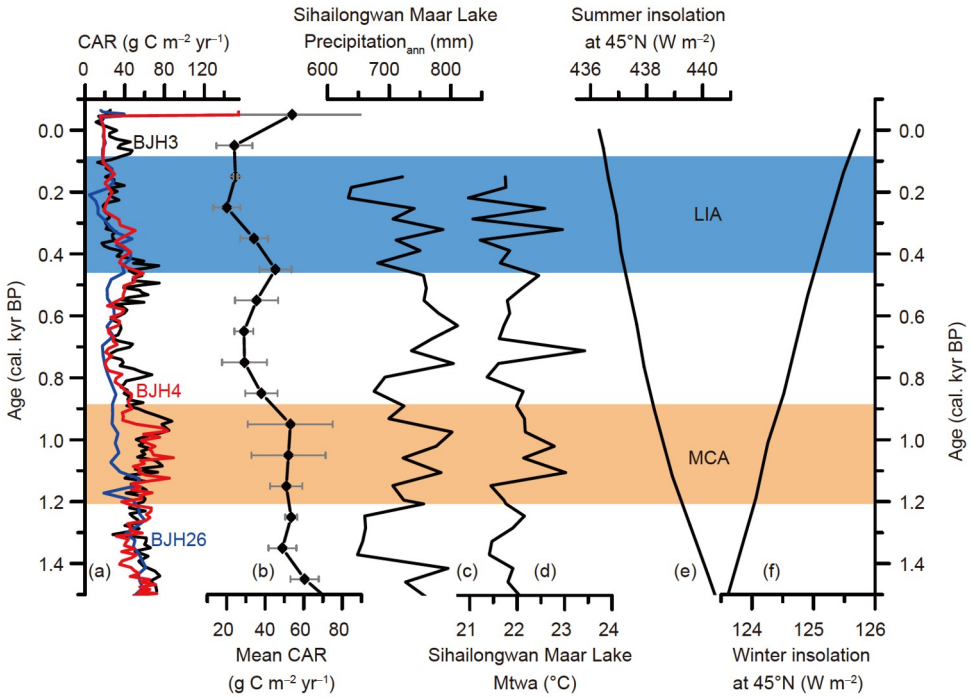

Figure 8 (a) The CAR for cores BJH3 (black solid line), BJH4 (red solid line), and BJH26 (blue solid line) from the BJH peatland for the last 1.5 cal. kyr BP. (b) Mean CAR for the BJH peatland for the last 1.5 cal. kyr BP. (c)–(d) Reconstructed mean annual precipitation and mean temperature of the warmest month (July) for the Sihailongwan Maar Lake (Stebich et al., 2015). (e)–(f) Summer and winter insolation curves at 45°N (Laskar et al., 2004). LIA: Little Ice Age, MCA: Medieval Climate Anomaly. The shaded orange areas indicate warm and wet conditions, while the blue areas indicate cool and dry conditions.

influenced by the EASM (Zhang et al., 2015, 2016; Xing et al., 2015b). Previous work (Xia et al., 2019) dealing with the same peatland presented CAR values for the BJH peatland which showed fluctuations between 26 and 127 g C m^{-2} yr^{-1} over different periods during the last 1.3 cal. kyr BP, which is much higher than those presented in this study. This might be attributed to less decomposition due to relatively late formation, the overestimated peat accumulation rates resulting from inaccuracies in the chronostratigraphic framework, or the anomalous results from a single core analysis.

6. Conclusions

The direction of peatland lateral expansion, plant composition, and peat characteristics indicate that BJH peatland formation initiated at 7.9 cal. kyr BP and laterally expanded through a process of paludification. Climate-related hydrological conditions were identified as the most important factors driving the expansion of this peatland. The warm and wet climate between 5 and 4 cal. kyr BP was favourable for the BJH peatland rapid lateral expansion. Both climatic and local conditions have exerted an important influence on the CAR in the BJH peatland since the middle Holocene, but the primary factors varied among the different periods. The carbon accumulation patterns between 5 and 1.5 cal. kyr BP were probably linked to local conditions, including topography, hydrological conditions, and plant composition, rather than the climatic setting. In particular, the correlation between *Sphagnum* spp. and CAR varied within different peat cores, indicating the complicated influence of plant composition on CAR. However, the consistently decreasing CAR values at all locations within the BJH peatland over the last 1.5 cal. kyr BP suggests primary control by climate factors, such as lower solar insolation and seasonality, lower regional temperatures, and less precipitation. The CAR values obtained from the three long peat cores were 36.3, 39.1 and 48.4 g C m^{-2} yr^{-1} and were higher than those found in the northern peatlands.

Acknowledgements *We are grateful to Dr. Yingyi CHEN from the Northeast Institute of Geography and Agroecology, Chinese Academy of Sciences, for the enthusiastic field support, and to engineer Shasha LIU and Ziping LIU from Northeast Normal University for the laboratory work. This research was supported by the National Key Research and Development Program of China (Grant No. 2016YFC0500407), and the National Natural Science Foundation of China (Grant Nos. 41771217 and 32071599).*

References

Blaauw M, Christen J A, Lopez A M A, Vazquez J E, Gonzalez V O M, Belding T, Theiler J, Gough B, Karney C. 2019. rbacon: Age-Depth Modelling using Bayesian Statistics. https://CRAN.R-project.org/package=rbacon

Blaauw M, Christen J A. 2011. Flexible paleoclimate age-depth models using an autoregressive gamma process. Bayesian Anal, 6: 457–474

Barber K E, Chambers F M, Maddy D. 2003. Holocene palaeoclimates from peat stratigraphy: macrofossil proxy climate records from three oceanic raised bogs in England and Ireland. Quat Sci Rev, 22: 521–539
Bragazza L, Freeman C. 2007. High nitrogen availability reduces polyphenol content in *Sphagnum* peat. Sci Total Environ, 377: 439–443
Bronk R C. 2009. Bayesian analysis of radiocarbon dates. Radiocarbon, 51: 337–360
Bunsen M S, Loisel J. 2020. Carbon storage dynamics in peatlands: Comparing recent- and long-term accumulation histories in southern Patagonia. Glob Change Biol, 26: 5778–5795
Cai C, Hong B, Zhu Y X, Hong Y T, Wang Y, Peng H J. 2013. Holocene peat accumulation rates and influence factors from the Hani peatland, northeast China (in Chinese). Earth Environ, 41: 597–604
Cai S S, Yu Z C. 2011. Response of a warm temperate peatland to Holocene climate change in northeastern Pennsylvania. Quat Res, 75: 531–540
Chai X. 1990. Peat Geology (in Chinese). Beijing: Science Press. 1–116
Charman D. 2002. Peatlands and Environment Change. Chichester: John Wiley & Sons
Charman D J, Amesbury M J, Hinchliffe W, Hughes P D M, Mallon G, Blake W H, Daley T J, Gallego-Sala A V, Mauquoy D. 2015. Drivers of Holocene peatland carbon accumulation across a climate gradient in northeastern North America. Quat Sci Rev, 121: 110–119
Charman D J, Beilman D W, Blaauw M, Booth R K, Brewer S, Chambers F M, Christen J A, Gallego-Sala A, Harrison S P, Hughes P D M, Jackson S T, Korhola A, Mauquoy D, Mitchell F J G, Prentice I C, van der Linden M, De Vleeschouwer F, Yu Z C, Alm J, Bauer I E, Corish Y M C, Garneau M, Hohl V, Huang Y, Karofeld E, Le Roux G, Loisel J, Moschen R, Nichols J E, Nieminen T M, MacDonald G M, Phadtare N R, Rausch N, Sillasoo Ü, Swindles G T, Tuittila E S, Ukonmaanaho L, Väliranta M, van Bellen S, van Geel B, Vitt D H, Zhao Y. 2013. Climate-related changes in peatland carbon accumulation during the last millennium. Biogeosciences, 10: 929–944
Chen R, Shen J, Li C H, Zhang E L, Sun W W, Ji M. 2014. Mid- to late-Holocene East Asian summer monsoon variability recorded in lacustrine sediments from Jingpo Lake, Northeastern China. Holocene, 25: 454–468
Chu G Q, Sun Q, Xie M M, Lin Y, Shang W Y, Zhu Q Z, Shan Y B, Xu D K, Rioual P, Wang L, Liu J Q. 2014. Holocene cyclic climatic variations and the role of the Pacific Ocean as recorded in varved sediments from northeastern China. Quat Sci Rev, 102: 85–95
Clymo R S. 1984. The limits to peat bog growth. Phil Trans R Soc Lond B, 303: 605–654
Dong Y M, Li H K, He H S, Wang S Z. 2021. Holocene peatland development, carbon accumulation and its response to climate forcing and local conditions in Laolike peatland, northeast China. Quat Sci Rev, 268: 107124
Dorrepaal E, Toet S, van Logtestijn R S P, Swart E, van de Weg M J, Callaghan T V, Aerts R. 2009. Carbon respiration from subsurface peat accelerated by climate warming in the subarctic. Nature, 460: 616–619
Dykoski C A, Edwards R L, Cheng H, Yuan D X, Cai Y J, Zhang M L, Lin Y S, Qing J M, An Z S, Revenaugh J. 2005. A high-resolution, absolute-dated Holocene and deglacial Asian monsoon record from Dongge Cave, China. Earth Planet Sci Lett, 233: 71–86
Frolking S, Talbot J, Jones M C, Treat C C, Kauffman J B, Tuittila E S, Roulet N. 2011. Peatlands in the Earth's 21st century climate system. Environ Rev, 19: 371–396
Gallego-Sala A V, Charman D J, Brewer S, Page S E, Prentice I C, Friedlingstein P, Moreton S, Amesbury M J, Beilman D W, Björck S, Blyakharchuk T, Bochicchio C, Booth R K, Bunbury J, Camill P, Carless D, Chimner R A, Clifford M, Cressey E, Courtney-Mustaphi C, De Vleeschouwer F, de Jong R, Fialkiewicz-Koziel B, Finkelstein S A, Garneau M, Githumbi E, Hribjlan J, Holmquist J, Hughes P D M, Jones C, Jones M C, Karofeld E, Klein E S, Kokfelt U, Korhola A, Lacourse T, Le Roux G, Lamentowicz M, Large D, Lavoie M, Loisel J, Mackay H, MacDonald G M, Makila M, Magnan G, Marchant R, Marcisz K, Martínez Cortizas A, Massa C, Mathijssen P, Mauquoy D, Mighall T, Mitchell F J G, Moss P, Nichols J, Oksanen P O, Orme L, Packalen M S, Robinson S, Roland T P, Sanderson N K, Sannel A B K, Silva-Sánchez N, Steinberg N, Swindles G T, Turner T E, Uglow J, Väliranta M, van Bellen S, van der Linden M, van Geel B, Wang G, Yu Z, Zaragoza-Castells J, Zhao Y. 2018. Latitudinal limits to the predicted increase of the peatland carbon sink with warming. Nat Clim Change, 8: 907–913
Holmquist J R, MacDonald G M. 2014. Peatland succession and long-term apparent carbon accumulation in central and northern Ontario, Canada. Holocene, 24: 1075–1089
Hong Y T, Hong B, Lin Q H, Shibata Y, Hirota M, Zhu Y X, Leng X T, Wang Y, Wang H, Yi L. 2005. Inverse phase oscillations between the East Asian and Indian Ocean summer monsoons during the last 12000 years and paleo-El Niño. Earth Planet Sci Lett, 231: 337–346
Ise T, Dunn A L, Wofsy S C, Moorcroft P R. 2008. High sensitivity of peat decomposition to climate change through water-table feedback. Nat Geosci, 1: 763–766
Jones M C, Yu Z C. 2010. Rapid deglacial and early Holocene expansion of peatlands in Alaska. Proc Natl Acad Sci USA, 107: 7347–7352
Korhola A A. 1996. Initiation of a sloping mire complex in southwestern Finland: Autogenic *versus* allogenic controls. Écoscience, 3: 216–222
Kuhry P, Vitt D H. 1996. Fossil carbon/nitrogen ratios as a measure of peat decomposition. Ecology, 77: 271–275
Lacourse T, Adeleye M A, Stewart J R. 2019. Peatland formation, succession and carbon accumulation at a mid-elevation poor fen in Pacific Canada. Holocene, 29: 1694–1707
Lacourse T, Davies M A. 2015. A multi-proxy peat study of Holocene vegetation history, bog development, and carbon accumulation on northern Vancouver Island, Pacific coast of Canada. Holocene, 25: 1165–1178
Laskar J, Robutel P, Joutel F, Gastineau M, Correia A C M, Levrard B. 2004. A long-term numerical solution for the insolation quantities of the Earth. Astron Astrophys, 428: 261–285
Liu L J, Chen H, Yu Z C, Zhu D, He Y X, Liu J L, Zhu Q A, Liu X W, Liu L F. 2020. Peatland development and carbon dynamics since the Last Glacial Maximum in the Hengduan Mountains Region. Catena, 190: 104525
Loisel J, van Bellen S, Pelletier L, Talbot J, Hugelius G, Karran D, Yu Z, Nichols J, Holmquist J. 2017. Insights and issues with estimating northern peatland carbon stocks and fluxes since the last glacial maximum. Earth-Sci Rev, 165: 59–80
Loisel J, Gallego-Sala A V, Amesbury M J, Magnan G, Anshari G, Beilman D W, Benavides J C, Blewett J, Camill P, Charman D J, Chawchai S, Hedgpeth A, Kleinen T, Korhola A, Large D, Mansilla C A, Müller J, van Bellen S, West J B, Yu Z, Bubier J L, Garneau M, Moore T, Sannel A B K, Page S, Väliranta M, Bechtold M, Brovkin V, Cole L E S, Chanton J P, Christensen T R, Davies M A, De Vleeschouwer F, Finkelstein S A, Frolking S, Gałka M, Gandois L, Girkin N, Harris L I, Heinemeyer A, Hoyt A M, Jones M C, Joos F, Juutinen S, Kaiser K, Lacourse T, Lamentowicz M, Larmola T, Leifeld J, Lohila A, Milner A M, Minkkinen K, Moss P, Naafs B D A, Nichols J, O'Donnell J, Payne R, Philben M, Piilo S, Quillet A, Ratnayake A S, Roland T P, Sjögersten S, Sonnentag O, Swindles G T, Swinnen W, Talbot J, Treat C, Valach A C, Wu J. 2021. Expert assessment of future vulnerability of the global peatland carbon sink. Nat Clim Chang, 11: 70–77
Loisel J, Yu Z, Beilman D W, Camill P, Alm J, Amesbury M J, Anderson D, Andersson S, Bochicchio C, Barber K, Belyea L R, Bunbury J, Chambers F M, Charman D J, De Vleeschouwer F, Fiałkiewicz-Kozieł B, Finkelstein S A, Gałka M, Garneau M, Hammarlund D, Hinchcliffe W, Holmquist J, Hughes P, Jones M C, Klein E S, Kokfelt U, Korhola

A, Kuhry P, Lamarre A, Lamentowicz M, Large D, Lavoie M, MacDonald G, Magnan G, Mäkilä M, Mallon G, Mathijssen P, Mauquoy D, McCarroll J, Moore T R, Nichols J, O'Reilly B, Oksanen P, Packalen M, Peteet D, Richard P J, Robinson S, Ronkainen T, Rundgren M, Sannel A B K, Tarnocai C, Thom T, Tuittila E S, Turetsky M, Väliranta M, van der Linden M, van Geel B, van Bellen S, Vitt D, Zhao Y, Zhou W. 2014. A database and synthesis of northern peatland soil properties and Holocene carbon and nitrogen accumulation. Holocene, 24: 1028–1042

Loisel J, Yu Z, Parsekian A, Nolan J, Slater L. 2013. Quantifying landscape morphology influence on peatland lateral expansion using ground-penetrating radar (GPR) and peat core analysis. J Geophys Res-Biogeosci, 118: 373–384

Loisel J, Yu Z C. 2013. Holocene peatland carbon dynamics in Patagonia. Quat Sci Rev, 69: 125–141

Lupascu M, Welker J M, Seibt U, Maseyk K, Xu X, Czimczik C I. 2014. High Arctic wetting reduces permafrost carbon feedbacks to climate warming. Nat Clim Change, 4: 51–55

Mäkilä M. 1997. Holocene lateral expansion, peat growth and carbon accumulation on Haukkasuo, a raised bog in southeastern Finland. Boreas, 26: 1–14

Mäkilä M, Moisanen M. 2007. Holocene lateral expansion and carbon accumulation of Luovuoma, a northern fen in finnish Lapland. Boreas, 36: 198–210

Mann M E, Zhang Z H, Rutherford S, Bradley R S, Hughes M K, Shindell D, Ammann C, Faluvegi G, Ni F. 2009. Global signatures and dynamical origins of the Little Ice Age and medieval climate anomaly. Science, 326: 1256–1260

Mathijssen P J H, Gałka M, Borken W, Knorr K H. 2019. Plant communities control long term carbon accumulation and biogeochemical gradients in a patagonian bog. Sci Total Environ, 684: 670–681

Mathijssen P J H, Väliranta M, Korrensalo A, Alekseychik P, Vesala T, Rinne J, Tuittila E S. 2016. Reconstruction of Holocene carbon dynamics in a large boreal peatland complex, southern Finland. Quat Sci Rev, 142: 1–15

Meyers P A. 1994. Preservation of elemental and isotopic source identification of sedimentary organic matter. Chem Geol, 114: 289–302

Nemani R R, Keeling C D, Hashimoto H, Jolly W M, Piper S C, Tucker C J, Myneni R B, Running S W. 2003. Climate-driven increases in global terrestrial net primary production from 1982 to 1999. Science, 300: 1560–1563

Niu Z G, Zhang H Y, Wang X W, Yao W B, Zhou D M, Zhao K Y, Zhao H, Li N N, Huang H B, Li C C, Yang J, Liu C X, Liu S, Wang L, Li Z, Yang Z Z, Qiao F, Zheng Y M, Chen Y L, Sheng Y W, Gao X H, Zhu W H, Wang W Q, Wang H, Weng Y L, Zhuang D F, Liu J Y, Luo Z C, Cheng X, Guo Z Q, Gong P. 2012. Mapping wetland changes in China between 1978 and 2008. Chin Sci Bull, 57: 2813–2823

Olsson I. 1986. Radiometric methods. In: Berglund B, ed. Handbook of Holocene Palaeoecolgy and Palaeohydrology. Chichester: John Wiley and Sons. 273–312

Panait A, Diaconu A, Galka M, Grindean R, Hutchinson S M, Hickler T, Lamentowicz M, Mulch A, Tanţău I, Werner C, Feurdean A. 2017. Hydrological conditions and carbon accumulation rates reconstructed from a mountain raised bog in the carpathians: A multi-proxy approach. Catena, 152: 57–68

R Development Core Team. 2019. R: A language and environment for statistical computing. https://www.r-project.org

Reimer P J, Austin W E N, Bard E, Bayliss A, Blackwell P G, Bronk Ramsey C, Butzin M, Cheng H, Edwards R L, Friedrich M, Grootes P M, Guilderson T P, Hajdas I, Heaton T J, Hogg A G, Hughen K A, Kromer B, Manning S W, Muscheler R, Palmer J G, Pearson C, van der Plicht J, Reimer R W, Richards D A, Scott E M, Southon J R, Turney C S M, Wacker L, Adolphi F, Büntgen U, Capano M, Fahrni S M, Fogtmann-Schulz A, Friedrich R, Köhler P, Kudsk S, Miyake F, Olsen J, Reinig F, Sakamoto M, Sookdeo A, Talamo S. 2020. The IntCal20 Northern Hemisphere radiocarbon age calibration curve (0–55 cal kBP). Radiocarbon, 62: 725–757

Ruppel M, Väliranta M, Virtanen T, Korhola A. 2013. Postglacial spatio-temporal peatland initiation and lateral expansion dynamics in North America and northern Europe. Holocene, 23: 1596–1606

Rydin H, Jeglum J K. 2013. The Biology of Peatlands. 2nd ed. Oxford: Oxford University Press

Stebich M, Rehfeld K, Schlütz F, Tarasov P E, Liu J, Mingram J. 2015. Holocene vegetation and climate dynamics of NE China based on the pollen record from Sihailongwan Maar lake. Quat Sci Rev, 124: 275–289

Sun J J, Li H C, Wang J, Zhao H Y, Wang S Z, Li H K, Yang Q N, Chou C Y, Kashyap S. 2019. Study of Jinchuan Mire in NE China II: Peatland development, carbon accumulation and climate change during the past 1000 years. Quat Int, 528: 18–29

Tolonen K, Turunen J. 1996. Accumulation rates of carbon in mires in Finland and implications for climate change. Holocene, 6: 171–178

Treat C C, Jones M C, Camill P, Gallego-Sala A, Garneau M, Harden J W, Hugelius G, Klein E S, Kokfelt U, Kuhry P, Loisel J, Mathijssen P J H, O'Donnell J A, Oksanen P O, Ronkainen T M, Sannel A B K, Talbot J, Tarnocai C, Väliranta M. 2016. Effects of permafrost aggradation on peat properties as determined from a pan-Arctic synthesis of plant macrofossils. J Geophys Res-Biogeosci, 121: 78–94

van Bellen S, Dallaire P L, Garneau M, Bergeron Y. 2011. Quantifying spatial and temporal Holocene carbon accumulation in ombrotrophic peatlands of the Eastmain region, Quebec, Canada. Glob Biogeochem Cycle, 25: GB2016

Wang B, LinHo B. 2002. Rainy season of the Asian-Pacific summer monsoon. J Clim, 15: 386–398

Wang M, Chen H, Wu N, Peng C H, Zhu Q A, Zhu D, Yang G, Wu J H, He Y X, Gao Y H, Tian J Q, Zhao X Q. 2014. Carbon dynamics of peatlands in China during the Holocene. Quat Sci Rev, 99: 34–41

Wang M, Yang G, Gao Y H, Chen H, Wu N, Peng C H, Zhu Q, Zhu D, Wu J H, He Y X, Tian J Q, Zhao X Q, Zhang Y. 2015. Higher recent peat C accumulation than that during the holocene on the zoige plateau. Quat Sci Rev, 114: 116–125

Xia Y Y, Li H C, Zhao H Y, Wang S Z, Li H K, Yan H. 2019. Peatland development and environmental change during the past 1600 years in Baijianghe Mire of Changbai Mountains, China. Quat Int, 528: 41–52

Xing W, Bao K, Gallego-Sala A V, Charman D J, Zhang Z, Gao C, Lu X, Wang G. 2015a. Climate controls on carbon accumulation in peatlands of Northeast China. Quat Sci Rev, 115: 78–88

Xing W, Bao K, Guo W, Lu X, Wang G. 2015b. Peatland initiation and carbon dynamics in northeast china: links to holocene climate variability. Boreas, 44: 575–587

Xu J, Morris P J, Liu J, Holden J. 2018. PEATMAP: Refining estimates of global peatland distribution based on a meta-analysis. Catena, 160: 134–140

Yu Z. 2006. Holocene carbon accumulation of fen peatlands in boreal western Canada: A complex ecosystem response to climate variation and disturbance. Ecosystems, 9: 1278–1288

Yu Z C, Beilman D W, Jones M C. 2009. Sensitivity of Northern Peatland Carbon Dynamics to Holocene Climate Change. In: Baird A, Belyea L, Comas X, Reeve A, Slater L, eds. Carbon Cycling in Northern Peatlands. Geophys Monog Ser, 184: 55–69

Yu Z, Joos F, Bauska T K, Stocker B D, Fischer H, Loisel J, Brovkin V, Hugelius G, Nehrbass-Ahles C, Kleinen T, Schmitt J. 2021. No support for carbon storage of >1,000 GtC in northern peatlands. Nat Geosci, 14: 465–467

Yu Z C, Vitt D H, Wieder R K. 2014. Continental fens in western Canada as effective carbon sinks during the Holocene. Holocene, 24: 1090–1104

Yu Z C. 2011. Holocene carbon flux histories of the world's peatlands. Holocene, 21: 761–774

Zhang M M, Bu Z J, Jiang M, Wang S Z, Liu S S, Jin Q, Shi P H. 2019a. Mid-late Holocene maar lake-mire transition in northeast China triggered by hydroclimatic variability. Quat Sci Rev, 220: 215–229

Zhang M M, Bu Z J, Jiang M, Wang S Z, Liu S S, Chen X, Hao J N, Liao W Y. 2019b. The development of Hani peatland in the Changbai mountains (NE China) and its response to the variations of the East Asian summer monsoon. Sci Total Environ, 692: 818–832

Zhang M M, Bu Z J, Wang S Z, Jiang M. 2020. Moisture changes in Northeast China since the last deglaciation: Spatiotemporal out-of-phase patterns and possible forcing mechanisms. Earth-Sci Rev, 201: 102984

Zhang Z Q, Wang G P, Liu X H, Jia H J. 2016. Holocene controls on wetland carbon accumulation in the Sanjiang Plain, China. J Paleolimnol, 56: 267–274

Zhang Z Q, Xing W, Wang G P, Tong S Z, Lv X G, Sun J M. 2015. The peatlands developing history in the Sanjiang Plain, NE China and its response to East Asian monsoon variation. Sci Rep, 5: 11316

Zhao Y, Yu Z C, Tang Y, Li H, Yang B, Li F R, Zhao W W, Sun J H, Chen J H, Li Q, Zhou A F. 2014. Peatland initiation and carbon accumulation in China over the last 50,000 years. Earth-Sci Rev, 128: 139–146

Zheng Y H, Pancost R D, Liu X D, Wang Z Z, Naafs B D A, Xie X J, Liu Z, Yu X F, Yang H. 2017. Atmospheric connections with the North Atlantic enhanced the deglacial warming in northeast China. Geology, 45: 1031–1034

(Responsible editor: Shilong PIAO)

Catena 216 (2022) 106412

Contents lists available at ScienceDirect

Catena

journal homepage: www.elsevier.com/locate/catena

Plant assemblages-based quantitative reconstruction of past mire surface wetness: A case study in the Changbai Mountains region, Northeast China

Qiannan Yang [a,b,1], Hongkai Li [a,b,c,1], Hongyan Zhao [a,b,c,*], Frank M. Chambers [d], Zhaojun Bu [a,b,c], Edith Bai [a,b,c], Guangyuan Xu [a,b,c]

[a] Key Laboratory of Geographical Processes and Ecological Security in Changbai Mountains, Ministry of Education, School of Geographical Science, Northeast Normal University, Changchun 130024, Jilin, China
[b] Institute for Peat & Mire Research, Northeast Normal University, Changchun 130024, Jilin, China
[c] State Environmental Protection Key Laboratory of Wetland Ecology and Vegetation Restoration, Northeast Normal University, Changchun 130024, Jilin, China
[d] Centre for Environmental Change and Quaternary Research, School of Natural and Social Sciences, University of Gloucestershire, Cheltenham GL50 4AZ, Gloucestershire, UK

ARTICLE INFO

Keywords:
Mire surface wetness
Transfer function
Plant macrofossils
Northeast China
Hydroclimate

ABSTRACT

Quantitative relationships between mire plant assemblages and environmental variables have been investigated widely in Europe and North America, but hitherto insufficiently addressed in the East Asian monsoon region. In this study, the plant assemblages of 274 plots along hydrological gradients in five peatlands from the Changbai Mountains region, Northeast China were investigated during the growing seasons (from May to October) from 2014 to 2016. Seven environmental variables of surface water including depth to water table (DWT), pH, electrical conductivity (EC), total nitrogen (TN), total phosphorus (TP), calcium (Ca) and magnesium (Mg) were measured. Canonical correspondence analysis (CCA) indicated that DWT was the principal environmental variable determining the plant assemblages. A transfer function for inferring DWT based on plant assemblages was developed and refined using four models. The transfer function was shown to have strong predictive power following thorough statistical and ecological tests. When the plant assemblages-based transfer function was applied to a 41 cm peat sequence from Laobaishan bog in the Changbai Mountains region, the reconstructed DWTs were essentially consistent, in the trend and vital details of mire surface wetness, with those inferred from a testate amoebae-transfer function, which has been verified to be robust for reconstructing water table in peatlands in the same region. This study suggests that the mire plant assemblages-based transfer function has great potential for quantitative reconstruction of past mire surface wetness, and allows for further research into palaeoclimatology, palaeohydrology and palaeoecology in the East Asian monsoon region using multi-proxy methods.

1. Introduction

Quantitative reconstruction of palaeoclimate and environmental change has been a priority in palaeoclimatological and palaeoecological research (Turner et al., 2013; Seddon et al., 2014). A practical tool for quantitative reconstruction of past climate and environmental variability is the transfer function (Väliranta et al., 2007; Ghosh et al., 2017). Transfer functions model empirical relationships between contemporary taxa and environmental variables (Wen et al., 2013; Krashevska et al., 2020). Based on uniformitarian principles of the relationships, the developed transfer functions are applied to reconstruct past climate and environment variability quantitatively from palaeoecological taxa (Amesbury et al., 2013; Swindles et al., 2015a) and even predict the trends of taxa shifts in the context of global warming (Mitchell et al., 2008; Tierney et al., 2020). Thus, transfer functions have been viewed to revolutionize palaeoecology (Payne et al., 2012). More advanced statistical techniques have been applied to evaluate the predictive power of transfer functions in extended geographical regions since the first transfer model was developed (Telford and Birks, 2009; Swindles et al., 2015b; Kurina and Li, 2019). Transfer functions are now

* Corresponding author at: Key Laboratory of Geographical Processes and Ecological Security in Changbai Mountains, Ministry of Education, School of Geographical Science, Northeast Normal University, Changchun 130024, Jilin, China.
E-mail address: hyzhao@nenu.edu.cn (H. Zhao).
[1] This author contributed equally to this work.

https://doi.org/10.1016/j.catena.2022.106412
Received 13 December 2021; Received in revised form 2 May 2022; Accepted 24 May 2022
Available online 31 May 2022
0341-8162/© 2022 Elsevier B.V. All rights reserved.

commonly applied to quantitative reconstruction of past environment and climate changes from different proxies in various archives, especially from fossil data of plants, such as pollen (Cao et al., 2014; Ghosh et al., 2017), phytoliths (Lu et al., 2006) and plant macrofossils (Väliranta et al., 2007).

Peatlands are unique and valuable ecosystems owing to their various functions such as storage of carbon, regulation of catchment hydrology, and archives of environmental change (Dise, 2009; Yu et al., 2010). Peatlands hold the equivalent of half the atmospheric carbon and approximately one-tenth global freshwater although they only cover about 3% of the Earth's land area (Dise, 2009; Xu et al., 2018). The carbon stored in peatlands originated predominantly from incompletely decomposed mire plants, which accumulate sequentially in situ. Thus, peatlands record a wealth of information pertaining to the development of the mire plant assemblages and environmental changes over time, and have become an important archive used to record past and contemporary environmental changes (Chambers and Charman, 2004; Hédl et al., 2017; Kapfer et al., 2017; Zhang et al., 2020). The vegetation succession of peatlands depends on individual mire plant responses to changes in regional and local conditions (Rydin and Jeglum, 2013). Different types of mire plants grow in different habitats according to variations in wetness, acidity and nutrition (Laine et al., 2018). The plant assemblages may be regulated by climate changes and anthropogenic land-use transformation (Mitchell et al., 2013). These indications of mire plant habitats are recorded by means of plant remains, especially plant macrofossils (> 125 μm) in peatlands. If plant macrofossils are found in a peat sequence, it is probable that their parent plants were growing in situ or very close by (Birks, 2007). In peat sequences, plant macrofossils, which often can be identified to species level, provide precise data on historical vegetation dynamics at a relatively high taxonomic resolution (Mauquoy and Barber, 2002; Väliranta et al., 2012; Mitchell et al. 2013; Piilo et al., 2020).

Researchers have demonstrated the close ecological coupling relationship between plant macrofossils and hydrological factors, for example surface wetness described by depth to water table (DWT), although acidity (pH) and trophic status of peatlands also influence growth of mire plants (Väliranta et al., 2007; Rydin and Jeglum, 2013; Castro et al., 2015). Mire surface wetness had been reconstructed using plant macrofossils in peatlands using qualitative (Barber, 1981) and semi-quantitative technique (Barber, 1994) before the 20th century. Later, several transfer functions between mire plant assemblages and surface wetness were generated and applied to reconstruct past surface wetness quantitatively using a modern calibration dataset mostly in Europe (Väliranta et al., 2007; Birks and van Dinter, 2010; Väliranta et al., 2012; Mitchell et al., 2013) and North America (Thompson et al., 2008). These transfer function models of local or regional scales have provided robust quantitative reconstruction of palaeoenvironment and palaeoclimate based on a sound ecological basis, for example the relationship between living plants and DWT (Väliranta et al., 2012). Nevertheless, different plant species from the same genus might grow in different geographical regions and respond to different environmental variables or have different optima for the same environmental variable, for example DWT (Mauquoy and van Geel, 2010; Yang et al., 2019). The reconstructed environmental variable may have a large deviation when regional-scale plant species not included in their training set are applied (Turner et al., 2013). Hence, the plant-based transfer functions need to be developed and strengthened to be applied at local and regional scales outside of Europe and North America. Furthermore, the performance of transfer functions should be thoroughly tested with statistical and ecological methods before application to fossil data. The need to estimate quantitatively past hydrological and climatic conditions from plant macrofossils with higher precision is becoming increasingly important. In this paper, we aim to (1) investigate whether DWT is the principal environmental variable determining coverage of mire plants in the Changbai Mountains region, Northeast China; (2) develop a transfer function between modern mire plant assemblages and the principal environmental variable; and (3) assess the potential application of a plant-based transfer function in the context of climatic change.

2. Regional setting and study sites

Changbai Mountains in Northeast China are located at the southern edge of temperate peatlands (Fig. 1). Climate in this region is primarily controlled by the East Asian monsoon. Mean annual temperature ranges from 2 to 6 °C. Mean monthly temperature ranges from −20 to −15 °C in January, and from 17 to 24 °C in July, respectively. Mean annual precipitation decreases from 900 to 700 mm from southeast to northwest. More than 60% of precipitation occurs in the growing season (from May to October). With the joint influence of the East Asian monsoon, frozen and volcanic activities, peatlands have developed widely since the Last Glacial Maximum in various landforms, varying from lava platforms, crater lakes to alpine valleys (Xing et al., 2015). The Changbai Mountains region has become one of the key regions for the reconstruction of peat-based palaeoclimate and palaeoenvironment since the Last Glacial Maximum (Hong et al., 2009; Zhou et al., 2010; Zhang et al., 2019, 2020).

Five peatlands, namely Hani (HN), Hanlongwan (HLW), Jinchuan (JC), Xinglong (XL) and Dongfanghong (DFH) in the Changbai Mountains region, were selected for this research. They represent a range of trophic status in peatlands from different latitudes, longitudes and altitudes in the Changbai Mountains region (Fig. 1, Table 1). HN mire is in a meso- to oligotrophic condition with differentiated vegetation zones from the margin to the centre of the mire (Schröder et al., 2007). The forest dominated by *Larix olgensis* at the margin becomes thinner with increasing distance from the mire edge, when shrubs including *Betula ovalifolia*, *Vaccinium uliginosum* and *Ledum palustre* take over. This latter zone is followed by species-rich sedge reeds that again merge into *L. olgensis* forest. The stands close to the river are dominated by *Cornus alba*-shrub or open sedge reed with high tussocks. HLW mire originated from a small marr lake with a diameter of about 500 m. Now the mire surface is occupied by *Carex lasiocarpa, C. limosa, Phragmites australis* and *Sphagnum amblyphyllum*. JC mire and XL mire are open rich fen with various plants species. The dominant plant communities are *B. ovalifolia–C. schmidtii–S. subsecundum*, *C. limosa* and *P. australis–C. pseudocuraica* from the edge of mire to the centre (Ma et al., 2020). DFH mire is in a mesotrophic–oligotrophic state. The vegetation is dominated by *L. olgensis*, *V. uliginosum*, *Eriophorum polystachion, C. schmidtii*, *S. magellanicum*, *S. fuscum* and *S. angustifolium*, but is also rich in vascular plants, such as *B. ovalifolia*, *L. palustre*, and *P. australis*. (Liu et al., 2020).

3. Materials and methods

3.1. Investigation of plant assemblages and determination of environmental variables

The investigation plots were selected along hydrological gradients in the above-mentioned five peatlands (HN, JC, HLW, XL and DFH) to ensure dominant mire plant species occur in at least three plots (Fig. 1). The longitude, latitude and altitude of the plot were recorded using a GPS. Investigation of extant plant assemblages was conducted in July or August once every year from 2014 to 2016. An area of 4 m × 4 m quadrats was investigated for woody plants, with 1 m × 1 m quadrat for herbaceous plants and 50 cm × 50 cm quadrats for mosses. The average coverage and height of each plant species in a quadrat and habitat types of each quadrat (hummocks, lawns and hollows) were mainly recorded in situ. More precise species identification was conducted in the laboratory under a stereomicroscope in detail if the plant species was not identified on site. DWT was measured in each quadrat by inserting a 3 cm-diameter plastic tube (with holes at different depths) and then a dry rod was inserted into the tube after 30 min to record the depth. Electrical conductivity (EC) and pH of mire surface water (0–10 cm) were

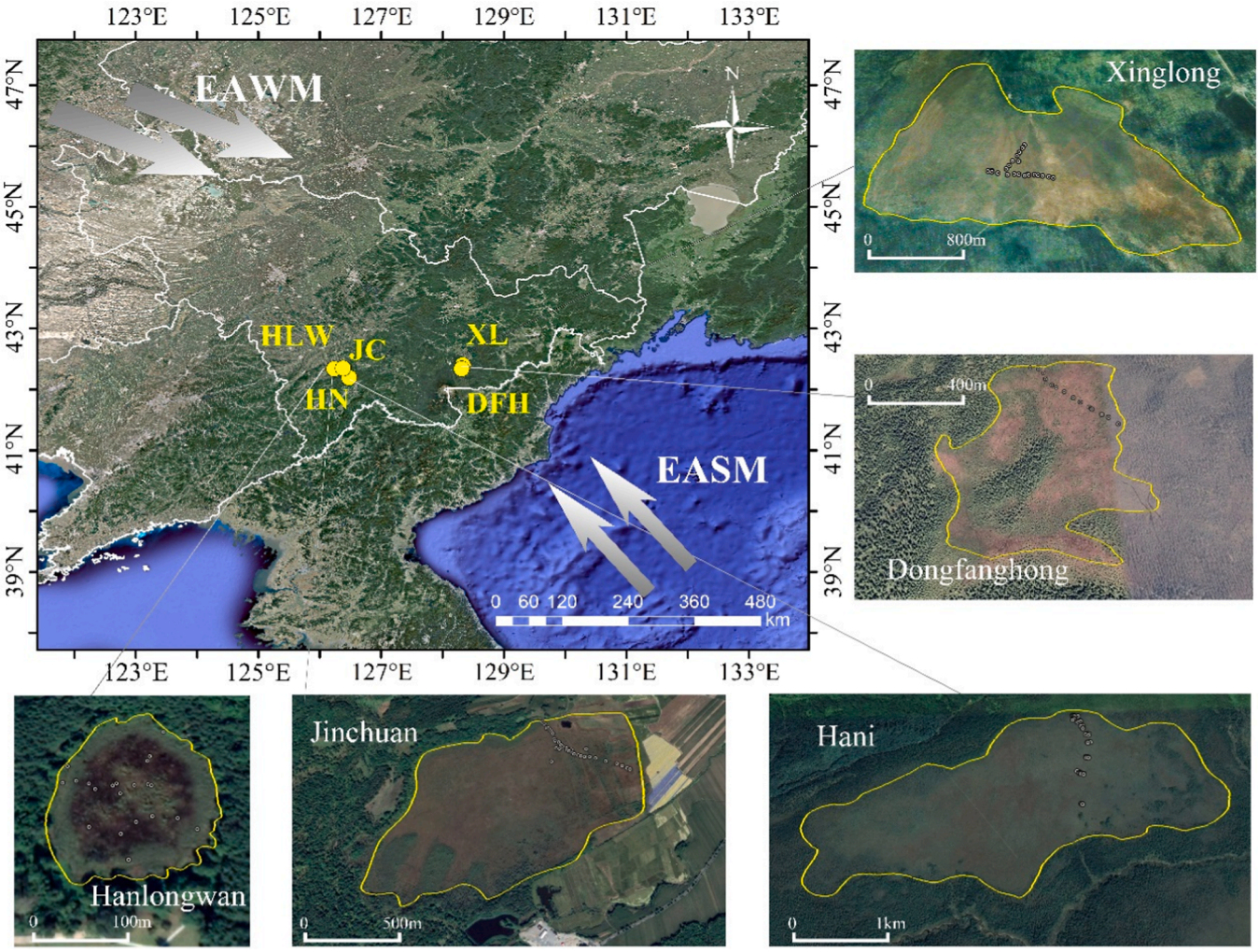

Fig. 1. Location of five peatlands (Hani, Jinchuan, Hanlongwan, Xinglong, Dongfanghong) and investigation plots in each peatland in the Changbai Mountains region. EASM: East Asian summer monsoon, EAWM: East Asian winter monsoon.

Table 1
Details of investigation sites with the ranges of environmental parameters.

Site	Hani	Hanlongwan	Jinchuan	Xinglong	Dongfanghong
Code	HN	HLW	JC	XL	DFH
Latitude (°N)	42°11′43″	42°20′18″	42°20′56″	42°24′09″	42°20′31″
Longitude (°E)	126°28′44″	126°13′55″	126°22′51″	128°19′50″	128°18′45″
Elevation (m a.s.l.)	882	782	616	694	1146
Sample number	96	29	58	30	61
DWT (cm)	−3.3–46.8	3.0–25.7	−12.3–21.2	−6.5–30.0	−2.5–58.5
pH	5.20–6.51	4.86–6.38	5.41–6.06	5.50–6.45	4.14–5.81
Conductivity (μS cm^{-1})	13–314	39–431	34–558	24–87	6–82
TN (mg L^{-1})	0.37–10.35	0.52–8.52	0.64–9.25	0.78–4.78	1.33–15.23
TP (mg L^{-1})	0.01–0.29	0.03–0.37	0.03–0.41	0.02–1.83	0.04–2.86
Ca (mg L^{-1})	2.41–30.99	4.14–15.66	5.38–18.84	7.47–30.17	4.10–36.40
Mg (mg L^{-1})	0.40–8.32	0.56–2.75	1.02–5.17	1.41–4.86	0.68–8.76

measured using a portable multi-parameter water quality analyzer (YSI 6600, Yellow Spring Instruments, USA). Two extra plastic bottles of surface water samples (100 ml each) were collected nearby each plant quadrat to measure physio-chemical properties, such as total nitrogen (TN), total phosphorus (TP), calcium (Ca) and magnesium (Mg). The concentrations of TN and TP were measured using a SmartChem 140 analyzer (AMS-Westco Scientific Instruments, Inc., Rome, Italy), and the concentrations of Ca and Mg were analyzed using ICP-OES in the Key Laboratory of Geographical Processes and Ecological Security in Changbai Mountains, Ministry of Education, Northeast Normal University. Each environmental variable was measured at least three times during every growing season (from May to October) between 2014 and 2016.

3.2. Data processing and statistical analysis

Two datasets of plant assemblages and environmental variables obtained from the investigation were compiled to explore the relationships between plant composition and seven environmental variables (DWT, pH, EC, TN, TP, Ca, Mg) using canonical correspondence analysis (CCA)

with CANOCO 5 (ter Braak and Šmilauer, 2012). Rare species in plant assemblages were downweighted. A Monte Carlo test with 999 permutations was used to test the significance of the environmental variables and ordination axis (Lepš and Šmilauer, 2003).

The transfer function was developed using weighted averaging (WA), weighted averaging partial least squares (WAPLS), modern analogue technique (MAT) and maximum likelihood (ML) with a R (R Development Core Team, 2020) package, the rioja (Juggins, 2013). The weighted averaging model was further divided into weighted averaging with inverse deshrinking (WA-inv), weighted averaging with classical deshrinking (WA-cla), tolerance downweighted weighted averaging with inverse deshrinking (WATOL-inv) and downweighted weighted averaging with classical deshrinking (WATOL-cla). The transfer function performance was assessed in term of R^2, the root mean square error of prediction (RMSEP), average bias and maximum bias. The leave-one-out (LOO) method was used to cross-validate the transfer function performance, and leave-one-site-out (LOSO) method was used to evaluate the impact of clustered sampling (Payne et al., 2012). Segment-wise RMSEPs were calculated to test the potential effect of uneven sampling along the DWT gradient (Telford and Birks, 2011). To identify spatial autocorrelation beyond the scale of inter-site differences, the random neighbourhood exclusion test was used to compare the effect of deleting geographically proximal versus random samples on model performance (Telford and Birks, 2009).

3.3. Quantitative reconstruction and comparison of past mire surface wetness

A 41 cm peat sequence from Laobaishan (LBS) bog (44°06′13″N, 128°02′37″E, 1691 m a.s.l.), located at the top of Zhangguangcai Mountain in the Changbai Mountains region, was applied to assess the potential of the plant assemblages-based transfer function for quantitative reconstruction of past mire surface wetness. Detrended correspondence analysis (DCA) was conducted on fossil plant assemblages of the LBS peat sequence. DWTs of the LBS peat sequence were quantitatively reconstructed applying the transfer function developed in this study. For comparison, DWTs in this sequence were also inferred with a well-developed transfer function between testate amoebae and DWT suitable for this region (Qin et al., 2021).

4. Results

4.1. The environmental variables

The details of investigation sites with the ranges of the environmental variables are shown in Table 1. The 55 kinds of mire plants that were investigated responded widely to seven physiochemical variables

Table 2
Full names and abbreviation of investigated mire plant taxa.

Full name	Abbreviation	Full name	Abbreviation
Aulacomnium palustre	*Aul. pal*	*Oxycoccus palustris*	*O. pal*
Betula ovalifolia	*B. ova*	*Phragmites australis*	*P. aus*
Calamagrostis angustifolia	*C. ang*	*Polygonum* spp.	*Polygonum*
Calliergonella cuspidata	*C. cus*	*Polytrichum strictum*	*P. str*
Caltha palustris	*Cal. pal*	*Potentilla fruticosa*	*P. fru*
Carex lasiocarpa	*C. las*	*Rhododendron parvifolium*	*R. par*
Carex limosa	*C. lim*	*S. amblyphyllum*	*S. amb*
Carex meyeriana	*C. mey*	*S. fallax*	*S. fal*
Carex pseudocuraica	*C. pse*	*S. fuscum*	*S. fus*
Carex rhynchophysa	*C. rhy*	*S. imbricatum*	*S. imb*
Carex schmidtii	*C. sch*	*S. magellanicum*	*S. mag*
Carex spp.	*Carex*	*S. palustre*	*S. palu*
Carex tenuiflora	*C. ten*	*S.* sect. *Acutifolia*	*S.* sect. *Acu*
Chamaedaphne calyculata	*C. cal*	*S.* sect. *Cuspidata*	*S.* sect. *Cus*
Comarum palustre	*Com. pal*	S. sect. Subsecunda	*S.* sect. *Sub*
Dicranum scoparium	*D. sco*	*Salix myrtilloides*	*S. myr*
Drepanocladus aduncus	*D. adu*	*Salix rosmarinifolia*	*S. ros*
Equisetum hyemale	*E. hye*	*Sanguisorba tenuifolia*	*S. ten*
Eriophorum polystachion	*E. pol*	*Saussurea* spp.	*Saussurea*
Eriophorum vaginatum	*E. vag*	*Scheuchzeria palustris*	*Sch. pal*
Gentiana spp.	*Gentiana*	*Scirpus* spp.	*Scirpus*
Iris spp.	*Iris*	*Smilacina trifolia*	*S. tri*
Juncus effusus	*J. eff*	*Sphagnum* spp.	*Spha*
Larix olgensis	*L. olg*	*Spiraea salicifolia*	*S. sal*
Ledum palustre	*L. pal*	*Thelypteris palustris*	*T. pal*
Lonicera edulis	*L. edu*	*Typha angustifolia*	*T. ang*
Lythrum salicaria	*Lythrum*	*Vaccinium uliginosum*	*V. uli*
Menyanthes trifoliata	*M. tri*		

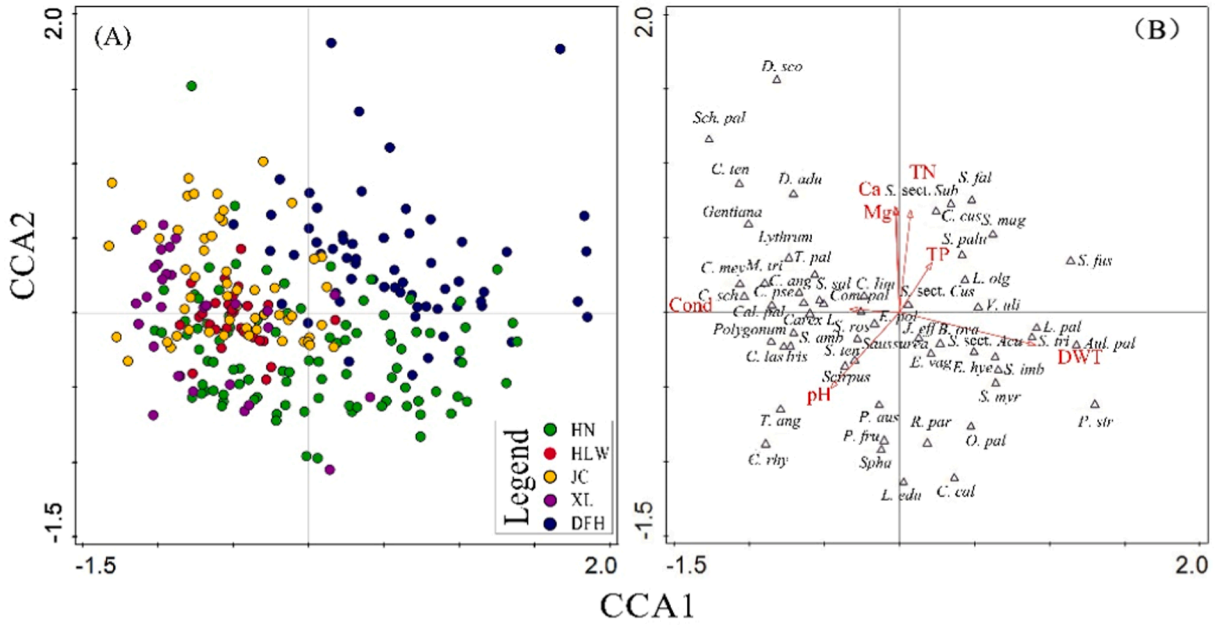

Fig. 2. Samples (Fig. 2A) / Species (Fig. 2B) -environmental variables ordination plot of canonical correspondence analysis (CCA) based on all samples. Different colors represented different peatlands (Fig. 2A). Full species names (Fig. 2B) were given in Table 2.

of mire surface water (Fig. 2; Table 2). In total, the DWT ranged from −12.3 cm to 58.5 cm, while the mire plants were adapted to acid to neutral water environments. Concentrations of Ca and Mg, as well as EC of mire surface water fluctuated from one to two orders of magnitude. Concentrations of TN changed from 0.37 mg L^{-1} to 15.23 mg L^{-1} while concentrations of TP ranged from 0.01 mg L^{-1} to 2.86 mg L^{-1}. Large changes in TN and TP concentrations indicates these peatlands are in different trophic level from oligotrophic, mesotrophic to eutrophic status. The relatively great fluctuation ranges of the environmental variables (such as DWT, TN, TP) may be related not only to various habitats involved in investigation from hummocks, lawns and hollows within a peatland and among peatlands with different trophic types, but also to various weather and climatic conditions at the time of sampling from May to October each year from 2014 to 2016.

4.2. Ordination analysis

Canonical correspondence analysis showed relatively even distribution of the investigated sites and considerable representativeness of different peatlands (Fig. 2A). In addition, CCA illustrated at least two groups of environmental gradients strongly determined plant assemblages (Fig. 2B). One was strongly correlated with surface wetness (DWT) as axis 1 indicated. Different types of plants were primarily separated along axis 1 among and within different peatlands. For example, species commonly inhabiting dry conditions with higher DWTs, such as *L. palustre*, *S. fuscum*, *S.* sect. *Acutifolia, Polytrichum strictum,* were on the right, whereas species in wet conditions, including *Menyanthes trifoliata* and *Scheuchzeria palustris* were toward the left end of axis 1 (Fig. 2B). The other group of environmental gradients, pointed out by axis 2, was a combination of pH, the concentrations of Ca and Mg, and to some extent correlated with nutrient availability (TN, TP). The CCA results showed that DWT had greater marginal effects than other six environmental variables (Table 3). Although axis 1 (eigenvalue = 0.355) and axis 2 (eigenvalue = 0.174) explained 11.6% of the variance in total (Table 3), DWT alone explained 3.6% of variability in total species, while other individual variables contributed less of the variance (<2.5% individually). The Monte Carlo permutation test showed that CCA axis 1 has a significant effect on the plant assemblages ($p = 0.001$, 999 random permutations). Ordination analysis provides a basis for the development of transfer functions between plant assemblages and DWT.

4.3. Transfer function development and performance

The performance and cross-validation results of four types of models are shown in Table 4. All of the models with the full dataset had relatively large RMSEP with relatively small R^2 when LOO cross validation or LOSO cross validation was applied. After model optimization by removing the outliers greater than one-fifth of the measured DWT range in the training set, all transfer function models performed better with a considerable increase in R^2 (14.27%–37.39%) and decrease in RMSEP (24.37%–42.89%), especially with reduction of maximum bias (Table 4; Fig. 3). The optimized models showed better predictive power in term of R^2 (almost greater than 0.5), RMSEP as well as average and maximum biases, especially with LOO cross validation. The WATOL-inv model performed best among four WA models and was therefore selected to further statistical test. The four types of transfer function models (WATOL-inv, WAPLS, ML and MAT) performed differently in terms of alternative performance measures. For R^2, the order of best performance was MAT > ML > WAPLS ≈ WATOL-inv, but the difference was relatively small. For RMSEP, the order changed into MAT > WATOL-inv > WAPLS > ML. In terms of the average and maximum biases, the WATOL-inv model generally performed best.

4.4. Mire surface wetness of the LBS peat sequence

The plant macrofossils diagram of the LBS peat sequence is shown in Fig. 4. Significant correlation between axis 1 scores obtained from DCA on fossil plant assemblages (Fig. 5A) and inferred DWTs from the plant assemblages-based transfer function (Fig. 5B) ($r^2 = 0.58$, $p < 0.01$, n = 41) provided good analogues for the plants in the contemporary training sets and fossil assemblages. This indicated that the plant assemblages-based function can be used on the LBS peat sequence. This was also shown by the significant correlation ($r^2 = 0.63$, $p < 0.01$, n = 41) between the inferred DWTs from the plant assemblages-based transfer function and the testate amoebae-based transfer function (Fig. 5C).

5. Discussion

5.1. The principal environmental variables determining growth of mire plants

The selected 55 mire plants (11 species of trees and shrubs, 29 species of graminoids and other herbs, and 15 species of mosses from genus to species) from five peatlands represent the common mire plant taxa in the Changbai Mountains region (Fig. 2; Table 2). It is noteworthy that most species in this region are the same as those that grow in the Greater Khingan Mountains and Lesser Khingan Mountains, which are representative of temperate montane peatlands, Northeast China, with woody plant *V. oxycoccus*, herbcaeous assemblages composed of *E. vaginatum*, *M. trifoliata*, and mosses (*S. palustre*, *Aulacomnium palustre*, and *S. fuscum*) (Lou et al., 2018). Although some plants are different at the level of species, they may be the same at the level of genus with mire plants in North America (Goud et al., 2018) or Europe under the control of continental climate (Mauquoy and Barber, 2002; Bragazza, 2006). Moreover, some mire plants in the Changbai Mountains region are also comparable to those in boreal peatlands in the regions influenced by oceanic climate (Mauquoy and van Geel, 2010; Jiroušek et al., 2013). This suggests most taxa have broad geographic distribution.

The relationship of mire plants and environmental variables suggested that DWT was the principal environmental variable determining compositions and distribution of plant assemblages (Fig. 2B). This was also evidenced by the highest marginal effect and the lowest variance inflation factor (VIF) of DWT among seven environmental variables (Table 3). It is reasonable that among three environmental gradients (wetness, acidity and nutrition) DWT is overriding in determining compositions of mire plant assemblages (Jiroušek et al., 2013; Potvin et al., 2015). Peatlands are kinds of transitional, amphibious ecosystems with special habitat between open water and terrestrial ecosystems (Rydin and Jeglum, 2013). The waterlogged, often poorly aerated condition is a key feature of peatlands. Thus, DWT directly influences colonization and growth of mire plant species, further compositions and succession of mire plant communities, as well as accumulation and decomposition of peat (Malhotra et al., 2016; Kokkonen et al., 2019). Following DWT, acidity (pH, Ca and Mg) and nutrient availability were subordinately responsible for the growth of mire plants (Fig. 2B, Table 3). The results are consistent with previous studies conducted in

Table 3
Variance inflation factors and marginal effect of seven environmental variables in CCA.

Variables	DWT	pH	Cond	TN	TP	Ca	Mg
Variance inflation factor	1.0620	1.1781	1.2653	1.7366	1.7673	8.0022	7.7524
Percentage variance	3.6%	2.3%	1.5%	1.7%	1.2%	1.4%	1.4%
Significance level	0.002	0.002	0.002	0.002	0.002	0.002	0.002

Table 4
Comparison of prediction performance of different models for DWT in cross validation. Data in normal are from all samples included in training sets; Data in parentheses are outliers filtered out. LOO: leave-one-out cross validation; LOSO: leave-one-site-out cross validation. WA-inv: weighted averaging inverse deshrinking; WA-cla: weighted averaging with classical deshrinking; WATOL-inv: tolerance downweighted weighted averaging inverse deshrinking; WATOL-cla: downweighted weighted averaging with classical deshrinking; WAPLS: weighted averaging partial least squares; ML: maximum likelihood; MAT: modern analogue technique.

	$RMSEP_{LOO}$	R^2_{LOO}	Average $Bias_{LOO}$	Maximum $Bias_{LOO}$	$RMSEP_{LOSO}$	R^2_{LOSO}	Average $Bias_{LOSO}$	Maximum $Bias_{LOSO}$
WA-inv	10.08	0.45	0.01	28.68	11.34	0.35	0.46	30.29
	(7.06)	(0.63)	(-0.01)	(10.47)	(8.22)	(0.54)	(0.19)	(11.96)
WA-cla	14.02	0.46	0.02	25.62	17.27	0.37	0.23	27.06
	(8.49)	(0.64)	(0.00)	(5.69)	(10.86)	(0.57)	(0.03)	(8.24)
WATOL-inv	10.13	0.45	0.06	28.15	11.86	0.32	0.32	30.53
	(6.99)	(0.64)	(0.05)	(10.69)	(8.41)	(0.51)	(0.20)	(12.71)
WATOL-cla	13.40	0.45	0.08	24.67	17.60	0.34	0.72	27.84
	(8.26)	(0.64)	(0.07)	(6.41)	(11.10)	(0.53)	(-0.18)	(8.70)
WAPLS	10.14	0.45	−0.86	27.70	11.43	0.35	−0.63	29.41
	(7.43)	(0.66)	(-0.49)	(14.70)	(8.61)	(0.57)	(-0.36)	(16.40)
ML	13.47	0.46	1.28	27.08	17.75	0.24	−1.58	26.81
	(7.77)	(0.74)	(0.96)	(5.77)	(12.05)	(0.45)	(-1.26)	(5.38)
MAT	9.25	0.54	0.68	23.06	11.64	0.36	2.15	29.56
	(6.08)	(0.77)	(0.46)	(16.8)	(7.92)	(0.59)	(1.91)	(22.93)

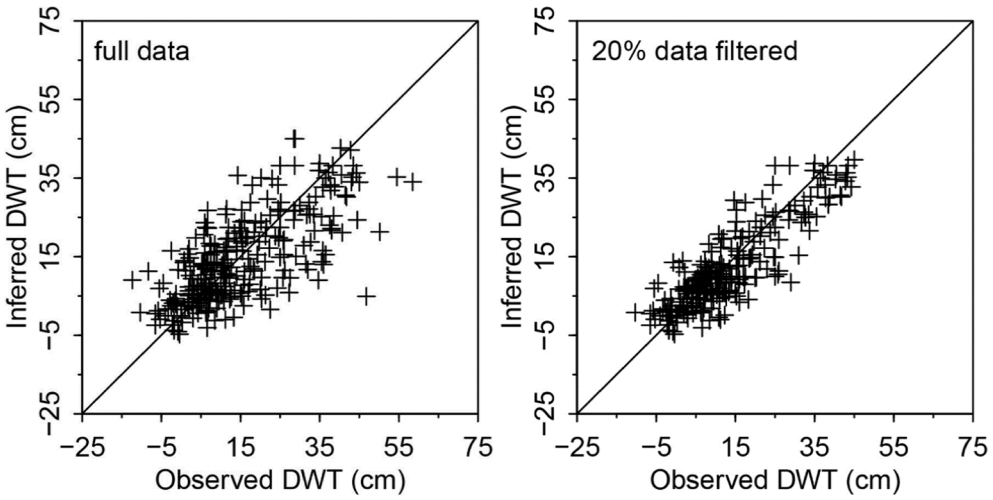

Fig. 3. Comparison of observed DWT and inferred DWT by the MAT model between full data and 20% filtered data. The 1:1 line was plotted for reference.

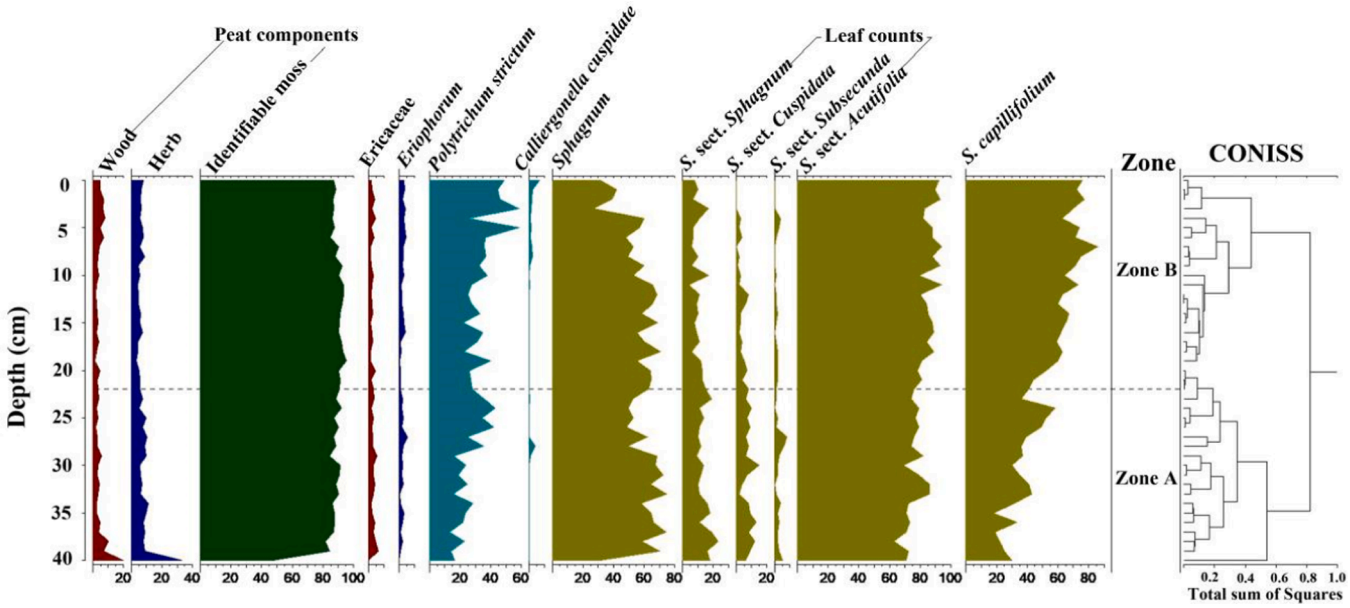

Fig. 4. Diagram for the plant macrofossils in the LBS peat sequence.

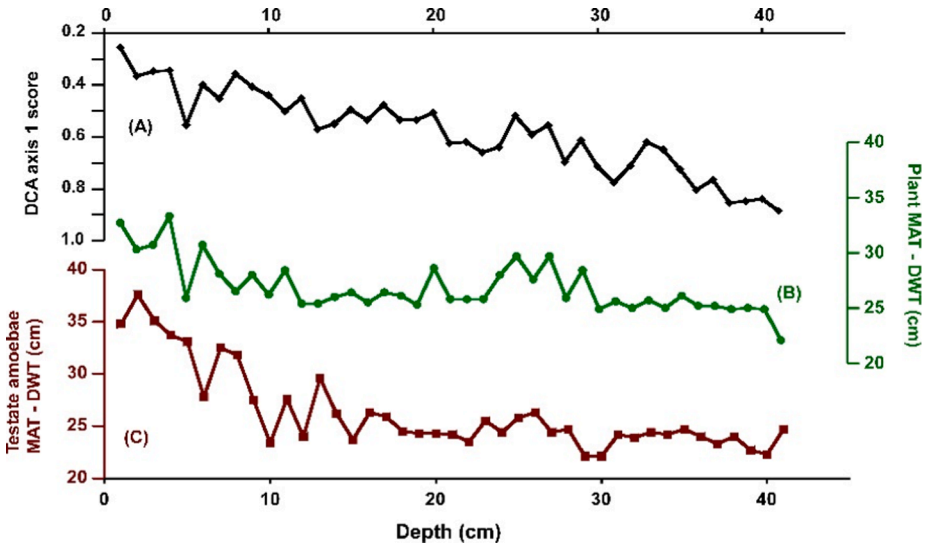

Fig. 5. (A) DCA axis 1 score: axis 1 score obtained from detrended correspondence analysis (DCA) on plant macrofossils; (B) Plant MAT - DWT: reconstructed DWT from plant macrofossils using the MAT model; (C) Testate amoebae MAT - DWT: reconstructed DWT from testate amoebae using the MAT model.

the peatlands of Europe and North America (Rydin and Jeglum, 2013; Mitchell et al., 2013).

5.2. *Statistical test of **performance** of mire plant assemblages-based function model*

Statistical testing of transfer function models is fundamental to make the output of transfer functions meaningful (Payne et al., 2012). Segment analysis was applied to assess the effect of uneven sampling along the water table gradient on model performance (Telford and Birks, 2011). The segment-wise RMSEP ($RMSEP_{SW}$) from testate amoebae-based transfer functions was also employed for comparison owing to less available segment analysis data from previous plant assemblages-based function models. After the removal of outliers with high residual values (Table 4), $RMSEP_{SW}$ in most DWT segments were 7–10 cm for the WATOL-inv and WAPLS models, 7–12 cm for the MAT model, and 10–17 cm for the ML model, respectively (Fig. 6). Although for all of the models, the $RMSEP_{SW}$ in most DWT segments were comparable to those in the published testate amoebae-based transfer functions (Amesbury et al., 2013; Li et al., 2015; Amesbury et al., 2016), the predictive power varied among models and in different DWT segments. The WATOL-inv and WAPLS models, which have almost the same curve, have the strongest predictive power owing to the lowest $RMSEP_{SW}$. Compared to the WATOL-inv and WAPLS models, the MAT model has quite similar $RMSEP_{SW}$ at a DWT range of 5–20 cm, 35–40 cm and above 45 cm, and relatively high $RMSEP_{SW}$ at a DWT range of 20–35 cm, as well as lower $RMSEP_{SW}$ at DWT segments below 5 cm and 40–45 cm with relatively fewer samples. The ML model has the poorest predictive power because its $RMSEP_{SW}$ exceeded the standard deviation of the water table (14.9 cm) in most DWT segments (Mitchell et al., 2013), particularly in the segment of DWT over 40 cm. Similarly, testate amoebae-based transfer functions also have relatively poor performance in dry conditions (Swindles et al., 2015b; van Bellen et al., 2014). This may be attributed to insufficient time for water equilibration in the driest sites with low saturated hydraulic conductivity, which may artificially induce the bias between real and measured DWTs (Swindles et al., 2015b; Zhang et al., 2017).

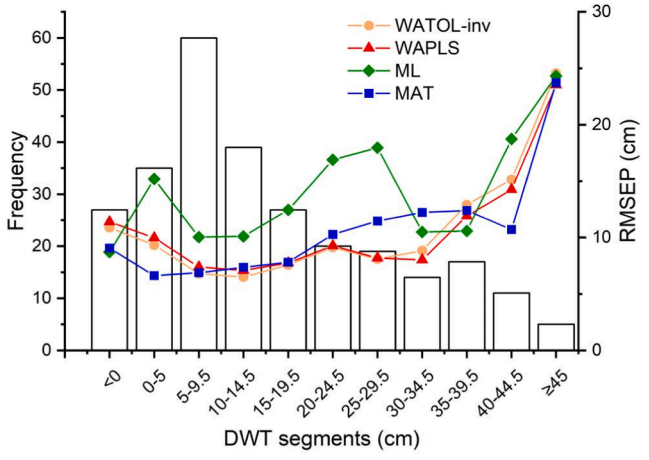

Fig. 6. Frequency and root mean square error of prediction (RMSEP) in different DWT segments of four types of models.

The LOSO test showed that the clustered sampling did overestimate the performance of these transfer function models (Telford and Birks, 2009). All of the models showed an apparent decrease in R^2_{loso} and increase in $RMSEP_{loso}$ when LOSO cross validation was used (Table 4), particularly for the ML model. This suggested that inter-site differences in plant assemblages have a considerable impact on performance of the transfer function (Telford and Birks, 2009). Another reason for performance deterioration in LOSO cross-validation might be that the large difference of sample number among five peatlands changed the size of the training set during the process of leave-one-site-out validation. For example, if the samples from Hani peatland were left out, around one-third of samples became excluded from the training set. Thus, the decrease of RMSEP would be unsurprising. However, in consideration that the $RMSEP_{LOSO}$ of all models were less than the standard deviation of measured DWT, all transfer function models built here still had their predictive power.

The effect of spatial autocorrelation on performance of the transfer function models is shown in Fig. 7. The results indicated that all models were robust to random sample deletion. The R^2 of all models remained stable, or only slightly decreased, even if more than half of samples were randomly deleted from the training set. When samples from geographical neighbourhoods were deleted, R^2 of all the models apparently decreased, but were still higher than when environmentally similar samples were deleted. This indicated that all the transfer models were affected, to different extents, by the spatial autocorrelation of the training set, which resulted from inter-site differences in plant assemblages rather than that the reconstructed DWTs were spatially

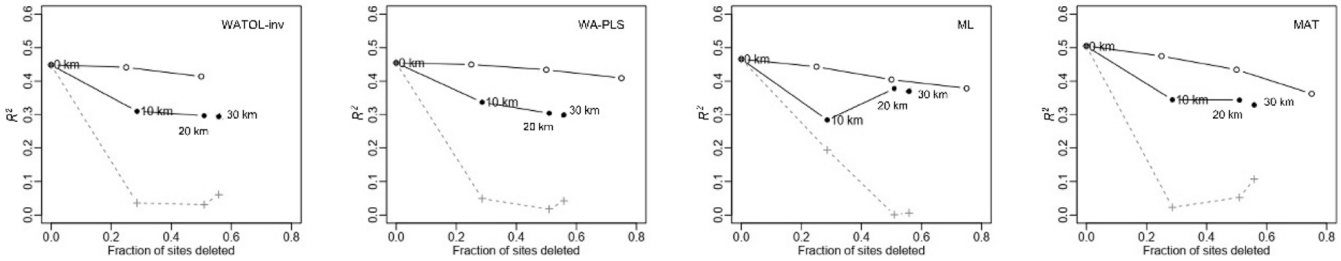

Fig. 7. The effect of spatial autocorrelation on performance (R^2) of four types of models.

autocorrelated. It is surprising that the MAT model, which is believed to be the most susceptible to spatial autocorrelation (Thompson et al., 2008), showed similar performance with WATOL-inv model in robustness to autocorrelation. This might be because that the results of spatial autocorrelation tests were complicated by the clustered nature of the training set (Amesbury et al, 2013). During the process of geographical neighbourhood deletion, it is always the case that all samples from certain sites within the geographical distance would be deleted. The resulting fewer samples in the training set can cause a decrease of R^2. However, since DWT of one site is independent of those from other sites,

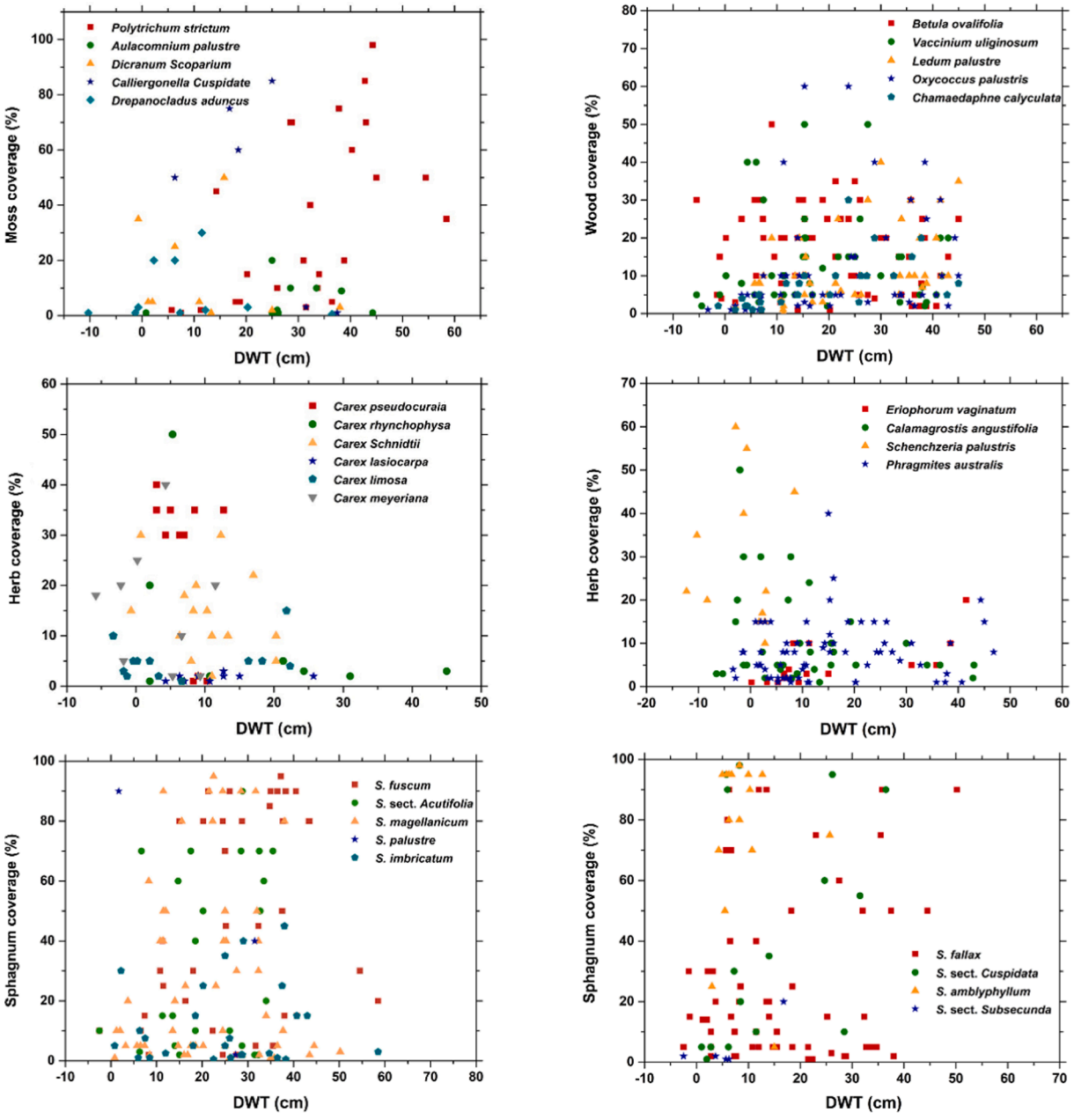

Fig. 8. Scatter plots of investigated DWT and coverage of selected moss, herb and wood species.

the remaining samples representing replicated microhabitats still had ability to model the ecological characteristics of most plant species.

5.3. Ecological assessment of mire plant assemblages-based function model

The potential of mire plant assemblages-based function for quantitative reconstruction of past mire surface wetness was assessed by comparing the DWTs of dominant mire plants in this study to the investigated DWTs in previous studies. The results from investigation on site (Fig. 8) and the model (Fig. 9) showed that most mire plants had similar DWT optima and tolerance to those in previous studies that were conducted in other temperate regions (Mauquoy and van Geel, 2010; Vicherová et al., 2017; Lou et al., 2018). For example, dwarf shrubs were generally found with DWT between 20 cm and 50 cm (Mauquoy and van Geel, 2010); *E. vaginatum*, with a wide range of moisture conditions (0–30 cm), inhabited most of the gradient; *S. palustre* settled at the sites (hollow or lawn) with lower DWT (~0 cm) (Bragazza, 2006); dry-preferring *Sphagnum* (for example *S.* section *Acutifolia*) and *P. strictum* preferred relatively dry conditions with greater DWT; wet-preferring *Sphagnum* (*S. fallax*, *S.* sect *Cuspidata* and *S.* sect *Subsecunda*) were in the hollow or lawn (Blaauw et al., 2004; Mauquoy and van Geel, 2010; Yang et al., 2019; Feurdean et al., 2019). However, several plant species had different adaptations to DWT compared to other research; for example, *Equisetum hyemale*, a variant species of *E. fluviatile*, investigated in this study grew on the hummocks with relatively high DWT. This is different from *E. fluviatile,* which usually inhabits hollow and lawn with relatively lower DWT (Mauquoy and van Geel, 2010).

In addition, different species of mire plants adapted to different fluctuation ranges of water table. The plant species (for example, *S. amblyphyllum*) that respond much more sensitively to variation in DWT have narrow fluctuation ranges of water table. Some species, including *E. vaginatum*, *V. oxycoccus*, *M. trifoliata*, have wider fluctuation ranges of water table than in previous research (Fig. 9) (Mauquoy and van Geel, 2010; Bu et al., 2011; Lou et al., 2018). This may be related to great fluctuation of DWT in the surface of the investigated peatlands during the growing season from 2014 to 2016 (Table 1). The relevant mechanism for this has been addressed by Lamentowicz et al. (2019), showing that the establishment of mire plants on peatlands may be a result of DWT extrema and their period of occurrence. Although absolute values and fluctuation ranges of DWTs may be much greater than in previous research, the optimal values of most mire plant species adapting to DWT were not significantly influenced. For example, *E. vaginatum* with a wide range of water table (0.2–41.5 cm) occupied most of the gradient from hollow through lawn to hummock; however, its optimum value (14.8 cm) was consistent with previous studies (14 cm) (Blaauw et al., 2004; Väliranta et al., 2012). The above analysis indicats that the mire plant assemblages-based function has great potential for reconstructing past surface wetness of mires in the Changbai Mountains region, and even to extend to peatlands with similar plant compositions in other regions.

5.4. Quantitative reconstruction of past mire surface wetness by a mire plant assemblages-based function

The DWTs of LBS peat sequence from bottom to top reconstructed by the mire plant assemblages-based transfer function have shown a very similar trend ($r^2 = 0.63$, $p < 0.01$, n = 41) to increased DWTs from a testate amoebae-based transfer function (Fig. 5), which has been widely applied to reconstruct past water tables in peatlands with relatively high accuracy and precision (Mitchell et al., 2008; Amesbury et al., 2016; Zhang et al., 2017; Qin et al., 2021). This suggests that mire plant assemblages-based transfer function is comparable to the testate amoebae-based transfer function in terms of reconstructed DWT. However, there is still some inconsistency in the magnitude of reconstructed DWT between the two curves, especially for the top 8 cm. The inconsistency was also found in reported studies (Väliranta et al., 2012; Mitchell et al., 2013). The reasons for the divergence may be attributed to different ecological habits and physiological characteristics of mire plants and testate amoebae. Testate amoebae have a very rapid life cycle with ten generations a year as a group of unicellular shelled microorganisms (Charman et al., 2000; Mitchell et al., 2008). Accordingly, testate amoebae can record more rapid variability of mire surface wetness at a seasonal level. However, most mire plants response to variability in DWT lags behind testate amoebae because they are perennial and can tolerate a relatively wide range of DWT fluctuation. Thus, the DWT inferred from plant macrofossils may represent the average condition at an annual level. Swindles et al. (2015a) also pointed out that estimated DWT based on the testate amoebae community reflected directional changes, with poor representations of real mean or median water table magnitudes for the study sites. Amesbury et al. (2016) suggested that interpretation of transfer function models should focus on shifts of mire surface wetness, avoiding potentially inaccurate conclusions relating to specific DWT. Compared to testate amoebae, plant macrofossils have their own advantages in quantitively reconstructing past mire surface wetness based on total trend and major shifts in DWT, especially for long-term time scales, for example the DWTs since the last deglaciation. Just as mentioned above, plant macrofossils are indicators of original mire plant communities at the time of peat accumulation (Barber et al., 1994; Väliranta et al., 2012). Once the plant macrofossils in the peat sequences from this region are identified, the past surface wetness in the peatlands can be derived based on the quantitative relationship indicated by the transfer function between water table dynamics and compositions of the current mire flora. This

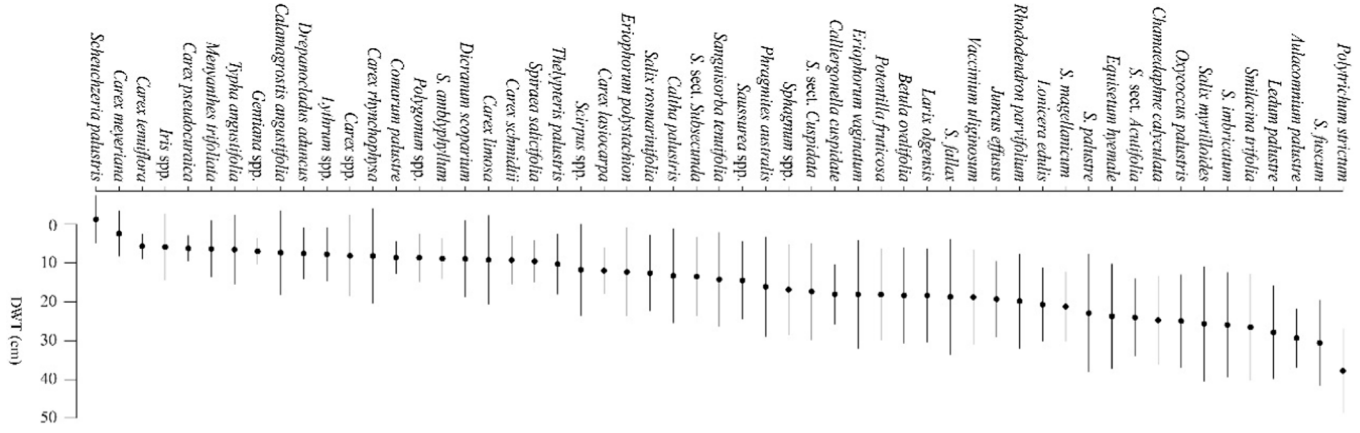

Fig. 9. Optima and tolerance of investigated species for DWT derived from the WA model.

allows for further research into past climate and hydrological changes since the last deglaciation.

6. Conclusions

(1) Datasets of mire plant assemblages and environmental variables were compiled from the Changbai Mountains region, Northeast China. Mire surface wetness (described as DWT) has been shown to be the principal variable that determined mire plant community composition, which provided a basis for the development of transfer functions between plant assemblages and DWT.
(2) The mire plant-DWT transfer function was successfully developed using four different types of models. The MAT model performed best although all of the models had their predictive power through a combination of statistical tests. The similar optima and tolerance of DWTs of dominant plant species to previous studies further indicated the potential of the plant assemblages-based function for reconstruction of mire surface wetness.
(3) Reconstructed DWTs of the LBS peat sequence by a plant assemblages-based transfer function showed high consistency in the trend and main shifts of surface wetness with those reconstructed by a testate amoebae-based transfer function. This demonstrated that the plant assemblages-based function has a great potential for quantitative reconstruction of past mire surface wetness.
(4) The modern calibration database built in this study fills a geographic gap with respect to quantitative relationships between mire plant assemblages and mire surface wetness in the temperate montane regions controlled by the East Asian monsoon. The quantitative reconstruction of past mire surface wetness is of great significance in vegetation science, community ecology, geographical modelling, global change biology, and especially in palaeoclimatology and palaeoecology.

CRediT authorship contribution statement

Qiannan Yang: Investigation, Writing – original draft. **Hongkai Li:** Methodology. **Hongyan Zhao:** Conceptualization, Writing – review & editing. **Frank M. Chambers:** Writing – review & editing. **Zhaojun Bu:** Investigation. **Edith Bai:** . **Guangyuan Xu:** Investigation.

Declaration of Competing Interest

The authors declare that they have no known competing financial interests or personal relationships that could have appeared to influence the work reported in this paper.

Acknowledgements

The authors thank Chuantao Song, Sipeng Zhang, Hanxiang Liu, Fangyuan Chen, Zheng Han, Chenxi Duan, Xiaokang Zhou, Xuanqi Zhao, Yiwen Cao, and Cong Xu for their help in the fieldwork. We are grateful to Xinhua Zhou, Na Xu, Yanmin Dong, Jingjing Sun, Yangyang Xia, and Jicheng Ma for their assistance with laboratory chemical analysis.

Funding

This work was supported financially by National Natural Science Foundation of China (No. 41471165, 41771217), Ministry of Science and Technology of China (2016YFC0500407), Jilin Provincial Department of Science and Technology (20190101025JH) and Jilin Provincial Department of Education (2016506).

References

Amesbury, M.J., Mallon, G., Charman, D.J., Hughes, P.D.M., Booth, R.K., Daley, T.J., Garneau, M., 2013. Statistical testing of a new testate amoeba-based transfer function for water-table depth reconstruction on ombrotrophic peatlands in north-eastern Canada and Maine, United States. J. Quat. Sci. 28 (1), 27–39. https://doi.org/10.1002/jqs.2584.

Amesbury, M.J., Swindles, G.T., Bobrov, A., Charman, D.J., Holden, J., Lamentowicz, M., Mallom, G., Mazei, Y., Mitchell, E.A.D., Payne, R.J., Roland, T.P., Turner, T.E., Warner, B.G., 2016. Development of a new pan-European testate amoeba transfer function for reconstructing peatland palaeohydrology. Quat. Sci. Rev. 152, 132–151. https://doi.org/10.1016/j.quascirev.2016.09.024.

Barber, K.E., 1981. Peat stratigraphy and climatic change: a palaeoecological test of the theory of cyclic peat bog regeneration. Cumbria England 219. https://doi.org/10.1016/j.quaint.2012.05.043.

Barber, K.E., Chambers, F.M., Maddy, D., Stoneman, R., Brew, J.S., 1994. A sensitive high-resolution record of late-Holocene climatic change from a raised bog in northern England. Holocene 4 (2), 198–205. https://doi.org/10.1177/095968369400400209.

Birks, H.H., 2007. Plant Macrofossil Introduction, in: Smol, J. P., Birks, H. J. B., Last, W. M. (Eds.), Tracking Environmental Change Using Lake Sediments. Volume 3: Terrestrial, Algal, and Siliceous Indicators. Kluwer Academic Publishers, Dordrecht, pp. 49–65. https://doi.org/10.1016/B978-0-12-409548-9.10499-3.

Birks, H.H., Van Dinter, M., 2010. Lateglacial and early Holocene vegetation and climate gradients in the Nordfjord - Ålesund area, western Norway. Boreas 39, 783–798. https://doi.org/10.1111/j.1502-3885.2010.00161.x.

Blaauw, M., van Geel, B., van der Plicht, J., 2004. Solar forcing of climatic change during the mid-Holocene: indications from raised bogs in the Netherlands. Holocene 14 (1), 35–44. https://doi.org/10.1191/0959683604hl687rp.

Bragazza, L., 2006. A decade of plant species changes on a mire in the Italian Alps vegetation-controlled or climate-driven mechanisms. Clim. Change 77 (3-4), 415–429. https://doi.org/10.1007/s10584-005-9034-x.

Bu, Z.J., Rydin, H., Chen, X., 2011. Direct and interaction-mediated effects of environmental changes on peatland bryophytes. Oecologia 166 (2), 555–563. https://doi.org/10.1007/s00442-010-1880-1.

Cao, X.Y., Herzschuh, U., Telford, R.J., Ni, J., 2014. A modern pollen - climate dataset from China and Mongolia: Assessing its potential for climate reconstruction. Rev. Palaeobot. Palynol. 211, 87–96. https://doi.org/10.1016/j.revpalbo.2014.08.007.

Castro, D., Souto, M., Garcica-Rodeja, E., Pontevedra-Pombal, X., Fraga, M.I., 2015. Climate change records between the mid- and late Holocene in a peat bog from Serra do Xistral (SW Europe) using plant macrofossils and peat humification analyses. Palaeogeogr. Palaeoclimatol. Palaeoecol. 420, 82–95. https://doi.org/10.1016/j.palaeo.2014.12.005.

Chambers, F.M., Charman, D.J., 2004. Holocene environmental change: contributions from the peatland archive. Holocene 14 (1), 1–6. https://doi.org/10.1191/0959683604hl684ed.

Charman, D.J., Hendon, D., Woodland, W.A., 2000. The identification of testate amoebae (Protozoa: Rhizopoda) in peats. QRA technical guide no. 9. https://doi.org/10.1016/j.quascirev.2004.03.008.

Dise, B.N., 2009. Peatland response to global change. Science 326 (5954), 810–811. https://doi.org/10.1126/science.1174268.

Feurdean, A., Gałka, M., Florescu, G., Diaconu, A.-C., Tanţău, I., Kirpotin, S., Hutchinson, S.M., 2019. 2000 years of variability in hydroclimate and carbon accumulation in western Siberia and the relationship with large-scale atmospheric circulation: a multi-proxy peat record. Quat. Sci. Rev. 226, 1–15. https://doi.org/10.1016/j.quascirev.2019.105948.

Ghosh, R., Bruch, A.A., Portmann, F., Bera, S., Paruya, D.K., Morthekai, P., Ali, S.N., 2017. A modern pollen - climate dataset from the Darjeeling area, eastern Himalaya: assessing its potential for past climate reconstruction. Quat. Sci. Rev. 174, 63–79. https://doi.org/10.1016/j.quascirev.2017.09.002.

Goud, E.M., Watt, C., Moore, T.M., 2018. Plant community composition along a peatland margin follows alternate successional pathways after hydrologic disturbance. Acta Oecologica 91, 65–72. https://doi.org/10.1016/j.actao.2018.06.006.

Hédl, R., Bernhardt-Römermann, M., Grytnes, J.-A., Jurasinski, G., Ewald, J., 2017. Resurvey of historical vegetation plots: a tool for understanding long-term dynamics of plant communities. Appl. Veg. Sci. 20 (2), 161–163. https://doi.org/10.1111/avsc.12307.

Hong, B., Liu, C.Q., Lin, Q.H., Shibata, Y., Leng, X.T., Wang, Y., Zhu, Y.X., Hong, Y.T., 2009. Temperature change recorded by $\delta^{18}O$ in Hani peat since 14000 a BP. Sci. China Ser. D Earth Sci. 39, 626–637. https://doi.org/10.1007/s11430-009-0086-z.

Jiroušek, M., Poulíčková, A., Kintrová, K., Opravilová, V., Hájková, P., Rybníček, K., Kočí, M., Bergová, K., Hnilica, R., Mikulášková, E., Králová, Š., Hájek, M., 2013. Long-term and contemporary environmental conditions as determinants of the species composition of bog organisms. Freshw. Biol. 58 (10), 2196–2207.

Juggins, S., 2013. Rioja: analysis of quaternary science data, R Package version 0.8-4.

Kapfer, J., Hédl, R., Jurasinski, G., Kopecký, M., Schei, F.H., Grytnes, J.-A., Bernhardt-Römermann, M., 2017. Resurveying historical vegetation data - opportunities and challenges. Appl. Veg. Sci. 20 (2), 164–171.

Kokkonen, N.A.K., Laine, A.M., Laine, J., Vasander, H., Kurki, K., Gong, J., Tuittila, E.-S., Collins, B., 2019. Responses of peatland vegetation to 15-year water level drawdown as mediated by fertility level. J. Veg. Sci. 30 (6), 1206–1216. https://doi.org/10.1111/jvs.12794.

Krashevska, V., Tsyganov, A.N., Esaulov, A.S., Mazei, Y.A., Hapsari, K.A., Saad, A., Sabiham, S., Behling, H., Biagioni, S., 2020. Testate amoeba species- and trait-based transfer functions for reconstruction of hydrological regime in tropical peatland of

Central Sumatra, Indonesia. Front. Ecol. Evol. 8 (225) https://doi.org/10.3389/fevo.2020.00225.
Kurina, I.V., Li, H., 2019. Why do testate amoeba optima related to water table depth vary? Microb. Ecol. 77 (1), 37–55. https://doi.org/10.1007/s00248-018-1202-4.
Laine, A.M., Selänpää, T., Oksanen, J., Seväkivi, M., Tuittila, E.-S., 2018. Plant diversity and functional trait composition during mire development. Mires Peat 21 (02), 1–19.
Lamentowicz, M., Gałka, M., Marcisz, K., Słowiński, M., Kajukało-Drygalska, K., Dayras, M.D., Jassey, V.E.J., 2019. Unveiling tipping points in long-term ecological records from *Sphagnum*-dominated peatlands. Biol. Lett. 15 (4), 20190043. https://doi.org/10.1098/rsbl.2019.0043.
Lepš, J., Smilauer, P., 2003. Multivariate analysis of ecological data using CANOCO. Cambridge University Press, Cambridge, p. (pp. 284)..
Li, H., Wang, S., Zhao, H., Wang, M., 2015. A testate amoebae transfer function from *Sphagnum*-dominated peatlands in the Lesser Khingan Mountains, NE China. J. Paleolimnol. 54 (2-3), 189–203. https://doi.org/10.1007/s10933-015-9846-2.
Liu, C., Bu, Z.-J., Mallik, A., Rochefort, L., Hu, X.-F., Yu, Z., 2020. Resource competition and allelopathy in two peat mosses: implication for niche differentiation. Plant Soil 446 (1-2), 229–242. https://doi.org/10.1007/s11104-019-04350-0.
Lou, Y.J., Gao, C.Y., Pan, Y.W., Xue, Z.S., Liu, Y., Tang, Z.H., Jiang, M., Lu, X.G., Rydin, H., 2018. Niche modelling of marsh plants based on occurrence and abundance data. Sci. Total Environ. 616–617, 198–207. https://doi.org/10.1016/j.scitotenv.2017.10.300.
Lu, H.-Y., Wu, N.-Q., Yang, X.-D., Jiang, H., Liu, K.-B., Liu, T.-S., 2006. Phytoliths as quantitative indicators for the reconstruction of past environmental conditions in China I: phytolith-based transfer functions. Quat. Sci. Rev. 25 (9-10), 945–959. https://doi.org/10.1016/j.quascirev.2005.07.014.
Ma, J.Z., Chen, X., Malik, A., Bu, Z.J., Zhang, M.M., Wang, S.Z., Sundberg, S., 2020. Environmental together with interspecific interactions determine bryophyte distribution in a protected mire of Northeast China. Front. Earth. Sci. 8 (32) https://doi.org/10.3389/feart.2020.00032.
Malhotra, A., Roulet, N.T., Wilson, P., Giroux-Bougard, X., Harris, L.I., 2016. Ecohydrological feedbacks in peatlands: an empirical test of the relationship among vegetation, microtopography and water table. Ecohydrology 9 (7), 1346–1357. https://doi.org/10.1002/eco.1731.
Mauquoy, D., Barber, K., 2002. Testing the sensitivity of the palaeoclimatic signal from ombrotrophic peat bogs in northern England and the Scottish Borders. Rev. Palaeobot. Palynol. 119 (3-4), 219–240. https://doi.org/10.1016/S0034-6667(01)00099-9.
Mauquoy, D., van Geel, B., 2010. Plant macrofossil methods and studies: mire and peat Macros. In: Elias, S.A. (Ed.), Encyclopedia of Quaternary Science, pp. 2315–2336.
Mitchell, E.A.D., Charman, D.J., Warner, B.G., 2008. Testate amoebae analysis in ecological and paleoecological studies of wetlands: past, present and future. Biodivers. Conserv. 17 (9), 2115–2137. https://doi.org/10.1007/s10531-007-9221-3.
Mitchell, E.A.D., Payne, R.J., van der Knaap, W.O., Lamentowicz, Ł., Gąbka, M., Lamentowicz, M., 2013. The performance of single- and multi-proxy transfer functions (testate amoebae, bryophytes, vascular plants) for reconstructing mire surface wetness and pH. Quat. Res. 79 (1), 6–13. https://doi.org/10.1016/j.yqres.2012.08.004.
Payne, R.J., Telford, R.J., Blackford, J.J., Blundell, A., Booth, R.K., Charman, D.J., Lamentowicz, Ł., Lamentowicz, M., Mitchell, E.AD., Potts, G., Swindles, G.T., Warner, B.G., Woodland, W., 2012. Testing peatland testate amoeba transfer functions: appropriate methods for clustered training-sets. Holocene 22 (7), 819–825. https://doi.org/10.1177/0959683611430412.
Piilo, S.R., Korhola, A., Heiskanen, L., Tuovinen, J.-P., Aurela, M., Juutinen, S., Marttila, H., Saari, M., Tuittila, E.-S., Turunen, J., Väliranta, M.M., 2020. Spatially varying peatland initiation, Holocene development, carbon accumulation patterns and radiative forcing within a subarctic fen. Quat. Sci. Rev. 248, 106596. https://doi.org/10.1016/j.quascirev.2020.106596.
Potvin, L.R., Kane, E.S., Chimner, R.A., Kolka, R.K., Lilleskov, E.A., 2015. Effects of water table position and plant functional group on plant community, aboveground production, and peat properties in a peatland mesocosm experiment (PEATcosm). Plant Soil 387 (1-2), 277–294. https://doi.org/10.1007/s11104-014-2301-8.
Qin, Y.M., Li, H.K., Mazei, Y., Kurina, I., Swindles, G.T., Bobrov, A., Tsyganov, A.N., Gu, Y.S., Huang, X.Y., Xue, J.T., Lamentowicz, M., Marcisz, K., Roland, T., Payne, R.J., Mitchell, E.A.D., Xie, S.C., 2021. Developing a continental-scale testate amoeba hydrological transfer function for Asian peatlands. Quat. Sci. Rev. 258, 1–17. https://doi.org/10.1016/j.quascirev.2021.106868.
R Development Core Team, 2020. R: a language and environment for statistical computing. https://www.r-project.org.
Rydin, H., Jeglum, J.K., 2013. The Biology of Peatlands, second ed. Oxford University press, Oxford, UK.
Schröder, C., Thiele, A., Wang, S.Z., Bu, Z.J., Joosten, H., 2007. Hani mire – A percolation mire in Northeast China. Peatland Int. 2, 20–24.
Seddon, A.W.R., Mackay, A.W., Baker, A.G., Birks, H.J.B., Breman, E., Buck, C.E., Ellis, E.C., Froyd, C.A., Gill, J.L., Gillson, L., Johnson, E.A., Jones, V.J., Juggins, S., Macias-Fauria, M., Mills, K., Morris, J.L., Nogués-Bravo, D., Punyasena, S.W., Roland, T.P., Tanentzap, A.J., Willis, K.J., Aberhan, M., Asperen, E.N., Austin, W.E.N., Battarbee, R.W., Bhagwat, S., Belanger, C.L., Bennett, K.D., Birks, H.H., Bronk Ramsey, C., Brooks, S.J., Bruyn, M., Butler, P.G., Chambers, F.M., Clarke, S.J., Davies, A.L., Dearing, J.A., Ezard, T.H.G., Feurdean, A., Flower, R.J., Gell, P., Hausmann, S., Hogan, E.J., Hopkins, M.J., Jeffers, E.S., Korhola, A.A., Marchant, R., Kiefer, T., Lamentowicz, M., Larocque-Tobler, I., López-Merino, L., Liow, L.H., McGowan, S., Miller, J.H., Montoya, E., Morton, O., Nogué, S., Onoufriou, C., Boush, L.P., Rodriguez-Sanchez, F., Rose, N.L., Sayer, C.D., Shaw, H.E., Payne, R., Simpson, G., Sohar, K., Whitehouse, N.J., Williams, J.W., Witkowski, A., McGlone, M., 2014. Looking forward through the past: identification of 50 priority research questions in palaeoecology. J. Ecol. 102 (1), 256–267.
Swindles, G.T., Amesbury, M.J., Turner, T.E., Carrivick, J.L., Woulds, C., Raby, C., Mullan, D., Roland, T.P., Galloway, J.M., Parry, L.E., Kokfelt, U., Garneau, M., Charman, D.J., Holden, J., 2015a. Evaluating the use of testate amoebae for palaeohydrological reconstruction in permafrost peatlands. Palaeogeogr. Palaeoclimatol. Palaeoecol. 424, 111–122. https://doi.org/10.1016/j.palaeo.2015.02.004.
Swindles, G.T., Holden, J., Raby, G.L., Turner, T.E., Blundell, A., Charman, D.J., Menberu, M.W., Kløve, B., 2015b. Testing peatland water-table depth transfer functions using high-resolution hydrological monitoring data. Quat. Sci. Rev. 120, 107–117. https://doi.org/10.1016/j.quascirev.2015.04.019.
Telford, R.J., Birks, H.J.B., 2009. Evaluation of transfer functions in spatially structured environments. Quat. Sci. Rev. 28 (13-14), 1309–1316. https://doi.org/10.1016/j.quascirev.2008.12.020.
Telford, R.J., Birks, H.J.B., 2011. Effect of uneven sampling along an environmental gradient on transfer-function performance. J. Paleolimnol. 46 (1), 99–106. https://doi.org/10.1007/s10933-011-9523-z.
ter Braak, C.J.F., Šmilauer, P., 2012. CANOCO Reference Manual and User's Guide: Software for Ordination (Version 5). Ithaca, Microcomputer Power.
Thompson, R.S., Anderson, K.H., Bartlein, P.J., 2008. Quantitative estimation of bioclimatic parameters from presence/absence vegetation data in North America by the modern analog technique. Quat. Sci. Rev. 27 (11-12), 1234–1254. https://doi.org/10.1016/j.quascirev.2008.02.014.
Tierney, J.E., Poulsen, C.J., Montañez, I.P., Bhattacharya, T., Feng, R., Ford, H.L., Hönisch, B., Inglis, G.B., Petersen, S.V., Sagoo, N., Tabor, C.R., Thirumalai, K., Zhu, J., Burls, N.J., Foster, G.L., Goddéris, Y., Huber, B.T., Ivany, L.C., Turner, S.K., Lunt, D.J., McElwain, J.C., Mills, B.J.W., Otto-Bliesner, B.L., Ridgwell, A., Zhang, Y.G., 2020. Past climates inform our future. Science 370 (6517). https://doi.org/10.1126/science.aay3701.
Turner, T.E., Swindles, G.T., Charman, D.J., Blundell, A., 2013. Comparing regional and supra-regional transfer functions for palaeohydrological reconstruction from Holocene peatlands. Palaeogeogr. Palaeoclimatol. Palaeoecol. 369, 395–408. https://doi.org/10.1016/j.palaeo.2012.11.005.
Van bellen, S., Mauquoy, D., Payne, R.J., Roland, T.P., Daley, T.J., Hughes, P.D.M., Loader, N.J., Street-perrott, F.A., Rice, E.M., Pancotto, V.A., 2014. Testate amoebae as a proxy for reconstructing Holocene water table dynamics in southern Patagonian peat bogs. J. Quat. Sci. 29 (5), 463–474. https://doi.org/10.1002/jqs.2719.
Väliranta, M., Korhola, A., Seppä, H., Tuittila, E.-S., Sarmaja-Korjonen, K., Laine, J., Alm, J., 2007. High-resolution reconstruction of wetness dynamics in a southern boreal raised bog, Finland, during the late Holocene: a quantitative approach. Holocene 17 (8), 1093–1107. https://doi.org/10.1177/0959683607082550.
Väliranta, M., Blundell, A., Charman, D.J., Karofeld, E., Korhola, A., Sillasoo, Ü., Tuittila, E.S., 2012. Reconstructing peatland water tables using transfer functions for plant macrofossils and testate amoebae: A methodological comparison. Quat. Int. 268, 34–43. https://doi.org/10.1016/j.quaint.2011.05.024.
Vicherová, E., Hájek, M., Šmilauer, P., Hájek, T., 2017. Sphagnum establishment in alkaline fens: Importance of weather and water chemistry. Sci. Total Environ. 580, 1429–1438. https://doi.org/10.1016/j.scitotenv.2016.12.109.
Wen, R.L., Xiao, J.L., Ma, Y.Z., Feng, Z.D., Li, Y.C., Xu, Q.H., 2013. Pollen-climate transfer functions intended for temperate eastern Asia. Quat. Int. 311, 3–11. https://doi.org/10.1016/j.quaint.2013.04.025.
Xing, W., Bao, K.S., Gallego-Sala, A.V., Charman, D.J., Zhang, Z.Q., Gao, C.Y., Lu, X.G., Wang, G.P., 2015. Climate controls on carbon accumulation in peatlands of Northeast China. Quat. Sci. Rev. 115, 78–88. https://doi.org/10.1016/j.quascirev.2015.03.005.
Xu, J., Morris, P.J., Liu, J., Holden, J., 2018. PEATMAP: Refining estimates of global peatland distribution based on a meta analysis. Catena 160, 134–140. https://doi.org/10.1016/j.
Yang, Q.N., Li, H.C., Zhao, H.Y., Li, H.K., Bu, Z.J., Wang, S.Z., Chou, C.Y., Liu, Z.P., 2019. Hydroclimate controls of the distribution and abundance of mosses in Hani mire, Northeast China: Modern vegetation survey and peat-core analysis. Quat. Int. 528, 30–40. https://doi.org/10.1016/j.quaint.2019.09.026.
Yu, Z., Loisel, J., Brosseau, D.P., Beilman, D.W., Hunt, S.J., 2010. Global peatland dynamics since the Last Glacial Maximum. Geophys. Res. Lett. 37 (13), n/a–n/a. https://doi.org/10.1029/2010GL043584.
Zhang, H., Amesbury, M.J., Ronkainen, T., Charman, D.J., Gallego-Sala, A.V., VÄliranta, M., 2017. Testate amoeba as palaeohydrological indicators in the permafrost peatlands of north-east European Russia and Finnish Lapland. J. Quat. Sci. 32 (7), 976–988. https://doi.org/10.1002/jqs.2970.
Zhang, M.M., Bu, Z.J., Jiang, M., Wang, S.Z., Liu, S.S., Chen, X., Hao, J.N., Liao, W.Y., 2019. The development of Hani peatland in the Changbai mountains (NE China) and its response to the variations of the East Asian summer monsoon. Sci Total Environ. 692, 818–832. https://doi.org/10.1016/j.scitotenv.2019.07.287.
Zhang, M., Bu, Z., Wang, S., Jiang, M., 2020. Moisture changes in Northeast China since the last deglaciation: Spatiotemporal out-of-phase patterns and possible forcing mechanisms. Earth-Sci Rev. 201, 102984. https://doi.org/10.1016/j.earscirev.2019.102984.
Zhou, W., Zheng, Y., Meyers, P.A., Jull, A.J.T., Xie, S., 2010. Postglacial climate change record in biomarker lipid compositions of the Hani peat sequence, Northeastern China. Earth Planet. Sci. Lett. 294 (1-2), 37–46. https://doi.org/10.1016/j.epsl.2010.02.035.

Quaternary Science Reviews 268 (2021) 107124

Contents lists available at ScienceDirect

Quaternary Science Reviews

journal homepage: www.elsevier.com/locate/quascirev

Holocene peatland development, carbon accumulation and its response to climate forcing and local conditions in Laolike peatland, northeast China

Yanmin Dong [a, b, 1], Hongkai Li [a, b, 1], Hongshi He [a, c], Shengzhong Wang [a, b, *]

[a] Key Laboratory of Geographical Process and Ecological Security in Changbai Mountains, Ministry of Education, School of Geographical Sciences, Northeast Normal University, Changchun, 130024, China
[b] State Environmental Protection Key Laboratory of Wetland Ecology and Vegetation Restoration, Institute for Peat and Mire Research, Northeast Normal University, Changchun, 130024, China
[c] School of Natural Resources, University of Missouri, MO, 65211, USA

ARTICLE INFO

Article history:
Received 6 April 2021
Received in revised form
23 July 2021
Accepted 24 July 2021
Available online xxx

Handling Editor: Yan Zhao

Keywords:
Peatland development
Carbon accumulation
Climate
Holocene
NE China

ABSTRACT

Peatlands are one of the most significant carbon reservoirs in the terrestrial ecosystem. Understanding past peatland carbon accumulation processes and their responses to varying external and internal forcing factors would help reveal the general development patterns of peatland ecosystems and provide useful insights into projecting the fate of carbon reservoirs into the future. In this paper, the basal ages of 17 peat cores were used to explore the lateral expansion processes of the Laolike peatland, northeast China. Two cores were selected to calculate carbon accumulation rates (CAR) and reconstruct moisture/precipitation records based on $\delta^{13}C$ and grain size analyses. The basal ages show that the peatland was initiated at 12.1 cal kyr BP, then laterally expanded with its fastest rate occurring during the early Holocene, and reached its largest area around 6 cal kyr BP. The time-weighted mean CAR in the Laolike peatland ranged from 31.1 to 52.9 g C/m^2/yr (with an average of 42 g C/m^2/yr) during the Holocene. The peatland experienced a high CAR of 52.5 g C/m^2/yr from 11.7 to 5 cal kyr BP, followed by a low CAR of 35.1 g C/m^2/yr after 5 cal kyr BP. Both lateral expansion and vertical accretion are consistent with the summer insolation, climate seasonality, and the strength of the East Asia summer monsoon (EASM) over multi-millennium timescales, where the CAR correlated well with $\delta^{13}C$ and grain size, implying moisture/precipitation might be the primary factors controlling carbon accumulation over millennium timescales. Local conditions, such as topography and hydrology, also played an important role in the process of peatland initiation and lateral expansion, as well as the discrepant CAR within the peatland. This study reveals the roles of climate and local conditions in peatland initiation, expansion, and CAR during the Holocene. In addition, we provide a window for a better understanding of the driving factors of peatland development in the temperate zones of the Northern Hemisphere.

© 2021 Elsevier Ltd. All rights reserved.

1. Introduction

Peatlands are carbon-rich ecosystems that develop where local conditions promote a persistent excess of plant productivity over ecosystem respiration (Clymo, 1984; Charman, 2002). With a total organic carbon storage of about 455–600 Pg (1 Pg = 10^{15} g) (Gorham, 1991; Yu et al., 2010), peatlands account for nearly one-third of the global soil carbon pool (Yu, 2012). According to the latest estimates of peatland carbon storage, northern peatlands carbon stocks amount to between 1016 and 1105 Pg (Nichlis and Peteet, 2019). Peatlands play a key role in the global carbon cycle as important long-term carbon sinks and major sources of methane (CH_4) emitted to the atmosphere (Frolking et al., 2011; Yu et al., 2011; Charman et al., 2013). Understanding the past lateral expansion and vertical accretion processes of peatlands and their links to various controls will help reveal the general development patterns of peatland ecosystems and provide useful insights into the fate of peatland carbon in the future.

* Corresponding author. Key Laboratory of Geographical Process and Ecological Security in Changbai Mountains, Ministry of Education, School of Geographical Sciences, Northeast Normal University, Changchun, 130024, China.
E-mail address: szwang@nenu.edu.cn (S. Wang).
[1] Both authors contributed equally.

https://doi.org/10.1016/j.quascirev.2021.107124
0277-3791/© 2021 Elsevier Ltd. All rights reserved.

Carbon accumulation in peatlands can be affected by a range of autogenic factors, such as hydrological conditions (Panait et al., 2017), topography (van Bellen et al., 2011), plant species composition (Charman et al., 2015), and allogenic factors, including climate (Jone and Yu, 2010; Charman et al., 2013; Morris et al., 2018; Zhao et al., 2014) over different temporal and spatial scales. Climate might regulate the hydrological conditions of peatlands by temperature, precipitation, and evaporation (Yu et al., 2009). Waterlogged conditions and stable water tables are necessary preconditions for carbon accumulation in peatlands (Charman, 2002), but the role of moisture in peatland carbon accumulation remains unclear (Jone and Yu, 2010; Klein et al., 2013; Panait et al., 2017). Some studies have argued that hydrological and decomposition processes may play an important role in carbon accumulation in many peatlands, such as those in Alaska (Klein et al., 2013), the Eastern Carpathians (Panait et al., 2017), Patagonian (Mathijssen et al., 2019), and the Zoige Plateau (Wang et al., 2015). Moreover, the hydrological characteristics of peatlands are often closely related to the local topography. Charman et al. (2015) have suggested that the early phase of high carbon accumulation in such peatlands before the main Holocene Thermal Maximum was probably locally controlled by topography and hydrology.

Peatlands always grow by vertical accretion, together with lateral expansion. To comprehensively understand the long-term carbon accumulation dynamics and associated driving factors, both vertical accretion and lateral expansion rates should be considered (Mathijseen et al., 2016). The initiation and expansion of peatlands have been suggested to be associated with summer insolation variations and climatic changes over large spatial scales (Jone and Yu, 2010; Yu et al., 2011; Zhao et al., 2014; Wang et al., 2014). Over local scales, environmental factors such as topography, substrate, hydrology, and vegetation may influence lateral peat expansion to a larger extent than the climate (Korhola, 1992;Mäkilä, 1997;Mäkilä and Moisanen, 2007). How local conditions influence lateral expansion may vary for different peatland types and regions (Ireland et al., 2013; Mäkilä and Moisanen, 2007; Peregon et al., 2009). Allogenic and autogenic factors operate simultaneously in the processes of peatland development and it is challenging to differentiate their contributions (Tuittila et al., 2007;Mathijseen et al., 2016; Loisel et al., 2013). Multiple core analyses should therefore be used to reconstruct the development of a peatland (Mäkilä and Moisanen, 2007; van Bellen et al., 2011).

Many syntheses and investigations have been carried out to explore the carbon accumulation processes of peatlands and their driving factors over different temporal and spatial scales around the world (Yu et al., 2010;Jone and Yu, 2010; Charman et al., 2013; Loisel et al., 2014, 2017, 2017; Gallego-Sala et al., 2018;Mathijseen et al., 2016). Most of these efforts have focused on northern peatlands, such as Western Siberia, Alaska (Jone and Yu, 2010; Klein et al., 2013), Canada (Yu, 2006), Finland (Mathijseen et al., 2016), and all of the northern peatland (Loisel et al., 2014, 2017, 2017; Charman et al., 2013). Northeast China (NE China) contains the largest area of peatland in the country, with 48 % of the nation's total wetland area (Niu et al., 2012). As an important component of the peatland area of NE China, the peatlands in the Changbai Mountains have been estimated to cover about 7580 km^2 and to have held about 0.72 Gt of carbon during the Holocene (Xing et al., 2015a). Previous studies in terms of the carbon dynamics of the NE China peatlands have mainly focused on the regional scale (Xing et al., 2015a, 2015b, 2015b; Zhao et al., 2014; Wang et al., 2014), with little attention paid to carbon accumulation and the associated forcing factors at local scales. Moreover, few carbon accumulation records cover the Holocene across NE China, which limits our understanding of peatland development processes and responses to climate change across this huge carbon pool of China and the temperate zones of the Northern Hemisphere.

In this study, a total of 17 peat cores were used to investigate the lateral expansion process, with two cores being used to reconstruct the carbon accumulation history of the Laolike peatland, NE China, during the Holocene. The objectives of this study are: (1) to present a new carbon accumulation rate (CAR) record over the Holocene for the Changbai mountains, NE China; (2) to reconstruct the lateral expansion and carbon accumulation processes of the peatland and their responses to climate change and local conditions; and (3) to discuss the influence of climate and local conditions on peatland carbon accumulation at local scales.

2. Study site

The Laolike peatland (128°39′59″E 42°28′47″N, 1475 m a.s.l.) is located on top of the planation surface of Zengfengling, a range of the Changbai Mountains (Fig. 1a). Its total area is about 0.15 km^2 and it is around 800 m long and 300 m wide (Fig. 1b). The vegetation surrounding it is a mixture of mixed coniferous and broad-leaved forests. The climate is strongly influenced by the East Asia summer monsoon (EASM) (Wang and Lin, 2002), where in summer, winds from the southeast ocean cause warm and wet conditions, while it is cold and dry in winter due to the continental winds from the northwest. According to meteorological data from Donggang station for the period from 1957 to 2014, the mean annual temperature (MAT) is about 3.6 °C and the mean annual precipitation (MAP) is around 824 mm (Fig. 1d). The rainy season lasts from June to September and accounts for at least 60 % of the MAP. The peatland was the headwaters of the Hailan River in the Changbai Mountains, and it was surrounded by rivers to its western, northern, and southern sides (Fig. 1b). Both surface runoff and precipitation are the water sources for the peatland.

Located on the top of the watershed, the peatland has generally retained its pristine state. Its surface elevation decreases from the west and south to the east and north. Due to the topography and hydrological conditions, the vegetation in the Laolike peatland has obvious heterogeneity, especially in the east-west direction (Fig. 1c). In the western part of the peatland, *Sphagnum* is dominant, with a coverage of over 85 %. The coverage of *Carex* increases along the slope towards the east and is dominant in the middle of the peatland. In the east, *Iris* and *Carex* are more abundant. Peat deposition generally becomes shallower from the center to the edge of the peatland. The average peat thickness is about 4 m with a maximum of 7.5 m in the southern part of the peatland (Fig. 2a).

3. Materials and methods

3.1. Field investigation and sampling

We conducted a detailed field investigation of the Laolike peatland, with the relative elevation of the peatland being measured continuously with a water level gauge at 100 measuring points across eight transects. The vegetation survey was conducted at 20 randomly selected 1 × 1 m^2 herbaceous quadrats in different parts of the peatland. The thickness of the peat deposits was surveyed at 56 points along 5 transects, and the peat depth contour was plotted using the ArcMap 10.3 software tool.

Samples for laboratory analysis were taken with a manual peat corer 5 cm in diameter and 50 cm in length. The basal ages of 17 cores were used to explore the lateral expansion processes, while two more continuous peat profiles (LLK17C and LLK-D-2019) of these cores were used to calculate the CAR and to reconstruct moisture/precipitation. Core LLK17C (499 cm in length) was

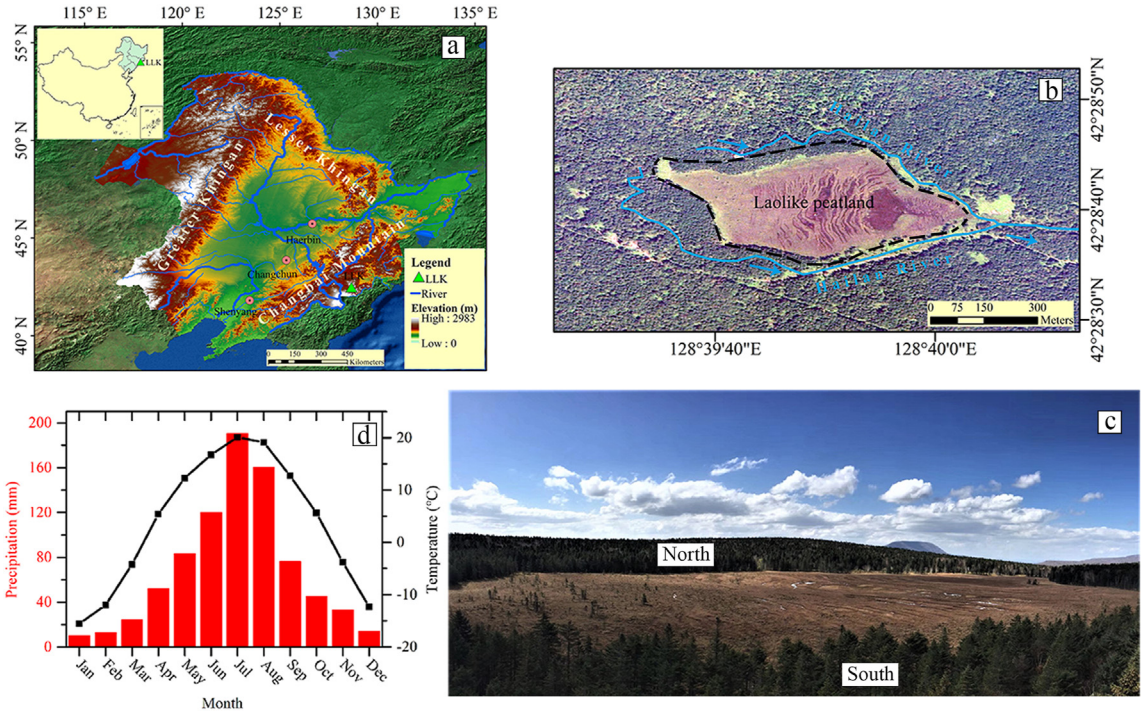

Fig. 1. (a) Map showing the location of the Laolike peatland in the Changbai Mountains, NE China (LLK: Laolike peatland). (b) Remote sensing image of the Laolike peatland. (c) Overlooking the Laolike peatland. (d) Temperature and precipitation characteristics of the Laolike peatland. The values shown are mean monthly temperature and precipitation as recorded by the Donggang station from 1957 to 2014.

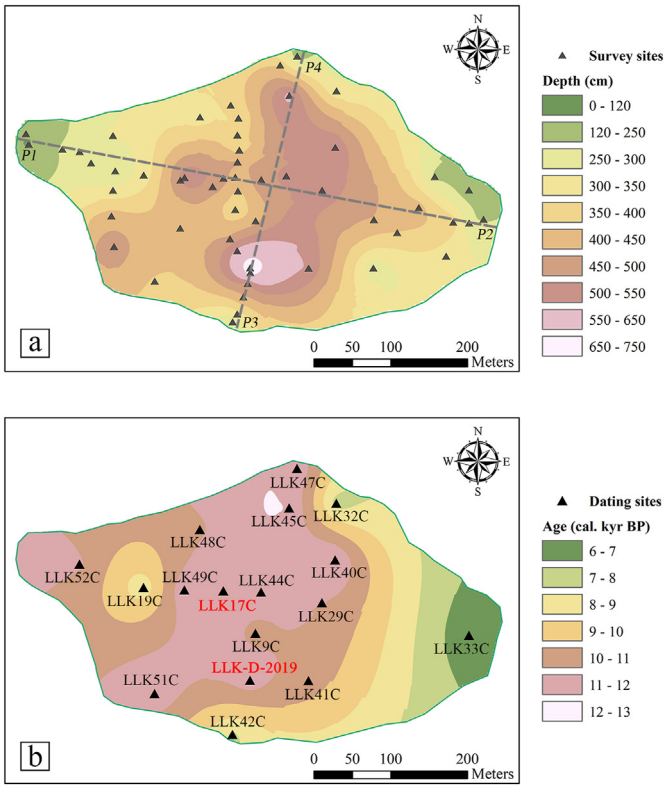

Fig. 2. (a) Peat thickness distribution and (b) pattern of peatland lateral expansion of the Laolike peatland. *P1—P2* and *P3—P4* in (a) refer to the starting point and terminus of the section line from the west to the east and from south to north, respectively. The gray dotted line in (a) refers to the section line shown in Fig. S6.

obtained near the center of the peatland and core LLK-D-2019 (750 cm in length) was obtained from the south of the peatland (Fig. 2b). After recording the sedimentary features and photographing each core (Supplementary Figs. S1—S3), all cores were segmented at an interval of 1 cm on-site, with all samples then put into labeled plastic zipper bags and taken to the laboratory for preservation.

3.2. Laboratory methods

3.2.1. Dating and depth-age modeling

The upper 28 cm of samples from core LLK17C were dated by ^{210}Pb and ^{137}Cs methods. These samples were first dried and ground, and then put into 7 ml centrifugal tubes and weighted before being sealed with sealing film. The activity of $^{210}Pb_{ex}$ and ^{137}Cs was directly measured using an ORTEC High-Purity Germanium (HPGe) Well Detector. The chronology for these sections was calculated using the constant rate of supply (CRS) model of $^{210}Pb_{ex}$ and validated with ^{137}Cs time markers. The dating results of the upper 28 cm in LLK17C are presented in Supplementary Fig. S4.

The ages from the core LLK-D-2019, basal peat samples from the 15 other cores, and the lower layer of core LLK17C were determined using accelerator mass spectrometry ^{14}C (AMS^{14}C). The layers in cores LLK17C and LLK-D-2019 with obvious changes of sedimentary features or organic carbon content were selected as the dating points. The basal peat samples of each core were determined according to the loss on ignition (LOI) and dry bulk density (DBD) methods, where we define basal peat as when the LOI is more than 30 % (Chai, 1990) (Supplementary Fig. S5). For most dating samples, *Sphagnum*, seeds, or above-ground parts of herbaceous plants were carefully hand-picked as the dating materials (Table 1), but bulk peat was also used for some highly decomposed samples.

All the AMS^{14}C dating samples were pretreated by standard acid-alkali-acid (Olsson, 1986), then freeze-dried in an ultra-low

Table 1
Radiocarbon dating (AMS14C) results for the cores LLK17C and LLK-D-2019 and the basal peat samples from this study.

Core	Sample code	Lab number	Depth (cm)	Material dated	^{14}C age ± error (yr BP ± yr)	Calibrated age (2σ range) (cal. yr BP)	Mean calibrated age (cal. kyr BP)
Basal sample	LLK9C	NENUR10647	425	Bulk sample	9452 ± 82	10,499–10,900	10.7
	LLK19C	NENUR10648	310	Bulk sample	7531 ± 78	8177–8461	8.3
	LLK29C	NENUR10649	520	Bulk sample	9683 ± 84	10,990–11,242	11.1
	LLK32C	NENUR10650	304	Bulk sample	6720 ± 72	7466–7685	7.6
	LLK33C	NENUR10651	248	Herb	5436 ± 70	6164–6324	6.2
	LLK40C	NENUR10652	550	Bulk sample	10,281 ± 80	11,811–12,474	12.1
	LLK41C	NENUR10653	517	Herb	9392 ± 86	10,339–10,815	10.6
	LLK42C	NENUR10654	230	Bulk sample	6996 ± 71	7683–7958	7.8
	LLK44C	NENUR10655	498	Bulk sample	9997 ± 82	11,248–11,758	11.5
	LLK45C	NENUR10656	590	Bulk sample	10,226 ± 79	11,614–12,201	11.9
	LLK47C	NENUR10657	193	Herb	10,192 ± 97	11,401–12,195	11.8
	LLK48C	NENUR10658	325	Herb	9484 ± 80	10,561–11,106	10.8
	LLK49C	Beta-594,671	573	Bulk sample	10,140 ± 30	11,688–11,886	11.8
	LLK51C	NENUR10660	396	Bulk sample	10,112 ± 77	11,391–11,946	11.7
	LLK52C	Beta-594,672	274	Bulk sample	9650 ± 30	11,068–11,188	11.1
LLK17C	LLK17C-1	NENUR10411	34	Herb	303 ± 62	271–502	0.4
	LLK17C-2	NENUR10412	50	Herb	512 ± 66	450–654	0.6
	LLK17C-3	NENUR10413	70	Herb	1199 ± 63	971–1274	1.1
	LLK17C-4	NENUR10414	92	Herb	1906 ± 65	1700–1993	1.8
	LLK17C-5	NENUR10415	112	Herb	2083 ± 69	1869–2182	2.0
	LLK17C-6	NENUR10416	129	Seed	2464 ± 78	2356–2726	2.5
	LLK17C-7	NENUR10417	136	Herb	2931 ± 69	2880–3254	3.1
	LLK17C-8	NENUR10418	150	Seed and Leaf	3333 ± 69	3441–3721	3.6
	LLK17C-9	NENUR10419	167	Herb	3757 ± 66	3962–4302	4.1
	LLK17C-10	NENUR10420	196	Herb	4211 ± 66	4530–4870	4.7
	LLK17C-11	NENUR10421	216	Herb	4466 ± 77	4876–5309	5.1
	LLK17C-12	NENUR10422	231	Seed	5093 ± 69	5658–5947	5.8
	LLK17C-13	NENUR10423	249	Seed	5257 ± 73	5903–6208	6.1
	LLK17C-14	NENUR10425	274	Leaf	6040 ± 77	6731–7079	6.9
	LLK17C-15	NENUR10426	292	Seed	6371 ± 70	7166–7425	7.3
	LLK17C-16	NENUR10427	309	Herb	6532 ± 74	7311–7573	7.4
	LLK17C-17	NENUR10428	321	Seed	7045 ± 91	7689–8016	7.9
	LLK17C-18	NENUR10429	359	Seed	7444 ± 80	8162–8391	8.3
	LLK17C-19	NENUR10430	371	Herb	7713 ± 104	8328–8780	8.6
	LLK17C-20	NENUR10431	395	Seed	8182 ± 74	8994–9326	9.2
	LLK17C-21	NENUR10432	415	Seed and Leaf	8893 ± 77	9711–10,211	10.0
	LLK17C-22	NENUR10433	431	Seed and Leaf	9623 ± 77	10,735–11,197	11.0
	LLK17C-23	NENUR10435	478	Seed	9807 ± 109	11,064–11,626	11.3
	LLK17C-24	NENUR10342	490	Herb	10,100 ± 86	11,311–11,946	11.6
LLK-D-2019	LLK-D-2019-1	NENUR10723	50	Herb	379 ± 83	284–545	0.4
	LLK-D-2019-2	NENUR10724	75	Seed	1120 ± 85	903–1191	1.0
	LLK-D-2019-3	NENUR10725	125	Herb	2391 ± 101	2301–2737	2.5
	LLK-D-2019-4	NENUR10726	175	Herb	3340 ± 86	3390–3731	3.6
	LLK-D-2019-5	NENUR10727	234	Seed and Leaf	4486 ± 87	4866–5323	5.1
	LLK-D-2019-6	NENUR10728	306	Bulk sample	4856 ± 91	5443–5755	5.6
	LLK-D-2019-7	NENUR10729	331	Bulk sample	5081 ± 86	5646–5996	5.8
	LLK-D-2019-8	NENUR10730	394	Herb	5374 ± 94	5934–6312	6.1
	LLK-D-2019-9	NENUR10731	430	Herb	5850 ± 90	6446–6888	6.7
	LLK-D-2019-10	NENUR10732	482	Bulk sample	6026 ± 88	6671–7076	6.9
	LLK-D-2019-11	NENUR10733	524	Herb	6861 ± 92	7571–7870	7.7
	LLK-D-2019-12	NENUR10735	618	Herb	7952 ± 97	8546–9027	8.8
	LLK-D-2019-13	NENUR10736	662	Seed	9652 ± 145	10,572–11,347	11.0
	LLK-D-2019-14	NENUR10738	736	Bulk sample	10,037 ± 108	11,246–11,886	11.6

temperature vacuum. The graphite target was prepared in a high-vacuum graphite target synthesis system at the Northeast Normal University. The AMS ^{14}C dating was carried out in the NTUAMS ^{14}C dating lab at the National Taiwan University and Beta Analytic. All ^{14}C ages of the basal peat samples were calibrated online using the OxCal 4.4 calibrate tool with the IntCal20 curve (Reimer et al., 2020). The depth-age models for the LLK17C and LLK-D-2019 cores were constructed using the Bacon model (Blaauw and Chriaten, 2011) with the rbacon package (Blaauw et al., 2020) in the R statistical software.

3.2.2. Cellulose extraction and stable isotope analysis

The α-cellulose was extracted at intervals of 1 cm from the LLK17C core to determine the stable carbon isotope composition (δ^{13}C). The extraction method following Daley (2007) was employed. A mixed solution of sodium chlorite ($NaClO_2$), glacial acetic acid (CH_3COOH), and sodium hydroxide alkali (NaOH) was used to extract the α-cellulose. To avoid interference from ligneous residues and roots on the stable isotope signals as much as possible, visible non-herbaceous plant residues and roots were removed before the process of cellulose extraction.

Samples of 70–90 μg cellulose were used for the stable carbon

isotope analysis. After wrapping the samples in foil paper cups, the $\delta^{13}C$ was determined using an isotope mass spectrometer (Thermo Fisher—Delta V Advantage). L-Glutamic Acid ($C_5H_9NO_4$) was used as the standard material, with the measurement precision being less than 0.15 ‰. Samples and standard material were measured repeatedly at an interval of 5 cm along the profile for accuracy control. The results showed that the systematic error was less than 0.2 ‰ and 0.15 ‰ in the repeated sample and standard material measurements, respectively.

3.2.3. Peat characteristics and carbon accumulation rates

Samples of 2 cm^3 of undisturbed peat were taken from each layer of the LLK17C and LLK-D-2019 cores and dried under 105 °C, then the DBD was calculated. The dried peat was then grounded and sieved through a 100-mesh sieve for total organic carbon content (TOC) analysis, which was done using an element analyzer (EURO VECTOR EA3000). All 499 sub-samples from the LLK17C core and odd-numbered samples from the LLK-D-2019 core were measured for TOC. Each sample from the LLK17C core was measured three times and the odd-numbered samples in core LLK-D-2019 were measured once. The measurement method of LOI in this study followed Li et al. (2017), where the LOI was calculated after 4 h ignition in a muffle furnace at 550 °C. The LOI analysis was only conducted for even-numbered samples from core LLK-D-2019. The CAR was calculated by the following equation:

$$CAR = r/1000 \times c \times d \quad (1)$$

where *CAR* represents the carbon accumulation rate (g $C/m^2/yr$), *r* is the rate of peat accretion (mm/yr), *c* is the total organic carbon content (g C/g dry weight), and *d* is dry bulk density (g/m^3). The CAR was calculated for each depth of LLK17C core and odd-numbered depth of LLK-D-2019. Additionally, the time-weighted CAR was also calculated for each core at a 100-years interval.

3.2.4. Grain size analysis

The samples used to calculate the LOI for core LLK-D-2019 were transferred to a quartz crucible and heated to 105 °C under an electric heating plate. Then, a small amount of hydrogen oxide (H_2O_2) solution was added to the crucible as many times as necessary until no bubbles were generated, then a small amount of 10 % hydrochloric acid (HCl) was added, again until no bubbles were generated. After the crucible cooled, the samples were transferred to a 15 ml plastic centrifuge tube, centrifuged, and cleaned to pH neutral. Finally, about 5 ml of 0.06 mol/L sodium hexametaphosphate solution ($(NaPO_3)_6$) was added and then vibrated in an ultrasonic oscillator for more than 2 h. The grain size was measured using the laser particle size analyzer (MICROTRAC S3500). The percentages of sand (>64 μm), silt (4–64 μm), and clay (<4 μm) were then calculated.

4. Results

4.1. Peatland lateral expansion and vertical accretion

Peat formation was first initiated at several separate depressed parts of the study site around the end of the last deglacial period (Table 1), then expanded laterally outward, especially towards an east-west direction, and reached its maximum area (0.15 km^2) around 6 cal kyr BP (Fig. 2b). The lateral expansion rate was highest between 12 and 10 cal kyr BP (0.03 km^2/kyr), followed by a decrease to 0.01 km^2/kyr during the period 9 to 6 cal kyr BP.

The AMS^{14}C dating of the cores revealed that peat formation was initiated almost simultaneously at cores LLK17C and LLK-D-2019 during the Holocene (Fig. 3), although the vertical accretion rates for the two cores were not consistent (Figs. 4c–5c). The relatively high mean peat accretion rates of 0.7 mm/yr in LLK-D-2019 resulted in thicker peat deposition than the 0.5 mm/yr rates inferred for core LLK17C. In addition, the peat accretion rates in LLK17C fluctuated more frequently than for LLK-D-2019. For core LLK17C, the peat accretion rates were higher during the periods 11.6 to 10.8 cal kyr BP, 8.2 to 6.8 cal kyr BP, 2.1 to 1.8 cal kyr BP, and the last 150 years. For LLK-D-2019, the peat accretion rate increased between 10.6 and 5.8 cal kyr BP, then decreased after 5.8 cal kyr BP.

4.2. Carbon accumulation rate

Generally, DBD and TOC varied moderately within core LLK17C and severely in core LLK-D-2019, and there were different characteristics of CAR between the two cores. The DBD ranged between 0.02 and 0.76 g/cm^3, with an average of 0.17 g/cm^3 in the LLK17C core (Fig. 4a), and between 0.02 and 0.93 g/cm^3 with an average of 0.3 g/cm^3 in core LLK-D-2019 (Fig. 5a). TOC was different between the two cores before 4.4 cal kyr BP, where for LLK17C it varied between 11.7 % and 57.1 % with an average of 46 % (Fig. 4b), while for LLK-D-2019 it was 5.5 %–57.7 % with an average of 32.3 % (Fig. 5b). There was extreme variation with the lowest TOC before 4.4 cal kyr BP in LLK-D-2019, after which it was generally consistent with LLK17C. The TOC in LLK17C was low and showed an increasing trend before 9 cal kyr BP and peaked during the period 9 to 7.5 cal kyr BP (Fig. 4b).

The CAR ranged between 9.5 and 147.7 g $C/m^2/yr$ with an average of 31.1 $C/m^2/yr$ in LLK17C (Fig. 4d) and between 14.2 and 119.8 g $C/m^2/yr$ with an average of 52.9 g $C/m^2/yr$ in LLK-D-2019 (Fig. 5d). There were obvious differences in CAR between the two cores between 11.6 and 4.4 cal kyr BP and had similar variation after 4.4 cal kyr BP. Particularly, CAR in LLK17C increased gradually from 10 cal kyr BP until high values were maintained during the period 8.2 to 6.8 cal kyr BP. It then decreased rapidly from 7 cal kyr BP and showed the lowest values during the period 7 to 4.4 cal kyr BP. CAR in LLK-D-2019 decreased until 7.3 cal kyr BP, but had high values between 7 and 4.4 cal kyr BP, which differed from the situation in LLK17C.

4.3. Stable carbon isotope

The $\delta^{13}C$ sequence in LLK17C ranged from −29.5 ‰ to −22.8 ‰ with an average of −25.1 ‰ during the Holocene (Fig. 4e). The variations in $\delta^{13}C$ can be divided into three stages: stage A (11.7–9 cal kyr BP) was characterized by low and gradually increasing $\delta^{13}C$ values from −29.5 ‰ to −24 ‰ with an average of −26.7 ‰. Stage B (9–4.5 cal kyr BP) was marked by an obvious increase of $\delta^{13}C$ from −27.9 ‰ to −22.8 ‰ and an average of −24.8 ‰. The lowest value of $\delta^{13}C$ occurred between 7 and 6 cal kyr BP. During stage B, the $\delta^{13}C$ was still higher but fluctuated more frequently than during the previous stage. Stage C (the last 4.5 cal kyr) was characterized by high and stable $\delta^{13}C$ values that ranged between −25.7 ‰ and −22.9 ‰, with an average of −24.4 ‰.

4.4. Grain size characteristics

The dominant components of the peat ash in core LLK-D-2019 were silt and sand (Fig. 5e–f). The percentage of silt ranged from 45.2% to 93.7 % with an average of 80.1 %, increasing over the Holocene with two abrupt decreases occurring between 8.6 and 8.1 cal kyr BP and 5.8 and 5 cal kyr BP (Fig. 5e). The sand content varied from 0.4 % to 54.4 % with an average of 15.1 % and was higher from 10.6 to 4.5 cal kyr BP (Fig. 5f). However, clay content showed a lower percentage during this period (Fig. 5e). The mean grain size

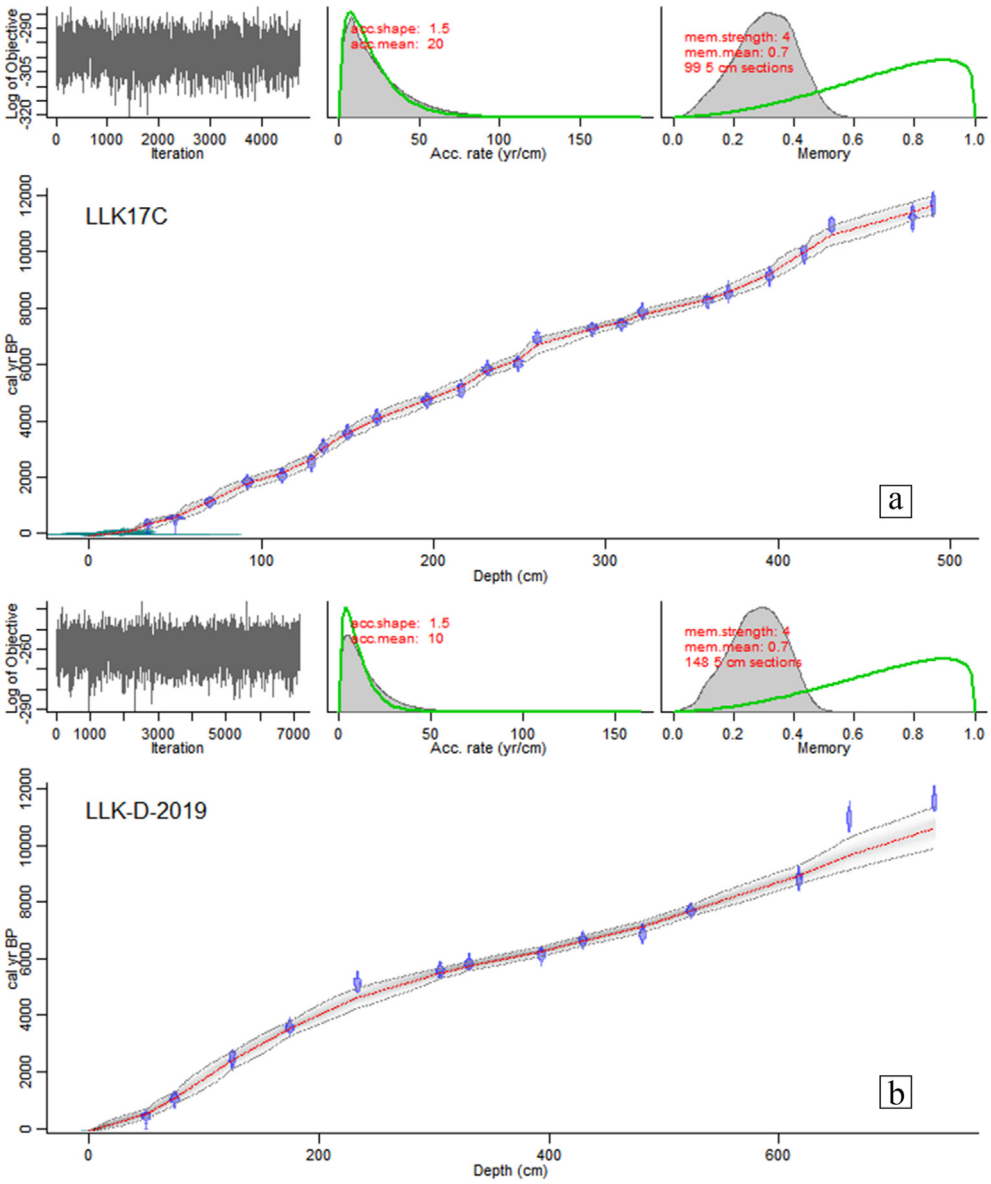

Fig. 3. Age-depth models produced by the BACON approach in R software tool for cores (a) LLK17C and (b) LLK-D-2019.

of peat ash ranged from 9 μm to 102.1 μm with an average of 31.4 μm through the Holocene, which was consistent with the variations in sand content (Fig. 5f).

5. Discussion

5.1. Moisture variations

5.1.1. Paleoclimate interpretation of $\delta^{13}C$ and grain size

In some previous studies, the $\delta^{13}C$ of peat cellulose was considered to be an effective indicator of surface effective moisture/precipitation in peatlands (Hong et al., 2003; Roland et al., 2015; Zhang et al., 2018). Here, we attempt to follow this argument that more negative values of $\delta^{13}C$ correspond to wetter peatland conditions and vice versa. This can be validated by the grain size of the peat ash (Figs. 4e–5f).

Grain size analysis of sediments is an important means to distinguish sedimentary conditions and environmental variation (Bao et al., 2010; Li et al., 2017). Different depositional patterns may have various grain size compositions and display different environmental indicators (Li et al., 2017). We suggest that the size of inorganic particles in the LLK-D-2019 core is mainly controlled by the strength of runoffs, as suggested by the following. 1) Sand dunes are densely distributed in the western part of NE China and far from the study area, where the vegetation is mixed coniferous and broadleaf forest. 2) The Laolike peatland is located in a small, but broad and shallow depression on the top of a watershed at an altitude of more than 1400 m (Fig. 1b). The favorable landform, together with abundant precipitation, allows the runoff from the south, north, and east to flow easily into the peatland carrying silt and sand particles. Therefore, we assume that the mean diameter (Mz) and sand content of the peat ash can be taken as a proxies for precipitation in the Laolike peatland. The coarser particles and higher sand content indicate more precipitation, resulting in more abundant surface runoff and stronger flow dynamics, while finer particles and lower sand content indicate a lower level of precipitation.

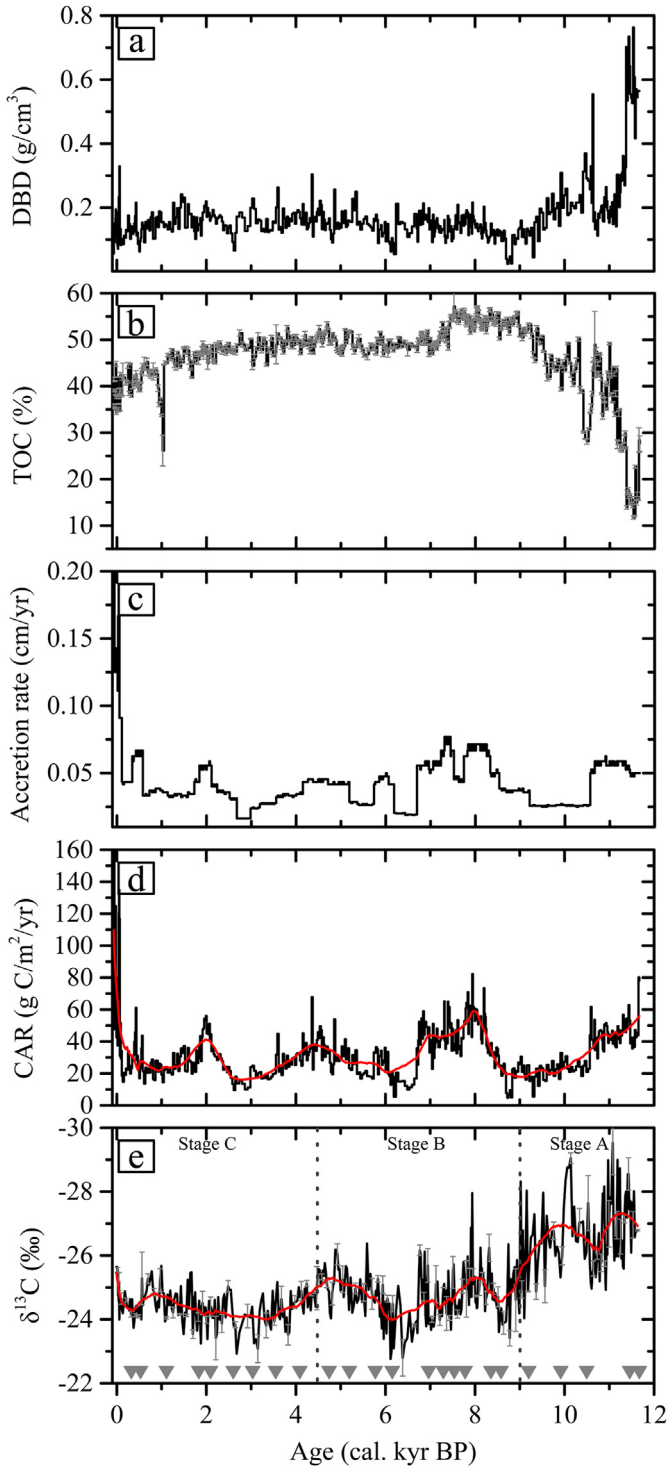

Fig. 4. Peat characteristics of the core LLK17C. (a) Dry bulk density (DBD). (b) Total organic carbon content (TOC). (c) Peat vertical accretion rate. (d) Carbon accumulation rate (CAR). (e) $\delta^{13}C$. The gray inverted triangle indicates the AMS^{14}C dating point. The red lines in (d) and (e) indicate the CAR and $\delta^{13}C$ after smoothing, respectively. (For interpretation of the references to colour in this figure legend, the reader is referred to the Web version of this article.)

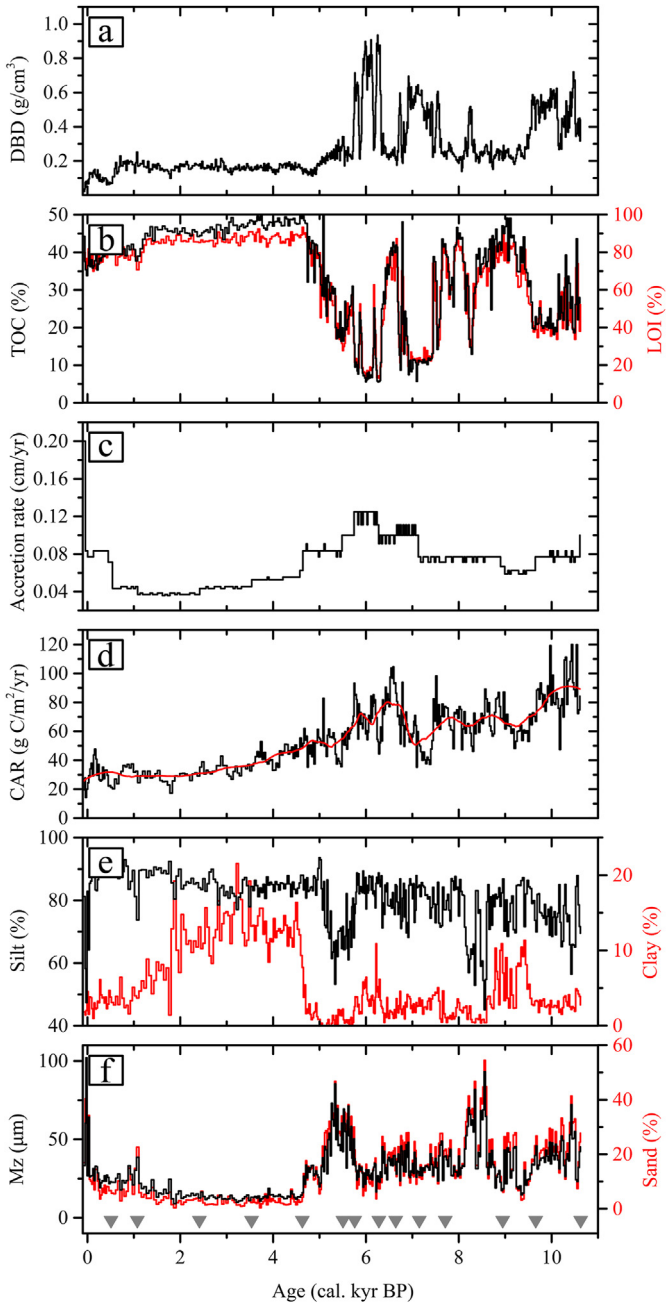

Fig. 5. Peat characteristics of the core LLK-D-2019. (a) Dry bulk density (DBD). (b) Total organic carbon (TOC) and loss on ignition (LOI). (c) Peat vertical accretion rate. (d) Carbon accumulation rate (CAR). (e) The silt and clay content. (f) The content of sand and mean diameter of peat ash (Mz). The gray inverted triangle indicates the AMS^{14}C dating point. The red line in (d) indicates the CAR after smoothing. (For interpretation of the references to colour in this figure legend, the reader is referred to the Web version of this article.)

5.1.2. *Moisture variation in laolike peatland*

Our $\delta^{13}C$ and grain size records from the Laolike peatland showed almost uniform synchronous changes (Figs. 4e–5f). The wettest conditions occurred during the early Holocene (12–9 cal kyr BP), followed by a decrease in peatland wetness, although there were still wet conditions during the middle Holocene (9–4.5 cal kyr BP), with the driest conditions during the late Holocene (the last 4.5 cal kyr).

The moisture changes in the Laolike peatland through the Holocene have been supported by many other paleoclimate records from NE China. The $\delta^{13}C$ sequence of the Hani peatland showed their lowest values during the early Holocene and an increasing trend until 5 cal kyr BP, suggesting wetter conditions during the

early to middle Holocene (Hong et al., 2003, 2005). Total nitrogen (TN) and C/N ratios of lacustrine depositions in the Erlongwan Maar lake were high between 11.4 and 9.1 cal kyr BP, together with coarse sediments, reflecting a warm-wet climate with abundant precipitation (You and Liu, 2012). At the Gushantun peatland, pollen data shows that *Betula* increased around 11.3 cal kyr BP, and percentages of broadleaved trees such as *Quercus*, *Ulmus*, *Alnus*, *Juglans*, and *Corylus* were high between 11.3 and 4.4 cal kyr BP (Liu, 1989). Pollen records from the Qindeli peatland also show that deciduous broadleaved forest trees, including *Ulmus*, *Quercus*, *Salix*, *Carpinus*, and *Corylus*, thrived from 10 to 5.5 cal kyr BP, indicating high levels of effective moisture during the growing season (Xia, 1988). Pollen diagrams from the Jinchuan peatland have a similar pattern as those from the Qindeli peatland, with a steady high percentage of broadleaved trees (such as *Quercus*, *Ulmus,* and *Juglans*) growing between 11.5 and 6/5 cal kyr BP (Jiang et al., 2008).

5.2. Peatland development and climate forcing

5.2.1. High lateral expansion rate and CAR during the early holocene

In general, peatland lateral expansion occurs in two different ways: terrestrialization, where a water body is filled with sediments and peat, and paludification, where dryland is converted to peatland due to rising water levels. This sees the basal peat being younger towards the peatland's edge as a result of paludification, while terrestrialization leads to younger basal peat towards the center (Charman, 2002). According to the basal ages of the 17 cores from the Laolike peatland, we assumed that the peatland initiated at several separate points and gradually connected under the process of paludification (Supplementary Fig. S6). The peat appears to have initiated first in the north of the center of the peatland and then expanded rapidly towards the center of the peatland (more depressed part) between 12 and 10 cal kyr BP, followed by expansion to the east and west at 10 cal kyr BP, but is mainly concentrated in the eastern part. However, there was a weak relationship between basal ages and peat thickness (Fig. 2a–b), where the western part of the peatland had almost the oldest basal ages, but had relatively shallow peat thickness compared to the central part, which might result from inconsistent peat accumulation rates at different locations of the peatland.

The highest lateral expansion rate in the Laolike peatland occurred during the early Holocene (12–9 cal kyr BP) (Fig. 6a), corresponding to the high prevalence of peatland formation in the northern peatlands (MacDonald et al., 2006) (Fig. 6b), northern peatlands in China (Fig. 6c) (Zhao et al., 2014), NE China (Fig. 6d) (Xing et al., 2015b), and the Qinghai-Tibetan Plateau (Fig. 6e) (Wang et al., 2014). Meanwhile, the CAR in the Laolike peatland showed similar patterns in terms of peak timing. The CAR in core LLK-D-2019 was high during the early to middle Holocene and low after 6 cal kyr BP (Fig. 7b), corresponding well with the high CAR found in the northern peatlands (Fig. 7c) (Yu et al., 2009). The similar patterns of peatland development in the Laolike peatland and northern peatlands during the Holocene reflects the consistent climate forcing for peatland development in these areas.

High summer insolation and the greater climate seasonality have been suggested as the main reasons for the high rate of peatland expansion and carbon accumulation during the Holocene in the northern peatlands (Yu et al., 2009, 2010;Jone and Yu, 2010). Hence, a similar mechanism might have applied to the Laolike peatland's development. After the Younger Dryas (YD), the summer insolation in the Northern Hemisphere and the temperatures in NE China recovered rapidly (Fig. 7e–f) (Berger and Loutre, 1991; Stebich et al., 2015). The high summer insolation and temperatures during the early Holocene would increase the length of the growing season, leading to higher net primary productivity (NPP) (Charman et al., 2013). In addition, the maximum summer and minimum winter insolation during that time might lead to increased productivity in warmer summers and reduced decomposition in colder seasons. While high temperatures during warmer summers would increase the rate of peat decomposition through accelerated microbial activity (Ise et al., 2008; Dorrepaal et al., 2009), the variability in NPP has a greater role in determining long-term carbon accumulation than decomposition (Charman et al., 2013; Xing et al., 2015a). Furthermore, in accordance with the strong EASM (Fig. 6f) (Dykoski et al., 2005), the $\delta^{13}C$ and grain size of peat ash in the Laolike peatland reveals conditions being wettest during the early Holocene (Fig. 7a). High moisture/precipitation conditions would

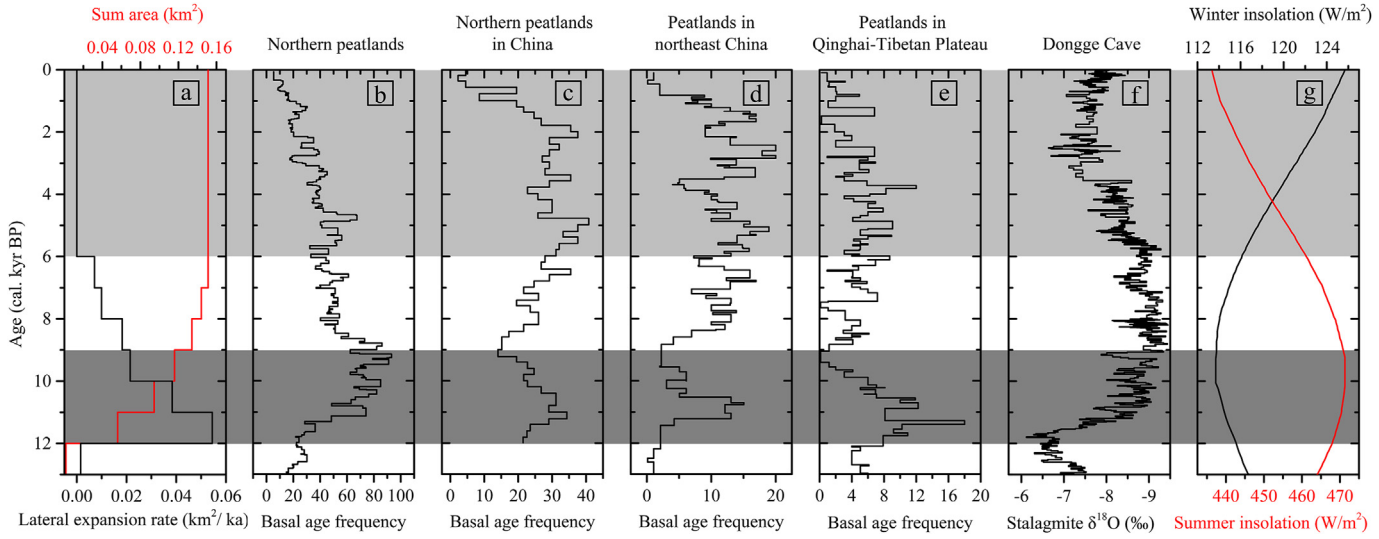

Fig. 6. (a) Lateral expansion rates and total area of the Laolike peatland during the Holocene. Frequency of peat basal dates from (b) the Northern peatlands (MacDonald et al., 2006), (c) Northern peatlands in China (Zhao et al., 2014), (d) NE China (Xing et al., 2015b), and (e) the Qinghai-Tibetan Plateau (Wang et al., 2014). (f) Oxygen isotope record from the Dongge Cave, southern China (Dykoski et al., 2005). (g) Summer and winter insolation curves at 60°N (Berger and Loutre, 1991). The dark and light gray shaded areas in the background indicate high and low rates of lateral expansion in the Laolike peatland, respectively.

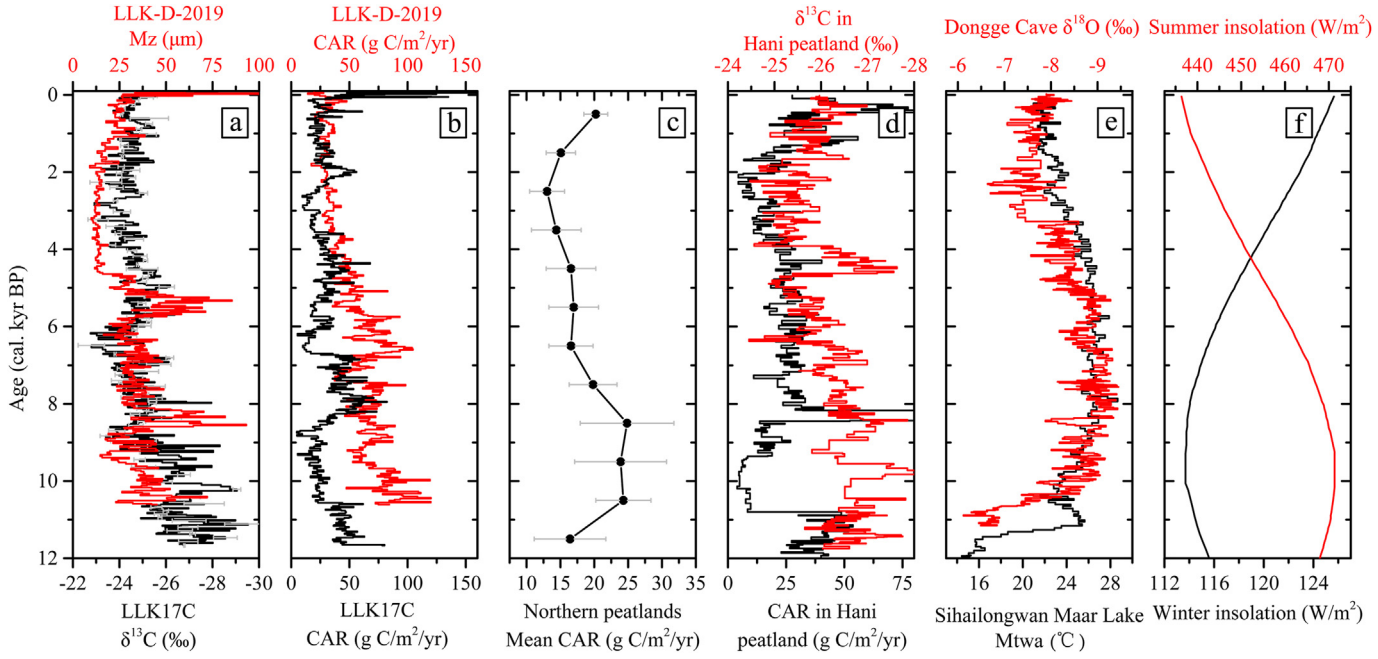

Fig. 7. The corresponding relationships between $\delta^{13}C$, Mz and CAR for the Laolike peatland and regional comparisons. (a) $\delta^{13}C$ and Mz for the Laolike peatland. (b) CAR from the cores LLK17C and LLK-D-2019. (c) Mean CAR from the northern peatlands (Yu et al., 2009). (d) $\delta^{13}C$ and CAR from the Hani peatland (Hong et al., 2005; Cai et al., 2013). (e) Oxygen isotope record from the Dongge Cave, southern China (Dykoski et al., 2005), and reconstructed temperatures (July) for Sihailongwan Maar lake (Stebich et al., 2015). (f) Summer and winter insolation curves at 60°N (Berger and Loutre, 1991).

promote plant growth and decreased peat decomposition, resulting in long-term peatland expansion and carbon accumulation (Charman et al., 2013; Lupascu et al., 2014; Panait et al., 2017).

In summary, peatland lateral expansion and CAR in the Laolike peatland showed consistent variation characteristics during the Holocene. The high lateral expansion rate and CAR values correspond to the high summer insolation, climate seasonality, regional temperatures, and the strong EASM, indicating the primary role of climatic conditions in the development of the Laolike peatland over multi-millennium timescales.

5.2.2. Consistency between moisture/precipitation and CAR over millennium scales

There were almost simultaneous variations between the CAR and the moisture/precipitation as identified in core LLK17C during the Holocene. The high CAR during the period 12 to 10.5 cal kyr BP corresponded to the wettest conditions and the decreasing CAR between 12 and 8.4 cal kyr BP is well correlated with the decreasing moisture/precipitation conditions during that period. There was higher CAR but lower moisture conditions during the period 8.2 to 6.8 cal kyr BP than during the early Holocene. The lowest CAR values are between 7 and 6 cal kyr BP corresponded to the driest conditions of the peatland during the Holocene (Fig. 7a–b). In addition, the low CAR during the periods 8.8 to 8.5 cal kyr BP and 3 to 2.6 cal kyr BP also corresponded to the dry conditions. These characteristics indicated that regional moisture/precipitation might play a key role in CAR over millennium timescales.

In addition to extending the length of the growing season and improving the productivity of the peatland, the increase in temperatures will also promote evaporation from the peatland, possibly resulting in dry conditions for the peatland's surface and the enhancement of microbial activity (Gillooly et al., 2001), which will lead to the aggravation of decomposition and the reduction of CAR (Gorham, 1991;McGuire et al., 2006). The increasing summer insolation, climate seasonality (Berger and Loutre, 1991), and temperature in NE China had the potential to result in high evaporation levels between 12 and 8.4 cal kyr BP in the Laolike peatland, but it may have been offset by the increasing regional precipitation. In this regard, effective moisture/precipitation is more important than total precipitation and has been validated by the $\delta^{13}C$ values. High effective moisture/precipitation conditions could promote the growth of plants in the peatland and inhibit decomposition. The increasing summer insolation, climate seasonality, and temperatures contributed to the higher CAR values during the early Holocene, but the effective moisture/precipitation regulated the variation of CAR during that time. The climate during the period 8.2 to 6.8 cal kyr BP was drier than during the early Holocene, but it was still wetter than for the rest of the Holocene (Fig. 7a). However, the CAR during the early Holocene was lower than that during the period 8.2 to 6.8 cal kyr BP, indicating that the influence of moisture/precipitation on CAR is complicated.

There were consistent variations in CAR and moisture/precipitation after 4.4 cal kyr BP (Fig. 7a–b). However, the CAR variations also corresponded to the decreasing summer insolation, climate seasonality, and lower temperatures across NE China (Fig. 7e–f). The low CAR might have resulted from the combination of low moisture/precipitation and low temperatures that induced a decreased NPP of the peatland and increased decomposition due to deeper acrotelm under the lower water table (Fig. 7a). Although winter insolation was high during that time (Fig. 7f), but organic production and decomposition during the cold seasons were almost negligible (Charman et al., 2013, 2015).

To verify this relationship between moisture/precipitation and CAR as revealed by the Laolike peatland, we examined this phenomenon at the Hani peatland, which is located 180 km away (Cai et al., 2013). The consistent variation of CAR and moisture/precipitation indicated a similar situation also occurred in the Hani peatland (Fig. 7d) (Cai et al., 2013; Hong et al., 2005), with increasing CAR that corresponded to increasing moisture/precipitation between 12 and 11 cal kyr BP. There were also consistent

variations in CAR and moisture/precipitation over the last 6 cal kyr BP, where the low CAR between 11 and 8.5 cal kyr BP possibly resulted mainly from volcanic ash deposition and unstable climatic conditions (Fig. 7d) (Cai et al., 2013; Hong et al., 2005). The results further confirmed that moisture/precipitation may be the primary control of CAR in these peatlands over millennium timescales.

5.3. Peatland development and local conditions

5.3.1. Topography and lateral expansion of the peatland

Previous studies have suggested that local conditions, such as topography, hydrology, slope, substrate, etc., are the main factors determining the lateral expansion of peatlands (Mäkilä, 1997;Mäkilä and Moisanen, 2007; Korhola, 1992). Such constraints, particularly the topography and associated hydrology, played an important role in the development of the Laolike peatland in terms of the location of peatland initiation, the direction of its lateral expansion, and the resulting extent of the peatland.

Early phases of peat accumulation appear to have been influenced by local environmental factors to a much greater extent, especially during fen peat development and early-stage succession (Holmquist and Macdonald, 2014). The peatland formation was initiated first at cores LLK49C (11.8 cal kyr BP) and LLK45C (11.9 cal kyr BP) rather than at the lowest-lying parts of the peatland (such as at cores LLK29C and LLK-D-2019) (see in Supplementary Fig. S6). We assumed this phenomenon might have resulted from the lowest-lying location of the peatland still being covered by ice due to lower temperatures during the YD, or that it was water-logged due to the melting ice/snow and increasing precipitation. The relatively flat topographic conditions at the other depressed parts (such as around cores LLK45C and LLK49C) might have led to moderate water conditions due to their relatively high locations compared to cores LLK29C and LLK-D-2019.

Independent of the peatland initiation processes, all peatlands may subsequently expand horizontally onto the surrounding land, which occurs when marginal areas of the peatlands become waterlogged due to excess water running off from the peatland surface or the surrounding area (Ruppel et al., 2013; Charman, 2002). Peatland lateral expansion in Laolike was concentrated in an east-west direction (Fig. 2b), which might be attributed to the direction of runoff of the peatland and the slope. There was runoff from west to east through the peatland due to the higher elevations to the west, north, and south (Fig. 2a). The sufficient water supply in the direction of runoff could facilitate peat formation and its lateral expansion, while the water needed for the expansion of the peatland in the north-south direction mainly came from runoffs from the east-west direction. In addition, the slope in the east-west direction is gentler than that in the north-south direction, making it more conducive to lateral expansion (Fig. 2a).

The Laolike peatland reached its present coverage at around 6 cal kyr BP, and may have been influenced by the steep slope along the margin of the peatland and its surroundings (Fig. 2b). The steep slopes at the northern and southern margins limit the lateral expansion of the peatland (Makila and Moisanen, 2007). Although there are low-lying topographic features and a gentle slope to the east of the peatland, it existed as an outfall of the peatland over the Holocene and the frequent runoff from the peatland made it unsuitable for peat accretion. Furthermore, the rivers around the north, south and west of the peatland may make it difficult to expand outwards, while the newly formed peat in the margin of the peatland might be washed away by floods during the rainy seasons, where field observations show that the margin of the peatland has been eroded.

5.3.2. Topographic influence on the internal differences of CAR

There were internal differences in the peat properties and CAR patterns under the same climatic conditions during the early to middle Holocene, indicating local conditions might also play an important role in determining long-term CAR over local scales.

The time-weighted CAR was 31.1 g C/m^2/yr (ranging from 9.5 to 147.7 g C/m^2/yr) in core LLK17C (Fig. 8b), while it ranged from 14.2 to 119.8 g C/m^2/yr (with an average of 52.9 g C/m^2/yr) in core LLK-D-2019. Such differences in CAR within a peatland are difficult to explain by climatic influences alone, hence, differences in local conditions (such as topography and hydrology) between these cores may also contribute to this situation.

Core LLK-D-2019 is located in the lowest-lying part of the peatland (Fig. 2a and Supplementary Fig. S6), which might be more frequently influenced by surface runoff. This was confirmed by the variations in DBD and TOC (Fig. 8d and e). The severe variations in DBD and TOC before 5 cal kyr BP indicate an increasing strength and frequency of runoffs. This location might, therefore, receive allogenic organic materials from surrounding forests or other locations of the peatland. Although TOC was low during that time, the higher vertical accretion rates (Fig. 8c) resulting from increasing runoffs could promote a higher CAR in LLK-D-2019 than LLK17C under the same climatic conditions.

The profile from core LLK17C showed a decreasing CAR between 8.4 and 5.2 cal kyr BP, with the lowest values occurring between 7 and 6 cal kyr BP while LLK-D-2019 showed an increasing trend with a peak between 7 and 6 cal kyr BP (Fig. 8b). As discussed above, the variation of CAR in core LLK17C is consistent with the moisture/precipitation records over millennium timescales (Fig. 8a), where the lowest values of CAR correspond to lower moisture/precipitation. The difference in the CAR in LLK-D-2019 and LLK17C indicates at least two things: 1) the CAR in LLK-D-2019 was less sensitive to moisture/precipitation conditions than in LLK17C during this period; and 2) there were allogenic factors included in the process of peat accumulation in LLK-D-2019, such as the received allogenic materials from the surrounding forest and organic matter from other locations of the peatland. Under the same climate, the different local conditions (e.g., topography and hydrology) between the two sites could explain this phenomenon to a large extent. The relatively wet conditions between 8.4 and 7 cal kyr BP benefited peat accumulation around LLK17C, but might lead to water-logged conditions around core LLK-D-2019 which are not suitable for peat accumulation due to the relatively low-lying topographic conditions (Supplementary Fig. S6). Subsequently, the location of LLK-D-2019 and the surrounding area might remain wet despite the low moisture/precipitation in other parts of the peatland between 7 and 6 cal kyr BP. The high TOC, low DBD, and higher accretion rates (Fig. 8d and e) indicate the local conditions were suitable for peat accumulation in LLK-D-2019 and still be supplied with allogenic materials supply (Fig. 8c). However, the differences in peat accretion induced by surface runoff gradually disappeared after 4.4 cal kyr BP, after which there is a similar variation in CAR (Fig. 8b). This may be the result of the gradually flattening surface of the peatland, which led to a decreased difference in hydrologic conditions, as well as in the peat accretion (Supplementary Fig. S6). The topography in LLK-D-2019 is consistent with that of other locations within the peatland after 4.4 cal kyr BP and no longer exhibits the influence of topography-related hydrological conditions, with climatic conditions becoming the primary control for CAR.

The internal differences in CAR within the Laolike peatland demonstrate the importance of local conditions (such as topography and hydrology) to CAR. This emphasizes the need for peat cores to be obtained from different locations within the same peatland to undertake multiple core analyses to reveal different CAR patterns and to resolve the sensitivity of CAR to climate change

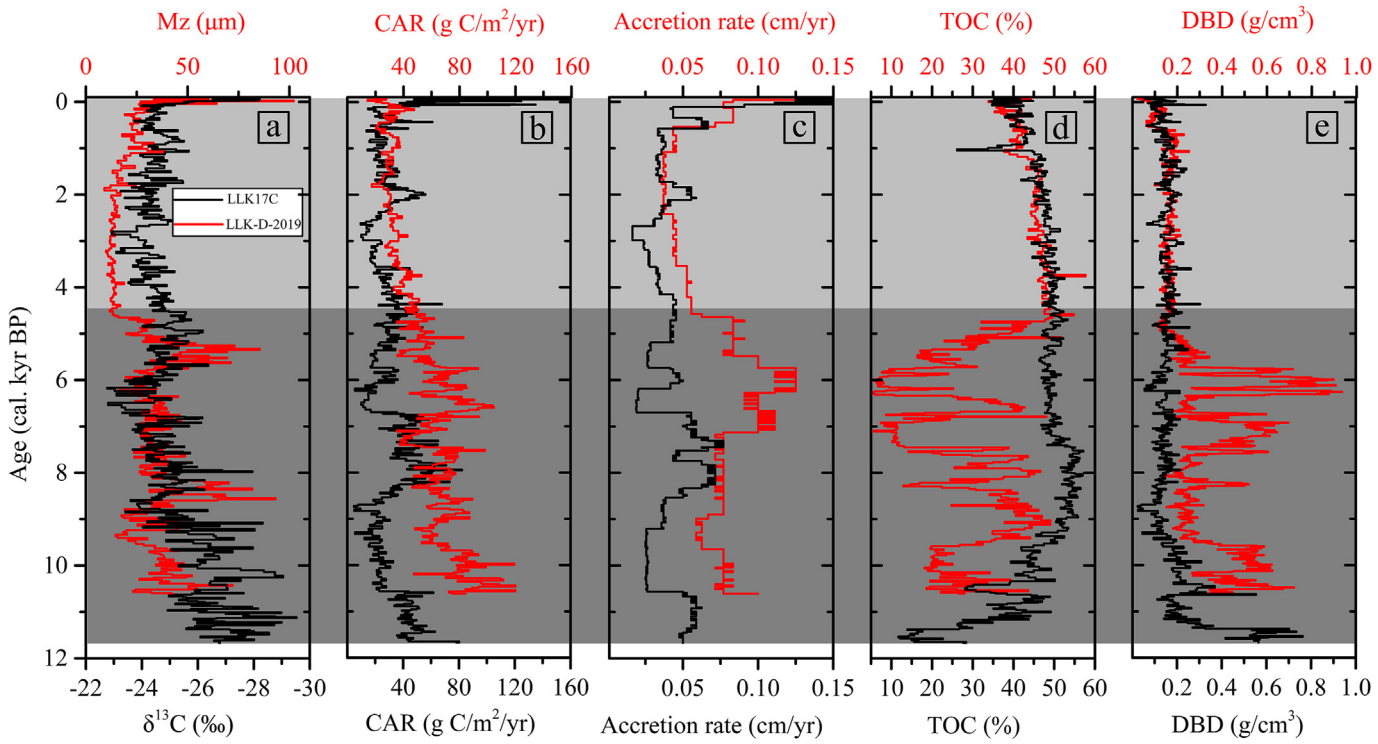

Fig. 8. (a) $\delta^{13}C$, Mz and comparisons between the cores LLK17C and LLK-D-2019. (b) Carbon accumulation rate (CAR). (c) Peat vertical accretion rate. (d) Total organic carbon (TOC). (e) Dry bulk density (DBD). The dark gray shaded areas in the background indicate the difference of CAR between cores LLK17C and LLK-D-2019, and the light gray shaded areas indicate the consistent variation in CAR.

(van Bellen et al., 2011; Mathijssen et al., 2016, 2019, 2019; Klein et al., 2013).

6. Conclusions

This study presented a case of how climate and local conditions both influence peatland development. The results contribute to a better understanding of the factors controlling long-term CAR and lateral expansion in the temperate zones of the Northern Hemisphere. The moisture and precipitation in the Laolike region decreased continually over the Holocene, with wet conditions during the early to middle Holocene and a dry climate during the late Holocene, consistent with the strength of the EASM and other climatic records from NE China. The peatland's formation was initiated at 12.1 cal kyr BP and experienced a rapid lateral expansion and a high CAR during the early Holocene. The time-weighted mean CAR in the Laolike peatland ranged from 31.1 to 52.9 g C/m^2/yr (with an average of 42 g C/m^2/yr) during the Holocene. Both lateral expansion and vertical accretion are consistent with the summer insolation, climate seasonality, and the strength of the EASM, which indicates the primary control of climate over multi-millennium timescales. However, the synchronicity between CAR and moisture/precipitation conditions implies that moisture/precipitation might be the primary control on CAR over millennium timescales. Local conditions, particularly topography, also play an important role in the lateral expansion of peatlands and the internal differences of CAR. This study, therefore, implied that both climate and local conditions are important in determining long-term carbon accumulation in peatlands over local spatial scales. Furthermore, multiple core analyses are recommended for a more comprehensive understanding of peatland development and its response to climate change.

Credit author statement

Yanmin Dong: Conceptualization, Investigation, Formal analysis, Writing – original draft. Hongkai Li: Validation, Writing- Reviewing and Editing. Hongshi He: Supervision, Project administration. Shengzhong Wang: Methodology, Resources, Funding acquisition.

Declaration of competing interest

The authors declare that they have no known competing financial interests or personal relationships that could have appeared to influence the work reported in this paper.

Acknowledgments

We are grateful to Dr. Chen Yingyi from Northeast Institule of Geography and Agroecology, China Academy of Sciences for the enthusiastic field supports. We also thank two anonymous reviewers for their helpful comments on the manuscript.

Appendix A. Supplementary data

Supplementary data to this article can be found online at https://doi.org/10.1016/j.quascirev.2021.107124.

Funding

This work was supported by the National Key Research and Development Program of China (2016YFC0500407), and the National Natural Science Foundation of China (No. 41771217).

References

Bao, K.S., Jia, L., Lu, X., Wang, G., 2010. Grain-size characteristics of sediment in Daniugou Peatland in Changbai Mountains, Northeast China: implications for atmospheric dust deposition. Chin. Geogr. Sci. 20 (6), 498–505.

Berger, A., Loutre, M.F., 1991. Insolation values for the climate of the last 10 million years. Quat. Sci. Rev. 10, 297–317.

Blaauw, M., Christen, J.A., 2011. Flexible paleoclimate age-depth models using an autoregressive gamma process. Bayesian Anal 6 (3), 457–474.

Blaauw, M., Christen, J.A., Aquino, M.A., et al., 2020. Age-Depth Modelling Using Bayesian Statistics.

Cai, C., Hong, B., Zhu, Y.X., et al., 2013. Holocene peat accumulation rates and influence factors from the Hani peatland, northeast China. Earth Environ. 41, 597–604 (in Chinese).

Chai, X., 1990. Peat Geology. Science Press. Beijing (in Chinese).

Charman, D., 2002. Peatlands and Environment Change. John Wiley, New York.

Charman, D., Amesbury, M., Hinchliffe, W., et al., 2015. Drivers of Holocene peatland carbon accumulation across a climate gradient in northeastern North America. Quat. Sci. Rev. 121, 110–119.

Charman, D., Beilman, D.W., Blaauw, M., et al., 2013. Climate-related changes in peatland carbon accumulation during the last millennium. Biogeosciences 10, 929–944.

Clymo, R.S., 1984. The limits to peat bog growth. Philos Trans. R. Soc. B 303, 605–654.

Daley, T.J., 2007. Tracking Holocene Climate Change Using Peat Bog Stable Isotopes. University of Southampton.

Dorrepaal, E., Toet, S., Logtestijn, R.S.P.V., et al., 2009. Carbon respiration from subsurface peat accelerated by climate warming in the subarctic. Nature 460 (7255), 616–619.

Dykoski, C.A., Edwards, R.L., Cheng, H., et al., 2005. A high-resolution, absolute-dated Holocene and deglacial Asian monsoon record from Dongge Cave, China. Earth Planet Sci. Lett. 233 (1–2), 71–86.

Frolking, S., Talbot, J., Jones, M.C., et al., 2011. Peatlands in the Earth's 21st century climate system. Environ. Rev. 19, 371–396.

Gallego-Sala, A.V., Charman, D., et al., 2018. Latitudinal limits to the predicted increase of the peatland carbon sink with warming. Nat. Clim. Change 8, 907–913.

Gillooly, J.F., Brown, J.H., West, G.B., et al., 2001. Effect of size and temperature on metabolic rate. Science 293, 2248–2251.

Gorham, E., 1991. Northern peatland: role in the carbon cycle and probably responses to global warming. Ecol. Appl. 1, 182–195.

Holmquist, J.R., Macdonald, G.M., 2014. Peatland succession and long-term apparent carbon accumulation in central and northern Ontario, Canada. Holocene 24 (9), 1075–1089.

Hong, Y.T., Hong, B., Lin, Q.H., et al., 2005. Inverse phase oscillations between the east asian and indian ocean summer monsoons during the last 12000 years and paleo-El Nino. Earth Planet Sci. Lett. 231 (3–4), 337–346.

Hong, Y.T., Hong, B., Lin, Q.H., et al., 2003. Correlation between Indian ocean summer monsoon and north atlantic climate during the holocene. Earth Planet Sci. Lett. 211, 371–380.

Ise, T., Dunn, A.L., Wofsy, S.C., Moorcroft, P.R., 2008. High sensitivity of peat decomposition to climate change through water-table feedback. Nat. Geosci. 1 (11), 763–766.

Ireland, A.W., Booth, R.K., Hotchkiss, S.C., Schmitz, J.E., 2013. A comparative study of within-basin and regional peatland development: implications for peatland carbon dynamics. Quat. Sci. Rev. 61, 85–95.

Jiang, W.Y., Leroy, S.A.G., Ogle, N., et al., 2008. Natural and anthropogenic forest fires recorded in the Holocene pollen record from a Jinchuan peat bog, northeastern China. Palaeogeography, Palaeoclimatology. Palaeoecology 261, 47–57.

Jones, M.C., Yu, Z.C., 2010. Rapid deglacial and early Holocene expansion of peatlands in Alaska. Proc. Natl. Acad. Sci. Unit. States Am. 107, 7347–7352.

Klein, E.S., Booth, R.K., Yu, Z.C., et al., 2013. Hydrology-mediated differential response of carbon accumulation to late holocene climate change at two peatlands in southcentral Alaska. Quat. Sci. Rev. 64, 61–75.

Korhola, A., 1992. Mire induction, ecosystem dynamics and lateral extension on raised bogs in the southern coastal area of Finland. Fennia 170, 25–94.

Li, N.N., Chambers, F.M., Yang, J.X., Jie, D.M., et al., 2017. Records of East Asian monsoon activities in Northeastern China since 15.6ka, based on grain size analysis of peaty sediments in the Changbai Mountains. Quat. Bar Int. 447, 158–169.

Liu, J., 1989. Vegetation and climatic changes at Gushantun bog in jinlin, northeast China, since 13,000 yr B.P. Acta Palaeontol. Sin. 28, 495–511 (in Chinese).

Loisel, J., Bellen, S.V., Pelletier, L., et al., 2017. Insights and issues with estimating northern peatland carbon stocks and fluxes since the last glacial maximum. Earth Sci. Rev. 165, 59–80.

Loisel, J., Yu, Z.C., Beilman, D.W., Camill, P., et al., 2014. A database and synthesis of northern peatland soil properties and holocene carbon and nitrogen accumulation. Holocene 24 (9), 1028–1042.

Loisel, J., Yu, Z.C., Parsekian, A., et al., 2013. Quantifying landscape morphology influence on peatland lateral expansion using ground-penetrating radar (GPR) and peat core analysis. J. Geophys. Res. Biogeosci. 118 (2), 373–384.

Lupascu, M., Welker, J.M., Seibt, U., et al., 2014. High Arctic wetting reduces permafrost carbon feedbacks to climate. Nat. Clim. Change 4, 51–55.

MacDonald, G.M., Beilman, D.M., Kremenetski, K.V., et al., 2006. Rapid early development of circumarctic peatlands and atmospheric CH4 and CO2 variations. Science 314, 285–288.

Mäkilä, M., 1997. Holocene lateral expansion, peat growth and carbon accumulation on Haukkasuo, a raised bog in southeastern Finland. Boreas 26, 1–14.

Mäkilä, M., Moisanen, M., 2007. Holocene lateral expansion and carbon accumulation of Luovuoma, a northern fen in Finnish Lapland. Boreas 36, 198–210.

Mathijssen, P.J.H., Galka, M., Borken, W., Knorr, K.H., 2019. Plant communities control long term carbon accumulation and biogeochemical gradients in a patagonian bog. Sci. Total Environ. 684 (SEP.20), 670–681.

Mathijssen, P.J.H., Väliranta, M., Korrensalo, A., et al., 2016. Reconstruction of Holocene carbon dynamics in a large boreal peatland complex, southern Finland. Quat. Sci. Rev. 142, 1–15.

McGuire, A.D., Chapin, F.S., 2006. Climate feedbacks in the Alaskan boreal forest. In: Verbyla, D.L. (Ed.), Alaska's Changing Boreal Forest. Oxford University Press, New York, USA, pp. 309–322. III.

Morris, P.J., Swindles, G.T., Valdes, P.J., et al., 2018. Global peatland initiation driven by regionally asynchronous warming. Proc. Natl. Acad. Sci. U.S.A. 115 (19), 4851.

Nichols, J.E., Peteet, D.M., 2019. Rapid expansion of northern peatlands and doubled estimate of carbon storage. Nat. Geosci. 12 (C8).

Niu, Z.G., Zhang, H.Y., Wang, X.W., et al., 2012. Mapping wetland changes in China between 1978 and 2008. China Sci. Bull. 57, 2813–2823.

Olsson, I., 1986. Radiometric methods. In: Berglund, B. (Ed.), Handbook of Holocene Palaeoecolgy and Palaeohydrology. John Wiley and Sons, Chichester, pp. 273–312.

Panait, A., Diaconu, A., Galka, M., et al., 2017. Hydrological conditions and carbon accumulation rates reconstructed from a mountain raised bog in the carpathians: a multi-proxy approach. Catena 152, 57–68.

Peregon, A., Uchida, M., Yamagata, Y., 2009. Lateral extension in Sphagnum mires along the southern margin of the boreal region, Western Siberia. Environ. Res. Lett. 4 (4), 45028.

Reimer, P., Austin, W., Bard, E., et al., 2020. The IntCal20 Northern Hemisphere radiocarbon age calibration curve (0–55 cal kBP). Radiocarbon 62, 725–757.

Roland, T.P., Daley, T.J., Caseldine, C.J., et al., 2015. The 5.2 ka climate event: evidence from stable isotope and multi-proxy palaeoecological peatland records in Ireland. Quat. Sci. Rev. 124, 209–223.

Ruppel, M., Väliranta, M., Virtanen, T., Korhlola, A., 2013. Postglacial spatiotemporal peatland initiation and lateral expansion dynamics in North America and northern Europe. Holocene 23 (11), 1596–1606.

Stebich, M., Rehfeld, K., Schlütz, F., et al., 2015. Holocene vegetation and climate dynamics of NE China based on the pollen record from Sihailongwan Maar lake. Quat. Sci. Rev. 124, 275–289.

Tuittila, E.S., Vliranta, M., Laine, J., Korhola, A., 2007. Quantifying patterns and controls of mire vegetation succession in a southern boreal bog in Finland using partial ordinations. J. Veg. Sci. 18, 891–902.

van Bellen, S., Dallaire, P.L., Garneau, M., Bergeron, Y., 2011. Quantifying Spatial and Temporal Holocene Carbon Accumulation in Ombrotrophic Peatlands of the Eastmain Region. Global Biogeochemical Cycles, 25, GB2016, Quebec, Canada.

Wang, B., Lin, H., 2002. Rainy season of the Asian-Pacific summer monsoon. J. Clim. 15, 386–398.

Wang, M., Chen, H., Wu, N., et al., 2014. Carbon dynamics of peatlands in China during the Holocene. Quat. Sci. Rev. 99, 34–41.

Wang, M., Yang, G., Gao, Y.H., et al., 2015. Higher recent peat C accumulation than that during the Holocene on the zoige plateau. Quat. Sci. Rev. 114, 116–125.

Xia, Y., 1988. A preliminary study of the vegetation development and climatic changes in the Sanjiang plain since 12,000 yr B.P. Scienta Sci.Geogr. Sin.Sinica 8, 240–249 (in Chinese).

Xing, W., Bao, K.S., Gallego-Sala, A.V., Charman, D.J., et al., 2015a. Climate controls on carbon accumulation in peatlands of Northeast China. Quat. Sci. Rev. 115, 78–88.

Xing, W., Bao, K.S., Guo, W.Y., Lu, X.G., Wang, G.P., 2015b. Peatland initiation and carbon dynamics in northeast china: links to holocene climate variability.BOREAS 372, 575–587.

You, H., Liu, J., 2012. High-resolution climate evolution derived from the sediment records of Erlongwan Maar Lake since 14 ka BP. Chin. Sci. Bull. 57 (27), 3610–3616.

Yu, Z., 2006. Holocene carbon accumulation of fen peatlands in boreal western Canada: a complex ecosystem response to climate variation and disturbance. Ecosystems 9 (8), 1278–1288.

Yu, Z., 2012. Northern peatland carbon stocks and dynamics: a review. Biogeosciences 9 (10), 4071–4085.

Yu, Z., Beilman, D.W., Frolking, S., et al., 2011. Peatlands and their role in global carbon cycle. Eos. Trans. Am. Geophy. Times Union 92, 97–98.

Yu, Z., Beilman, D.W., Jones, M.C., 2009. Sensitivity of northern peatland carbon dynamics to holocene climate change. In: Baird, A.J., Belyea, L.R., Comas, X., Reeve, A.S., Slater, L.D. (Eds.), Carbon Cycling in Northern Peatlands. Geophysical Monograph, vol. 184. Am Geophys Union, Washington, DC, pp. 55–69.

Yu, Z., Loisel, J., Brosseau, D.P., et al., 2010. Global peatland dynamics since the last glacial maximum. Geophys. Res. Lett. 37, L13402.

Zhang, D., Feng, Z., Yang, Y., et al., 2018. Peat δ13C celluose -recorded wetting trend during the past 8000 years in the southern Altai Mountains, northern Xinjiang, NW China. J. Asian Earth Sci. 156, 174–179.

Zhao, Y., Yu, Z.C., Tang, Y., et al., 2014. Peatland initiation and carbon accumulation in China over the last 50,000 years. Earth Sci. Rev. 128 (128), 139–146.

Quaternary Science Reviews 258 (2021) 106868

Contents lists available at ScienceDirect

Quaternary Science Reviews

journal homepage: www.elsevier.com/locate/quascirev

Developing a continental-scale testate amoeba hydrological transfer function for Asian peatlands

Yangmin Qin [a, b, *], Hongkai Li [c, 1], Yuri Mazei [d, e], Irina Kurina [f], Graeme T. Swindles [g, h], Anatoly Bobrov [d], Andrey N. Tsyganov [d, e], Yansheng Gu [b], Xianyu Huang [a, b], Jiantao Xue [b, i], Mariusz Lamentowicz [j], Katarzyna Marcisz [j], Thomas Roland [k], Richard J. Payne [d, l], Edward A.D. Mitchell [m, n], Shucheng Xie [a, b]

[a] Hubei Key Laboratory of Critical Zone Evolution, School of Geography and Information Engineering, China University of Geosciences, Wuhan, 430074, China
[b] Key Laboratory of Regional Ecology and Environmental Change, China University of Geosciences, Wuhan, 430074, China
[c] Key Laboratory of Geographical Processes and Ecological Security of Changbai Mountains, Ministry of Education, Northeast Normal University, Changchun, 130024, China
[d] Lomonosov Moscow State University, Leninskie Gori, Moscow, 119991, Russia
[e] Severtsov Institute of Ecology and Evolution, Russian Academy of Sciences, Leninskiy prospekt, 33, 119071, Moscow, Russia
[f] Laboratory of Monitoring of Forest Ecosystems, Institute of Monitoring of Climatic and Ecological Systems, Siberian Branch of the Russian Academy of Sciences, Tomsk, 634055, Russia
[g] Geography, School of Natural and Built Environment, Queen's University Belfast, Belfast, UK
[h] Geoscience Centre and Department of Earth Sciences, Carleton University, ON, K1S 5B6, Canada
[i] School of Environmental Ecology and Biological Engineering, Wuhan Institute of Technology, Wuhan, 430073, China
[j] Climate Change Ecology Research Unit, Adam Mickiewicz University, Bogumiła Krygowskiego 10, 61-680, Poznań, Poland
[k] Geography, College of Life and Environmental Sciences, University of Exeter, UK
[l] Environment Geography, University of York, Heslington, York, YO10 5DD, UK
[m] Laboratory of Soil Biodiversity, University of Neuchâtel, Rue Emile Argand 11, CH-2000, Neuchâtel, Switzerland
[n] Jardin Botanique de Neuchâtel, Chemin du Pertuis-du-Sault 58, CH-2000, Neuchâtel, Switzerland

ARTICLE INFO

Article history:
Received 5 November 2020
Received in revised form
14 February 2021
Accepted 22 February 2021
Available online xxx

Handling Editor: P Rioual

Keywords:
Testate amoebae
Water table depth
Palaeohydrology
Dataset harmonisation
Consensus taxonomy
Palaeoecology
Asia

ABSTRACT

Testate amoebae (TA) are a common and diverse group of protists and are especially abundant in peatlands. The structure of peatland TA communities is well correlated to surface moisture and water table depth (WTD). For that reason, TA are widely used as proxy indicators in ecological and palaeoecological studies. Peatlands are abundant across Asia, but the diversity and ecology of the TA that inhabit these systems are poorly documented. It is therefore unclear whether TA can be used as palaeohydrological indicators in the manner in which they commonly are in Europe and North-America. There is particular uncertainty as to the efficacy of this approach in the lower latitudes. We compiled existing and new data on testate amoebae from 1124 *Sphagnum*-dominated samples from 42 individual peatlands covering broad latitudinal (25°–66° N) and longitudinal (68°–129° E) ranges. Using a consensus taxonomic framework, we built a checklist of TA and developed TA-based hydrological transfer functions for Asian peatlands. The results showed that three models, weighted averaging (WA), weighted average partial least squares (WA-PLS), and maximum likelihood (ML), predicted similar WTD values for full samples, while the modern analogue technique (MAT) produced the strongest (R^2_{boot} = 0.58) relationship between observed and estimated water-table depths (WTDs). Removing outlier samples improved the R^2 values of observed vs. estimated WTDs, with ML then demonstrating the strongest predictive power (R^2_{boot} = 0.68, $RMSEP_{boot}$ = 8.98 cm). The predictive capability of the

* Corresponding author. Hubei Key Laboratory of Critical Zone Evolution, School of Geography and Information Engineering, China University of Geosciences, Wuhan, 430074, China.
E-mail address: qinyangmin2005@163.com (Y. Qin).
[1] This author contributed equally to this work.

https://doi.org/10.1016/j.quascirev.2021.106868
0277-3791/© 2021 Elsevier Ltd. All rights reserved.

developed WTD transfer function is comparable to equivalent models for Europe and North America and thus can be used for palaeohydrological reconstructions for boreal to subtropical peatlands in Asia.
© 2021 Elsevier Ltd. All rights reserved.

1. Introduction

Testate amoebae are a group of eukaryotic micro-organisms which are widespread in wetlands, soils, freshwaters and coastal habitats globally (Beyens and Meisterfeld, 2001; Meisterfeld, 2002; Mitchell et al., 2008). They play important functional roles in many ecosystems (Wilkinson, 2008; Wilkinson and Mitchell, 2010). Testate amoebae are considered useful bioindicators due to their abundance, diversity, characteristic morphology and the good preservation of their shell (test) in peats and sediments (Mitchell et al., 2008; Payne, 2013). They are commonly used in palaeoecological studies from lakes, saltmarshes and particularly from peatlands (Beyens and Meisterfeld, 2001). In the last two decades, testate amoebae have been mainly used to reconstruct changes in hydrological conditions in peatlands, typically expressed as water table depth (WTD) (Charman and Warner, 1992; Warner and Charman, 1994; Woodland, 1998; Bobrov et al., 1999; Mitchell et al., 1999; Charman et al., 2004; Payne et al., 2008; Booth, 2010; Lamentowicz et al., 2515; Swindles et al., 2019).

A prerequisite for using testate amoebae in palaeoecological studies is the combined analysis of contemporary testate amoeba assemblages with associated hydrological data. These correlations are used to build models, named transfer functions, to correlate subfossil communities with past environmental data. More than thirty transfer functions have been now produced from around the world (Booth, 2001; Lamentowicz and Mitchell, 2005; Charman et al., 2007; Payne et al., 2008; Swindles et al., 2009, 2014; Amesbury et al., 2016, 2018; van Bellen et al., 2014, 2017). These WTD transfer functions have successfully been used to reconstruct past hydrological change (Lamentowicz et al., 2010; Swindles et al., 2015, 2019; van Bellen et al., 2017) and results were tested by cross-validations and against instrumental data (Charman, 2004; Booth, 2011). The sensitivity of testate amoebae to water table changes has also recently been validated by manipulative experiments (Marcisz et al., 2014; Koenig et al., 2017, 2018).

Peatlands play an important role in the global carbon cycle, the rate of C sequestration and storage under a changing climate (Yu, 2010; Charman et al., 2015). Peatlands expanded rapidly as a result of Asian monsoon-driven hydrological changes occurring at the end of the last glaciation (Xie et al., 2013; Qin et al., 2020) and, by 1990 CE, covered an estimated near 1.6×10^6 km^2 in Asia, corresponding to 40% of the world total (about 3.9×10^6 km^2) (Joosten, 2010). However, despite this abundance previous research on the contemporary ecology and palaeoecology of testate amoebae in peatlands has been heavily skewed towards North America and northern Europe. More recently similar approaches have been extended to Asia.

Asia is home to both the most extensive peatland region (The West Siberian Lowland) and the largest peatland in the world (The Great Vasyugan Mire, 55 000 km^2 or 2% of the world's peatlands). The huge amount of carbon stored in Asian peatlands is potentially threatened by climate change and direct human impact (Yu, 2012; Zhao et al., 2014). An estimated 1.97×10^5 km^2 of Asian peatland considered as degraded (12.7% of the total peatland area) and therefore represents a substantial source of CO_2. In 2008 CE, China was the 3rd largest CO_2 contributor from degraded peatlands in the world after the European part of Russia and Indonesia (Joosten, 2010). As the hydrological condition is the main factor governing the functioning of peatlands, it is important to develop reliable tools to assess past and on-going hydrological changes occurring in peatlands (Beilman et al., 2009; Sheng et al., 2004). Asian peatlands are the most abundant in the boreal domain (i.e. Siberia and the Russian Far East, Mongolia, northern China, Korea and Japan), more scattered in the sub-tropical zone of China and again abundant in the tropical zone (especially Borneo and New Guinea). Research on peatland testate amoeba ecology has been developing rapidly in the last 5–10 years in Asia (Kurina, 2011; Li et al., 2015; Qin et al., 2013; Ratcliffe et al., 2017; Krashevska et al., 2020) and testate amoeba analysis has been used in several palaeoecological studies (Klimaschewski et al., 2015).

Recently, there has been a movement towards the construction of training sets at larger spatial scales by combining multiple regional datasets (such as Amesbury et al., 2013; Booth, 2008). This approach has culminated in the production of continental-scale training sets for both Europe (Amesbury et al., 2016) and North America (Amesbury et al., 2018). The advantage of transfer functions based on these training sets is that a larger dataset will include a greater number of records for each species and span a greater range of environmental conditions, increasing the likelihood of accurately reflecting conditions found in the palaeoecological archive (Payne et al., 2016). Two disadvantages are that such transfer functions rely on the combination of hydrological data based on point measurements in different locations at different times and that the identification of some taxa may not be consistent among studies requiring taxonomic harmonisation (i.e. reduction in taxonomic resolution to a common denominator). Both factors might be expected to impair model performance but cross-validated performance statistics for such models are often comparable to individual regional studies and palaeoecological reconstructions for well-studied sites are likewise often very similar to regional transfer functions (Amesbury et al., 2016, 2018; Turner et al., 2013). The current prevailing view is therefore that the advantages of wide coverage outweigh the disadvantages of inconsistent environmental data and that, while results should never be accepted uncritically, continental-scale transfer functions are a useful tool in the palaeoecologist's toolkit. Our focus in this study is to i) combine multiple regional training sets to produce a continental-scale training set for the peatlands of Asia; ii) to develop a trans-regional Asian transfer function model, and iii) to apply the model to a palaeoecological record from an Asian peatland.

2. Methods

2.1. Features of datasets used

We combined datasets from 42 individual peatlands, including unpublished data from 29 sites (Table 1). These peatlands ranged in latitude from 25° N to 66° N and 68° E to 129° E in longitude (Fig. 1). They cover a broad range of topographic settings and vegetation types, spanning from the sub-tropics to the edge of the sub-Arctic climatic zone (Table 1; Fig. 1). Most sites are bogs but sites also include poor fens. The majority are in remote regions and relatively undisturbed by human activity, although one site has been burned

Table 1
Summary information on the 42 peatlands sites included in the study. Code of ecoregion types: TCF = Temperate Conifer Forests, TBMF = Temperate Broadleaf and Mixed Forests, SMBF=Subtropical Moist Broadleaf Forests, MGM = Montane Grasslands and Meadows.

Peatland name (code)	Latitude (N)	Longitude (E)	Altitude (m)	Location	Site description	Ecoregion type	Range of WTD (cm)	Range of pH	References
(1) Gutian (GT)	26°05′03″	110°22′13″	1692	South central China	Subtropical poor fen	SMBF	8.5 to 42	4.40 to 4.60	Qin unpublished data
(2) Wangdongyang (WDY)	27°40′46″	119°38′13″	1398	SE China	Subtropical poor fen	SMBF	−1 to 23	4.47 to 5.93	Qin unpublished data
(3) Zhaogongting (ZGT)	26°24′29‴	114°04′59″	1793	South central China	Subtropical poor fen	SMBF	3 to 30.5	4.45 to 6.19	Qin unpublished data
(4) Xinjiang1 (XJ-ATM)	48°49′48″	86°54′44″	1728	NW China	*Sphagnum* bog	MGM	3 to 44	NA	Qin unpublished data
(5) Xinjiang2 (XJ-C4-S)	48°48′09″	86°55′47″	1753	NW China	*Sphagnum* bog	MGM	−5 to 50	NA	Qin unpublished data
(6) Tiandouyang (TDY)	25°54′44″	117°28′57″	1183	South China	Subtropical poor fen	SMBF	8 to 30	5.54 to 6.13	Qin unpublished data
(7) Ruoergai (REG)	33°48′54″	102°43′.57″	3444	Tibetan plateau, West China	Subtropical poor fen	MGM	−1.0 to 22	6.85 to8.48	Qin unpublished data
(8) Erxianyan (EXY)	29°43′35″	108°48′08″	1530	Central China	Subtropical poor fen	SMBF	3.0 to 28.4	4.77 to 6.48	Qin et al. (2013)
(9) Qizimeishan (QZM)	29°57′51″	109°45′10″	1800	Central China	Subtropical poor fen	SMBF	−6.6 to 22.9	4.62 to 5.88	Qin et al. (2013)
(10) Dajiuhu (DJH)	31°29′35″	109°59′48″	1700	South central China	Subtropical poor fen	SMBF	−8.6 to 43	3.21 to 5.73	Qin unpublished data
(11) Changying (CY)	52°51′47	123°19′34″	555	NE China	Forested boreal bog	TCF	0 to 38	4.6 to 6.04	Li unpublished data
(12) Gaodi (GD)	52°14′26″	122°26′10″	725	NE China	Forested boreal bog	TCF	1 to 46	4.2 to 4.98	Li unpublished data
(13) Gushantun (GS)	42°18′19″	126°16′49″	515	NE China	Forested boreal bog	TBMF	8 to 37	4.92 to 6.24	Li unpublished data
(14) Hani (HN)	42°13′34″	126°31′06″	900	NE China	*Sphagnum* bog	TBMF	4 to 53	4.84 to 6.76	Li unpublished data
(15) Jinbei (JB)	41°58′48″	127°37′09″	900	NE China	Forested boreal bog	TBMF	10 to 75	4.46 to 5.05	Li unpublished data
(16) Jinchuan (JC)	42°20′53″	126°21′39″	620	NE China	Forested boreal bog	TBMF	4 to 36	4.86 to 5.94	Li unpublished data
(17) Mangui (MG)	52°15′46″	122°13′08″	685	NE China	Forested boreal bog	TCF	2 to 48	4.53 to 5.66	Li unpublished data
(18) Sandaohu (SDH)	42°21′24″	126°53′39″	600	NE China	Forested boreal bog	TBMF	5 to 33	5.15 to 6.17	Li unpublished data
(19) Tangbei (TBA)	48°25′08″	129°04′52″	490	NE China	Forested boreal bog	TBMF	7 to 48	4.78 to 5.56	Li et al. (2015)
(20) Tangbei (TBB)	48°25′57″	129°9′12″	475	NE China	Forested boreal bog	TBMF	0 to 68	4.72 to 5.27	Li et al. (2015)
(21) Tanghongling (THL)	48°39′46″	129°28′54″	350	NE China	Forested boreal bog	TBMF	0 to 51	4.84 to 5.99	Li et al. (2015)
(22) Tuqiang (TQ)	52°56′29″	122°51′24″	480	NE China	Forested boreal bog	TCF	3 to 44	4.59 to 6.16	Li unpublished data
(23) Yuanchi (YC)	42°01′58″	128°25′57″	1290	NE China	*Sphagnum* bog	TBMF	0 to 61	4.65 to 5.55	Li unpublished data
(24) Zhuanglin (ZL)	52°44′40″	122°39′02″	555	NE China	Forested boreal bog	TCF	5 to 47	4.41 to 5.74	Li unpublished data
(25) Bakchar mire (BK1-4)	56°58′33″	82°36′27″	104	Western Siberia, Russia	*Sphagnum* bog	TCF	0.1 to 46	3.30 to 4.00	Kurina and Li (2019)
(26) Bakchar mire (BK1-6)	56°58′26″	82°35′08″	115	Western Siberia, Russia	*Sphagnum* bog	TCF	6 to 38	3.40 to 4.30	Kurina and Li (2019)
(27) Samara mire (SM2-1)	56°55′17″	82°30′49″	111	Western Siberia, Russia	*Sphagnum* bog	TCF	3 to 48	3.50 to 6.00	Kurina and Li (2019)
(28) Gorno-Slinkino village (GSV1)	58°47′24″	68°47′24″	65	Western Siberia, Russia	*Sphagnum* bog	TCF	NA	NA	Mazei and Tsyganov, 2006
(29) Gorno-Slinkino village (GSV2)	58°46′48″	68°46′48″	65	Western Siberia, Russia	*Sphagnum* bog	TCF	NA	NA	Mazei and Tsyganov, 2006
(30) Vinokurova village (VV1)	58°18′55″	68°20′0″	90	Western Siberia, Russia	*Sphagnum* bog	TCF	NA	NA	Mazei unpublished data
(31) Vinokurova village (VV2)	58°19′34.4″	68°19′10″	90	Western Siberia, Russia	*Sphagnum* bog	TCF	NA	NA	Mazei unpublished data
(32) Zapolyarnyi village (ZV)	66°24′00″	79°1′	20	Western Siberia, Russia	*Sphagnum* bog	TCF	NA	NA	Mazei unpublished data
(33) Urengoi-town (UT)	65°35′00″	77°35′	15	Western Siberia, Russia	*Sphagnum* bog	TCF	NA	NA	Mazei unpublished data
(34) Surgut region (SR)	60°7′00″	71°30′	40	Western Siberia, Russia	*Sphagnum* bog	TCF	NA	NA	Mazei unpublished data
(35) Tobolsk region (TR)	58°14′00″	68°13′	90	Western Siberia, Russia	*Sphagnum* bog	TCF	NA	NA	Mazei unpublished data
(36) Listvyanka-bog1 (LYB)	51°57′28″	104°43′15″	550	Baikal, Russia	*Sphagnum* bog	TBMF	0 to 60	4.3 to 6.4	Mazei unpublished data
(37) Bayandai boggy (BBF)	53°2′31″	105°33′32″	650	Baikal, Russia	*Sphagnum* bog	TCF	NA	4.1 to 5.9	Mazei unpublished data

(*continued on next page*)

Table 1 (*continued*)

Peatland name (code)	Latitude (N)	Longitude (E)	Altitude (m)	Location	Site description	Ecoregion type	Range of WTD (cm)	Range of pH	References
(38) Listvyanka-bog2 (LB2)	52°0′39″	104°39′50″	550	Baikal, Russia	*Sphagnum* bog	TBMF	0 to 50	4.0 to 6.1	Mazei unpublished data
(39) Listvyanka-bog3 (LB3)	52°2′27″	104°38′13″	550	Baikal, Russia	*Sphagnum* bog	TBMF	5 to 50	5.2 to 6.2	Mazei unpublished data
(40) Listvyanka-bog4 (LB4)	52°4′12″	104°35′38″	550	Baikal, Russia	*Sphagnum* bog	TBMF	3 to 15	5.8 to 6.3	Mazei unpublished data
(41) Nanwenghe (NWH)	51°5′28″	125°12′23″	460	NE China	*Sphagnum* bog	TCF	NA	5.2 TO 6.8	Qin et al. (2017)
(42) Mukhrino (MUK)	60°53′36″	68°40′57″	80	W Siberia, Russia	*Sphagnum* bog	TCF	−15 to 54	3 to 3.8	Lamentowicz et al. (2015)

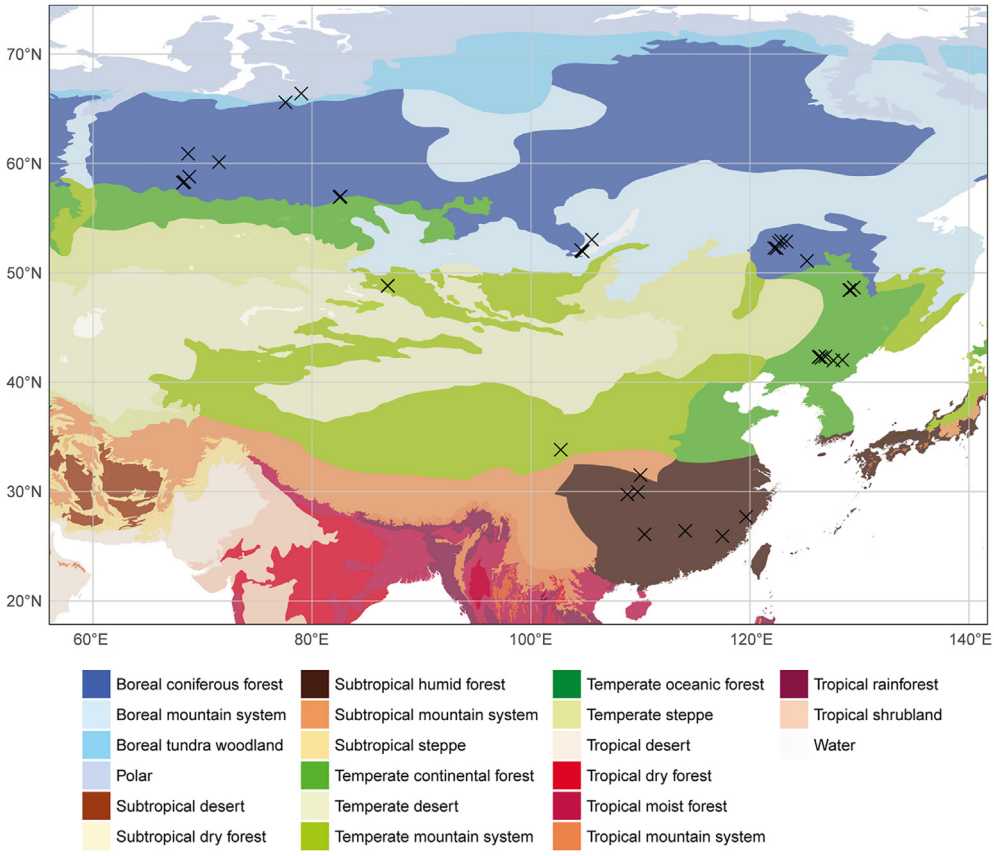

Fig. 1. Map showing the location of the 42 studied peatlands in Asia. The background map shows the global ecological zones according to FAO (2012). See Table 1 for detailed information.

by wildfire (Qin et al., 2017). We did not include some datasets from western Asia (Payne, 2011; Payne et al., 2008, 2010). These sites are a great distance from the sites included in this study and considered geographically and ecologically 'European', as demonstrated by their inclusion in a similar continent-scale study from Europe (Amesbury et al., 2016) and pan-European-American peatlands dataset(Amesbury et al., 2018). Finally, data from several published sites were not included (such as sites from the Kamchatka Peninsula in Russia and the Korean peninsula) as the original data were unavailable (Chung et al., 1992; Qin and Xie, 2011; Qin et al., 2018; Song et al., 2014; Payne et al., 2020).

Full details of the sites, selection criteria and how the sampling was undertaken are included in the original publications (Table 1). Typically, sampling points were selected to reflect the main microtopographic range of the peatland including hummocks, hollows, lawns and pools (where present). Most samples analysed were from the upper 5 cm of *Sphagnum* moss but datasets also included samples from brown mosses and locations with vascular plants. The environmental data collected as part of field sampling also varied among datasets leading to some inconsistencies. In most studies, water table depth was measured by making a hole adjacent to the sampling point, leaving this to equilibrate and then manually measuring depth. In many studies, samples were dried on return to the laboratory to calculate gravimetric moisture content. In some studies, pH and conductivity were measured, either on surface water or on peat suspensions.

Sample preparation for testate amoeba analysis typically involved washing through a 250 μm mesh and sometimes a second wash through a finer (15 μm) mesh to remove fine material (cf. Hendon and Charman, 1997). Samples were mounted on slides and

amoebae were identified under a light-microscopy at 100–400× magnification. Count totals for most samples exceeded 150 tests (Payne and Mitchell, 2009).

2.2. Harmonisation of datasets

An important stage in studies of this type is the attempt to harmonise datasets to a standard taxonomy. Datasets have been produced by a range of analysts and the taxonomy of testate amoebae is not always clear-cut; different research groups have opted for differing degrees of 'lumping' or 'splitting' taxa. We developed a consistent approach to data harmonisation through a process of dialogue between the researchers involved. Given the clear risks of taxonomic inconsistency (Payne et al., 2011), we aimed for the maximal taxonomic resolution possible which we could have confidence was consistent between analysts. To do this we used a conservative "morpho-type" approach, similar to that generally used in palaeoecological studies and implemented in previous similar studies (Mitchell et al., 2014). A lower-resolution taxonomic approach of this type has recently been shown to give similar model performance results to identification based on higher taxonomic resolution (Mitchell et al., 2014; Amesbury et al., 2016).

We firstly adjusted the taxonomic schemes of the original studies to currently accepted taxonomy (Kosakyan et al., 2016). *Amphitrema flavum* was changed as *Archerella flavum*. *Nebela carinata* type and *N. marginata* were updated to *Planocarina carinata* and *P. marginata* respectively, while *Nebela maxima* and *N. speciosa* were changed as *Gibbocarina maxima* and *G. speciosa* respectively. *Nebela dentistoma* and *N. caudata* were updated to *Argynnia dentistoma* and *A. caudata* respectively.

We next grouped taxa where we considered there was at least the possibility for taxonomic inconsistency. We grouped *Phryganella acropodia, P. acropodia penardi* and *P. hemisphaerica* (now synonymized to *Phryganella acropodia* by Dumack et al., 2020) into *Cyclopyxis arcelloides* type. *Netzelia (Difflugia) oviformis* and *Netzelia (Difflugia) compressa* were combined into *Difflugia angulostoma* type. Another two taxa: *Schoenbornia smithi* and *Schoenbornia c.f. smithi* were included within *Difflugia pristis* type (Table 2). Taxa in the genus *Argynnia* were grouped in *Argynnia dentistoma* type with *A. caudata* considered separately. Five *Nebela* taxa with keels on their shells were included in *Gibbocarina gracilis* type. *Padaungiella lageniformis, P. wailesi, Nebela minor, N. wetekampi* and *P. tubulata* were included in *Padaungiella lageniformis* type. A few types combined by other authors and in other compilations were considered separately here, notably *Corythion-Trinema* type (Charman et al., 2000) is here included as the separate taxa *Corythion dubium* and *Trinema lineare* (Table 2). Very rare species that appeared only in one or two samples with low abundance were excluded from the dataset (Supplementary Table 1).

2.3. Data analysis

2.3.1. Ordination

We used ordination to explore the data structure and test for the links between assemblage composition and environmental variables. We first conducted non-metric multidimensional scaling (NMDS) ordinations on the full dataset. Species occurring in less than 10 samples or with highest abundance less than 5% were removed prior to analysis. Species data were square root transformed with Wisconsin double standardization and Bray-Curtis dissimilarities were calculated (Bray and Curtis, 1957). Environmental variables were projected into the NMDS space.

Secondly, we used redundancy analysis (RDA) to quantify the relationships between abiotic variables and biotic communities. We focus on three variables previously shown to be linked to testate amoeba assemblages: moisture content, water table depth (WTD) and pH. However, of these data, many samples lack one, two, even all three variables. Among 1124 samples, only 888 samples had WTD values, 771 samples had moisture values, 819 samples had pH values and 15 samples had none of these three environmental variables. This means that we needed to conduct analyses with differing combinations of environmental data. We considered three sets of samples: (1) all valid 1068 samples (Fig. 2); (2) 862 samples having WTD, longitude and latitude (Table 3, Fig. 3); (3) 546 samples including WTD, pH, moisture, longitude and latitude (Supplementary Figure 1). A Hellinger-transformed (Legendre and Gallagher, 2001) testate amoeba community matrix was used as the response matrix. The significance of the model, axes, and variables was tested using a Monte Carlo test with 999 permutations (Lepš and Šmilauer, 2003). Computations were performed in R 3.0.1 (R Development Core Team, 2014) using the vegan package (Oksanen et al., 2012).

2.3.2. Transfer function development and testing

Transfer function models were developed for WTD using a suite of techniques commonly applied in the palaeoecological literature: weighted averaging (WA), weighted average partial least squares (WA-PLS), maximum likelihood (ML) and the modern analogue technique (MAT) (Birks, 1995; Birks et al., 1990; Overpeck et al., 1985; ter Braak and Juggins, 1993). Transfer functions were developed in R (R Development Core Team, 2014), primarily using the package rioja (Juggins, 2009). MAT was based on squared chord distance and WA included variants based on both classical and inverse deshrinking regressions and, with and without tolerance down-weighting. Additional WA-PLS components were included where they resulted in a >5% improvement in R^2 and had a significant P-value ($P < 0.05$) when tested following van der Voet (1994). Transfer function studies have typically excluded species with small numbers of records as species optima will be difficult to characterise from small sample sizes (Payne et al., 2006). Here we applied a precautionary criterion of ten occurrences and therefore excluded *Pontigulasia elisa* and *Difflugia labiosa* from the dataset used for model development.

Transfer function performance can often be impaired by a small proportion of samples where the model performs poorly, which in many cases can be traced to samples with atypical assemblages or inaccurate environmental data (Payne et al., 2008; Woodland et al., 1998). Consequently, it has been common practice to present and apply 'pruned' models with high residual samples excluded. Here we excluded samples with residuals greater than 20% of the total measured water table range; a criterion which has been used in previous studies (Amesbury et al., 2016). For each model, we repeated model building and cross-validation using a dataset from which samples with initial residual values greater than this criterion (17.04 cm) were excluded. Some previous studies have also applied an additional step of removing sites considered unrepresentative (due to e.g. nutrient status: Amesbury et al. (2016)) before building models but we did not consider this necessary with our data. Model performance was assessed based on root mean squared error of prediction (RMSEP), R^2 between measured and predicted values, average bias and maximum bias. We selected preferred models primarily based on RMSEP (small) and R^2 (high), which generally showed opposite trends (i.e. low RMSEP corresponding to high R^2).

To establish the performance of the transfer functions, we used statistical cross-validation approaches to test model performance with subsets of the same training set used for model development. Three methods were implemented: leave-one-out ('jack-knife'), bootstrapping (1000 cycles) and leave-one-site-out cross-validation (LOSO) (Birks, 1995; Payne et al., 2012). Of these approaches

Table 2
Taxonomic harmonisation applied in this study.

Taxa grouping in this study	Taxa included (or synonym)
Arcella discoides type	*Arcella discoides* type
ARC-DIS	*Arcella discoides difficilis*
	Arcella discoides scutelliformis
	Arcella discoides foveosa
Arcella gibbosa type	*Arcella bathystoma*
ARC-GIB	*Arcella costata*
	Arcella gibbosa
	Arcella gibbosa laevis
	Arcella intermedia laevis
Arcella hemisphaerica	*Arcella hemisphaerica*
ARC-HEM	*Arcella hemisphaerica undulata*
	Arcella rotundata
	Arcella rotundata stenostoma
	Arcella rotundata stenostoma undulate
	Arcella pygmaea
Arcella arenaria type	*Arcella arenaria*
ARC-ARE	*Arcella arenaria compressa*
	Arcella arenaria sphagnicola
	Arcella catinus
	Arcella polyphora
	Arcella polyphora undulata
	Arcella vulgaris
	Arcella vulgaris polymorpha
Archerella flavum	*Amphitrema flavum*
(ARC-FLA)	
Amphitrema wrightianum	*Amphitrema wrightianum*
(AMP-WRI)	
Assulina muscorum	*Assulina muscorum*
(ASS-MUS)	
Assulina seminulum	*Assulina seminulum*
(ASS-SEM)	*Assulina scandinavica*
Bullinularia indica	*Bullinularia indica*
(BUL-IND)	*Bullinularia indica minor*
Centropyxis aculeata type	*Centropyxis aculeata*
(CEN-ACU)	*Centropyxis aculeata grandis*
	Centropyxis aculeata minima
	Centropyxis gibba inermis
	Centropyxis discoides
Centropyxis aerophila type (CEN-AER)	*Centropyxis aerophila*
	Centropyxis aerophila sphagnicola
	Centropyxis cassis type
	Centropyxis constricta
	Centropyxis constricta minima
	Centropyxis ecornis type
	Centropyxis sylvatica minor
	Centropyxis sylvatica
	Centropyxis orbicularis
	Centropyxis minuta
Centropyxis platystoma type	*Centropyxis platystoma*
(CEN-PLA)	*Centropyxis elongata*
Corythion dubium	*Corythion dubium*
(COR-DUB)	*Corythion dubium minima*
	Corythion dubium terricola
	Corythion dubium orbicularis (Corythion orbicularis)
	Corythion delamarei
Cryptodifflugia oviformis type	*Cryptodifflugia oviformis*
(CRY-OVI)	*Cryptodifflugia oviformis fusca*
	Cryptodifflugia minuta
	Cryptodifflugia bassini
	Cryptodifflugia cf voigti
	Cryptodifflugia sacculus sacotschawi
Cyclopyxis arcelloides type	*Cyclopyxis arcelloides*
(CYC-ARC)	*Cyclopyxis arcelloides large form*
	Cyclopyxis eurystoma
	Cyclopyxis eurystoma parvula
	Difflugia globulosa
	Cyclopyxis kahli
	Cyclopyxis plana
	Phryganella acropodia
	Phryganella acropodia penardi
	Phryganella hemisphaerica
Cyphoderia ampulla type	*Cyphoderia ampulla papillata*
(CYP-AMP)	*Cyphoderia ampulla*
	Cyphoderia trochus

Table 2 (*continued*)

Taxa grouping in this study	Taxa included (or synonym)
Difflugia acuminata type (DIF-ACU)	*Difflugia acutisimella*
	Difflugia acuminata type
	Difflugia bacillariarum
	Difflugia elegans
	Difflugia styla
Difflugia angulostoma type (DIF-ANG)	*Difflugia angulostoma*
	Difflugia minuta
	Netzelia (Difflugia) oviformis
	Netzelia (Difflugia) compressa
	Difflugia globulus
	Difflugia geosphaerica
	Difflugia lobostoma
Difflugia lucida type (DIF-LUC)	*Difflugia lucida* type
	Difflugia penardi
	Difflugia petricola
	Difflugia lanceolata
Difflugia labiosa type (DIF-LAB)	*Difflugia labiosa* type
	Difflugia decloitrei
	Difflugia amphora
	Difflugia molesta
	Difflugia ovalisina
	Difflugia pecac
	Difflugia ampullula
	Difflugia ampla
	Difflugia amphoralis
Difflugia leidyi (DIF-LEI)	*Difflugia leidyi*
Difflugia oblonga type (DIF-OBL)	*Difflugia oblonga*
	Difflugia bacillifera
	Difflugia gassowskii
	Difflugia parva
	Difflugia pyriformis
	Difflugia rubescens
Difflugia pristis type (DIF-PRI)	*Difflugia pristis*
	Difflugia pulex
	Schoenbornia smithi
	Schoenbornia cf. smithi
Euglypha rotunda (EUG-ROT)	*Euglypha anodonta*
	Euglypha rotunda
	Euglypha rotunda obliqua
	Euglypha capsiosa
	Euglypha denticulata
	Euglypha laevis
	Euglypha simplex
Euglypha ciliata type (EUG-CIL)	*Euglypha bryophila*
	Euglypha ciliata
	Euglypha ciliata glabra
	Euglypha compressa
	Euglypha compressa glabra
	Euglypha cristata
	Euglypha cristata decora
	Euglypha cristata major
	Euglypha filifera
	Euglypha filifera pyriformis
	Euglypha filifera spinosa
	Euglypha scutigera
	Euglypha strigosa
	Euglypha strigosa glabra
	Euglypha strigosa heterosphina
	Euglypha strigosa muscorum
Euglypha tuberculata (EUG-TUB)	*Euglypha tuberculata*
	Euglypha tuberculata minor
Heleopera sphagni (HEL-SPH)	*Heleopera petricola*
	Heleopera petricola amethystea
	Heleopera rosea
	Heleopera sphagni
Heleopera sylvatica (HEL-SYL)	*Heleopera sylvatica*
Hyalosphenia elegans (HYA-ELE)	*Hyalosphenia elegans*
Hyalosphenia papilio (HYA-PAP)	*Hyalosphenia papilio*
	Hyalosphenia subflava
Lesqueresia spiralis type (LES-SPI)	*Lesquereusia modesta type*
	Lesquereusia spiralis

(*continued on next page*)

Table 2 (*continued*)

Taxa grouping in this study	Taxa included (or synonym)
	Lesquereusia epistomium
Nebela tincta type	*Nebela bohemica*
(NEB-TIN)	*Nebela tincta type*
	Nebela parvula
Nebela collaris type	*Nebela collaris type*
(NEB-COL)	
Planocarina carinata type	*Planocarina (Nebela) carinata* type
(PLA-CAR)	*Planocarina (Nebela) marginata*
	Gibbocarina (Nebela) maxima
Argynnia dentistoma type	*Argynnia (Nebela) dentistoma*
(ARG-DEN)	*Argynnia (Nebela) dentistoma lacustris*
	Argynnia (Nebela) dentistoma laevis
	Argynnia (Nebela) vitraea
	Argynnia (Nebela) vitraea minor
	Argynnia (Nebela) vitraea sphagni
Argynnia caudata	*Argynnia caudata*
ARG-CAU	
Gibbocarina gracilis type	*Nebela penardiana*
(GIB-GRA)	*Gibbocarina (Nebela) galeata*
	Gibbocarina (Nebela) galeata orbicularis
	Gibbocarina (Nebela) gracilis
	Gibbocarina (Nebela) tubulosa
Physochila griseola	*Physochila (Nebela) griseola*
(PHY-GRI)	*Physochila (Nebela) tenella*
Padaungiella lageniformis type	*Padaungiella (Nebela) lageniformis*
(PAD-LAG)	*Padaungiella (Nebela) wailesi*
	Nebela minor
	Nebela wetekampi
	Padaungiella (Nebela) tubulata
Alabasta militaris type	*Nebela militaris*
(ALA-MIT)	
Placocista spinosa type	*Placocista spinosa type*
(PLA-SPI)	*Placocista glabra*
	Placocista jurassica
	Placocista lens
Plagiopyxis callida type	*Plagiopyxis callida*
(PLA-CAL)	*Plagiopyxis declivis*
	Plagiopyxis labiata
	Plagiopyxis penardi
Pontigulasia elisa type	*Pontigulasia compressa*
(PON-ELI)	*Pontigulasia compressoidea*
	Pontigulasia elisa
	Pontigulasia sp
Quadrulella symmetrica type	*Mrabella (Quadrulella) subcarinata*
(QUA-SYM)	*Quadrulella symmetrica*
Sphenoderia lenta type	*Sphenoderia fissirostris*
(SPH-LEN)	*Sphenoderia lenta*
Tracheleuglypha dentata type	*Tracheleuglypha dentata*
(TRA DEN)	
Trigonopyxis arcula type	*Trigonopyxis arcula*
(TRI-ARC)	*Trigonopyxis arcula major*
	Trigonopyxis microstoma
	Trigonopyxis minuta
Trinema lineare type	*Trinema chardezi*
(TRI-LIN)	*Trinema complanatum*
	Trinema complanatum elongata
	Trinema complanatum platystoma
	Trinema enchelys
	Trinema lineare
	Trinema lineare truncatum
	Trinema penardi

LOSO is often the most conservative and arguably the most robust as it accounts for the between-site differences which can often be substantial in testate amoeba datasets (Payne et al., 2012). We used these tests to identify the optimum model and then applied two further tests to the final selected model. To identify spatial autocorrelation beyond the scale of inter-site differences we used the random neighbour exclusion (rne) test of Telford and Birks (2009) which compares the effect of deleting geographically proximal versus random samples on model performance. We constructed a matrix of geographic distances using the Vincenty Ellipsoid method in the R package 'geosphere' (Hijmans et al., 2015) and implemented in 'palaeoSig' (Telford, 2011). To address the impact of uneven sampling along environmental gradients on model performance we applied the segment-wise RMSEP method of Telford and Birks (2011) to boot-strap cross-validated data.

In addition to the cross-validation techniques, we tested the model performance using an independent test-set (i.e. real data) so taking advantage of the large pool of samples in our region for

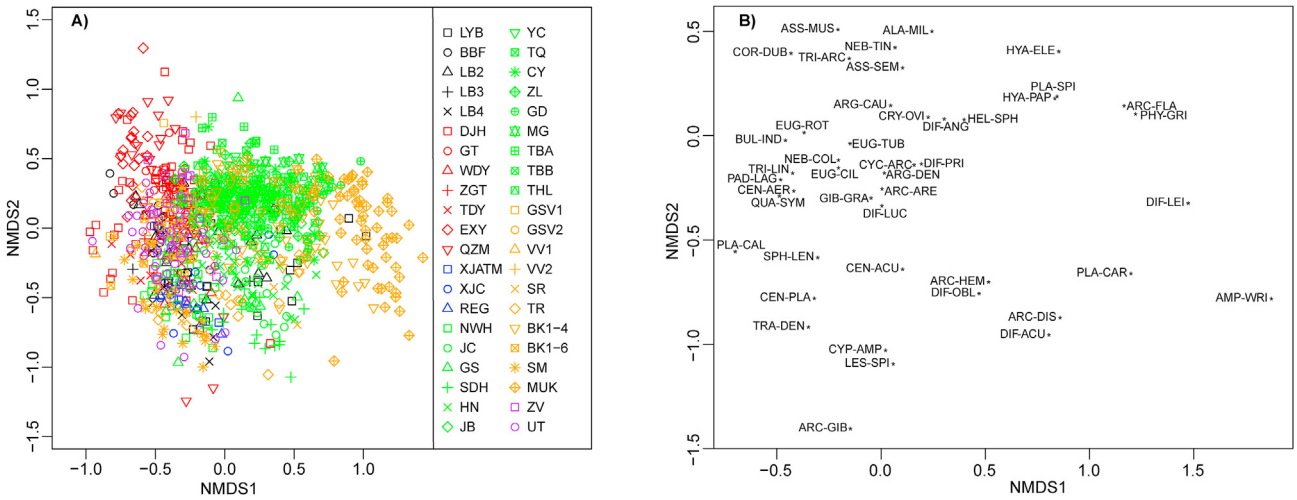

Fig. 2. NMDS of testate amoeba community data from 42 Asian peatlands (A: sites, B: species). Colours of points represent individual sampling sites. Plot based on the 1068 samples, stress = 0.14. Full species names are given in Table 2.

Table 3
Percentage explained variance by environmental variables and axes in RDA of testate amoeba data from 42 Asian peatlands (862 samples, see text for details).

	Axis 1	Axis 2	All	WTD	Longitude	Latitude
% variance explained in species data	10.53	8.58	15.08	4.73	3.32	6.37

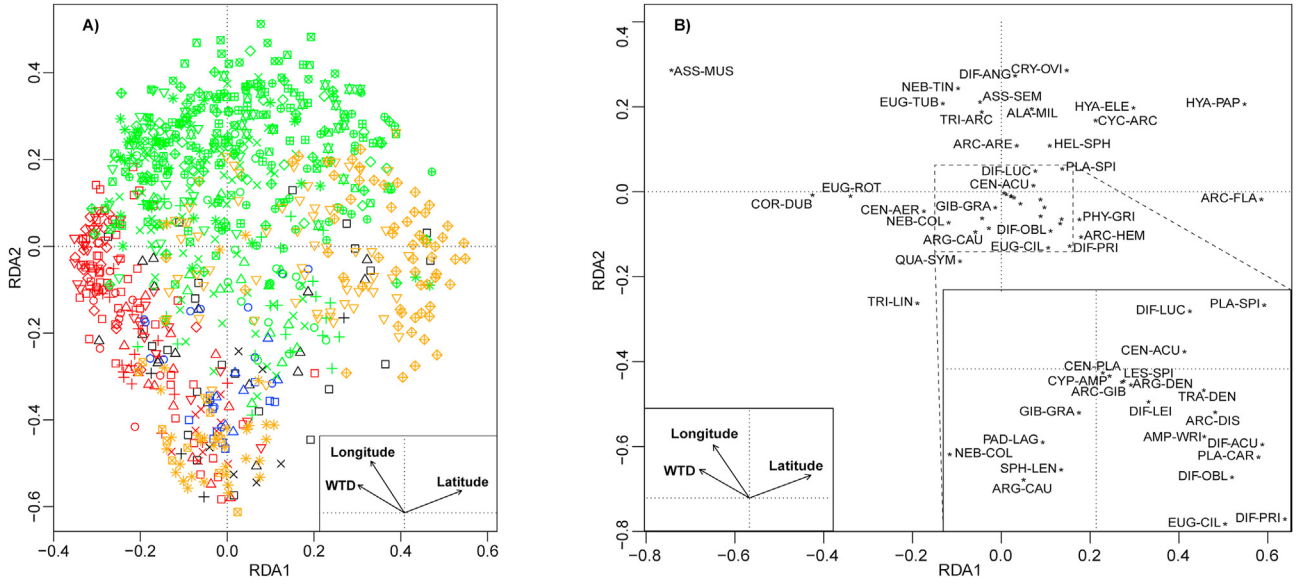

Fig. 3. RDA biplots of testate amoeba community composition from Asian peatlands (862 samples, 42 sites) showing the relations of environmental variables with sites (A), and species (B). Each site is illustrated by a different symbol (for legend see Fig. 2). Full species names are given in Table 2.

which moisture content was measured, but not water table depth (n = 191). Water table depth has generally been preferred in testate amoeba transfer function development as it is a relatively robust and easy-to-measure variable which significantly explains variance in testate amoeba assemblages, despite the indirect mechanistic link to testate amoebae typically living many centimetres above the water table. However, WTD and moisture content are typically correlated and we have many samples for which only moisture content data is available. Water table correlations with moisture are frequently strong, although the relationship can break down in conditions with very deep water tables and in certain peatland environments (Price, 1997). Nevertheless, we can reasonably expect that if a transfer function performs well, predicted water tables for sites not included in the training set will be correlated with measured surface moisture content. We applied our final selected transfer function to all samples for which moisture content, but not WTD data, were available (n = 191) and compared the strength of correlation to that between moisture content and WTD where both were measured (n = 580).

Finally, we applied the transfer function to a palaeoecological dataset. This dataset is derived from a short near-surface core from Dajiuhu peatland, a site in central China with surface samples

included in the training set (Qin et al., 2013, see details in Table 1, site (10)). We harmonised the taxonomies and applied the selected WA-PLS transfer function to the dataset with boot-strap confidence intervals calculated. We calculated a number of measures of transfer function fit to the palaeoecological dataset comprising the proportion of shared taxa, the proportion of fossil samples with poor modern analogues and the squared residual lengths (Supplementary Table 3).

Previous continental-scale studies have addressed the question of sub-continental differences in testate amoeba ecological preferences by considering differences between training sets based on different ecoregions (Amesbury et al., 2016). Here we follow this example for our Asian sites. All sampling locations were assigned to one of the global terrestrial ecoregions following Olson et al. (2001) using the 'speciesgeocode' package (Zizka and Antonelli, 2015). Sampling sites occur in four ecoregions: Subtropical Moist Broadleaf Forests (n = 105); Temperate Broadleaf and Mixed Forests (n = 499); Temperate Conifer Forests (n = 227) and Montane Grasslands and Shrublands (n = 31). Of these ecoregions, all except for Montane Grasslands & Shrublands were considered to contain sufficient samples for model development. For comparability, ecoregion transfer functions were developed using the same pruned dataset and optimal model structure selected for the entire dataset (two-component WA-PLS). Each ecoregion transfer function was applied to the palaeoecological dataset (derives from the Temperate Broadleaf and Mixed Forests ecoregion).

3. Results

3.1. Testate amoeba ecology and biogeography

Given the large climatic range and different ecoregions sampled, there is surprisingly little difference in peatland testate amoeba assemblage composition across the region. From Siberia to subtropical China there is considerable similarity in the relative abundance of testate amoeba taxa in different sites. Most testate amoebae taxa reported in this study are broadly distributed in peatlands across the world. The most abundant and frequent species is *Assulina muscorum* which appeared in almost all samples. As the samples included in this study spanned wide geographic and climatic ranges, some rare taxa were recorded and the data include species with contrasted geographical distributions (See details in Table 2 and supplementary Table 1). For example, *Hyalosphenia papilio* and *H. elegans* are abundant in boreal peatlands while *Cornutheca* (*Nebela*) *jiuhuensis* and *Argynnia caudata* are more frequent in subtropical regions. In order to assess the potential influence of the biogeographic distribution on transfer functions, we removed the sites from subtropical regions. The results showed that the performance of transfer functions slightly increased in terms of higher R^2 and lower RMSEP values (Supplementary Table 4). However, the number of samples was reduced with only 62% of the full data set included (699 in 1124 samples).

3.2. Ordination

The NMDS showed considerable overlap in assemblage composition between sites with most samples tightly clustered (Supplementary Table 2, Fig. 2A and B). In the analysis of samples with WTD data, WTD was strongly correlated with axis 2 (R = −0.63). In the analysis of samples with longitude data, longitude was strongly correlated with axis 2 (R = −0.74), while latitude was strongly correlated with axis 1 (R = 0.95) (Supplementary Table 2).

In RDA ordinations, WTD and latitude were correlated with axis 1, while longitude was correlated with axis 2 (Fig. 3A and B). The included environmental variables (WTD, latitude, and longitude) were correlated explain 15.08% of variance in the full data, where WTD explained 4.73% of the variance in assemblage composition (Table 3). While this is a small proportion, this figure is broadly concordant with previous studies and the result is highly significant. This significant correlation provides a basis for the development of transfer functions.

3.3. Transfer function development and performance

Full transfer function cross-validation results are presented in Table 4. Following initial testing, we found that a two-component WA-PLS model and weighted averaging with tolerance down-weighting and inverse deshrinking were the optimal models in their classes. With the full dataset two-component, WA-PLS was the optimal model in terms of RMSEP while MAT was often superior in terms of R^2. However, MAT showed a particularly large reduction in performance when using LOSO cross-validation, suggesting that inter-site differences in assemblage have a considerable impact on performance. All models showed poorer performance in LOSO testing than with LOO or boot-strapping, with the deterioration in performance most apparent in R^2. Even before data-pruning, almost all models had an RMSEP value lower than the standard deviation of the water table (13.1 cm), implying that they have predictive power (Fig. 4).

Following data pruning, there was a considerable improvement in model performance based on all metrics, with the improvement in Maximum Bias particularly marked (Table 4). Data pruning also substantially reduced the difference between LOSO and the other cross-validation methods. Following this data filtering, different models performed differently in terms of alternative performance measures. In terms of RMSEP, WA-PLS was generally optimal but was marginally out-performed by MAT in LOO cross-validation. In terms of R^2, ML performed well. Considering the overall results, we opted for a two-component WA-PLS as the preferred model structure based on generally good performance across measures and limited deterioration in performance when using LOSO as compared to LOO and bootstrapping. This model had an $RMSEP_{Boot}$ of 8.98 cm and cross-validation results showed a strong relationship ($R^2_{boot} = 0.68$) between measured and predicted values with considerable overlap between samples from different ecoregions (Fig. 4). This model, based on 814 samples, was taken for further evaluation.

Tests of the role of the training set spatial autocorrelation showed some evidence for impacts on model performance (Table 4, Fig. 4). As expected from LOSO, the results showed a marked deterioration in performance when deleting very proximal samples from the same site and further, but somewhat lower, deterioration with additional deletion. Spatial autocorrelation may therefore lead performance statistics to be over-optimistic and this caveat should be borne in mind when applying the transfer function, particularly to regions where no samples were collected (Telford and Birks, 2009). Segment-wise RMSEP showed that model performance was strongest towards the centre of the water table gradient, where there was the greatest data density. In the central segment, RMSEP was only 5.3 cm but performance is weaker at the extremes of the gradient and particularly at the drier end; paralleling many previous findings showing weaker links between WTD and amoeba assemblages in very dry sites (Booth, 2002, 2008). $RMSEP_{segment-wise}$ was 9.3 cm, higher than overall results but still comfortably within the range of RMSEP for published testate amoeba transfer functions and broadly comparable to values from similar, continental-scale studies (Amesbury et al., 2016, 2018).

In terms of the hydrological preferences of individual taxa, weighted average results showed a considerable range

Table 4
Full details of Asian peatland testate amoeba water table depth transfer function performance in cross-validation.

	$RMSEP_{loo}$	R^2_{loo}	Ave $Bias_{loo}$	Max $Bias_{loo}$	$RMSEP_{boot}$	R^2_{boot}	Ave $Bias_{boot}$	Max $Bias_{boot}$	$RMSEP_{loso}$	R^2_{loso}	Ave $Bias_{loso}$	Max $Bias_{loso}$
Full data												
WA Inv (tol)	9.94	0.42	0.00	43.22	9.98	0.42	0.01	43.29	10.23	0.38	0.06	43.97
WA-PLS (2)	9.91	0.44	0.05	41.50	9.78	0.43	0.02	41.54	10.25	0.38	0.04	42.44
ML	13.03	0.45	−1.20	28.46	13.22	0.43	−1.30	27.42	13.61	0.40	−1.45	30.75
MAT	8.57	0.57	−0.75	29.97	9.39	0.58	−0.78	30.79	10.26	0.40	−1.19	33.97
Pruned												
WA Inv (tol)	8.03	0.48	−0.01	16.56	8.06	0.49	−0.02	16.58	8.29	0.45	0.05	17.08
WA-PLS (2)	7.92	0.51	0.02	15.40	8.02	0.51	0.04	15.29	8.32	0.46	0.10	16.10
ML	8.96	0.68	−0.91	28.50	8.98	0.68	−0.85	29.28	9.31	0.64	−1.06	30.52
MAT	6.93	0.67	−0.67	16.27	7.68	0.67	−0.71	16.42	8.57	0.50	−1.13	16.47

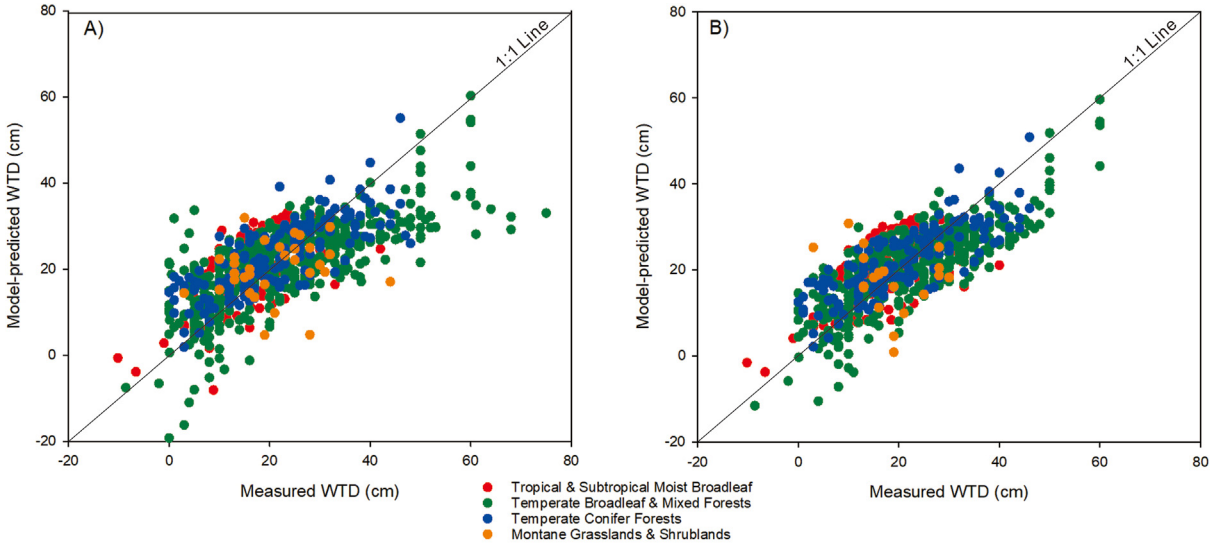

Fig. 4. Biplots of observed and predicted (Bootstrap cross-validated) water-table depth using the Asian peatland testate amoeba transfer function, for the full dataset (A), and the pruned dataset (B). The 1:1 line is plotted for reference. (blue circle = Temperate Conifer Forests, green circle = Temperate Broadleaf and Mixed Forests, red circle = Subtropical Moist Broadleaf Forests, orange circle = Montane Grasslands and Meadows).

(Supplementary Figure 3). At the wetter end of the gradient are taxa such as *Pontigulasia elisa, Amphitrema wrightianum* and *Difflugia acuminata*. At the drier end of the gradient are taxa such as *Bullinularia indica, Assulina seminulum* and *Trigonopyxis arcula*. More generally, most taxa belonging to the genera *Assulina, Bullinularia*, *Corythion, Cyclopyxis, Euglypha*, *Trinema* and *Trigonopyxis,* were indicative for the driest conditions, and most taxa in genera *Argynnia*, *Centropyxis, Difflugia, Pontigulasia* and *Quadrulella* were associated with the wettest conditions (Supplementary Figure 3).

3.4. Testing against moisture content data

Our novel test of transfer function performance using sites with measured moisture content data adds further nuance to these results (Supplementary Figure 2; Table 5). In the training set there is a moderately strong correlation between measured moisture content and water table depth (R^2 = 0.4; Supplementary Figure 2A). This result sets a maximum strength of correlation which could be reasonably expected when the transfer function is applied to predict water table depth in the sites with only moisture data available. Correlations with this independent test set are far weaker (R^2 = 0.06; Supplementary Figure 2B). However, this weak correlation is primarily due to the high proportion of sites with very low moisture content, often samples from non-*Sphagnum* habitats. If only the proportion of the moisture gradient also represented in the training set is considered, the results are much more comparable (R^2 = 0.28). While the limited strength of the correlation between WTD and moisture limits what can be concluded from such testing our results add a level of confidence that the model output has predictive ability.

Table 5
Performance of selected transfer function when applied to samples with measured moisture content (also shown in supplementary Figure 2) and, for comparability, moisture content versus water table depth for training set samples.

	Measured WTD vs moisture (training set)	Predicted WTD vs measured moisture (independent samples)	Predicted WTD vs measured moisture (independent samples within same range)
N	580	191	140
RMSE	3.00	21.6	7.42
R^2	0.40	0.06	0.283

3.5. Palaeoecological application

We subsequently applied the selected transfer function to a palaeoecological record from one of the sites, the Dajiuhu peatland (Fig. 5). The diversity in the 129-cm deep peat core is relatively high, with the dominate taxa being *Assulina muscorum*, *Centropyxis aculeate*, *Difflugia oblonga* type, *D. pristis* type, *Euglypha rotunda* type, *Alabasta militaris* type, *Pontigulasia elisa* and *Trinema lineare* type (Supplementary Figure 4). The fit of the transfer function to the palaeoecological data was adequate and within the range of previous studies (Supplementary Table 3). The resulting reconstruction implies a general increase in WTD from sampling depth of 43 cm followed by a fall at a sampling depth of 11 cm and a subsequent increase towards the surface. The bootstrap standard error of prediction values (mean = 8.2 cm) are at the lower end of the range typical for testate amoeba reconstructions of peatland water table depth.

3.6. Ecoregion-specific models

Performance of the three ecoregion models was variable (Table 6). The model for the 'Subtropical Moist Broadleaf Forests' sites had the weakest performance overall with a high Maximum Bias and a notably low R^2, particularly in LOSO cross-validation. Performance for the other two models was generally comparable, and sometimes superior, to the full continental model. Across most measures, model performance was strongest for the 'Temperate Conifer Forests' sites. Plots of cross-validated (LOSO) model predictions versus measured values show reasonably strong correlations (Fig. 6).

When applied to the palaeoecological data series the reconstructions differed markedly in absolute values with the 'Temperate Broadleaf and Mixed Forests' ecoregion model giving much higher WTD values than the others (Fig. 7). This is most likely a consequence of the greater measured range in this region, which included most of the drier sites sampled (Fig. 7). All models showed similar trends in the reconstruction, including the trough from 15 to 7 cm and minor peaks at 10 and 29 cm. When results were expressed as z-scores (standardised residuals) rather than absolute values (Swindles et al., 2015) the reconstructions were highly concordant with only minor discrepancies, most apparent in the lowermost sample (Fig. 7B).

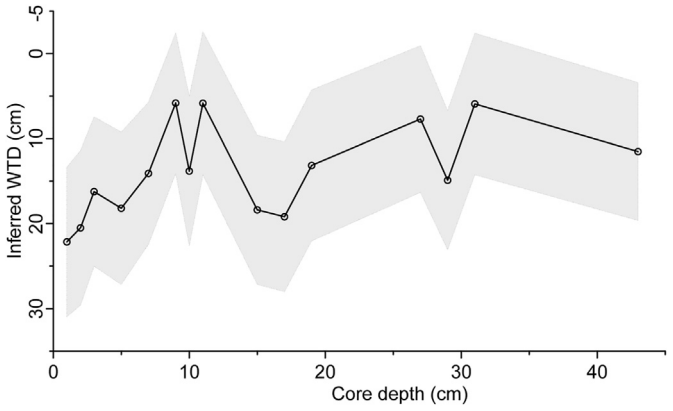

Fig. 5. Water-table depth reconstruction for the Dajiuhu peatland (Shennongjia mountains, central China) based on the selected WA-PLS testate amoeba-based transfer function with bootstrap-derived standard errors of prediction.

4. Discussion

4.1. Diversity and biogeography consideration

Most testate amoeba taxa in this study have a broad distribution across the Holarctic or beyond. However, some species such as *Hyalosphenia papilio* are common in northern peatlands, but rare or absent from subtropical regions. *Archerella flavum* and *Amphitrema wrightianum,* two very common species in boreal peatlands, have not yet been reported in subtropical peatlands of Asia. *Arcella arenaria*, *Hyalosphenia papilio* and *Planocarina marginata* were reported only recently from peatlands in north Asia (Li et al., 2010; Qin et al., 2012; Kurina and Li, 2019). By contrast, *Cornutheca jiuhuensis* and *Argynnia caudata* were only reported from subtropical peatlands (Qin et al., 2013, 2016). Some species were only found at one or two sites (Supplementary Table 1), possibly suggesting that their ecological optimum is not within *Sphagnum*-dominated peatlands and that they only occur there accidentally (Bonnet et al., 1981; Qin et al., 2013, 2016). In some cases, however, taxonomic confusion could lead to erroneous records and this was the main reason for pooling species into conservative morphotypes that would minimise observers' bias. The downside of doing so is that some individual species within morpho-species may differ in ecological optima or geographical distribution (Charman and Warner, 1997; Booth and Zygmunt, 2005; Charman et al., 2007; Swindles et al., 2009; Qin et al., 2013; Mitchell et al., 2014; Singer et al., 2018). The fact that, despite taxonomic harmonisation, longitude and latitude were correlated with axis 2 in the RDA could thus either be interpreted as revealing a geographical signal, an ecological signal, or the fact that different people analysed the samples. This calls for a more detailed analysis of the geographical distribution of testate amoebae, greater sampling efforts along ecological gradients and across broad geographical ranges and the use of a well-defined consistent taxonomic framework in future work.

4.2. Community composition responding to hydrological conditions

The ordination results revealed that surface wetness, represented by water table depth, is a controlling factor for testate amoeba community compositions, in agreement with previous studies. In recent years, studies in the ecology of testate amoebae suggested that the correlation between community composition and the hydrological gradient is reflected at fine (hummock – hollow gradient), broad (among sites), regional and continental to pan-continental scales (Qin et al., 2013; Li et al., 2015; Amesbury et al., 2013, 2016; Swindles et al., 2016). This was also reflected in the horizontal or vertical distribution patterns of testate amoebae at fine scales along micro-topographic and hence moisture gradients in *Sphagnum* peatlands (Mitchell et al., 2000; Jassey et al., 2011; Qin et al., 2013).

Results of ordination map and hydrological transfer function show similar responding trends to previous studies elsewhere in the world (Charman, 1997; Bobrov et al., 1999; Booth, 2001; Lamentowicz and Mitchell, 2005; Payne et al., 2008; Swindles et al., 2009; Amesbury et al., 2016). Taxa indicators for relatively dry conditions are *Assulina muscorum*, *A. seminulum*, *Bullinularia indica, Euglypha rotunda, Corythion dubium, Alabasta militaris* type, *Nebela tincta, Trinema lineare* and *Trigonopyxis arcula* type. Indicators for wet biotopes are *Arcella gibbosa* type, *Arcella hemisphaerica*, *Pontigulasia elisa, Amphitrema wrightianum* and *Difflugia acuminata, D. leidy, D. oblonga*, *Planocarina carinata* type and *Physochila griseola*.

In general, the species richness of Arcellinida taxa is higher in wetter conditions. Also, taxa at the wetter end of the hydrological gradient seem to have a larger size than most of those at the drier

Table 6
Performance of peatland testate amoeba water table depth transfer function models from three Asian ecoregions in cross-validation.

	$RMSEP_{loo}$	R^2_{loo}	Ave $Bias_{loo}$	Max $Bias_{loo}$	$RMSEP_{boot}$	R^2_{boot}	Ave $Bias_{boot}$	Max $Bias_{boot}$	$RMSEP_{loso}$	R^2_{loso}	Ave $Bias_{loso}$	Max $Bias_{loso}$
Temperate Conifer Forests												
WA-PLS (2)	7.10	0.65	0.01	11.28	7.33	0.65	0.01	11.38	9.32	0.44	0.84	16.28
Temperate Broadleaf & Mixed Forests												
WA-PLS (2)	7.79	0.52	0.11	13.98	7.98	0.52	0.17	14.15	8.65	0.43	−0.05	14.70
Subtropical Moist Broadleaf Forests												
WA-PLS (2)	6.69	0.33	−0.05	21.42	6.92	0.35	−0.07	6.92	7.88	0.12	−0.99	26.80

end. This has been confirmed by some recent studies on shell functional traits of testate amoebae in peatlands, which implied that the shell size and biovolume are negatively correlated with WTD, among the Arcellinida (Fournier et al., 2015; van Bellen et al., 2017; McKeown et al., 2019). Functional traits analyses of testate amoebae have started to be used in ecological studies and palaeoenvironmental reconstructions (Marcisz et al., 2020), and our results show that this potential also exists in Asian peatlands.

4.3. Asian testate amoeba-based hydrological transfer function

An increasing number of hydrological transfer function based on testate amoebae in peatlands have been built in the past two decades. The current trend is now to develop larger-scale models to be applied in palaeohydrological reconstructions in peatlands across larger regions. In Asia, several hydrological transfer functions using testate amoebae in peatlands have recently been developed (Qin et al., 2013, 2018; Li et al., 2015; Kurina and Li, 2019). However, a larger scale transfer function with numerous training datasets will have a broader scale application because it can better represent testate amoeba ecology than local or regional scale models with lower number of samples (Amesbury et al., 2016). We, therefore, hope that the new large-scale transfer function presented here will be widely used for palaeohydrological reconstructions of peatlands in Asia.

The cross-validation method used in the model development showed poorer performance in LOSO testing than with LOO or boot-strapping in all model types, with ML performance consistently best. Considering the small differences of R^2 values between different performance and previous studies (Payne et al., 2012; Qin et al., 2013), LOO, boot-strapping and LOSO cross-validation methods are similar and robust in model development. For the full dataset, with WA, WA-PLS and MAT, the models predicted similar WTD values for full samples, while with MAT, there was a strongest ($RMSEP_{boot}$ = 9.39 cm, R^2_{boot} = 0.58) relationship between observed and estimated values. For the pruned dataset, R^2 values of observed and estimated by WA, WA-PLS and MAT are higher than the full dataset, while ML showed the strongest predicted power ($RMSEP_{boot}$ = 8.98 cm, R^2_{boot} = 0.68). The predictive capability of the Asian peatlands WTD transfer function is as good as other large/continental-scale hydrological transfer functions, such as the European ($RMSEP_{Jack}$ = 5.65 cm, R^2_{Jack} = 0.71, Charman et al., 2007), pan-European ($RMSEP_{LOO}$ = 7.72 cm, R^2_{LOO} = 0.59, Amesbury et al., 2016) and Northern American peatlands ($RMSEP_{LOO}$ = 6.83 cm, R^2_{LOO} = 0.79, Amesbury et al., 2018), which suggested that the transfer functions can be used for palaeohydrological reconstructions in Asian peatlands.

For moisture, however, it should be noted that the model performance for surface moisture was relatively poor. With WA-PLS, relations between measured WTD and moisture show low values (R^2 = 0.4, RMSE = 3%, N = 580). The poor performance for moisture can be caused by sampling strategy or the error made during measurements. A larger training set and validation of our model with independent data are therefore desirable before the transfer function can be applied to palaeoecological records (Qin et al., 2013).

4.4. Ecoregional transfer function and hydrological reconstruction

The performance of transfer functions for the three ecoregion training sets showed that the WAPLS models were robust for temperate conifer forests (R^2 = 0.67) and temperate broadleaf and mixed forests (R^2 = 0.61). Both bootstrapping and LOO values for the WA-PLS model in the two ecoregions in temperate forests are good, and similar to other studies.

However, the 'Subtropical moist broadleaf forests' models performed poorly (R^2_{boot} = 0.37). This suggests that the model should only be used with extreme caution in tropical sites. These poor results are in strong contrast with a previous study in Amazonian peatlands using WA-PLS ($R^2_{apparent}$ = 0.76, RMSE = 4.29 cm; R^2_{loo} = 0.68, RMSEP = 5.18 cm) (Swindles et al., 2014). We interpret this result as an indication that most subtropical peatlands included in this study were disturbed and indeed it is unclear if a sufficient number of relatively pristine peatlands still exist in the region to study the ecology of testate amoebae in a natural setting (Qin et al., 2016, 2020). By contrast, many peatlands in Amazonia are still well preserved.

This was further confirmed in our example of palaeohydrological application where the reconstruction based on the models for each ecoregion differed substantially in absolute values, with the 'Temperate Broadleaf & Mixed Forests' ecoregion model giving much higher WTD values (i.e. drier) than the others (Fig. 7). This is most likely a consequence of the greater measured range in this region, which included most of the drier sites sampled.

5. Conclusion

We studied the community ecology and species-environment relationships of testate amoebae across Asian peatlands based on 1124 samples from 42 sites. Consistent with many previous ecological studies on testate amoebae, our results showed that water table depth is the key variable with which testate amoeba communities are correlated in peatlands. Based on these data, we developed a large-scale testate amoeba-based palaeohydrological transfer function for boreal to subtropical Asian peatlands. The predictive capability of the Asian peatlands WTD transfer function is comparable with other large/continental-scale hydrological transfer functions, suggesting that the model can be used for palaeohydrological reconstructions in the peatlands of Asia. This tool will be useful for studies which aim to reconstruct past climatic change in the region and thus to assess the extent to which ongoing climate changes differ from the long-term record (Booth, 2010). This, in turn, will be useful in determining potential threats to the functioning of Asian peatlands under future climate warming scenarios, which, when the high proportion of global soil organic carbon that is currently stored in Asian peatlands is considered, could represent a considerable positive feedback loop in the ongoing rise in atmospheric carbon concentration.

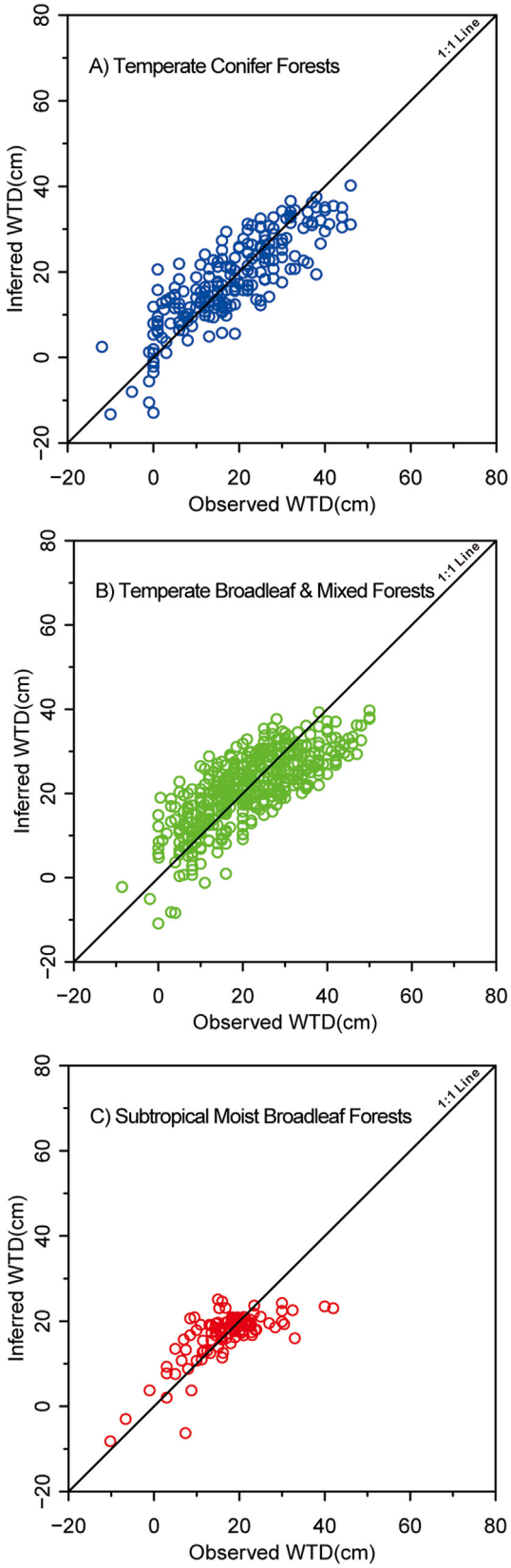

Fig. 6. Plots of measured peatland water-table depth versus testate amoeba-based transfer function predictions (LOSO cross-validation) for Asian ecoregion-specific transfer functions: Temperate Conifer Forests (A), Temperate Broadleaf and Mixed Forests (B) and Subtropical Moist Broadleaf Forests (C).

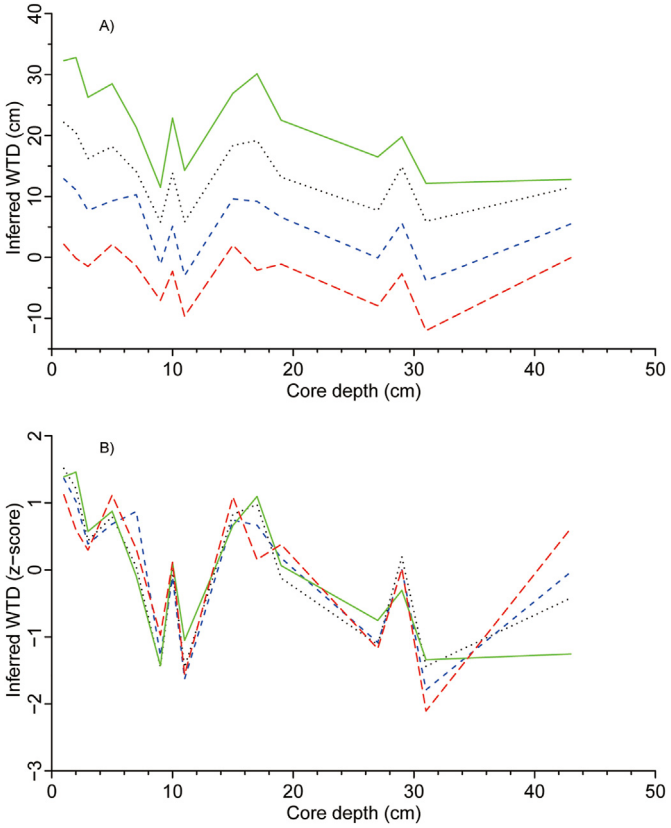

Fig. 7. Comparison of water table depth reconstructions by the core from Dajiuhu peatland based on the Asian testate amoeba transfer function and models for three ecoregions. Black dotted line: full dataset, blue: temperate Conifer Forests, green: temperate Broadleaf and Mixed Forests, red: subtropical Moist Broadleaf Forests. Top panel (A) shows reconstructed values, lower panel (B) shows z-scores. Error bars omitted for clarity.

Author statement

All members in the authorship have contributed a lot to this work either on providing samples, field works and original data, or on editing and writings. Some persons were mentioned in the Acknowledgement section.

Declaration of competing interest

The authors declare that they have no known competing financial interests or personal relationships that could have appeared to influence the work reported in this paper.

Acknowledgments

We dedicate this study to our late colleague Dr Richard J. Payne who passed away in 2019 in a mountaineering accident in the Himalayas. Richard was instrumental in making this study happen and he ran the transfer function analyses for this study. The first draft of the manuscript was written by YQ, RJP and HL with contributions from all authors.

This work was supported by National Science Foundation of China (NO. 41502167, 41771217) and the '111 project' of China (grant No. BP0820004), 'Belt and Road Project' in CUG (T2018014), and Russian Science Foundation (grant No. 19-14-00102). We thank Guillaume Lentendu for preparing the Fig. 1. We thank the two anonymous reviewers for their constructive comments.

Appendix A. Supplementary data

Supplementary data to this article can be found online at https://doi.org/10.1016/j.quascirev.2021.106868.

References

van Bellen, S., Mauquoy, D., Payne, R.J., Roland, T.P., Daley, T.J., Hughes, P.D.M., Loader, N.J., Street-Perrott, F.A., Rice, E.M., Pancotto, V.A., 2014. Testate amoebae as a proxy for reconstructing Holocene water table dynamics in southern Patagonian peat bogs. J. Quat. Sci. 29, 463–474. https://doi.org/10.1002/jqs.2719.

Amesbury, M.J., Mallon, G., Charman, D.J., Hughes, P.D.M., Booth, R.K., Daley, T.J., Garneau, M., 2013. Statistical testing of a new testate amoeba-based transfer function for water-table depth reconstruction on ombrotrophic peatlands in north-eastern Canada and Maine, United States. J. Quat. Sci. 28, 27–39. https://doi.org/10.1002/jqs.2584.

Amesbury, M.J., Swindles, G.T., Bobrov, A., Charman, D.J., Holden, J., Lamentowicz, M., Mallon, G., Mazei, Y., Mitchell, E.A.D., Payne, R.J., Roland, T.P., Turner, T.E., Warner, B.G., 2016. Development of a new pan-European testate amoeba transfer function for reconstructing peatland palaeohydrology. Quat. Sci. Rev. 152, 132–151. https://doi.org/10.1016/j.quascirev.2016.09.024.

Amesbury, M.J., Booth, R.K., Roland, T.P., Bunbury, J., Clifford, M.J., Charman, D.J., Elliott, S., Finkelstein, S., Garneau, M., Hughes, P.D.M., Lamarre, A., Loisel, J., Mackay, H., Magnan, G., Markel, E.R., Mitchell, E.A.D., Payne, R.J., Pelletier, N., Roe, H., Sullivan, M.E., Swindles, G.T., Talbot, J., van Bellen, S., Warner, B.G., 2018. Towards a Holarctic synthesis of peatland testate amoeba ecology: development of a new continental-scale palaeohydrological transfer function for North America and comparison to European data. Quat. Sci. Rev. 201, 483–500. https://doi.org/10.1016/j.quascirev.2018.10.034.

Beilman, D.W., MacDonald, G.M., Smith, L.C., Reimer, P.J., 2009. Carbon accumulation in peatlands of West Siberia over the last 2000 years. Global Biogeochem. Cycles 23, GB1012. https://doi.org/10.1029/2007GB003112.

Beyens, L., Meisterfeld, R., 2001. Protozoa: testate amoebae. In: Smol, J.P., Birks, H.J.B., Last, W.M. (Eds.), Tracking Environmental Change Using Lake Sediments, ume 3. Terrestrial, Algal, and Siliceous Indicators. Kluwer, Dordrecht, pp. 119–153.

Birks, H.J.B., 1995. Quantitative palaeoenvironmental reconstructions. In: Maddy, D., Brew, J.S. (Eds.), Statistical Modelling of Quaternary Science Data. Quaternary Research Association, Cambridge, pp. 161–254.

Birks, H.J.B., Line, J.M., Juggins, S., Stevenson, A.C., Ter Braak, C.J.F., 1990. Diatoms and pH reconstruction. Philosophical transactions of the royal society of london.B. Biol. Sci. 327, 263–278.

Bobrov, A.A., Charman, D.J., Warner, B.G., 1999. Ecology of testate amoebae (Protozoa: rhizopoda) on peatlands in western Russia with special attention to niche separation in closely related taxa. Protist 150, 125–136.

Bonnet, L., Brabet, J., Comoy, N., Guitard, J., 1981. Nouvelle données sur le thécamoebien filosia *Amphitrema flavum* (Archer 1877) Penard 1902. PROTISTOLOGICA 17, 225–233.

Booth, R.K., 2001. Ecology of testate amoebae (Protozoa) in two lake superior coastal wetlands: implications for palaeoecology and environmental monitoring. Wetlands 21, 564–576.

Booth, R.K., 2002. Testate amoebae as palaeoindicators of surface-moisture changes on Michigan peatlands: modern ecology and hydrological calibration. J. Paleolimnol. 28, 329–348.

Booth, R.K., 2008. Testate amoebae as proxies for mean annual water-table depth in *Sphagnum*-dominated peatlands of North America. J. Quat. Sci. 23, 43–57. https://doi.org/10.1002/jqs.1114.

Booth, R.K., 2010. Testing the climate sensitivity of peat-based paleoclimate reconstructions in mid-continental North America. Quat. Sci. Rev. 29, 720–731. https://doi.org/10.1016/j.quascirev.2009.11.018.

Booth, R.K., Zygmunt, J.R., 2005. Biogeography and comparative ecology of testate amoebae inhabiting *Sphagnum*-dominated peatlands in the Great Lakes and Rocky Mountain regions of North America. Divers. Distrib. 11, 577–590. https://doi.org/10.1111/j.1366-9516.2005.00154.x.

Bray, J.R., Curtis, J.T., 1957. An ordination of the upland forest communities of southern Wisconsin. Ecol. Monogr. 27, 325–349.

Charman, D.J., 1997. Modelling hydrological relationships of testate amoebae (Protozoa: rhizopoda) on New Zealand peatlands. J. Roy. Soc. N. Z. 27, 465–483.

Charman, D.J., Warner, B.G., 1992. Relationship between testate amoebae (Protozoa, Rhizopoda) and microenvironmental parameters on a forested peatland in northeastern Ontario. Can. J. Zool. 70, 2474–2482.

Charman, D.J., Warner, B.G., 1997. The ecology of testate amoebae (Protozoa: rhizopoda) in oceanic peatlands in Newfoundland, Canada: modelling hydrological relationships for paleoenvironmental reconstruction. Ecoscience 4, 555–562.

Charman, D.J., Hendon, D., Woodland, A.A., 2000. The Identification of Testate Amoebae (Protozoa: Rhizopoda) from British Oligotrophic Peats. Quaternary Research Association Technical Guide Series, Cambridge, UK.

Charman, D.J., Brown, A.D., Hendon, D., Karofeld, E., 2004. Testing the relationship between Holocene peatland palaeoclimate reconstructions and instrumental data at two European sites. Quat. Sci. Rev. 23, 137–143. https://doi.org/10.1016/j.quascirev.2003.10.006.

Charman, D.J., Blundell, A., Accrotelm, M E M B E R S, 2007. A new European testate amoebae transfer function for palaeohydrological reconstruction on ombrotrophic peatlands. J. Quat. Sci. 22, 209–221. https://doi.org/10.1002/jqs.1026.

Charman, D.J., Amesbury, M.J., Hinchliffe, W., Hughes, P.D.M., Mallon, G., Blake, W.H., Daley, T.J., Gallego-Sala, A.V., Mauquoy, D., 2015. Drivers of Holocene peatland carbon accumulation across a climate gradient in northeastern North America. Quat. Sci. Rev. 121, 110–119. https://doi.org/10.1016/j.quascirev.2015.05.012.

Chung, W.H., Kang, S.B., Choi, J.B., 1992. A taxonomic study of order Arcellinida (Protozoa: sarcomastigophora: Rhizopoda) from Korea. Korean J. Syst. Zool. 8, 11–18.

Dumack, K., Görzen, D., González-Miguéns, R., Siemensma, F., Lahr, D.J.G., Lara, E., Bonkowski, M., 2020. Molecular investigation of *Phryganella acropodia* Hertwig et Lesser, 1874 (Arcellinida, Amoebozoa). Eur. J. Protistol. 75 https://doi.org/10.1016/j.ejop.2020.125707.

FAO., 2012. Global Ecological Zones for FAO Forest Reporting: 2010 Update Forest Resources Assessment Working Paper 179. UN Food and Agriculture Organization, Rome, Italy.

Fournier, B., Lara, E., Jassey, V.E.J., Mitchell, E.A.D., 2015. Functional traits as a new approach for interpreting testate amoeba palaeo-records in peatlands and assessing the causes and consequences of past changes in species composition. Holocene 25, 1375–1383. https://doi.org/10.1177/0959683615585842.

Hendon, D., Charman, D.J., 1997. The preparation of testate amoebae (Protozoa: rhizopoda) samples from peat. Holocene 7, 199–205.

Hijmans, R.J., Williams, E., Vennes, C., 2015. Geosphere: spherical trigonometry. R package https://CRAN. R-project. org/package = geosphere, version 1. 3-11.

Jassey, V.E.J., Chiapusio, G., Mitchell, E.A.D., Binet, P., Toussaint, M.L., Gilbert, D., 2011. Fine-scale horizontal and vertical micro-distribution patterns of testate amoebae along a narrow Fen/Bog gradient. Microb. Ecol. 61, 374–385. https://doi.org/10.1007/s00248-010-9756-9.

Joosten, H., 2010. The Global Peatland CO_2 Picture - peatland status and drainage related emissions in all countries of the world. In: Wetlands International (Ed.), p. 36.

Juggins, S., 2009. rioja: analysis of Quaternary science data. R package version 0.5-6. URL http://cran.r-project.org/package = rioja.

Klimaschewski, A., Barnekow, L., Bennett, K.D., Andreev, A.A., Andren, E., Bobrov, A.A., Hammarlund, D., 2015. Holocene environmental changes in southern Kamchatka, Far Eastern Russia, inferred from a pollen and testate amoebae peat succession record. Global Planet. Change 134, 142–154. https://doi.org/10.1016/j.gloplacha.2015.09.010.

Koenig, I., Schwendener, F., Mulot, M., Mitchell, E.A.D., 2017. Response of *Sphagnum* testate amoebae to drainage, subsequent Re-wetting and associated changes in the moss carpet. Acta Protozool. 56, 191–210. https://doi.org/10.4467/16890027AP.17.017.7498.

Koenig, I., Mulot, M., Mitchell, E.A.D., 2018. Taxonomic and functional traits responses of *Sphagnum* peatland testate amoebae to experimentally manipulated water table. Ecol. Indicat. 85, 342–351. https://doi.org/10.1016/j.ecolind.2017.10.017.

Kosakyan, A., Gomaa, F., Lara, E., Lahr, D.J., 2016. Current and future perspectives on the systematics, taxonomy and nomenclature of testate amoebae. Eur. J. Protistol. 55, 105–117. https://doi.org/10.1016/j.ejop.2016.02.001.

Krashevska, V., Tsyganov, A.N., Esaulov, A.S., Mazei, Y.A., Hapsari, K.A., Saad, A., Sabiham, S., Behling, H., Biagioni, S., 2020. Testate amoeba species- and trait-based transfer functions for reconstruction of hydrological regime in tropical peatland of central sumatra, Indonesia. Front. Ecol. Evol. 8 (225) https://doi.org/10.3389/fevo.2020.00225.

Kurina, I.V., 2011. Ecology of testate amoebae as hydrological regime indicators in oligotrophic peatlands in the southern taiga of Western Siberia. Izvestia Penzenskogo gosudarstvennogo pedagogicheskogo universiteta 25, 368–375.

Kurina, I.V., Li, H., 2019. Why do testate amoeba optima related to water table depth vary? Microb. Ecol. 77, 37–55. https://doi.org/10.1007/s00248-018-1202-4.

Lamentowicz, M., Mitchell, E.A.D., 2005. The ecology of testate amoebae (Protists) in *Sphagnum* in north-western Poland in relation to peatland ecology. Microb. Ecol. 50, 48–63. https://doi.org/10.1007/s00248-004-0105-8.

Lamentowicz, M., Lamentowicz, Ł., van der Knaap, W.O., Gąbka, M., Mitchell, E.A.D., 2010. Contrasting species-environment relationships in communities of testate amoebae, bryophytes and vascular plants along the fen-bog gradient. Microb. Ecol. 59, 499–510. https://doi.org/10.1007/s00248-009-9617-6.

Lamentowicz, M., Słowiński, M., Marcisz, K., Zielińska, M., Kaliszan, K., Lapshina, E., Gilbert, D., Buttler, A., Fiałkiewicz-Kozieł, B., Jassey, V.E.J., Laggoun-Defarge, F., Kołaczek, P., 2015. Hydrological dynamics and fire history of the last 1300 years in western Siberia reconstructed from a high-resolution, ombrotrophic peat archive. Quat. Res. 84, 312–325. https://doi.org/10.1016/j.yqres.2015.09.002.

Legendre, P., Gallagher, E.D., 2001. Ecologically meaningful transformations for ordination of species data. Oecologia 129, 271–280.

Lepš, J., Šmilauer, P., 2003. Multivariate Analysis of Ecological Data Using CANOCO. Cambridge University Press, Cambridge, p. 284 pp.

Li, H.K., Wang, S., Bu, Z., Zhao, H., An, Z., Mitchell, E.A.D., Ma, Y., 2010. The testate amoebae in *Sphagnum* peatlands in Changbai Mountains. Wetl. Sci. 8, 249–255 (in Chinese).

Li, H., Wang, S., Zhao, H., Wang, M., 2015. A testate amoebae transfer function from *Sphagnum*-dominated peatlands in the Lesser Khingan Mountains, NE China. J. Paleolimnol. 54, 189–203. https://doi.org/10.1007/s10933-015-9846-2.

Marcisz, K., Fournier, B., Gilbert, D., Lamentowicz, M., Mitchell, E.A.D., 2014. Response of *Sphagnum* peatland testate amoebae to a 1-year transplantation experiment along an artificial hydrological gradient. Microb. Ecol. 67, 810–818.

https://doi.org/10.1007/s00248-014-0367-8.
Marcisz, K., Jassey, V.E.J., Kosakyan, A., Krashevska, V., Lahr, D.G.J., Lara, E., Lamentowicz, M., Lamentowicz, M., Macumber, A., Mazei, Y., Mitchell, E.A.D., Nasser, N.A., Patterson, R.T., Roe, H.M., Singer, D., Tsyganov, A.N., Fournier, B., 2020. Testate amoeba functional traits and their use in paleoecology. Front. Ecol. Evol. https://doi.org/10.3389/fevo.2020.575966.
Mazei, Y., Tsyganov, A., 2006. Freshwater Testate Amoebae. KMK, Moscow in Russian.
Mckeown, M.M., Wilmshurst, J.M., Duckert, C., Wood, J.R., Mitchell, E.A.D., 2019. Assessing the ecological value of small testate amoebae (<45 μm) in New Zealand peatlands. Eur. J. Protistol. 68, 1–15. https://doi.org/10.1016/j.ejop.2018.12.002.
Meisterfeld, R., 2002. Testate amoebae with filopodia. The illustrated guide to the protozoa 2, 1054–1084.
Mitchell, E.A.D., Buttler, A.J., Warner, B.G., Gobat, J.-M., 1999. Ecology of testate ameobae (Protozoa: rhizopoda) in *Sphagnum* peatlands in the Jura mountains, Switzerland and France. Ecoscience 6, 565–576.
Mitchell, E.A.D., Borcard, D., Buttler, A.J., Grosvernier, P., Gilbert, D., Gobat, J.M., 2000. Horizontal distribution patterns of testate amoebae (Protozoa) in a *Sphagnum magellanicum* carpet. Microb. Ecol. 39, 290–300.
Mitchell, E.A.D., Charman, D.J., Warner, B.G., 2008. Testate amoebae analysis in ecological and paleoecological studies of wetlands: past, present and future. Biodivers. Conserv. 17, 2115–2137. https://doi.org/10.1007/s10531-007-9221-3.
Mitchell, E.A.D., Lamentowicz, M., Payne, R.J., Mazei, Y., 2014. Effect of taxonomic resolution on ecological and palaeoecological inference - a test using testate amoeba water-table depth transfer functions. Quat. Sci. Rev. 91, 62–69. https://doi.org/10.1016/j.quascirev.2014.03.006.
Oksanen, J., Blanchet, F.G., Kindt, R., Legendre, P., Minchin, P.R., O'Hara, R.B., Simpson, G.L., Solymos, P., Henry, M., Stevens, H., Wagner, H., 2012. Vegan: community ecology package. http://CRAN.R-project.org/package = vegan.
Olson, D.M., Dinerstein, E., Wikramanayake, E.D., Burgess, N.D., Powell, G.V., Underwood, E.C., D'amico, J.A., Itoua, I., Strand, H.E., Morrison, J.C., 2001. Terrestrial Ecoregions of the World: a New Map of Life on Earth: a new global map of terrestrial ecoregions provides an innovative tool for conserving biodiversity. Bioscience 51, 933–938.
Overpeck, J., Webb, T., Prentice, I., 1985. Quantitative interpretation of fossil pollen spectra: dissimilarity coefficients and the method of modern analogs. Quat. Res. 23, 87–108.
Payne, R.J., 2011. Can testate amoeba-based palaeohydrology be extended to fens? J. Quat. Sci. 26, 15–27. https://doi.org/10.1002/jqs.1412.
Payne, R.J., 2013. Seven reasons why protists make useful bioindicators. Acta Protozool. 52, 105–113.
Payne, R.J., Mitchell, E.A.D., 2009. How many is enough? Determining optimal count totals for ecological and palaeoecological studies of testate amoebae. J. Paleolimnol. 42, 483–495. https://doi.org/10.1007/s10933-008-9299-y.
Payne, R.J., Kishaba, K., Blackford, J.J., Mitchell, E.A.D., 2006. Ecology of testate amoebae (Protista) in south-central Alaska peatlands: building transfer-function models for palaeoenvironmental studies. Holocene 16, 403–414. https://doi.org/10.1191/0959683606hl936rp.
Payne, R.J., Charman, D.J., Matthews, S., Eastwood, W.J., 2008. Testate amoebae as palaeohydrological proxies in Sürmene Ağaçbaşi Yaylasi peatland (northeast Turkey). Wetlands 28, 311–323. https://doi.org/10.1672/07-42.1.
Payne, R.J., Ryan, P.A., Nishri, A., Gophen, M., 2010. Testate amoeba communities of the drained Hula wetland (Israel): implications for ecosystem development and conservation management. Wetl. Ecol. Manag. 18, 177–189. https://doi.org/10.1007/s11273-009-9158-2.
Payne, R.J., Lamentowicz, M., Mitchell, E.A.D., 2011. The perils of taxonomic inconsistency in quantitative palaeoecology: experiments with testate amoeba data. Boreas 40, 15–27. https://doi.org/10.1111/j.1502-3885.2010.00174.x.
Payne, R.J., Telford, R.J., Blackford, J.J., Blundell, A., Booth, R.K., Charman, D.J., Lamentowicz, Ł., Lamentowicz, M., Mitchell, E.A.D., Potts, G., Swindles, G.T., Warner, B.G., Woodland, W., 2012. Testing peatland testate amoeba transfer functions: appropriate methods for clustered training-sets. Holocene 22, 819–825. https://doi.org/10.1177/0959683611430412.
Payne, R.J., Babeshko, K.V., van Bellen, S., Blackford, J.J., Booth, R.K., Charman, D.J., Ellershaw, M.R., Gilbert, D., Hughes, P.D.M., Jassey, V.E.J., Lamentowicz, Ł., Lamentowicz, M., Malysheva, E.A., Mauquoy, D., Mazei, Y., Mitchell, E.A.D., Swindles, G.T., Tsyganov, A.N., Turner, T.E., Telford, R.J., 2016. Significance testing testate amoeba water table reconstructions. Quat. Sci. Rev. 138, 131–135. https://doi.org/10.1016/j.quascirev.2016.01.030.
Payne, R.J., Bobrov, A.A., Tsyganov, A.N., Babeshko, K.V., Sloan, T.J., Kay, M., Kupriyanov, D.A., Surkov, N.V., Novenko, E.Y., Andreev, A.A., Mazei, Y.A., 2020. First records of contemporary testate amoeba assemblages from the Kamchatka Peninsula, Russia and potentialfor palaeoenvironmental reconstruction. Boreas. https://doi.org/10.1111/bor.12469. ISSN 0300–9483.
Price, J., 1997. Soil moisture, water tension, and water table relationships in a managed cutover bog. J. Hydrol 202, 21–32.
Qin, Y., Xie, S., 2011. Moss-dwelling testate amoebae and their community in Dajiuhu peatland of Shennongjia Mountains, China. J. Freshwater Ecol 26, 3–9. https://doi.org/10.1080/02705060.2011.553810.
Qin, Y., Payne, R.J., Gu, Y., Huang, X., Wang, H., 2012. Ecology of testate amoebae in Dajiuhu peatland of Shennongjia Mountains, China, in relation to hydrology. Front. Earth Sci. 6, 57–65. https://doi.org/10.1007/s11707-012-0307-1.
Qin, Y., Mitchell, E.A.D., Lamentowicz, M., Payne, R.J., Lara, E., Gu, Y., Huang, X., Wang, H., 2013. Ecology of testate amoebae in peatlands of central China and development of a transfer function for paleohydrological reconstruction. J. Paleolimnol. 50, 319–330. https://doi.org/10.1007/s10933-013-9726-6.
Qin, Y., Man, B., Kosakyan, A., Lara, E., Gu, Y., Wang, H., Mitchell, E.A.D., 2016. *Nebela jiuhuensis* nov. sp. (Amoebozoa; Arcellinida; Hyalospheniidae): a new member of the *Nebela saccifera-equicalceus–ansata* group described from *Sphagnum* peatlands in South-Central China. J. Eukaryot. Microbiol. 63, 558–566. https://doi.org/10.1111/jeu.12300.
Qin, Y., Payne, R., Gu, Y., Mazei, Y., Wang, Y., 2017. Short-term response of testate amoebae to wildfire. Appl. Soil Ecol. 116, 64–69. https://doi.org/10.1016/j.apsoil.2017.03.018.
Qin, Y., Gong, J., Gu, Y., Xuen, J., Xiang, C., Wu, W., Ge, J., 2018. Ecological monitoring and environmental significance of testate amoebae in subalpine peatlands in western Hubei Province, China. Earth Sci. 43, 4036–4045 (in Chinese).
Qin, Y., Puppe, D., Payne, R.J., Li, L., Li, J., Zhang, Z., Xie, S., 2020. Land-use change effects on protozoic silicon pools in the Dajiuhu National Wetland Park, China. Geoderma 368, 114305. https://doi.org/10.1016/j.geoderma.2020.114305.
R Development Core Team, 2014. R: a language and environment for statistical computing. R foundation for Statistical Computing.
Ratcliffe, J.L., Creevy, A., Andersen, R., Zarov, E., Gaffney, P.P.J., Taggart, M.A., Mazei, Y., Tsyganov, A.N., Rowson, J.G., Lapshina, E.D., Payne, R.J., 2017. Ecological and environmental transition across the forested-to-open bog ecotone in a west Siberian peatland. Sci. Total Environ. 607, 816–828. https://doi.org/10.1016/j.scitotenv.2017.06.276.
Sheng, Y., Smith, L.C., MacDonald, G.M., Kremenetski, K.V., Frey, K.E., Velichko, A.A., Lee, M., Beilman, D.W., Dubinin, P., 2004. A high-resolution GIS-based inventory of the west Siberian peat carbon pool. Global Biogeochem. Cycles 18, GB3004. https://doi.org/10.1029/2003GB002190.
Singer, D., Kosakyan, A., Seppey, C.V.W., Pillonel, A., Fernandez, L.D., Fontaneto, D., Mitchell, E.A.D., Lara, E., 2018. Environmental filtering and phylogenetic clustering correlate with the distribution patterns of cryptic protist species. Ecology 99, 904–914. https://doi.org/10.1002/ecy.2161. Epub 2018 Mar 25.
Song, L., Li, H., Wang, K., Wu, D., Wu, H., 2014. Ecology of testate amoebae and their potential use as palaeohydrologic indicators from peatland in Sanjiang Plain, Northeast China. Front. Earth Sci. 8, 564–572. https://doi.org/10.1007/s11707-014-0435-x.
Swindles, G.T., Charman, D.J., Roe, H.M., Sansum, P.A., 2009. Environmental controls on peatland testate amoebae (Protozoa: rhizopoda) in the North of Ireland: implications for Holocene palaeoclimate studies. J. Paleolimnol. 42, 123–140. https://doi.org/10.1007/s10933-008-9266-7.
Swindles, G.T., Reczuga, M., Lamentowicz, M., Raby, C.L., Turner, T.E., Charman, D.J., Gallego-Sala, A., Coronado, E.N.H., Roucoux, K.H., Raker, T., Mullan, D.J., 2014. Ecology of testate amoebae in an amazonian peatland and development of a transfer function for palaeohydrological reconstruction. Microb. Ecol. 68, 284–298. https://doi.org/10.1007/s00248-014-0378-5.
Swindles, G.T., Holden, J., Raby, C.L., Turner, T.E., Blundell, A., Charman, D.J., Menberu, M.W., Kløve, B., 2015. Testing peatland water-table depth transfer functions using high-resolution hydrological monitoring data. Quat. Sci. Rev. 120, 107–117. https://doi.org/10.1016/j.quascirev.2015.04.019.
Swindles, G.T., Morris, P.J., Wheeler, J., Smith, M., Bacon, K.L., Turner, T.E., Headley, A., Galloway, J.M., 2016. Resilience of peatland ecosystem services over millennial timescales: evidence from a degraded British bog. J. Ecol. 104, 621–636. https://doi.org/10.1111/1365-2745.12565.
Swindles, G.T., Morris, P.J., Mullan, D.J., Payne, R.J., Roland, T.P., Amesbury, M.J., Lamentowicz, M., Turner, T.E., Gallego-Sala, A., Sim, T., Barr, I.D., Blaauw, M., Blundell, A., Chambers, F.M., Charman, D.J., Feurdean, A., Galloway, J.M., Galka, M., Green, S.M., Kajukalo, K., Karofeld, E., Korhola, A., Lamentowicz, L., Langdon, P., Marcisz, K., Mauquoy, D., Mazei, Y.A., Mckeown, M.M., Mitchell, E.A.D., Plunkett, G., Roe, H.M., Schoning, K., Sillasoo, U., Tsyganov, A.N., Van der Linden, M., Väliranta, M., Wanner, B., 2019. Widespread drying of European peatlands in recent centuries. Nat. Geosci. 12, 922–928. https://doi.org/10.1038/s41561-019-0462-z.
Telford, R., 2011. palaeoSig: significance tests of quantitative palaeoenvironmental reconstructions. R package, version 1.
Telford, R., Birks, H., 2009. Evaluation of transfer functions in spatially structured environments. Quat. Sci. Rev. 28, 1309–1316. https://doi.org/10.1016/j.quascirev.2008.12.020.
Telford, R.J., Birks, H.J.B., 2011. Effect of uneven sampling along an environmental gradient on transfer-function performance. J. Paleolimnol. 46, 99–106. https://doi.org/10.1007/s10933-011-9523-z.
ter Braak, C.J.F., Juggins, S., 1993. Weighted averaging partial least squares regression (WA-PLS): an improved method for reconstructing environmental variables from species assemblages. Hydrobiologia 269, 485–502.
Turner, T.E., Swindles, G.T., Charman, D.J., Blundell, A., 2013. Comparing regional and supra-regional transfer functions for palaeohydrological reconstruction from Holocene peatlands. Palaeogeogr. Palaeoclimatol. Palaeoecol. 369, 395–408. https://doi.org/10.1016/j.palaeo.2012.11.005.
van Bellen, S., Mauquoy, D., Payne, R.J., Roland, T.P., Hughes, P.D.M., Daley, T.J., Loader, N.J., Street-Perrott, F.A., Rice, E.M., Pancotto, V.A., 2017. An alternative approach to transfer functions? Testing the performance of a functional trait-based model for testate amoebae. Palaeogeogr. Palaeoclimatol. Palaeoecol. 468, 173–183. https://doi.org/10.1016/j.palaeo.2016.12.005.
van der Voet, H., 1994. Comparing the predictive accuracy of models using a simple randomization test. Chemometr. Intell. Lab. Syst. 25, 313–323.
Warner, B.G., Charman, D.J., 1994. Holocene soil moisture changes on a peatland in northwestern Ontario based on fossil testate amoebae (Protozoa) analysis.

Boreas 23, 270–279.
Wilkinson, D.M., 2008. Testate amoebae and nutrient cycling: peering into the black box of soil ecology. Trends Ecol. Evol. 23, 596–599. https://doi.org/10.1016/j.tree.2008.07.006.
Wilkinson, D.M., Mitchell, E.A.D., 2010. Testate amoebae and nutrient cycling with particular reference to soils. Geomicrobiol. J. 27, 520–533. https://doi.org/10.1080/01490451003702925.
Woodland, W., Charman, D.J., Sims, P.C., 1998. Quantitative estimates of water tables and soil moisture in Holocene peatlands from testate amoebae. Holocene 8, 261–273. https://doi.org/10.1191/095968398667004497.
Xie, S., Evershed, R.P., Huang, X., Zhu, Z., Pancost, R.D., Meyers, P.A., Gong, L., Hu, C., Huang, J., Zhang, S., Gu, Y., Zhu, J., 2013. Concordant monsoon-driven postglacial hydrological changes in peat and stalagmite records and their impacts on prehistoric cultures in central China. Geology 41, 827–830. https://doi.org/10.1130/G34318.1.
Yu, Z.C., 2012. Northern peatland carbon stocks and dynamics: a review. Biogeosciences 9, 4071–4085. https://doi.org/10.5194/bg.9-4071-2012.
Yu, Z.C., Loisel, J., Brosseau, D.P., Beilman, D.W., Hunt, S.J., 2010. Global peatland dynamics since the. Last Glacial Maximum. Geophys. Res. Lett. 37 https://doi.org/10.1029/2010GL043584.
Zhao, Y., Tang, Y., Yu, Z., Li, H., Yang, B., Zhao, W., Li, F., Li, Q., 2014. Holocene peatland initiation, lateral expansion, and carbon dynamics in the Zoige Basin of the eastern Tibetan Plateau. Holocene 24, 1137–1145. https://doi.org/10.1029/2010GL04358410.1177/0959683614538077.
Zizka, A., Antonelli, A., 2015. Species geocode R: an R package for linking species occurrences, user-defined regions and phylogenetic trees for biogeography, ecology and evolution. bioRxiv. https://doi.org/10.1101/032755, 032755.

Author's personal copy

J Paleolimnol (2015) 54:189–203
DOI 10.1007/s10933-015-9846-2

A testate amoebae transfer function from *Sphagnum*-dominated peatlands in the Lesser Khingan Mountains, NE China

Hongkai Li · Shengzhong Wang · Hongyan Zhao · Ming Wang

Received: 19 November 2013 / Accepted: 31 May 2015 / Published online: 6 June 2015
© Springer Science+Business Media Dordrecht 2015

Abstract We present a testate amoebae training set for building a paleohydrology transfer function. Ninety-one samples were collected from three *Sphagnum* peatlands in the Lesser Khingan Mountains, NE China. Redundancy analysis revealed that depth to the water table (DWT) and moisture content (% water) are the primary factors that control testate amoebae assemblages. Transfer functions for prediction of these two environmental variables were developed. The root mean square error (RMSEP) for DWT and moisture content were 6.74 cm and 1.49 %, respectively, assessed with "leave-one-out" cross validation. We applied a more robust cross validation method for clustered structure data, "leave-one-site-out," and the RMSEP of the best performance model increased to 6.90 cm and 1.67 %, but all models still had predictive power. The effect of uneven sampling was tested using new statistical approaches. Greater numbers of samples in the middle range of the gradient yielded smaller RMSEP values than did samples from the extreme wet and dry ends of the spectrum, where there were fewer samples. Our results indicate this training set is a potentially important tool for paleoenvironmental reconstruction in the Lesser Khingan Mountains, NE China. It will contribute to understanding climate change, particularly past monsoon activity, in this region.

Keywords Testate amoebae · Transfer function · *Sphagnum* peatlands · Lesser Khingan Mountains · Water table

Introduction

Testate amoebae are a group of protists that produce decay-resistant, taxonomically distinct thecae, i.e. outer coverings. These single-celled organisms occur extensively in environments such as lakes, rivers, wetlands and soils, and they are especially abundant and diverse in *Sphagnum* peatlands (Charman 2001; Mitchell et al. 2008). Their sensitive response to environmental changes makes them important ecological and paleoecological indicators. In oligotrophic peatlands, the relative abundance of taxa in the testate amoeba assemblage is controlled primarily by surface wetness, often expressed as depth to the water table (DWT) and moisture content (% water). The biological explanation for this is that the water film on the host substrate is the

Electronic supplementary material The online version of this article (doi:10.1007/s10933-015-9846-2) contains supplementary material, which is available to authorized users.

H. Li (✉) · S. Wang · H. Zhao · M. Wang
Institute for Peat and Mire, School of Geographical Science, Northeast Normal University, Changchun 130024, China
e-mail: lihk431@nenu.edu.cn

H. Li · S. Wang · H. Zhao
State Environment Protection Key Laboratory of Wetland and Vegetation Restoration, Northeast Normal University, Changchun 130024, China

Author's personal copy

living space for the amoebae. The thickness of the water film affects the size and shape of the organisms inhabiting the substrate, and thus the taxonomic composition of testate amoebae assemblages.

During the last two decades, transfer functions have been developed to infer environmental conditions, using testate amoebae assemblages in surface peats from many regions of the world (Amesbury et al. 2013; Booth 2007; Payne et al. 2008; Qin et al. 2013; Swindles et al. 2009; Turner et al. 2013; Wilmshurst et al. 2003; Woodland et al. 1998). Some transfer functions have been applied to peat profiles to reconstruct past environmental change quantitatively (Booth 2010; Charman et al. 2012). Researchers have tested the value of testate amoebae in paleoenvironmental studies by comparing the testate amoeba-inferred DWT with instrumental climate data or long-term measurements of water table depth (Booth 2010; Charman 2007; Charman et al. 2004, 2009; Lamentowicz et al. 2010; Schoning et al. 2005), comparing inferred water table depths within a region (Hendon et al. 2001), or by comparison with other paleoenvironmental variables from the same profile (Lamentowicz et al. 2008b, 2010; Mauquoy and Barber 1999; Swindles et al. 2012; Väliranta et al. 2012). Testate amoebae in peats are now used routinely as proxies for paleoenvironmental reconstruction.

Previously, environmental transfer functions that use testate amoebae were largely developed in Europe (Charman et al. 2007; Lamentowicz and Mitchell 2005; Swindles et al. 2009) and North America (Amesbury et al. 2013; Booth 2007; Lamarre et al. 2013; Payne et al. 2006; Turner et al. 2013). A few studies were done in New Zealand (Charman 1997; Wilmshurst et al. 2003) and recently, in South America (Swindles et al. 2014; Van Bellen et al. 2014). Studies revealed that most testate amoebae taxa have similar hydrological preferences across different regions. Nevertheless, to fully understand and model the relations between testate amoebae communities and environmental variables, more data are needed from different geographic areas, especially from less sampled regions. In practice, application of transfer functions developed in one region to another region is problematic (Payne et al. 2012; Turner et al. 2013). Therefore, reliable quantitative reconstructions of hydrologic change need to use transfer functions developed with a modern training set from the same geographic setting as profile samples.

China possesses important, widely distributed peatlands. Knowledge of testate amoebae ecology throughout the region, however, is still limited (Li et al. 2009; Qin et al. 2013; Song et al. 2014). In the Lesser Khingan Mountains, northeast China, peatlands are widely distributed because of the cold and wet climate. Some peatlands have evolved to an oligotrophic stage and apparently possess several testate amoebae taxa and assemblages that have not been encountered in previous studies. The region lies at the northern margin of the Asian monsoon. Peatlands in the area may be very sensitive to environmental changes, which are recorded by proxy variables in peat cores. Several studies have inferred past environment conditions using pollen (Xia 2000; Yang 2003) or stable isotopes of carbon (Lin et al. 2004), but such paleoenvironmental studies have not been undertaken using testate amoebae. In the Lesser Khingan Mountains, temperature and precipitation are strongly affected by the activity of the summer and winter monsoon. By linking the reconstructed water table depth in peatlands, inferred from a testate amoebae transfer function, with climate drivers (Charman et al. 2009), we can better understand past climate change in this region and historical variability of the East Asian monsoon (An et al. 2000).

This study (1) describes the testate amoebae community in Northeast China, (2) explores the relations between testate amoebae assemblage composition and environmental variables, and (3) develops a testate amoeba-based transfer function for paleohydrological reconstruction to understand past climate change, in particular monsoon activity, in this region.

Study sites

We carried out the study in the Lesser Khingan Mountain range of northeast China, which is near the China–Russia border and extends about 500 km in a northwest–southeast direction (Fig. 1). Long-term fluvial planation has created relatively gentle topography. This area lies along the northern margin of the East Asian monsoon. The climate is characterized by long, cold winters with a mean annual temperature between −1 and 1 °C and mean temperatures in the coldest month (January) of −28 to −23 °C. Precipitation ranges from 400 to 600 mm annually and is concentrated in summer. Vegetation is mixed conifer/

Author's personal copy

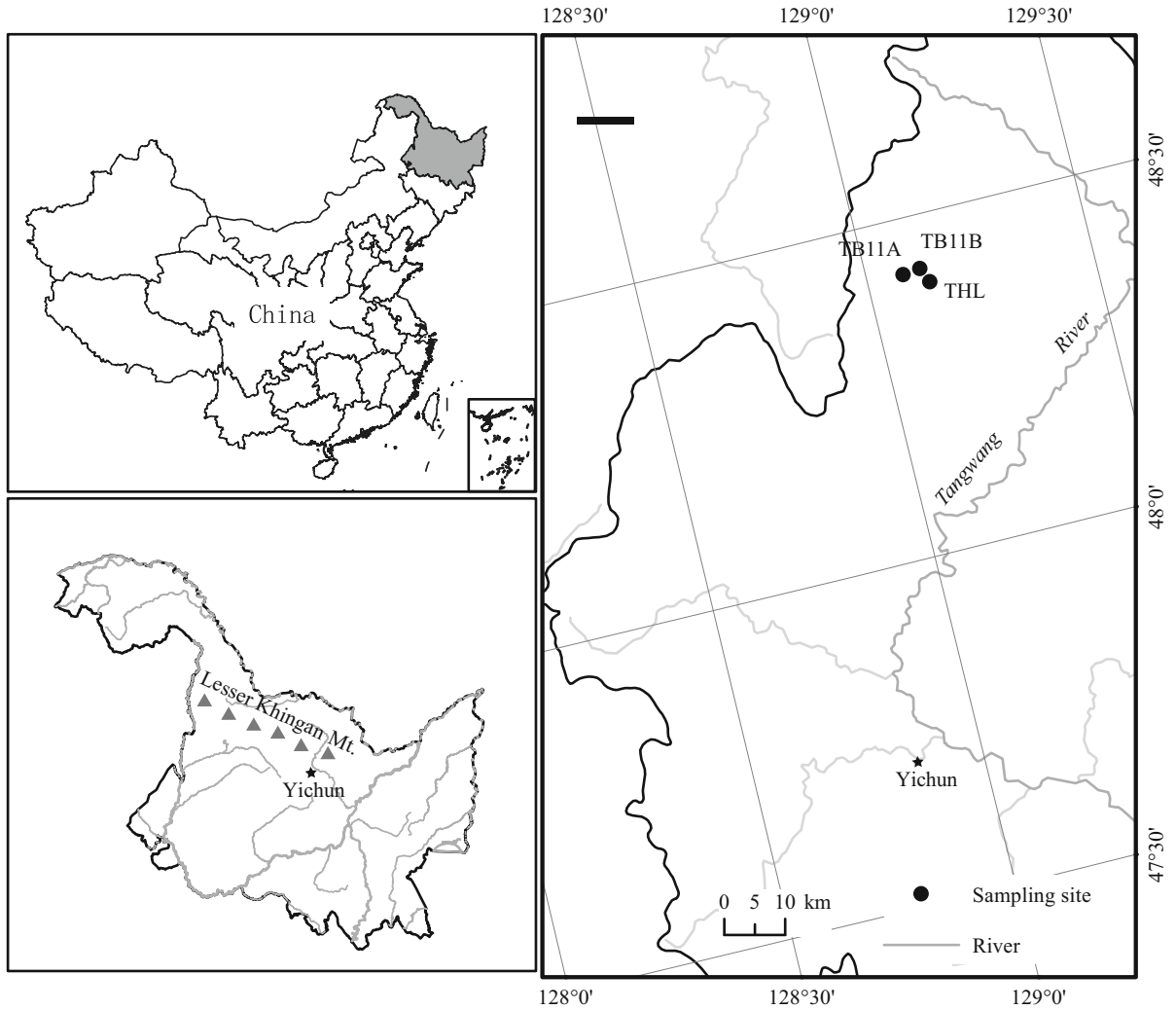

Fig. 1 Map showing the location of study sites

broadleaf forest. The cold and wet climate, together with the relatively flat terrain, open river valley, and sporadic permafrost, give rise to scattered patches of peatlands. In this study, three *Sphagnum* peatlands, TB11A (48°25′05″N, 129°04′52″E, 493 masl), TB11B (48°25′15″N, 129°07′15″E, 478 masl) and THL (48°23′54″N, 129°08′06″E, 484 masl) were selected for study of modern samples, given their accessibility. These peatlands all developed from *Larix gmelinii* (Rupr.) Kuzen forest, through paludification. Dominant plant species include *L. gmelinii*, *Ledum palustre* var. *angustum* E. Buch, *Vaccinium uliginosum* Linn and *Chamaedaphne calyculata* (Linn.) Moench. Mosses include mainly *Sphagnum magellanicum* Brid, *S. girgensohnii* Russ, *S. palustre* Linn., *S. nemoreum* Scop., *Aulacomnium palustre* (Hedw.) Schwägr. and *Polytrichum juniperum* Hedw.

Materials and methods

Field methods

Fieldwork was carried out in the middle of August 2011. Samples were taken from different microhabitats, including pools, lawns, hollows and hummocks. A total of 91 samples (33 in TB11A, 27 in TB11B, 31 in THL) were collected. At each sampling site, two

Author's personal copy

adjacent columns of surface moss approximately 5 cm in diameter and 5 cm long were removed. One was put in a plastic bag labeled "A" and transported to the laboratory to measure moisture content and bulk density. The other was divided into two parts. One 10-ml subsample was placed in 50 ml of distilled water in a lidded bottle for several hours, and used to measure pH and electrical conductivity (Stanek 1973) with a portable pH/EC meter. The balance of that sample was placed in a plastic bag labeled "B" to be used for testate amoebae analysis. Depth to the water table (DWT) was determined by digging a small hole in the peat at the sampling site and measuring DWT after at least 30 min. The datum (zero level) was defined as the top of the moss.

Laboratory procedures

In the laboratory, sample A was weighed, dried at 105 °C, weighed again, combusted at 550 °C and weighed once more to determine bulk density, moisture content and organic content [loss on in ignition (LOI)]. Testate amoebae samples were prepared following the methods of Hendon and Charman (1997) and Booth (2010). Sample B was weighed and immersed in distilled water in a beaker for about 24 h. Rose Bengal was added to stain living and encysted individuals. The material was then washed repeatedly to remove testate amoebae from the substrate, sieved through 300-µm mesh and back-sieved through 10-µm mesh. The fraction remaining on the 10-µm mesh was washed into a 15-ml tube. After centrifugation at 3,000 rpm for 5 min, the supernatant was poured off and the remainder was stored at 4 °C in a refrigerator. Testate amoebae were identified at 200× and 400× magnification with a light microscope. A minimum of 150 tests was counted in each sample. Identification guides consulted in this study included Charman et al. (2000), Meisterfeld (2002a, b), Ogden and Hedley (1980) and Penard (1902).

Numerical analysis

Relations between community structure of testate amoebae and environmental variables were explored using redundancy analysis (RDA). Six environmental variables (DWT, moisture content, pH, conductivity, bulk density and LOI) were tested as explanatory variables. Assemblage data were expressed as relative abundances, i.e. percent of each testate amoeba taxon in each sample. Nine species that occurred in fewer than four samples or had a maximum abundance of <1 % were excluded from the data set. Prior to RDA, species data were Hellinger-transformed, which allows use of Euclidian-based methods such as RDA rather than Chi squared methods such as CCA (Legendre and Gallagher 2001). Ordination analysis was carried out using the *vegan* package (Oksanen et al. 2013) for R language (R Development Core Team 2013).

Transfer functions were built and improved employing four common approaches, namely weighted averaging (WA), weighted averaging partial least squares (WAPLS), maximum likelihood (ML) and the modern analogue technique (MAT). The WA model included weighted averaging with inverse deshrinking (WA.inv), weighted averaging with classical deshrinking (WA.-cla), tolerance downweighted weighted averaging with inverse deshrinking (WA.inv.tol), tolerance down-weighted weighted averaging with classical deshrinking (WA.cal.tol). Model performance was assessed using the regression value r^2, the root mean squared error of prediction (RMSEP) and the maximum bias. The leave-one-out (LOO) technique was used to cross validate the models. To examine the effect of clustered sampling on transfer function performance, leave-one-site-out (LOSO) cross validation was carried out (Payne et al. 2012). To account for the effect of uneven sampling, segment-wise RMSEPs were calculated (Telford and Birks 2011). These analyses were done by using the *rioja* package for R language (Juggins 2013). Another R package, *paleoSig*, was used to test the impact of spatial autocorrelation on the prediction power of the transfer function (Telford 2013; Telford and Birks 2009). To test the applicability of the transfer functions, we applied them to an independent testate amoebae training set from the Changbai Mountains in northeast China, about 700 km from our sampling sites (Li et al. 2013).

Results

Testate amoebae assemblages and environmental variables

A total of 51 testate amoebae taxa were found in 91 peat samples. Species richness ranged between 8 and 31, with an average of 20.3 ($\sigma = 4.41$). Correlation analysis showed that species richness was significantly

Author's personal copy

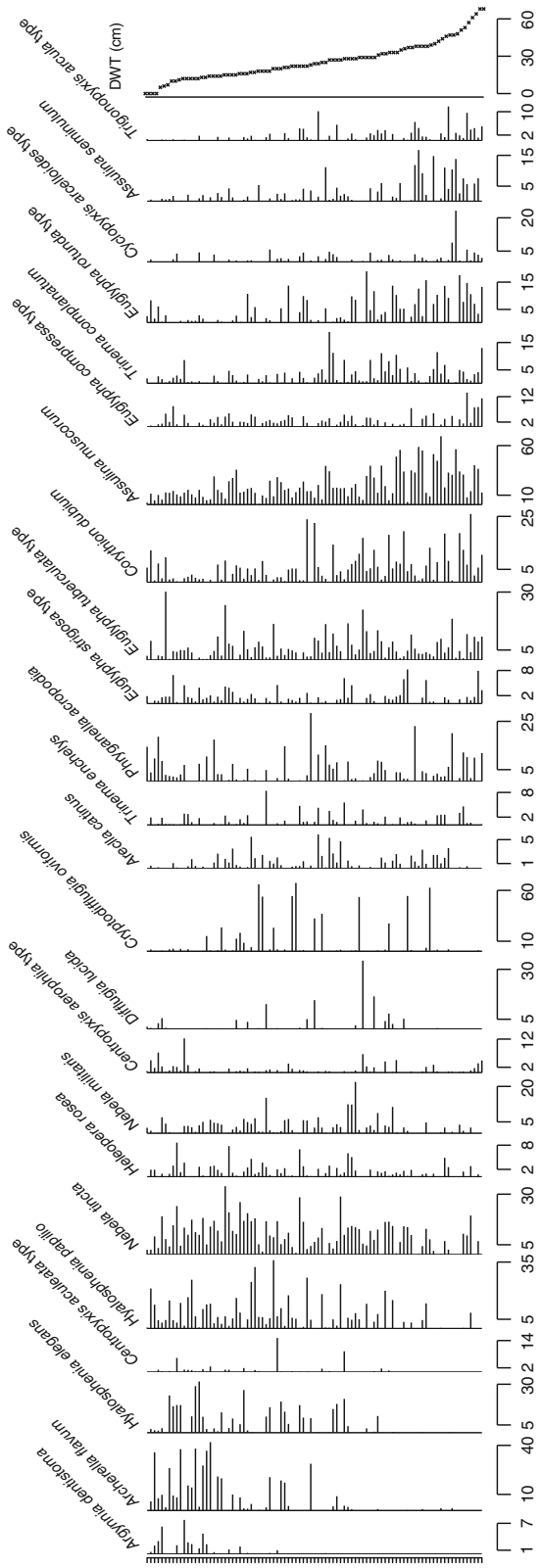

◀**Fig. 2** Relative abundance diagram of testate amoebae in all samples. Samples are arranged according to measured water table depth (DWT). Taxa are ordered from wet on the *left* to dry on the *right* by optima derived from the WA mode. Taxa occurring in <9 samples or having a maximum abundance <5 % were removed

positively correlated with moisture content ($r = 0.44$, $p < 0.001$) and significantly negatively correlated with DWT ($r = -0.59$, $p < 0.001$) and pH ($r = -0.29$, $p < 0.01$). Dominant species were *Assulina muscorum*, *Nebela tincta*, *Archerella flavum*, *Cryptodifflugia oviformis*, *Hyalosphenia papilio*, *Euglypha tuberculata* type, *Hyalosphenia elegans*, *Corythion dubium*, *Phryganella acropodia* and *Euglypha rotunda* type (Fig. 2). These 10 species represented 76.6 % of the total community composition. In terms of frequency, *A. muscorum* was most common, followed by *E. tuberculata* type, *C. dubium*, *Trinema complanatum*, *Euglypha compressa* type, *N. tincta*, *P. acropodia*, *Euglypha strigosa* type, *H. papilio* and *Heleopera rosea*.

In RDA, all six environmental variables explained 23.44 % of the variation in species data, with 76.56 % left unexplained. Permutation tests showed that axis 1 and axis 2 are significant ($p < 0.01$) and explain 13.21 and 3.98 % of the variation in species data, respectively. In partial RDA, DWT and moisture have relatively greater marginal effects. They explained 12.21 and 8.44 % of total species variation on their own, respectively, or 14.25 % together. Correlation analysis revealed that both DWT and moisture were significantly ($p < 0.01$) correlated with axis 1. In an ordination plot, DWT and moisture have a small angle with axis 1 and relatively longer arrow (Fig. 3). Therefore, these two variables were selected to build transfer functions. Four other environmental variables had relatively lower marginal effects (Bulk density: 3.5 %, $p < 0.01$; pH: 2.19 %, $p < 0.05$; Conductivity: 1.6 %, $p = 0.19$; LOI: 1.5 %, $p = 0.18$) and were associated with axis 2 in an ordination plot.

The testate amoebae species are also primarily separated along axis 1, except *C. oviformis*, which lies far from the others in the ordination plot (Fig. 4). Several species commonly associated with dry habitats, such as *A. muscorum*, *T. arcula*., *C. dubium*, *E. rotunda* type, were on the left end of axis 1, whereas *A. flavum*, *H. elegans*, *H. papilio*, *N. tincta* were on the right side. Samples from wet sites have high scores on

Author's personal copy

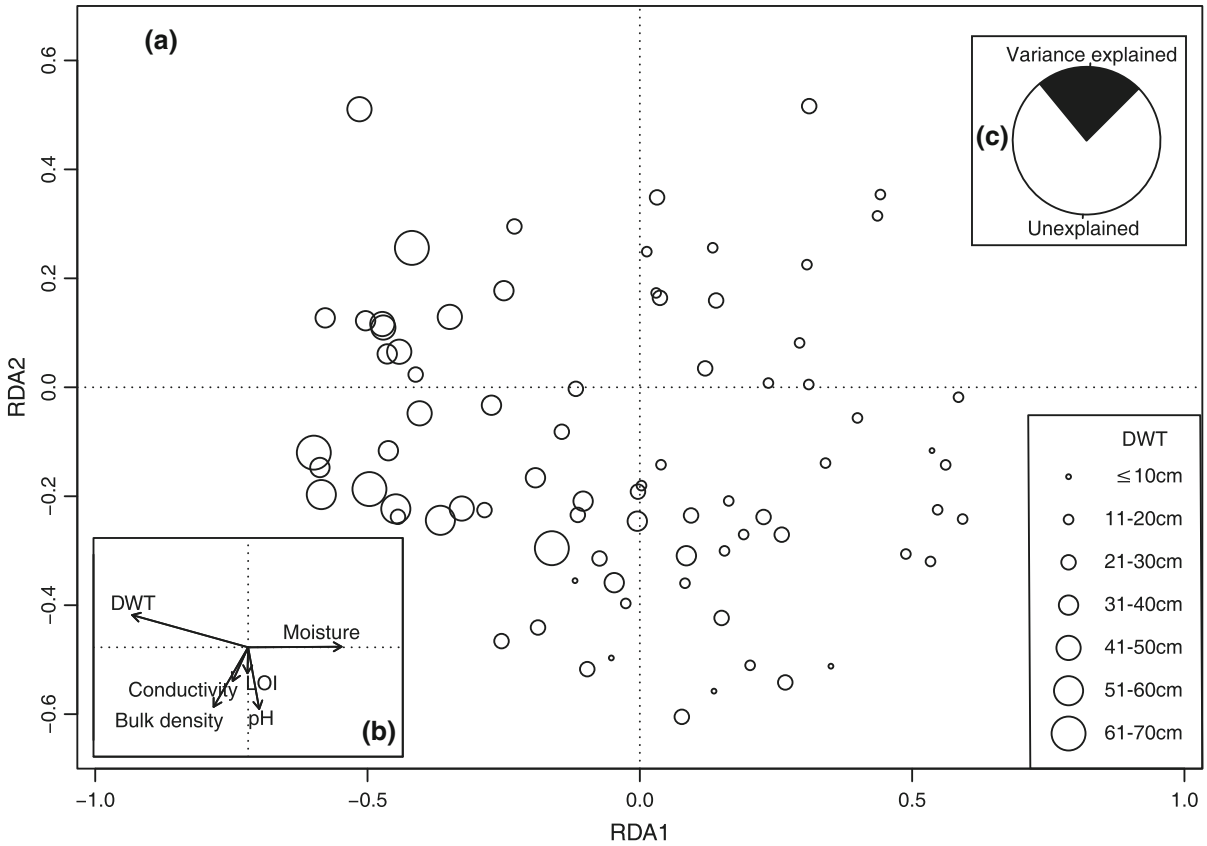

Fig. 3 **a** Sample ordination plot of Redundancy Analysis (RDA) based on all 91 samples. The larger radius of *open circles* indicates higher values of DWT. **b** Relationships of environmental variables with ordination axis 1 and axis 2. **c** Percent variance explained by RDA (see text for details)

axis 1 on the right side, whilst ones from dry sites have low scores on the left side.

Transfer function development

Transfer functions were developed for DWT and moisture content. All 91 samples were included in the training set at first. Model performance is shown in Table 1. The performance of the different transfer function models was similar in leave-one-out cross validation. In terms of $RMSEP_{LOO}$ and r^2_{LOO}, WMAT outperformed the other models for predicting DWT ($RMSEP_{LOO} = 9.31$ cm, $r^2_{LOO} = 0.62$), whereas WAPLS (component 2) yielded the best models for estimating moisture content ($RMESP_{LOO} = 2.20$ %, $r^2_{LOO} = 0.46$).

Outliers often dramatically influence the performance of transfer function models. Consequently, outliers are removed in testate amoeba calibration studies to improve the accuracy of transfer functions. As for most previous studies (Charman et al. 2007; Payne et al. 2006; Swindles et al. 2014; Van Bellen et al. 2014), the cut-off point was set at 20 % of the environmental gradient in this study. This allowed comparison of results to other studies. Samples with a residual of >13.60 cm for DWT or 3.32 % for moisture content were removed from the training set. Excluded samples are listed in Electronic Supplementary Material (ESM) Table 1. Most of the removed samples came from the extremes of the dry–wet range (Fig. 5). After removing outliers, all transfer function models for DWT and moisture content performed better, with a considerable decrease in RMSEP and increase in r^2. WA.inv.tol is the best model for DWT ($RMSEP_{LOO} = 6.74$, $r^2_{LOO} = 0.67$) and WAPLS (component 2) is the best for peat moisture content ($RMSEP_{LOO} = 1.49$ %, $r^2_{LOO} = 0.61$).

Author's personal copy

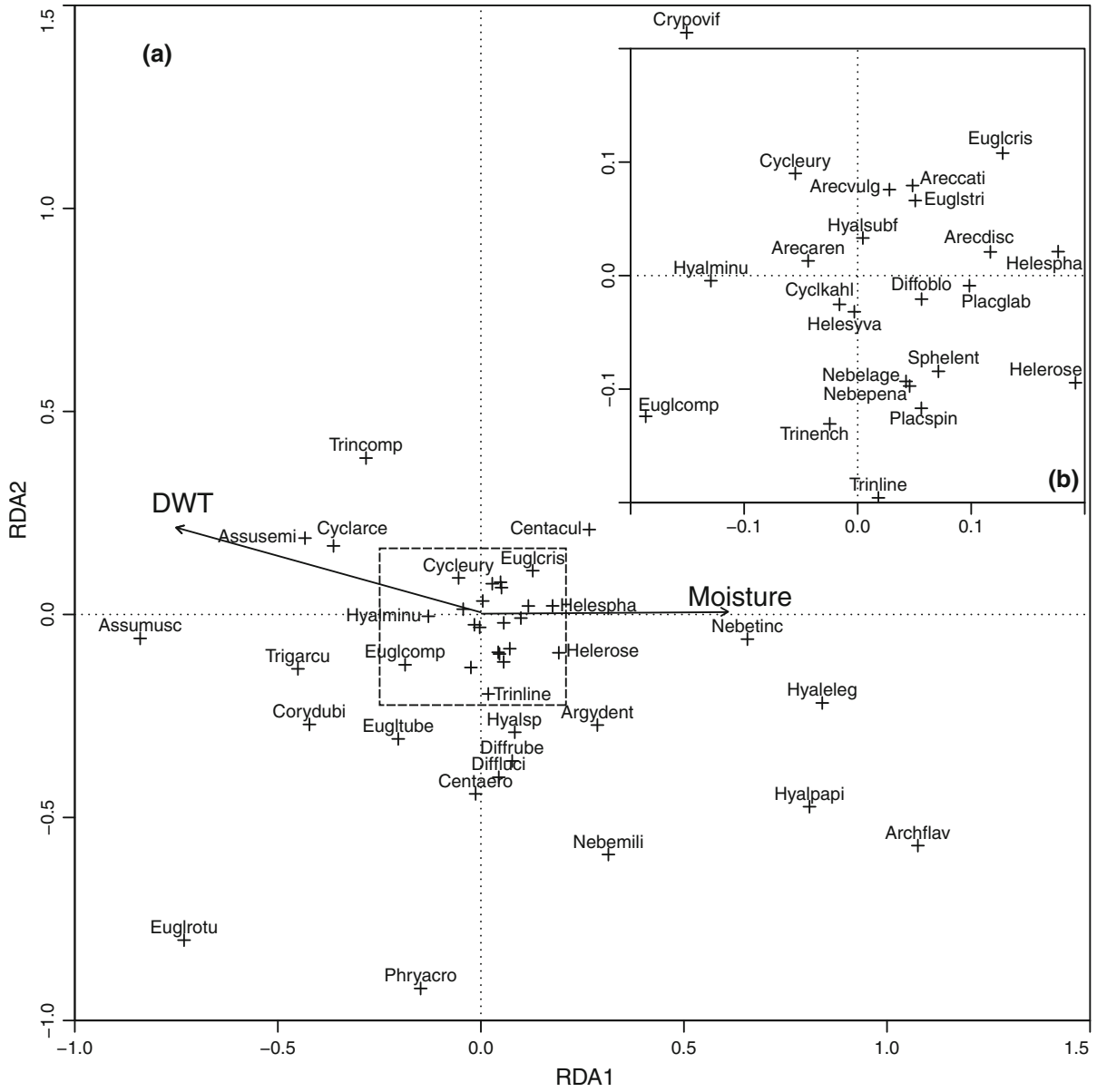

Fig. 4 **a** Species ordination plot of RDA. Only the most important environmental variables, DWT and Moisture are shown on the ordination plot. **b** Enlarged view of *dashed rectangle* in plot **a**. The abbreviated names of testate amoebae taxa are: Arcearen, *Arcella arenaria*; Arcecati, *Arcella catinus*; Arcedisc, *Arcella discoides* type; Arcevulg, *Arcella vulgaris*; Archflav, *Archerella flavum*; Argydent, *Argynnia dentistoma*; Assumusc, *Assulina muscorum*; Assusemi, *Assulina seminulum*; Centaero, *Centropyxis aerophila* type; Centacul, *Centropyxis aculeata* type; Cyclarce, *Cyclopyxis arcelloides* type; Cycleury, *Cyclopyxis eurystoma*; Cyclkahl, *Cyclopyxis kahli*; Corydubi, *Corythion dubium*; Crypovif, *Cryptodifflugia oviformis*; Difffluci, *Difflugia lucida*; Diffoblo, *Difflugia oblonga* type; Diffrube, *Difflugia rubesens* type; Euglcomp, *Euglypha compressa* type; Euglcris, *Euglypha cristata*; Euglrotu, *Euglypha rotunda* type; Euglstri, *Euglypha strigosa* type; Eugltube, *Euglypha tuberculata* type; Helespha, *Heleopera sphagni*; Helerose, *Heleopera rosea*; Helesyva, *Heleopera sylvatica*; Hyaleleg, *Hyalosphenia elegans*; Hyalminu, *Hyalosphenia minuta*; Hyalpapi, *Hyalosphenia papilio*; Hyalsubf, *Hyalosphenia subflava*; Hyalsp, *Hyalosphenia* sp; Nebemili, *Nebela militaris*; Nebetinc, *Nebela tincta*; Nebepena, *Nebela penardiana*; Nebelage, *Nebela lageniformis*; Phryacro, *Phryganella acropodia*; Placspin, *Placocista spinosa*; Placglab, *Placocista glabra*; Sphelent, *Sphenoderia lenta*; Trigarcu, *Trigonopyxis arcula*; Trincomp, *Trinema complanatum*; Trinench, *Trinema enchelys*; Trinline, *Trinema lineare*

Author's personal copy

Table 1 Performance statistics for transfer function models

	Water table depth			Moisture content		
	RMSEP (cm)	r^2	Maximum bias (cm)	RMSEP (cm)	r^2	Maximum bias (cm)
WA.inv	10.58	0.51	27.57	2.31 %	0.40	6.75 %
	(6.82)	(0.65)	(11.06)	(1.58 %)	(0.56)	(3.47 %)
	7.12	0.62	11.88	1.68 %	0.50	2.87 %
WA.cla	13.35	0.51	18.54	3.02 %	0.41	3.37 %
	(7.75)	(0.66)	(6.17)	(1.91 %)	(0.57)	(1.19 %)
	7.90	0.62	7.91	1.98 %	0.51	1.64 %
WA.inv.tol	10.07	0.55	25.88	2.29 %	0.41	6.86 %
	(6.74)	(0.66)	(11.15)	(1.63 %)	(0.53)	(3.58 %)
	6.90	0.65	11.75	1.67 %	0.51	3.53 %
WA.cla.tol	12.2	0.56	17.47	3.03 %	0.42	4.73 %
	(7.50)	(0.67)	(6.64)	(1.94 %)	(0.54)	(1.43 %)
	7.54	0.65	8.22	1.92 %	0.52	1.98 %
WAPLS	9.65	0.59	25.67	2.20 %	0.46	5.93 %
Component 2	(7.51)	(0.63)	(10.02)	(1.49 %)	(0.61)	(2.47 %)
	8.91	0.51	9.11	1.67 %	0.51	2.78 %
ML	10.15	0.65	10.78	2.64 %	0.49	5.47 %
	(7.31)	(0.80)	(7.76)	(2.07 %)	(0.61)	(6.02 %)
	11.65	0.54	21.40	2.17 %	0.57	6.00 %
MAT	9.31	0.62	20.20	2.38 %	0.36	7.59 %
	(7.28)	(0.70)	(22.00)	(1.66 %)	(0.49)	(4.54 %)
	7.75	0.65	29.40	2.38 %	0.36	6.39 %
WMAT	9.37	0.62	20.09	2.40 %	0.35	7.71 %
	(7.00)	(0.72)	(21.01)	(1.88 %)	(0.41)	(4.20 %)
	7.75	0.65	28.45	2.40 %	0.35	7.71 %

Normal: all samples included in training sets, leave-one-out cross validation. Parentheses: outliers filtered out, leave-one-out cross validation. Italics: outliers filtered out, leave-one-site-out cross validation. Abbreviated model names can be found in the text

Discussion

Ecology of testate amoebae

This study filled a geographic gap in knowledge about testate amoebae ecology in the Lesser Khingan Mountains, northeast China. Most species present there also occur in other parts of world. Nevertheless, we also recorded a potential new species, *Hyalosphenia* sp. The shell of this species is colorless or yellow, proteinaceous, smooth, pyriform and laterally flattened. The aperture is terminal and is a strongly compressed rectangle with rounded angles (ESM Fig. 1). Recent efforts in testate amoebae research across new sampling regions have discovered new species. For instance, Markel et al. (2010) described a previously unknown taxon from Alaskan peatlands and Swindles et al. (2014) recorded a potential new species of *Arcella*. Such studies are providing evidence that will resolve the debate as to whether this group of protozoans is cosmopolitan or endemic.

Relations between the testate amoebae community and environmental variables in the Lesser Khingan Mountains are similar to those reported for other regions. In this study, DWT and moisture content are primary factors that control composition of the testate amoebae assemblage, as found in almost all previous studies. Percentages of variation in the testate amoebae community explained by DWT and moisture content were 12.21 and 8.44 %, respectively,

Author's personal copy

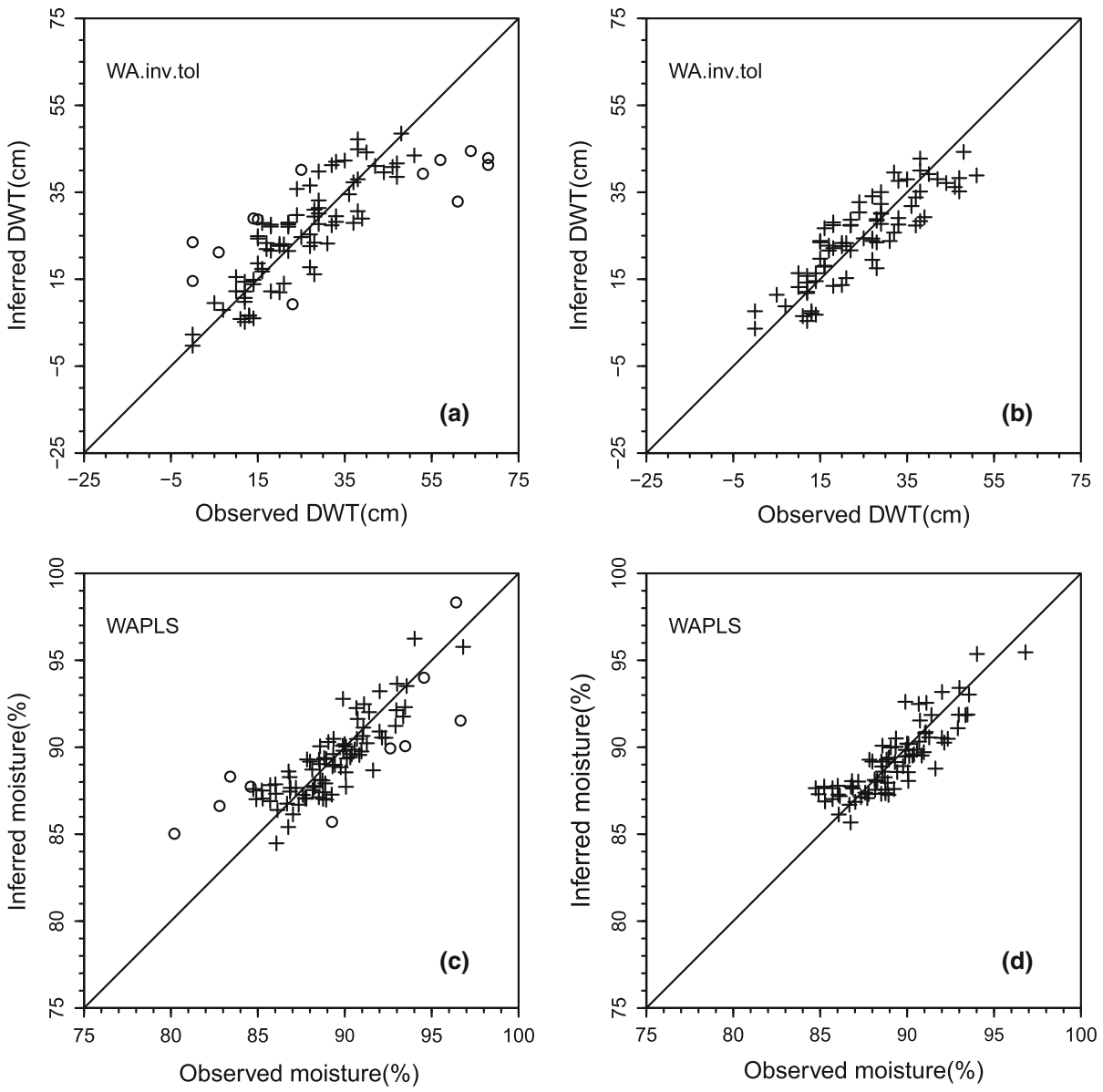

Fig. 5 Predicted values from the best performance model against observed values for water table (**a**, **b**) and moisture (**c**, **d**), pre-filtering (**a**, **c**) and post-filtering (**b**, **d**). The *open circles* in **a** and **c** are the samples removed in transfer function improvement

comparable to other studies (DWT: 9.1 %, moisture: 5.2 % (Charman 1997); DWT: 8.9 %, moisture: 7.5 % (Booth 2001); DWT: 15.8 %, moisture: 5.5 % (Swindles et al. 2009)).

pH has sometimes been considered an important controlling factor when samples came from a relatively broad pH gradient (Booth 2001; Lamentowicz and Mitchell 2005; Payne and Mitchell 2007). In this study, pH ranged from 4.72 to 5.99 in the 91 samples. This short pH gradient produced a smaller, marginal effect of only 2.19 %, low relative to other studies (pH 10.4 % (Booth 2001); DWT and pH 21 %, (Lamentowicz and Mitchell 2005). This led us to abandon any attempt to build a transfer function for pH. In some studies, bulk density has emerged as a significant variable in ordination analysis (Charman et al. 2007; Swindles et al. 2009), but it was never chosen to build a transfer function because its paleoenvironmental

Author's personal copy

implications are not understood. Here, bulk density had an even higher effect (3.53 %) than pH. Conductivity and LOI were not significant in controlling testate amoebae composition in this study.

Preferences of testate amoebae taxa in the Lesser Khingan Mountains are reasonably similar to those of testate rhizopods in peatlands of other regions. Water table depth and moisture content optima and tolerance were calculated with weighted averaging (Fig. 6). We assessed the rank position of testate amoebae taxa that occurred in at least four samples, with respect to water table depth and moisture gradients. The rank difference was expressed as water table depth rank minus moisture content rank (Fig. 7). Most taxa occurred in similar rank positions on the two gradients, with rank differences no greater than five. This makes sense, given the strong negative correlation between DWT and moisture content ($r = -0.72$, $p = 1.24e^{-15}$). There were, however, some exceptions, including *Cyclopyxis kahli*, *Phryganella acropodia*, *Cryptodifflugia oviformis*, *Nebela militaris*, *Difflugia lucida* and *Heleopera sylvatica.* Two of these taxa, *Cyclopyxis kahli* and *Heleopera sylvatica* are probably exceptions because of their low frequencies, which tend to yield large errors for optima estimates. When we examined the other four exceptional taxa closely, we found that, similar to what has been discovered in research on European testate amoebae transfer functions (Charman et al. 2007), their rank distances for depth to water table and moisture gradients were small. A relatively larger rank difference may result because ranking is not linear, i.e. each rank only represents a small difference in this part of the gradient. The rank difference indicates it might be better to reconstruct both water table depth and moisture changes in peat profiles, to recover a more complete picture of hydrological change. Nevertheless, it is unlikely that there will be large differences between the two variables, unless the testate amoebae assemblage is dominated by these exceptional taxa.

Some previous studies revealed that wet species generally have a narrower tolerance than dry species (Amesbury et al. 2013; Charman 1997; Charman et al. 2007; Lamentowicz et al. 2008a; Lamentowicz and Mitchell 2005; Mitchell et al. 1999). Stenotopic wet species are therefore more sensitive to hydrologic changes than are eurytopic dry species. A similar pattern was also found in the Lesser Khingan Mountains (ESM Fig. 2). The tolerance and optimum for DWT are positively correlated ($r = 0.65$, $p = 2.70e^{-6}$). Thus we anticipate that reconstructions of wetter phases are likely to be more accurate and precise than those in dry phases.

Mitchell et al. (2008) suggested that comparison of the ecological preferences of testate amoebae across broad geographic areas could provide a way to verify the ecology of species that remain constant through time. Several previous studies attempted to compare the relative position of testate amoebae along the water table gradient, among different regions (Booth 2001; Lamentowicz and Mitchell 2005; Payne et al. 2006). Most species demonstrated a similar preference for water table depth, although the methods for DWT measurement were different among the studies. We compared the optima of some common testate amoebae taxa in 19 studies published in the last two decades (ESM Fig. 3). Results showed that most taxa exhibit a relatively consistent hydrological preference across the different sampling regions. The optima for most taxa in this study are generally located near the middle of the range of optima for that species in other regions of the world. This agreement provides new support for using testate amoebae as biological indicators in paleoecology research. Some uncertainty, however, cannot be overlooked, e.g. for *Cyclopyxis arcelloides* type. Taxonomic inconsistency among studies may cause problems for comparisons, and this group consisted of several similar taxa that were distinguished in other studies (Charman et al. 2000; Mitchell et al. 2008; Payne et al. 2011).

Performance of the transfer function

In recent studies, it was reported that leave-one-out cross validation tended to overestimate the performance of transfer functions because of the training set having clustered structure, with many observations from each site. In such cases, leave-one-site-out (LOSO) is probably a more appropriate cross validation method (Payne et al. 2012). In this study, the number of observations from each site ranged from 27 to 33. Therefore, the training set also had a clustered structure. When LOSO was applied, most models performed relatively more poorly than before (Table 1). This is probably because we only have three sites. This means that LOSO cross validation removed approximately one-third of the samples from the training set. This over-filtering is one reason for the

Author's personal copy

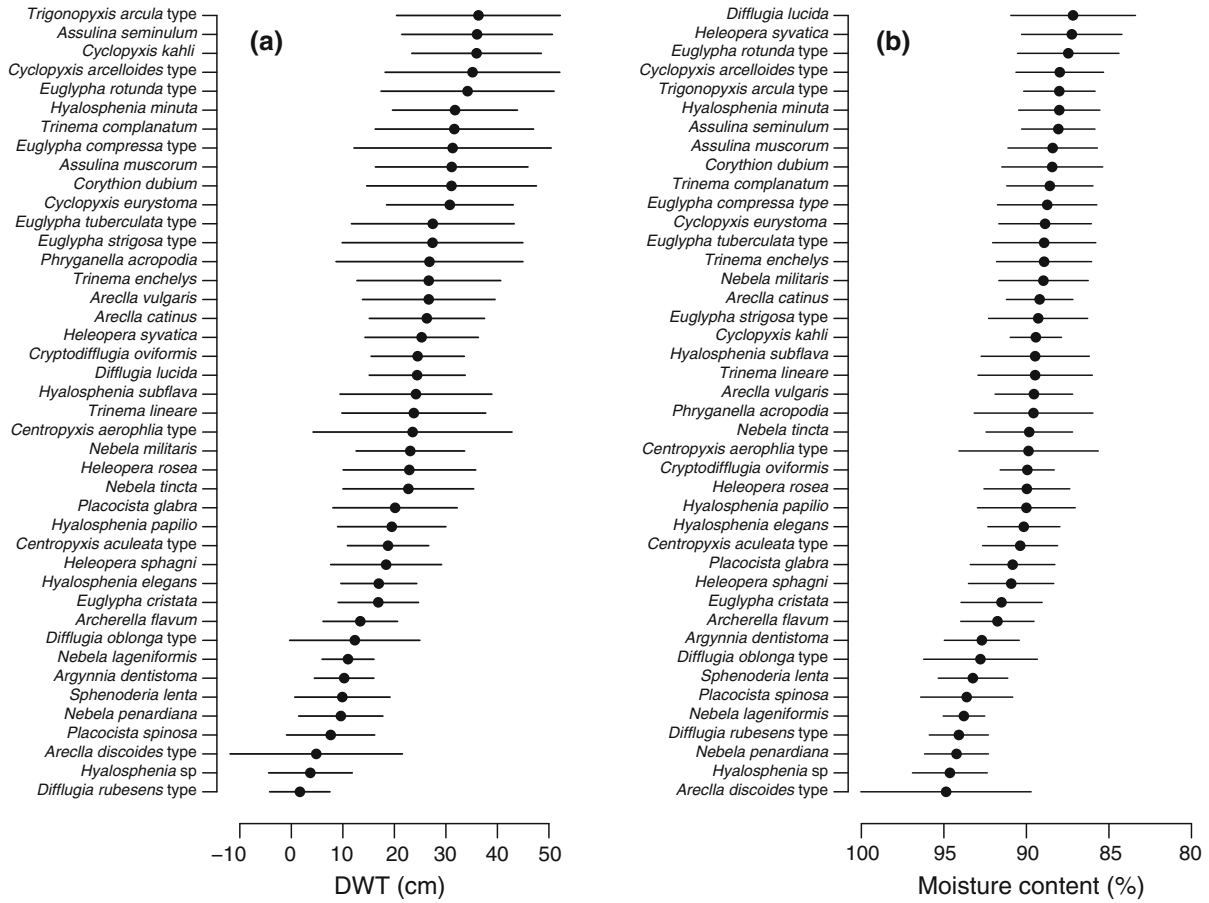

Fig. 6 Optima and tolerances from the entire data set based on weighted averaging for **a** depth to water table and **b** moisture

deterioration of model performance with LOSO. To obtain a reliable and objective assessment of the transfer function performance, samples from more sites are necessary. Nevertheless, because the training set samples were taken from very similar sites and observations at each site were relatively even along the gradient, the RMSEP difference between LOO and LOSO and was not large in this study, especially for a weighted averaging model, which is believed to be the most robust to clustered sampling (Payne et al. 2012).

Telford and Birks (2011) reported that the WA transfer function is sensitve to uneven sampling along the enviornmental gradient. To explore this source of bias, water table gradient was divided into 12 segments at 5-cm intervals and moisture was divided into seven segments at intervals of 2 %. The RMSEPs for the two variables were calculated for every segment. Results show that most samples were in the middle of the hydrological gradient (Fig. 8). For DWT, RMSEPs were relatively stable, ranging from 4.62 to 6.52 cm in the range from 11 to 40 cm, and lower than the $RMSEP_{LOO}$ of the whole gradient. On the dry end, RMSEPs were particularly high because of the small number of samples in the training set, but still lower than the standard deviation of observed water table depths (SD = 11.65 cm, n = 78), which suggests the transfer function has predictive capacity over the whole gradient. A similar pattern also occurred for moisture gradient. The middle range, from 86.01 to 94 %, has relatively smaller RMSEPs, whereas RMSEPs on both the wet and dry ends are high, but still lower than the standard deviation of observed values (SD = 2.42 %, n = 81), ensuring that the transfer function has predictive capacity over the whole moisture gradient.

Spatial autocorrelation is another factor that leads to overly optimistic estimates of model predictive power (Telford and Birks 2005, 2009). Figure 9 illustrates that spatial autocorrelation has limited impact on the

Author's personal copy

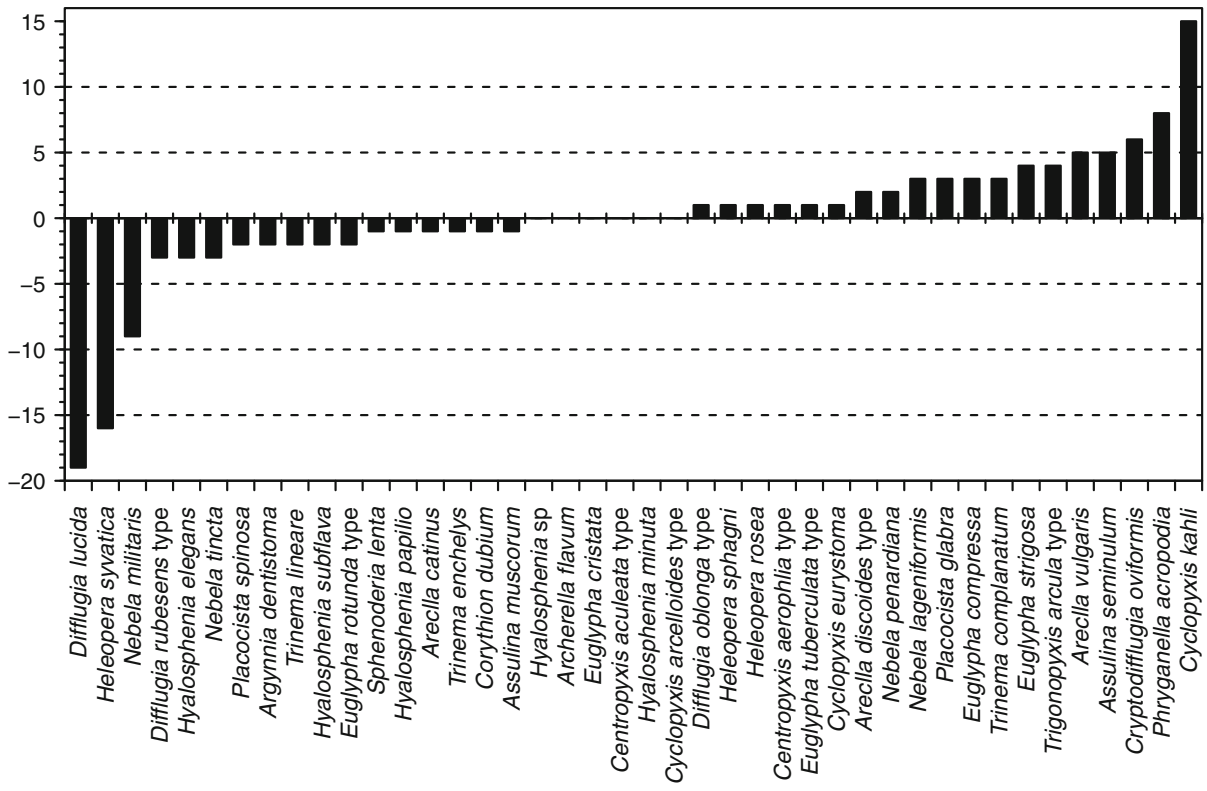

Fig. 7 Differences in the relative ranking of taxa along the water table and moisture gradients. Taxa with n < 4 are excluded. The rank difference is expressed as the water table rank minus the moisture content rank

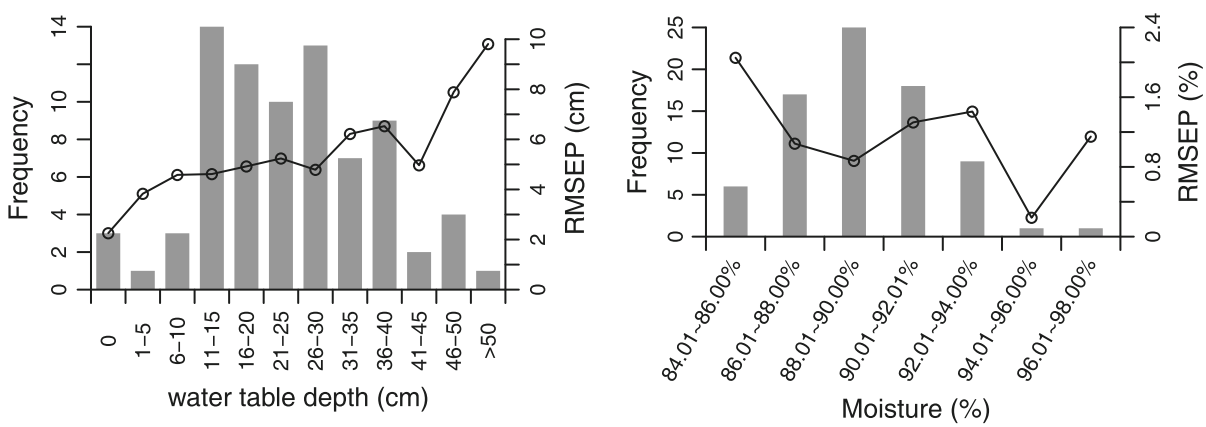

Fig. 8 Uneven sampling effect on best performing transfer functions models, measured by $RMSEP_{jack}$. The water table depth gradient (*left*) was divided into 12 segments at 5-cm intervals and the moisture gradient (*right*) was divided into 7 segments at 2 % intervals

performance of our transfer function models. We applied the models to an independent testate amoebae training set derived from the Changbai Mountains in northeast China, about 700 km from the sampling sites in this study (Li et al. 2013). The mean prediction errors of all models, for both DWT and moisture, are greater than $RMSEP_{LOO}$ and $RMSEP_{LOSO}$ (Table 2). This was not surprising, considering the differences in geographic context, water chemistry, and plant communities between Changbai and Lesser Khingan. The

Author's personal copy

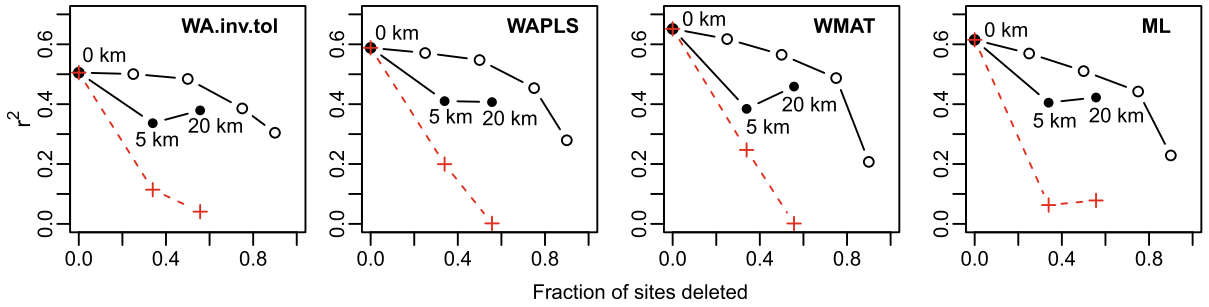

Fig. 9 Plot showing effect of spatial autocorrelation on r^2 for all model types by deleting sites at random (*open circles*), from the geographic area of the test site (*filled circles*), or that are most environmentally similar (*crosses*), during cross-validation

Table 2 RMSEP of the prediction with applying transfer function models to Changbai data (n = 52 samples)

	RMSEP	
	DWT (cm)	Moisture (%)
WA.inv	7.28	3.27
WA.cla	8.23	2.94
WA.inv.tol	6.77	3.36
WA.cla.tol	7.31	3.07
WAPLS	8.46	3.28
ML	9.57	3.31
MAT	10.42	3.89
WMAT	10.41	3.94

The model names as in Table 1

mean prediction errors are still far lower than the standard deviation of observed values for the Changbai data (SD_{DWT} = 12.85, $SD_{Moisture}$ = 4.47 %, n = 52), suggesting the predicted results are generally acceptable. For DWT, the best model assessed with LOO/LOSO, WA.inv.tol, produces the most precise prediction. For moisture, however, the $RMSEP_{pred}$ of the best model, WAPLS, is greater than WA.cla and WA.cla.tol. This also indicates that the best model training set, assessed with cross validation, does not necessarily perform best in paleohydrological reconstruction. We should therefore be very careful in choosing reconstruction models.

Conclusions

This study filled a geographic gap with respect to regions that have been sampled for testate amoebae. It provided new data from northeast China and added to our knowledge of testate amoebae ecology and biogeography. DWT and peat moisture are the principal factors that control testate amoebae community composition in *Sphagnum* peatlands of the Lesser Khingan Mountains, northeast China. The best performing transfer function models for DWT and moisture content produced $RMSEP_{LOO}$ values of 6.74 cm and 1.49 %, respectively. When a more robust cross validation method for clustered structure data, leave-one-site-out, was applied, the $RMSEP_{LOSO}$ of the best models increased, to 6.90 cm and 1.67 %, but all models still had predictive power. Uneven sampling along the environmental gradients also influenced the prediction performance. More samples in the middle range of the gradient produced smaller RMSEPs than did the extreme wet and dry ends of the gradient, where fewer samples were collected. Results of this study were comparable to those of other studies, suggesting this training set is a potentially important tool for peat-based paleoclimate reconstruction in the Lesser Khingan Mountains, northeast China. The study will contribute to a better understanding of past climate change, particularly monsoon activity, in this region.

Acknowledgments This work was supported by a Grant from the National Natural Science Foundation of China (No. 41001121). Students Youbao Pu, Xiaoling Yang, Songmai Wang, and Congyang Wang helped with fieldwork and sample processing. Dr. Matt Amesbury and an anonymous reviewer provided valuable comments on this paper.

References

Amesbury MJ, Mallon G, Charman DJ, Hughes PDM, Booth RK, Daley TJ, Garneau M (2013) Statistical testing of a new testate amoeba-based transfer function for water-table

Author's personal copy

depth reconstruction on ombrotrophic peatlands in north-eastern Canada and Maine, United States. J Quat Sci 28:27–39

An Z, Porter SC, Kutzbach JE, Xihao W, Suming W, Xiaodong L, Xiaoqiang L, Weijian Z (2000) Asynchronous Holocene optimum of the East Asian monsoon. Quat Sci Rev 19:743–762

Booth RK (2001) Ecology of testate amoebae (Protozoa) in two Lake Superior coastal wetlands: implications for paleoecology and environmental monitoring. Wetlands 21:564–576

Booth RK (2007) Testate amoebae as proxies for mean annual water-table depth in Sphagnum-dominated peatlands of North America. J Quat Sci 23:43–57

Booth RK (2010) Testing the climate sensitivity of peat-based paleoclimate reconstructions in mid-continental North America. Quat Sci Rev 29:720–731

Charman DJ (1997) Modelling hydrological relationships of testate amoebae (Protozoa: Rhizopoda) on New Zealand peatlands. J R Soc N Z 27:465–483

Charman DJ (2001) Biostratigraphic and palaeoenvironmental applications of testate amoebae. Quat Sci Rev 20:1753–1764

Charman DJ (2007) Summer water deficit variability controls on peatland water-table changes: implications for Holocene palaeoclimate reconstructions. Holocene 17:217–227

Charman DJ, Hendon D, Woodland WA (2000) The idendification of testate amoebae (Protozoa: Rhizopoda) in peats. QRA technical guide no. 9. Quaternary Research Association, London

Charman DJ, Brown AD, Hendon D, Karofeld E (2004) Testing the relationship between Holocene peatland palaeoclimate reconstructions and instrumental data at two European sites. Quat Sci Rev 23:137–143

Charman DJ, Blundell A, Members ACCROTELM (2007) A new European testate amoebae transfer function for palaeohydrological reconstruction on ombrotrophic peatlands. J Quat Sci 22:209–221

Charman DJ, Barber KE, Blaauw M, Langdon PG, Mauquoy D, Daley TJ, Hughes PDM, Karofeld E (2009) Climate drivers for peatland palaeoclimate records. Quat Sci Rev 28:1811–1819

Charman DJ, Hohl V, Blundell A, Mitchell F, Newberry J, Oksanen P (2012) A 1000-year reconstruction of summer precipitation from Ireland: calibration of a peat-based palaeoclimate record. Quat Int 268:87–97

Hendon D, Charman DJ, Kent M (2001) Palaeohydrological records derived from testate amoebae analysis from peatlands in northern England: within-site variability, between-site comparability and palaeoclimatic implications. Holocene 11:127–148

Juggins S (2013) Rioja: analysis of quaternary science data, R Package version 0.8-4

Lamarre A, Magnan G, Garneau M, Boucher É (2013) A testate amoeba-based transfer function for paleohydrological reconstruction from boreal and subarctic peatlands in northeastern Canada. Quat Int 306:88–96

Lamentowicz M, Mitchell EAD (2005) The ecology of testate amoebae (protists) in Sphagnum in north-western Poland in relation to peatland ecology. Microbial Ecol 50:48–63

Lamentowicz Ł, Lamentowicz M, Gabka M (2008a) Testate amoebae ecology and a local transfer function from a peatland in western Poland. Wetlands 28:164–175

Lamentowicz M, Cedro A, Gałka M, Goslar T (2008b) Last millennium palaeoenvironmental changes from a Baltic bog (Poland) inferred from stable isotopes, pollen, plant macrofossils and testate amoebae. Palaeogeogr Palaeoclimatol Palaeoecol 265:93–106

Lamentowicz M, Lamentowicz Ł, van Der Knaap WO, Gabka M, Mitchell EAD (2010) Contrasting species-environment relationships in communities of testate amoebae, bryophytes and vascular plants along the Fen-Bog Gradient. Microbial Ecol 59:499–510

Legendre P, Gallagher ED (2001) Ecologically meaningful transformations for ordination of species data. Oecologia 129:271–280

Li HK, Bu ZJ, Wang SZ, An ZS, Zhao HY, Ma YY, Chen X (2009) Environmental implications of the modern testate amoebae in the peatlands in Changbai Mountains. Quat Sci 29:817–824

Li HK, Li WW, Pu YB, Wang CY, Wang SM, Yang XL (2013) Building transfer functions between testate amoeba and environmental variables with 'rioja' package. Sci Geogr Sinica 33:1022–1028

Lin QH, Leng XT, Hong B (2004) Peat $\delta^{13}C$ record of climate change in Xiao Xinganling in the past 5000 years. Earth Environ 32:50–54

Markel ER, Booth RK, Qin Y (2010) Testate amoebae and δ13c of sphagnum as surface-moisture proxies in Alaskan peatlands. Holocene 20:463–475

Mauquoy D, Barber K (1999) A replicated 3000 yr proxy-climate record from Coom Rigg Moss and Felecia Moss, the Border Mires, northern England. J Quat Sci 14:263–275

Meisterfeld R (2002a) Order Arcellinida Kent, 1880. In: Lee JJ, Leedale GF, Bradbury P (eds) The illustrated guide to the protozoa. Society of protozoologists, Lawrence, pp 827–860

Meisterfeld R (2002b) Testate amoebae with filopodia. In: Lee JJ, Leedale GF, Bradbury P (eds) The illustrated guide to the protozoa. Society of protozoologists, Lawrence, pp 1054–1084

Mitchell EAD, Buttler AJ, Warner BG, Gobat JM (1999) Ecology of testate amoebae (Protozoa: Rhizopoda) in Sphagnum peatlands in the Jura mountains, Switzerland and France. Ecoscience 6:565–576

Mitchell EAD, Charman DJ, Warner BG (2008) Testate amoebae analysis in ecological and paleoecological studies of wetlands: past, present and future. Biodivers Conserv 17:2115–2137

Ogden CG, Hedley RH (1980) An atlas of freshwater testate amoebae. British Museum (Natural History) and Oxford University Press, London

Oksanen J, Blanchet FG, Kindt R, Legendre P, Minchin PR, O'Hara RB, Simpson GL, Solymos P, Stevens MHH, Wagner H (2013) vegan: community ecology package. R package version 2.0-10

Payne RJ, Mitchell EAD (2007) Ecology of testate amoebae from mires in the central Rhodope Mountains, Greece and development of a transfer function for palaeohydrological reconstruction. Protist 158:159–171

Author's personal copy

Payne RJ, Kishaba K, Blackford JJ, Mitchell EAD (2006) Ecology of testate amoebae (protista) in south-central Alaska peatlands: building transfer-function models for palaeoenvironmental studies. Holocene 16:403–414

Payne RJ, Charman DJ, Matthews S (2008) Testate amoebae as paleohydrological proxies in Sürmene Ağaçbaşi Yaylasi pealtand (Northeast Turkey). Wetlands 28:311–323

Payne R, Lamentowicz M, Mitchell EAD (2011) The perils of taxonomic inconsistency in quantitative palaeoecology: experiments with testate amoeba data. Boreas 40:15–27

Payne RJ, Telford RJ, Blackford JJ, Blundell A, Booth RK, Charman DJ, Lamentowicz Ł, Lamentowicz M, Mitchell EAD, Potts G, Swindles GT, Warner BG, Woodland W (2012) Testing peatland testate amoeba transfer functions: appropriate methods for clustered training-sets. Holocene 22:819–825

Penard E (1902) Faune rhizopodique tu bassin du Léman. Henry Kündig, Genève

Qin Y, Mitchell EAD, Lamentowicz M, Payne R, Lara E, Gu Y, Huang X, Wang H (2013) Ecology of testate amoebae in peatlands of central China and development of a transfer function for paleohydrological reconstruction. J Paleolimnol 50:319–330

R Development Core Team (2013) R: a language and environment for statistical computing. R Foundation for Statistical Computing, Vienna

Schoning K, Charman DJ, Wastegaård S (2005) Reconstructed water tables from two ombrotrophic mires in eastern central Sweden compared with instrumental meteorological data. Holocene 15:111–118

Song L, Li H, Wang K, Wu D, Wu H (2014) Ecology of testate amoebae and their potential use as palaeohydrologic indicators from peatland in Sanjiang Plain, Northeast China. Front Earth Sci 8:564–572

Stanek W (1973) Comparisons of methods of pH determination for organic terrain surveys. Can J Soil Sci 53:177–183

Swindles GT, Charman DJ, Roe HM, Sansum PA (2009) Environmental controls on peatland testate amoebae (Protozoa: Rhizopoda) in the North of Ireland: implications for Holocene palaeoclimate studies. J Paleolimnol 42:123–140

Swindles GT, Blaauw M, Blundell A, Turner TE (2012) Examining the uncertainties in a 'tuned and stacked' peatland water table reconstruction. Quat Int 268:58–64

Swindles GT, Reczuga M, Lamentowicz M, Raby CL, Turner TE, Charman DJ, Gallego-Sala A, Valderrama E, Williams C, Draper F, Honorio Coronado EN, Roucoux KH, Baker T, Mullan DJ (2014) Ecology of testate amoebae in an Amazonian peatland and development of a transfer function for palaeohydrological reconstruction. Microbial Ecol 68:284–298

Telford RJ (2013) palaeoSig: significance tests of quantitative palaeoenvironmental reconstructions. R package version 1.1-2

Telford RJ, Birks HJB (2005) The secret assumption of transfer functions: problems with spatial autocorrelation in evaluating model performance. Quat Sci Rev 24:2173–2179

Telford RJ, Birks HJB (2009) Evaluation of transfer functions in spatially structured environments. Quat Sci Rev 28:1309–1316

Telford RJ, Birks HJB (2011) Effect of uneven sampling along an environmental gradient on transfer-function performance. J Paleolimnol 46:99–106

Turner TE, Swindles GT, Charman DJ, Blundell A (2013) Comparing regional and supra-regional transfer functions for palaeohydrological reconstruction from Holocene peatlands. Palaeogeogr Palaeoclimatol Palaeoecol 369:395–408

Väliranta M, Blundell A, Charman DJ, Karofeld E, Korhola A, Sillasoo Ü, Tuittila ES (2012) Reconstructing peatland water tables using transfer functions for plant macrofossils and testate amoebae: a methodological comparison. Quat Int 268:34–43

Van Bellen S, Mauquoy D, Payne RJ, Roland TP, Daley TJ, Hughes PDM, Loader NJ, Street-Perrott FA, Rice EM, Pancotto VA (2014) Testate amoebae as a proxy for reconstructing Holocene water table dynamics in southern Patagonian peat bogs. J Quat Sci 29:463–474

Wilmshurst JM, Wiser SK, Charman DJ (2003) Reconstructing Holocene water tables in New Zealand using testate amoebae: differential preservation of tests and implications for the use of transfer functions. Holocene 13:61–72

Woodland WA, Charman DJ, Sims PC (1998) Quantitative estimates of water tables and soil moisture in Holocene peatlands from testate amoebae. Holocene 8:261–273

Xia YM (2000) Spore and pollen recoreds from peat deposits and the paleoenvironmental reconstruction in the Da Hingganling and Xiao Hingganling Moutains of northeast China. Acta Micropalaeontol Sin 17:218–227

Yang YX (2003) Study on formation and development of forest swamp and paleoenvironmental changes since the Holocene in the east part of the Xiaoxinganling Moutains. Oceanol Limnol Sin 34:74–82